

**Rational Synthesis
of Tubular and Belt-Like Aromatic Systems**

**Dissertation
zur Erlangung des Doktorgrades
der Mathematisch-Naturwissenschaftlichen Fakultät
der Christian-Albrechts-Universität
zu Kiel**

vorgelegt von
Venkataramana Rajuri

Kiel 2009

Referent: Prof. Dr. Rainer Herges

Koreferent: Prof. Dr. U. Lüning

Tag der mündlichen Prüfung: 30.01.09

Zum Druck genehmigt: Kiel, 06.07.09

Prof. Dr. L. Kipp, Dekan

Die vorliegende Arbeit wurde auf Anregung und unter Anleitung von
Herrn Prof. Dr. Rainer Herges
am Otto-Diels-Institut für Organische Chemie
der Christian-Albrechts-Universität zu Kiel
im Zeitraum von Oktober 2004 bis Februar 2009 angefertigt.

Eidesstattliche Erklärung

Hiermit erkläre ich an Eides statt, dass

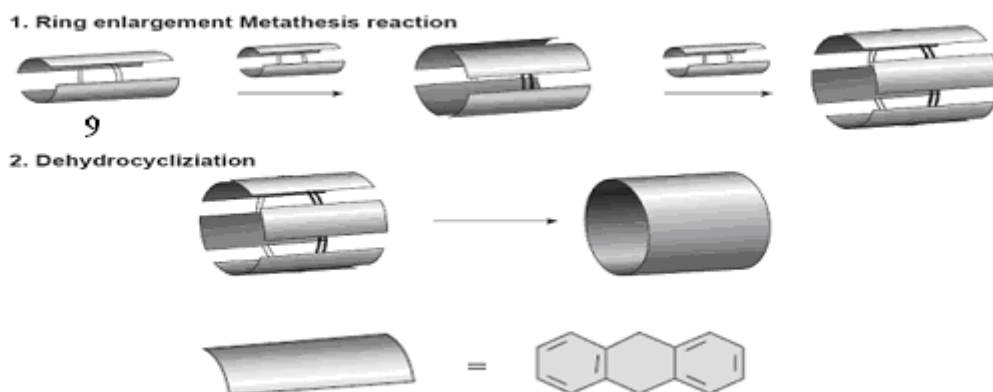
- a) diese Abhandlung - abgesehen von der Beratung durch die Betreuerin oder den Betreuer - nach Inhalt und Form meine eigene Arbeit ist;
- b) dass diese Arbeit noch nicht ganz oder zum Teil schon einer anderen Stelle im Rahmen eines Prüfungsverfahrens vorgelegen hat, veröffentlicht worden ist oder zur Veröffentlichung eingereicht wurde;
- c) dass diese Arbeit unter Einhaltung der Regeln guter wissenschaftlicher Praxis entstanden ist.

Kiel, den _____

Unterschrift: _____

Abstract

Nanotubes: Our approach towards the rational synthesis of nanotubes is based on the ring enlargement metathesis reaction. The starting materials are compounds with at least two aromatic “plates”, which are connected by at least two quinoid double bonds conjugated to the aromatic units. Using ring enlargement metathesis larger cyclic oligomers are formed. In a second independent step the tube walls are supposed to be closed by cyclodehydration.



Scheme: Our approach towards the synthesis of nanotubes.

Tetrahydrodianthracene (TDDA) **9** has been used as a building block for the ring enlargement metathesis reactions. This study was aimed at the synthesis of tubes with a larger diameter and at the extension of the short tubes in the prefabricated diameter and helicity. Furthermore, metal complexation with the synthesized tubular molecules was successfully achieved and verified by X-ray structure analysis.

Möbius aromatics: Our approach towards the synthesis of Möbius aromatics is based on the combination of inplane aromaticity and normal aromaticity which stabilize the Möbius structures and to facilitate their synthesis.

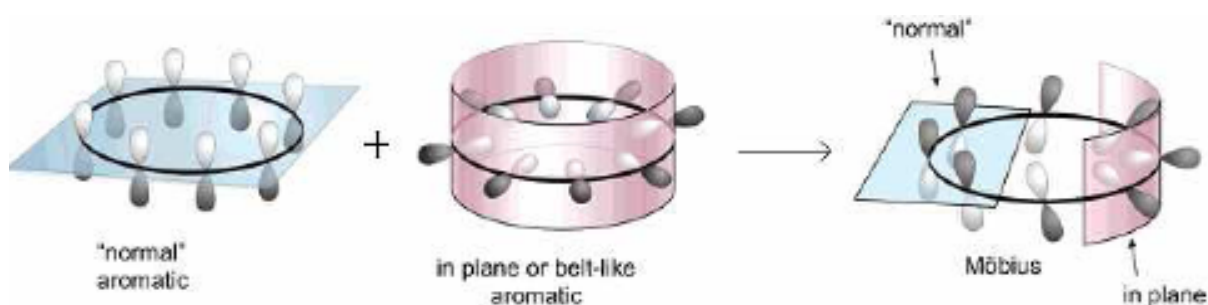
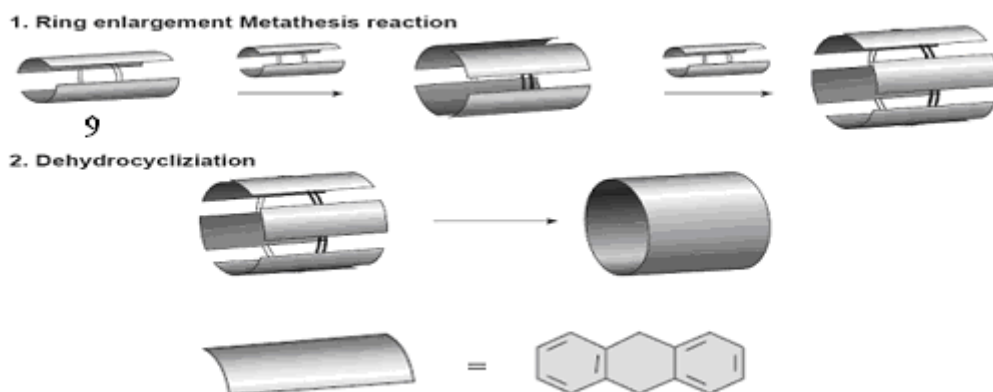


Figure: Our approach towards synthesis of Möbius aromatics.

Kurzzusammenfassung

Nanoröhren: Unser Ansatz zur rationalen Synthese von Nanoröhren basiert auf der Ringerweiterungsmetathese. Die Edukte weisen mindestens zwei aromatische Systeme auf, die jeweils durch mindestens zwei chinoide Doppelbindungen miteinander verbunden sind. Durch die Ringerweiterungsmetathese werden größere cyclische Oligomere gebildet. In einem zweiten, unabhängigen Schritt sollen die Röhrenwände durch Cyclodehydrierung geschlossen werden.



Schema: Unser Ansatz zur rationalen Synthese von Nanoröhren.

Tetradehydroanthracen (TDDA) **9** wurde als Baustein für die Ringerweiterungsmetathese eingesetzt. Das Ziel dieser Studie war die Herstellung röhrenförmiger Systeme mit einem größeren Durchmesser sowie die Verlängerung kürzerer Röhren in definiertem Durchmesser und Helicität. Darüber hinaus wurde die Komplexierung von Metallkationen an die hergestellten röhrenförmigen Systeme erfolgreich durch Röntgenstrukturen nachgewiesen.

Möbius-Aromaten: Unser Ansatz zur Synthese von Möbius-Aromaten basiert auf der Kombination von „in-plane“- und normaler Aromatizität, die die Möbius-Strukturen stabilisieren sowie ihre Synthese erleichtern sollen.

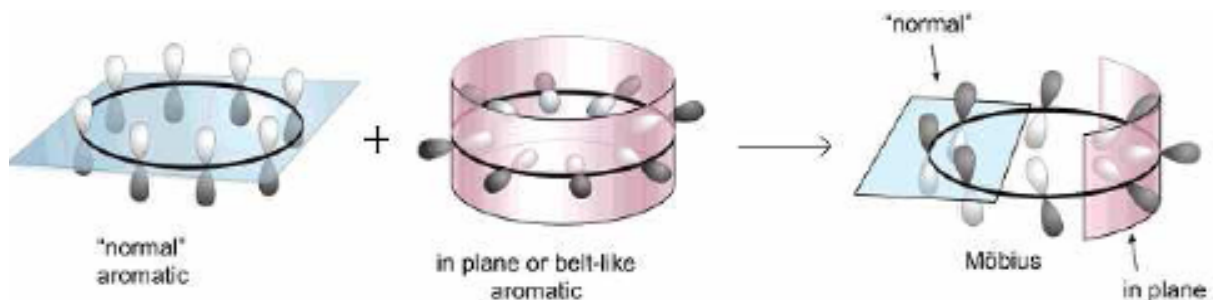


Abbildung: Unser Ansatz zur Synthese von Möbius-Aromaten.

ACKNOWLEDGEMENT

It was my privilege to work under the guidance of **Prof. Dr. Rainer Herges**, an eminent teacher and an excellent human being for my thesis work. I owe a great debt of gratitude for his indispensable guidance, kind cooperation, persistent encouragement and timely advice throughout my thesis.

I express sincere thanks to all of colleagues in the lab, Claudia Bornholdt, Catrin Goeschen, Dr. Anke Krüger, Regina Meinlschmidt, Eva Mucke, Hannelore Pohl, Jan Bornhöft, Dr. Bengt Buchhein-Stehn, Dr. Felix Köhler, Jens Kubitschke, Ali Mohebbi, Jens Walther, Dr. Torsten Winkler, Dr. Jan siegwarth, Hanno sell, Gaston Schaller, Benjamin Sahlmann, Thore Wendler, Marscha Ried, Dr. Umasish Jana, Anika Gehl, and Steffen Thies who were friendly and helpful during my thesis project work.

I specially thank Dr. Torsten Winkler and Dr. Anke Krüger for helping me in completion of my thesis.

I thank institute members of analytical department for measuring NMR and mass spectra.

Finally, I would like to thank my family for their constant encouragement and support through out my academic training.

Meinen Eltern

Table of Contents

1 Introduction	1
1.1 Molecular Tubes and Belts	1
1.1.1 Types of Nanotubes and Related Structures	1
1.1.1.1 Multiwalled Nanotubes	1
1.1.1.2 Single Walled Nanotubes	2
1.1.1.3 Nanotori	3
1.1.1.4 Nanobuds	3
1.1.2 Cyclacenes	4
1.1.3 Belt-like Benzoannulenes	5
1.1.4 Cyclo[n]phenacenes	5
1.1.5 Cyclic Paraphenylene Ethynylenes	6
1.1.6 Picotubes	7
1.2 Our Approach	8
2 9,9',10,10'-Tetrahydroanthracene (TDDA)	11
2.1 Synthesis of TDDA	11
2.2 Synthesis of <i>o</i> -Mesitylenesulfonylhydroxylamine (Carpino's Reagent)	12
2.3 Characterization of TDDA	13
2.4 Reactivity	14
2.4.1 Electrophilic addition to TDDA	14
2.4.2 Nucleophilic Additions to TDDA	15
2.4.3 Diels-Alder Reactions with Electron-Rich Dienes	16
2.4.4 Diels-Alder Reaction with Electron-Poor Dienes	17
2.4.5 Photochemically Induced Metathesis Reactions of TDDA	18
2.4.5.1 Photochemical Reaction with Cycloalkenes	18
2.4.5.2 Photodimerization of TDDA	18
2.4.5.3 Synthesis of Kammerphane	19
2.5 Conclusion	19
3 9,9',9'',10,10',10''-Hexadehydrotrianthracene (Trimer)	21
3.1 General	21
3.2 Bromination of the Semitrimer	23
3.3 Iodination of the Semitrimer	27

3.4 Diels-Alder Reaction of TDDA with Phthalazines	29
3.5 Treatment with Schlosser's Base	33
3.6 <i>N</i> -Bromo Succinimide Treatment of the <i>o</i> -Chinodimethane Adducts	36
3.7 Diels-Alder Reaction of TDDA with <i>o</i> -Chloranil and Tetrachlorothiopene Dioxide	37
3.8 Conclusion	39
4 Photochemical Reactions of the Tetramer	41
4.1 Synthesis of the Tetramer	41
4.2 Pyrolysis of the Tetramer	45
4.3 Solid State Irradiation of the Tetramer	47
4.4 Heating of the Tetramer	49
4.5 Conclusion	49
5 Möbius Aromatic Compounds	51
5.1 Introduction	51
5.2 Möbius Band of NbSe ₃ Crystals	52
5.3 Non Conjugated Molecular Möbius Strips	53
5.4 Design and Synthesis of the First Möbius Annulene	54
5.5 Möbius Aromaticity in Expanded Porphyrins	56
5.5.1 A Hückel-Möbius Aromaticity Switch	56
5.5.2 Möbius Aromaticity by Metallation	57
5.6 Diels-Alder Reaction of the (CH) ₄ Adduct with Pyridazine	58
5.7 Irradiation of the Semitrimer	59
5.8 Reaction of TDDA with 2,3-Bis (dibromomethyl) Naphthalene	65
5.9 Reaction of the (CH) ₄ Adduct with Tetrachlorothiopene Dioxide	66
5.9.1 Photochemical Irradiation of the Closed Isomer	71
5.9.2 Thermally Induced Ring Opening	72
5.10 Conclusion	74
6 Metal Complexations	75
6.1 Introduction	75
6.2 Copper Complexation of the Semitrimer	77
6.3 Silver Complex of the Semitrimer	78
6.3.1 Reaction with Silver Hexafluorophosphate	78
6.3.2 Reaction with silver hexafluoroantimonate	80

6.4 Silver Complexation of the Naphthalene System	81
6.5 Conclusion	83
7. Optimization of Mass Spectrometry	85
7.1 Electrospray Ionization	85
7.2 Matrix-Assisted Laser Desorption/Ionization (MALDI)	86
7.3 Conclusion	87
8 Summary	89
9 Experimental Part	95
9.1 Apparatus	95
9.2 Common Procedure	96
9.3 Rational Synthesis of Nanotubes and Möbius Aromatics	97
9.3.1 Synthesis of TDDA	97
9.3.1.1 Synthesis of 9-Bromoanthracene	97
9.3.1.2 Synthesis of 9, 10'-Dibromodianthracene	98
9.3.1.3 Synthesis of Bistriazolindianthracene	98
9.3.1.4 Synthesis of <i>N</i> -aminobistraizolinedianthracene	98
9.3.1.5 Synthesis of Tetradehydrodianthracene	99
9.3.2 Synthesis of <i>o</i> -Mesitylensulfonylhydroxylamin (Carpino's Reagent)	100
9.3.2.1 Synthesis of <i>tert</i> -Butyl Phenyl Carbonate	100
9.3.2.2 Synthesis of <i>tert</i> -Butyl Carbazate	100
9.3.2.3 Synthesis of <i>tert</i> -Butyl Azidoformate	101
9.3.2.4 Synthesis of <i>tert</i> -Butyl <i>N</i> -hydroxycarbamate	101
9.3.2.5 Synthesis of <i>tert</i> -butyl- <i>N</i> - <i>p</i> -toluenesulfonylcarbamate	102
9.3.2.6 Synthesis of Hydroxyl Amine- <i>o</i> -Mesitylene Sulfonate (Carpino's Reagent)	102
9.3.3 Synthesis of the Semitrimer	103
9.3.4 Attempted Trimer Synthesis	104
9.3.4.1 Preparation of 1,4-Dibromophthalazine	104
9.3.4.2 Attempted Diels-Alder Reaction of 1,4-Dibromophthalazine with TDDA	104
9.3.4.3 Attempted Diels alder reaction of 1,4 dichloro phthalazine with TDDA	104
9.3.4.4 Solid state reaction of 1,4 dihalophthalazine with TDDA	104
9.3.4.5 Reaction of Schlosser's Base with the Semitrimer	105
9.3.4.6 Halogenation of the Semitrimer	105
9.3.4.6.1 Bromination of the Semitrimer in Non-polar Solvents	105

9.3.4.6.2 Bromination of the Semitrimer in Polar Solvents	106
9.3.4.7 <i>N</i> -Bromo Succinimide Treatment of the <i>o</i> -Chinodimethane Adduct	106
9.3.4.7.1 Synthesis of the <i>o</i> -Chinodimethane Adduct	106
9.3.4.7.2 Treatment of the <i>o</i> -Chinodimethane Adduct with NBS	107
9.3.4.8 Diels-Alder Reaction of TDDA with <i>o</i> -Chloranil	107
9.3.5 Synthesis of the Tetramer	108
9.3.6 Attempted Synthesis of Möbius Hydrocarbons	108
9.3.6.1 Synthesis of the (CH) ₄ Adduct	108
9.3.6.2 Synthesis of the Naphthalene System	109
9.3.6.3 Attempted Diels-Alder Reaction of the (CH) ₄ Adduct with Pyridazine	110
9.3.6.4 Reaction of the (CH) ₄ Adduct with Tetrachlorothiopene Dioxide	111
9.3.6.4.1 Preparation of Tetrachlorothiopene Dioxide (TTD)	111
9.3.6.4.2 Reaction of TTD with the (CH) ₄ Adduct	111
9.4 Silver complexation of Semitrimer	113
9.5 X-ray Structure Data	114
9.5.1 Semitrimer	114
9.5.2 Naphthalene System	120
9.5.3 Iodine attacked naphthalene system	126
9.5.4 C _s Ring-Closed	132
9.5.5 C _s Ring-Opened	136
9.5.6 Silver Complex	141
10 References	154

1 Introduction

Carbon occurs in nature in different allotropes. Graphite and diamond are natural allotropes which differ both chemically and physically because of different hybridization and chemical structure. Since the discovery of fullerenes (also called as bucky balls) in 1985 by Kroto and Smalley^[1] different allotropes of carbon were discovered. Huffman and Krätschmer evaporated graphite in the electrical arc in 1990, thus enabling the chemical and physical examination of fullerenes. Under similar conditions Iijima^[3] observed in 1991 that not only spherical nanoparticles and fullerenes but also longer carbon tubes are formed which consist of several rolled graphite layers, which were later designated as multi-walled carbon nanotubes (MWNT). Soon after this discovery Ajayan and Ebbesen published a large scale synthesis of these compounds.^[4] Thereafter many articles were published based on theory, synthesis, characterization, properties and applications.

Nanotubes produced under these crude conditions occur in a number of different structures, different diameter, length, helicity etc. along with amorphous carbon. In the case of the fullerenes efficient separation techniques made it possible to isolate C₆₀ and C₇₀ in larger amounts with high purity, however, the purification of carbon nanotubes is still a distant prospect (except on the molecular level by single molecule manipulation in an AFM device). The rational synthesis of carbon nanotubes which could provide uniform structures with well defined physical properties is considered to be one of the “holy grails” of nanotechnology.^[5] The present work is aimed at taking the first steps toward this ambitious goal.

1.1 Molecular Tubes and Belts

1.1.1 Types of Nanotubes and Related Structures

1.1.1.1 Multi Walled Nanotubes

Multi-walled nanotubes (MWNT) are made up of concentric cylinders placed around a common central hollow.^[6] MWNTs are either wrapped into multiple layers like a parchment scroll or are constructed of multiple cylinders, one inside the other. The interlayer distance in multi-walled nanotubes is close to the distance between graphene layers in graphite, approximately 3.4 Å.

1.1.1.2 Single Walled Nanotubes

Single walled nano tubes (SWNT's) are formed by rolling a graphite sheet into a seamless cylinder.^[6] The tubes can be characterized by two integer numbers n and m . Rolling along the horizontal zig-zag line and superimposing the points $(0,0)$ and $(n,0)$ leads to a $(n,0)$ zig-zag nanotubes. If the zig-zag line and the rolling vector α form an angle of 30° armchair tubes are generated. For example superimposing $(0,0)$ and $(7,7)$ gives an $(7,7)$ armchair nanotube. Rolling angles α between 0° and 30° lead to chiral tubes with $n \neq m$ and $n, m \neq 0$.

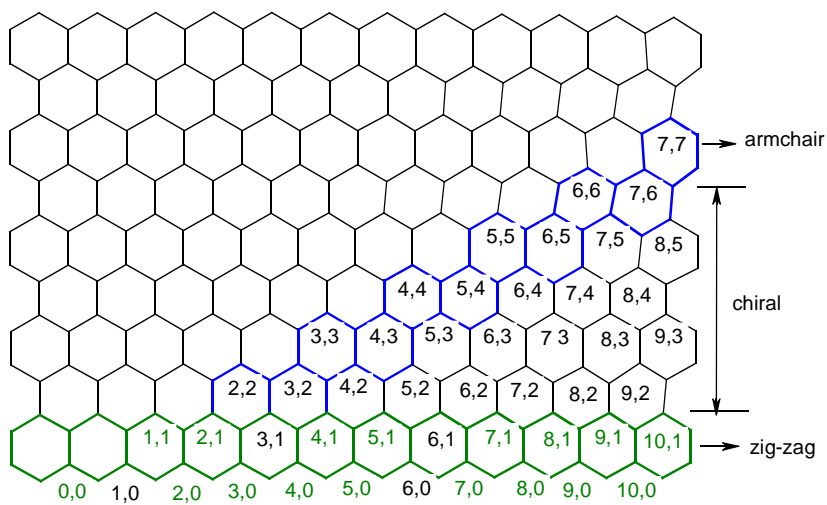


Figure 1.1: Vector notation of belts and tubes. The structures are characterized by integers n and m . Rolling up the wire mesh from $(0,0)$ to (n,m) and superimposing these two points leads to a (n,m) nanotube.

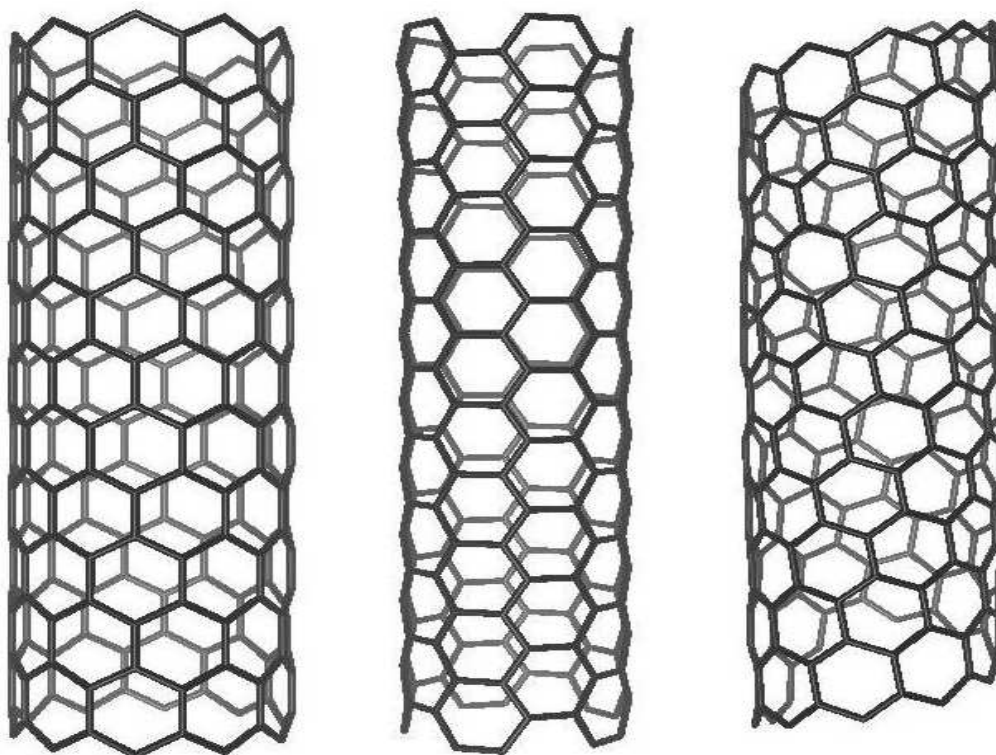


Figure 1.2: Models of nanotubes with different helicity: (10,0)-nano tube (zigzag, left) (5,5) nanotube (armchair, middle) (9,2) Nanotube (chiral, right).

1.1.1.3 Nanotori

A Carbon nanotorus can be considered to be constructed by bending a nanotube, then connecting its two open ends. The radii of a nanotorus are typically ranged between 300 and 500 nm, much larger than their width (5–30 nm), which may be used as building blocks for nanometer-scale electromagnetic devices. Properties such as magnetic moment, thermal stability, etc. vary widely depending on radius of the torus and radius of the tube.^[7,8]

1.1.1.4 Nanobuds

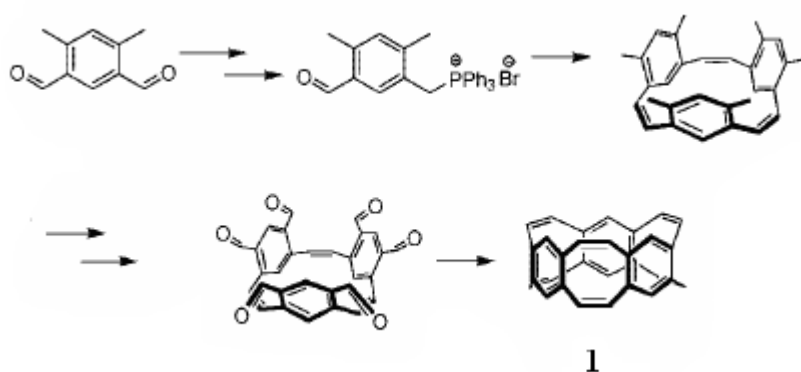
Nanobuds are novel hybrid materials that combine fullerenes and SWNT's into a single structure in which the fullerenes are covalently bonded to the outer surface of the SWNTs^[9] (figure 1.3). This hybrid material has useful properties of both fullerenes and carbon nanotubes. In particular, they have been found to be exceptionally good field emitters.^[10]



Figure 1.3: A stable nanobud structure.

1.1.2 Cyclacenes

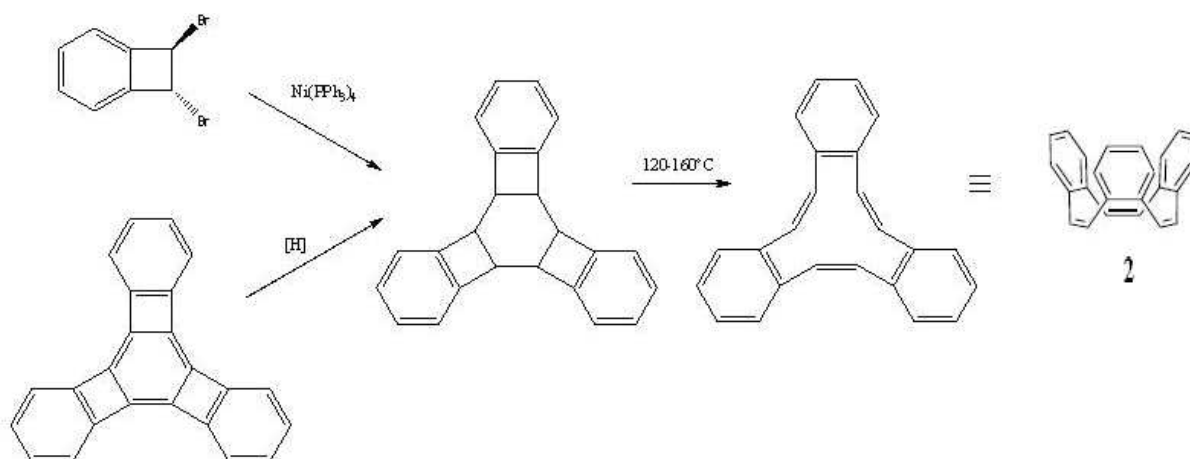
One of the synthetic challenges is the synthesis of cyclacenes, i.e. the (n,0)-zigzag unit of carbon nanotubes. Corey^[11,12] and Stoddard^[13,14,15] among other researchers, have tried to pick up this challenge, but unfortunately, neither one has achieved the aromatization of their respective cyclic precursors. These fully hoop-shaped cyclophanes are of interest with respect to their conjugation, their spectroscopic properties and their cavities. Recently, Gleiter et al^[16] developed a new synthesis strategy for [6.8]₃ cyclacene **1** as the first purely hydrocarbon cyclacene by stepwise synthesis (scheme 1.1). It is the smallest and most strained member of the [6.8]_n series which consisted of annelated six- and eight-membered rings.



Scheme 1.1: Synthesis of [6.8]₃ cyclacene.^[16]

1.1.3 Belt-like Benzoannulenes

All-*Z*-tribenzo[12]annulene (**2**) was synthesized by Iyoda^[17] and Vollhardt^[18] by [2+2+2] cycloreversion of tris (benzocyclobutadieno) benzene (scheme 1.2). Also, higher ring sizes of benzoannulene with all-*Z*-configurations were synthesized by same group. Like other π -spherands **2** forms 1:1 complexes with Ag^+ **3** and Cu^+ **4** (figure 1.4)^[19].



Scheme 1.2: Synthesis of *all-Z*-tribenzo [12]annulene^[17,18].

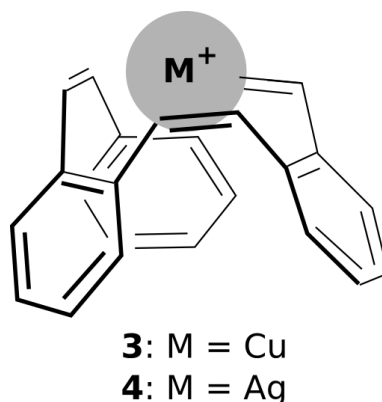
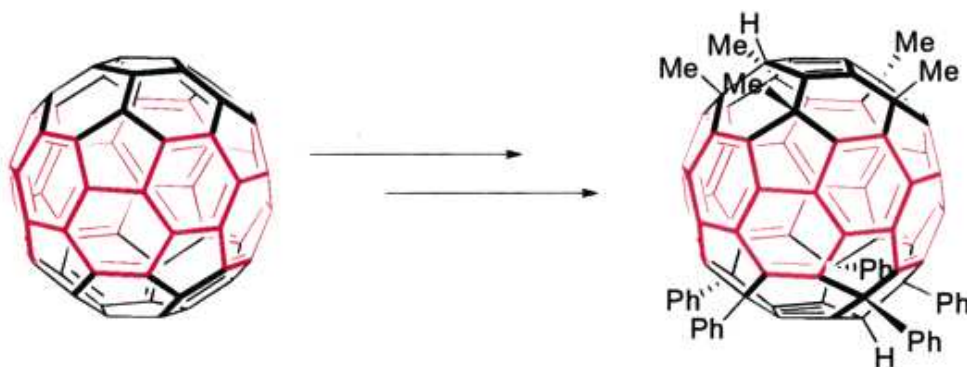


Figure 1.4: Metal complexation properties of *all-Z*-tribenzo [12]annulene.

1.1.4 Cyclo[n]phenacenes

The synthesis of cyclo[n]phenacenes which also contain double stranded π systems has been another target. Nakamura and Matsuo *et al.* succeeded in the first synthesis of a cyclo[10]phenacene derivative by the site selective alkylation/arylation of [60]fullerene as shown in Scheme 1.3, where the cyclo[10]phenacene substructure embedded in the [60]fullerene framework is highlighted.^[20,21]



Scheme 1.3: Synthesis of a [10]cyclophenacene from C_{60} .

1.1.5 Cyclic Paraphenylene Ethynylenes

Cyclic paraphenylene-ethynylenes are viewed as hybrids of cyclic paraphenylenes and cyclo[n]carbons. Hexameric and octameric cyclic paraphenylene-ethynylenes, [2₆]- and [2₈]paracyclophynes **5** and **6** respectively, were synthesized by Kawase and Oda *et al.* by bromination/dehydrobromination of the corresponding paracyclophenes, which were in turn obtained by the McMurry coupling of *p*-formylstyrene with a low-valent titanium reagent^[22] (figure 1.5).

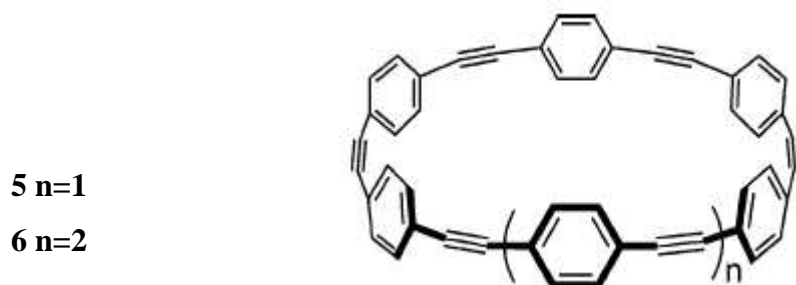


Figure 1.5: Structures of [2₆] and [2₈]paracyclophynes.

Because of the pyramidalization of the sp^2 carbon atoms, the electron densities and electrostatic potentials between the inner and outer surfaces of the cyclic paraphenylene-ethynylenes are different. This property gives rise to unique supramolecular behaviour of this class of compounds (figure 1.6). Such molecules have been attracting interest as precursors of carbon clusters.^[21]

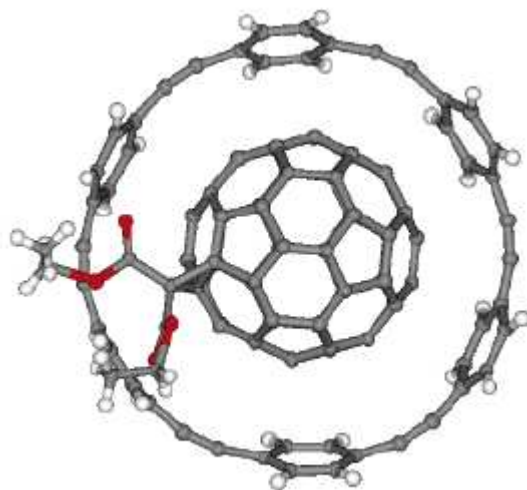
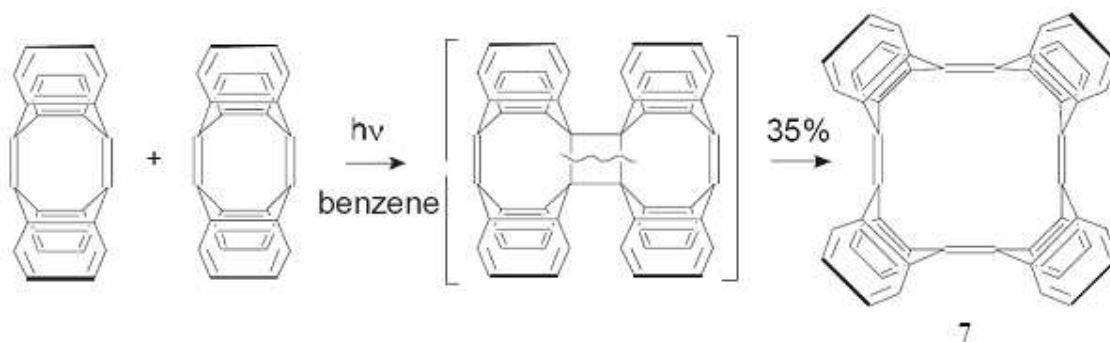


Figure 1.6: Side view of the X-ray crystallographic structure of the complex of [26]paracyclophane **5** with a [60]fullerene derivative.^[23]

1.1.6 Picotubes

Based upon a ring enlargement metathesis reaction Herges *et al.*^[24] were able to synthesize a belt- and tube-like fully conjugated molecule. The compound was termed picotube **7** because it is a small and short substructure of the larger carbon nanotubes (scheme 1.4).



Scheme 1.4: Synthesis of a picotube.

In a similar approach, Kammerphane **8**^[25] was synthesized as a fully conjugated tubular compound (figure 1.7).

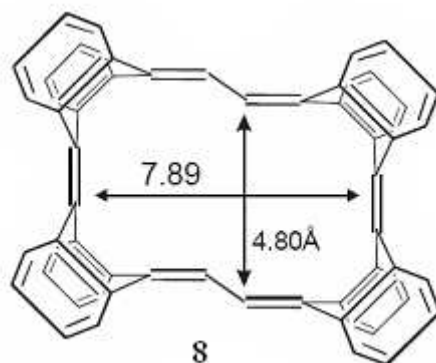


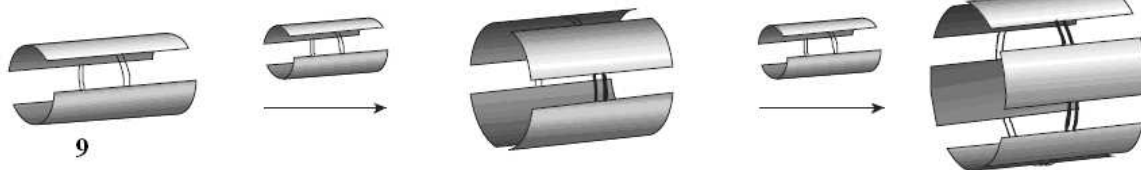
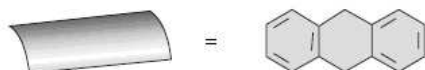
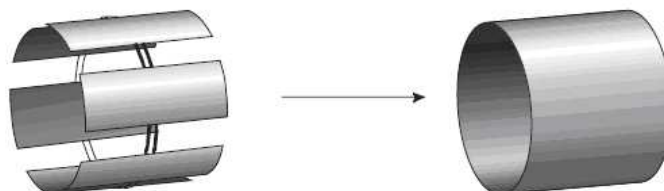
Figure 1.7: Structure of Kammerphane **8**.^[45]

1.2 Our Approach

Today, nanotechnology has found a great interest in research areas of different scientific fields. Indeed, nanoparticles and nanodevices exhibit new and promising properties for a number of applications. Chemistry is useful in the preparation of such nanometer sized systems because it allows a construction atom by atom, also called "bottom up" approach.

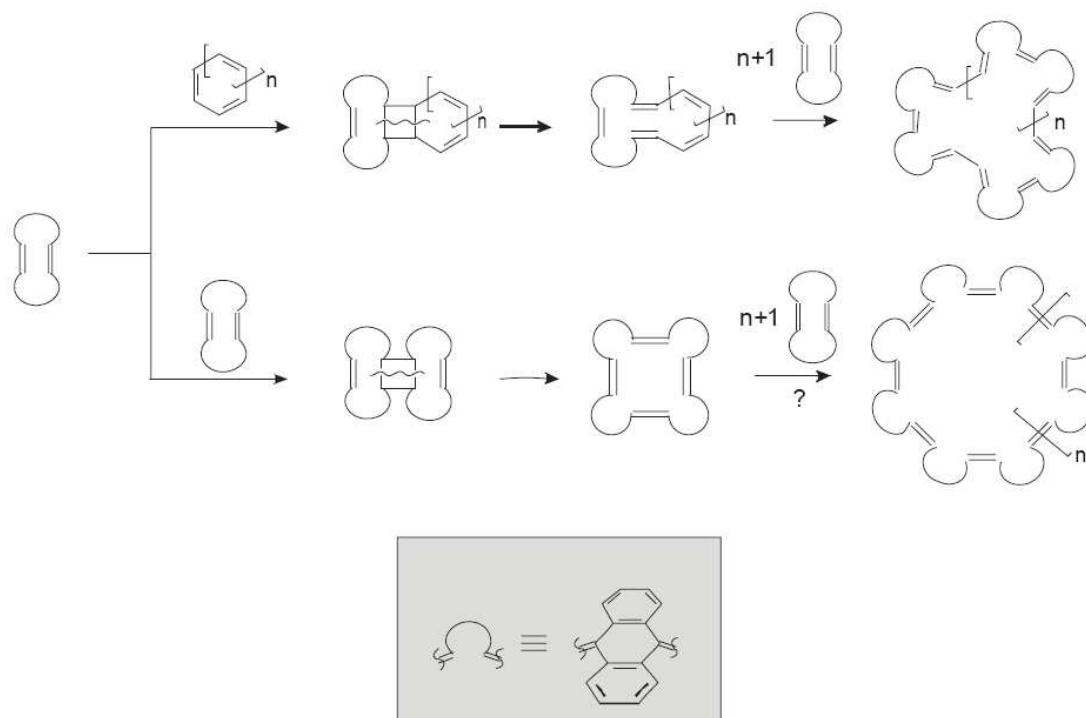
Nanotubes are technically produced by vaporization of graphite and chemical vapour deposition (CVD) at very high temperatures. Under these rough conditions, the tubes are generated with different lengths, diameters, helicities, and endcappings. For technical applications, however, tubes with a uniform geometry and thus with well defined physical properties are needed. A rational synthesis of carbon nanotubes was therefore considered.

Our approach starts out from a strategy which is based on the ring enlargement metathesis reaction. The starting material contains two small "graphitic plates" which are connected by at least two double bonds. Larger, cyclic oligomers are produced by metathesis reaction. In a further independent step the tube walls are closed by cyclodehydration (scheme 1.5).

1. Ring enlargement Metathesis reaction**2. Dehydrocyclization**

Scheme 1.5: Our approach towards rational synthesis of nanotubes.^[45]

Tetradehydrodianthracene (TDDA) **9** has been used as a building block in the ring enlargement metathesis reactions. A number of new belt-like and tubular aromatic compounds were constructed by metathesis of the highly reactive quinoid bridgehead double bond of TDDA **9** with [n]annulenes or by the dimerization reaction of two TDDA units (scheme 1.6). Targets of this study are aimed at the synthesis of tubes with a larger diameter and at the extension of the short tubes in the prefabricated diameter and helicity.

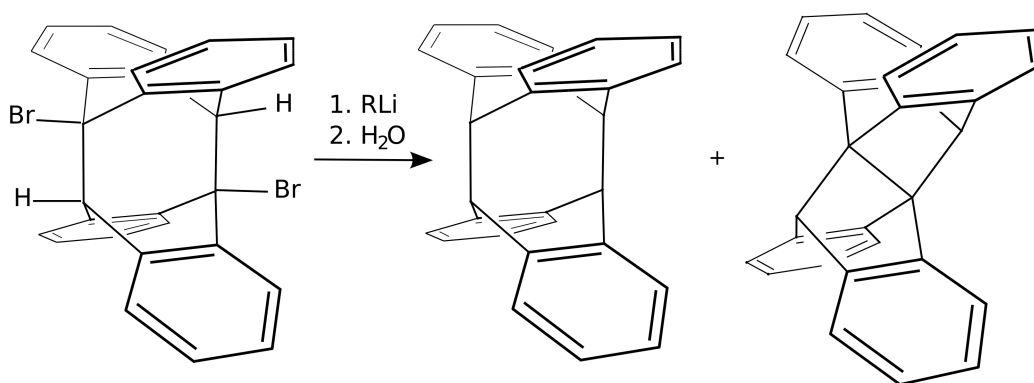


Scheme 1.6: Synthesis of molecular belts and tubes from the TDDA.

2 9,9',10,10'-Tetrahydrodianthracene (TDDA)

2.1 Synthesis of TDDA

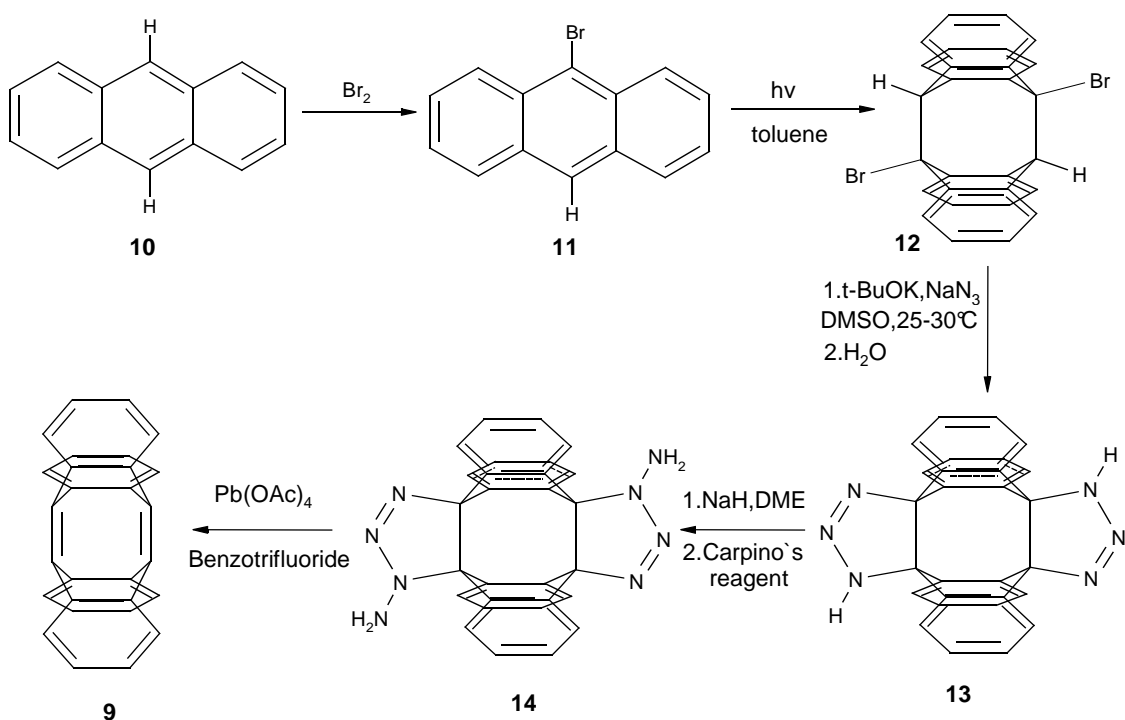
The synthesis of TDDA **9** looks very simple at first sight but because of the strained bridged double bonds the synthesis is very difficult. The bromination of anthracene **10** to get bromoanthracene **11** is followed by a [4+4] cycloaddition which yields 9,10'-dibromodianthracene **12**. Applequist *et al.*^[26] tried to synthesize TDDA on the basis of elimination of HBr from the 9,10'-dibromodianthracene **12**. They used organolithium reagents but they ended up with compounds **15,16** (scheme 2.1). With strong bases TDDA may be formed as an intermediate, but it will react with the elimination reagent as soon as it is formed.



Scheme 2.1: Attempts to eliminate HBr from the dibromodianthracene **12** (Applequist *et al.*).

In order to overcome these difficulties Green *et al.*^[27] used a sequence of formation, protection and subsequent regeneration of the reactive double bond. As shown in scheme 2.2, the reactive double bonds were generated by dehydrohalogenation of 9,10'-dibromodianthracene **12** to TDDA **9** and captured *in situ* with an excess of sodium azide by 1,3-dipolar cycloadditions. In a second step the triazoline **13** was converted to the *N*-aminotriazoline **14** by Carpino's reagent^[28] **15**. In the deprotection step oxidation of the *N*-amino triazoline **14** with lead tetraacetate yields TDDA **9**.

Because of the difficulties to reproduce the synthesis procedure of Greene *et al.* remained unused for a long time. In 1993 Neumann *et al.*^[29] optimized the synthesis of TDDA to obtain in grams. The optimized synthesis is as follows (scheme 2)

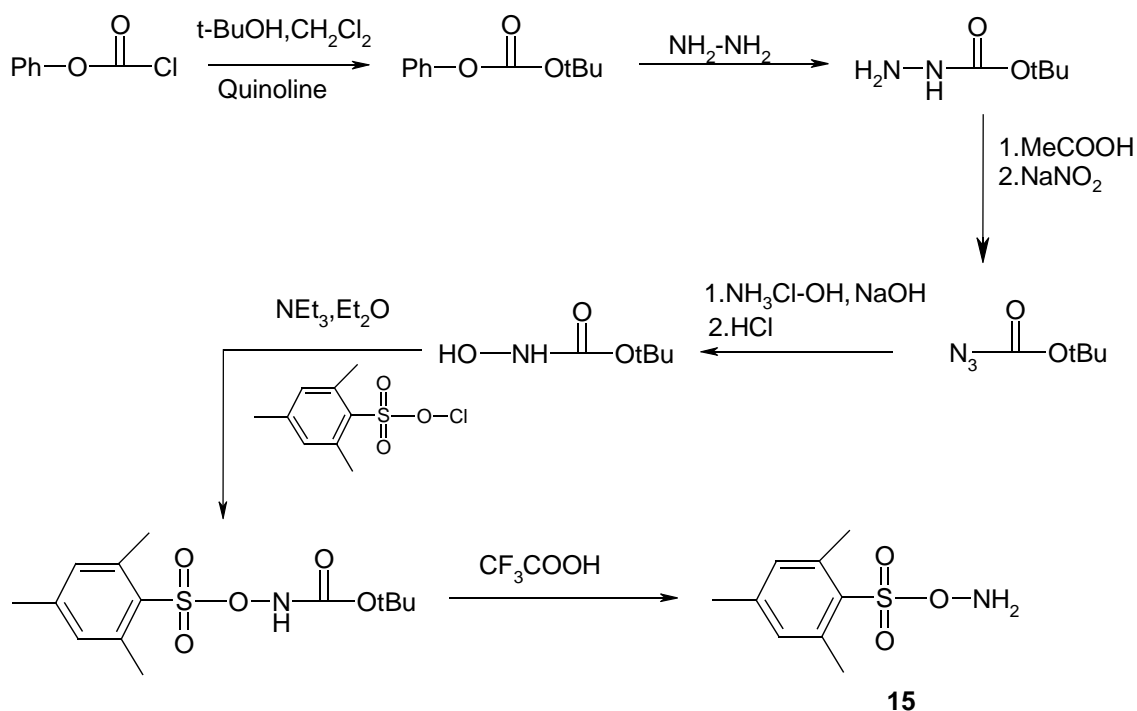


Scheme 2.2: Synthesis of TDDA **9**.^[45]

Bromoanthracene **11** was prepared from anthracene **10** by direct bromination or treatment with NBS. In both cases small amounts of anthracene **10** are left, but its presence will not affect the following step. Dibromodianthracene **12** is made from bromoanthracene **11** by photochemical [4+4] cycloaddition. Bromoanthracene **11** is irradiated in toluene. Due to low solubility, the formed dibromodianthracene **12** precipitates and does not obstruct the surface to further exposure of light. After monitoring of the azide protection reaction Neumann^[29] found that the reaction time should be changed from 2 days to 2 weeks. In the oxidation step, dichloromethane was replaced by α,α,α trifluoro toluene to prevent solvent addition to TDDA **9** and finally ultrasonic irradiation improved the yield of the last two steps.

2.2 Synthesis of *o*-Mesitylenesulfonylhydroxylamine (Carpino's Reagent) **15**

An important and difficult step in the synthesis of TDDA is the preparation of Carpino's reagent **15**. It is a multi step synthesis and time consuming. Since crystalline Carpino's reagent **15** is explosive, it should be made freshly (scheme 2.3).



Scheme 2.3: Synthesis of Carpino's reagent **15**.^[45]

2.3 Characterization of TDDA **9**

The structure of TDDA has some special features (figure 2.1).

- (1) the bridgehead carbon-carbon double bond distance (1.35 Å).
- (2) the pyramidalization angle of bridgehead atoms (35°).
- (3) the distance between the double bonds (2.4 Å), which is considerably smaller than the sum of the van der Waals radii of the corresponding sp^2 carbon atoms.

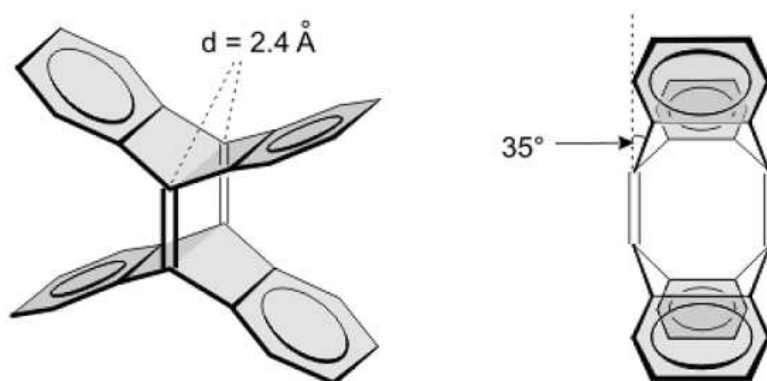
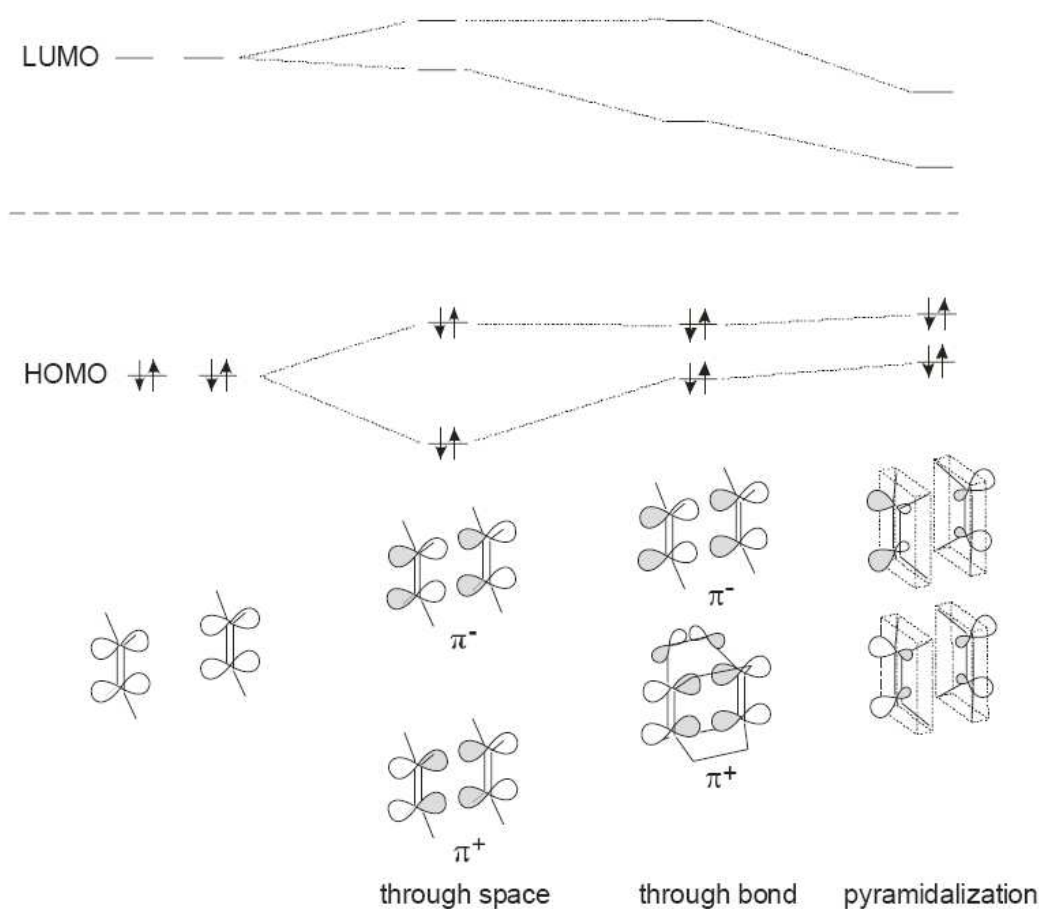


Figure 2.1: Structure of TDDA **9**.^[45]

From simple MO considerations, the following assumptions can be made (scheme 2.4). Through-space interaction leads to a splitting of HOMO and LUMO each into a bonding π^+ and antibonding π^- combination. Through-bond interaction through the benzo bridge raises the energy of the occupied π^+ and lowers the unoccupied π^- orbitals.^[30] The π orbital remains almost unchanged. Pyramidalization lowers the LUMO considerably and raises the HOMO.^[31] Thus, an enhanced reactivity towards electrophiles and particularly towards nucleophiles can be expected. Consequently, in Diels-Alder reactions TDDA **9** is more reactive as an electron deficient dienophile than maleic anhydride^[32] and therefore TDDA **9** should react with electron-rich and electron-poor dienes.



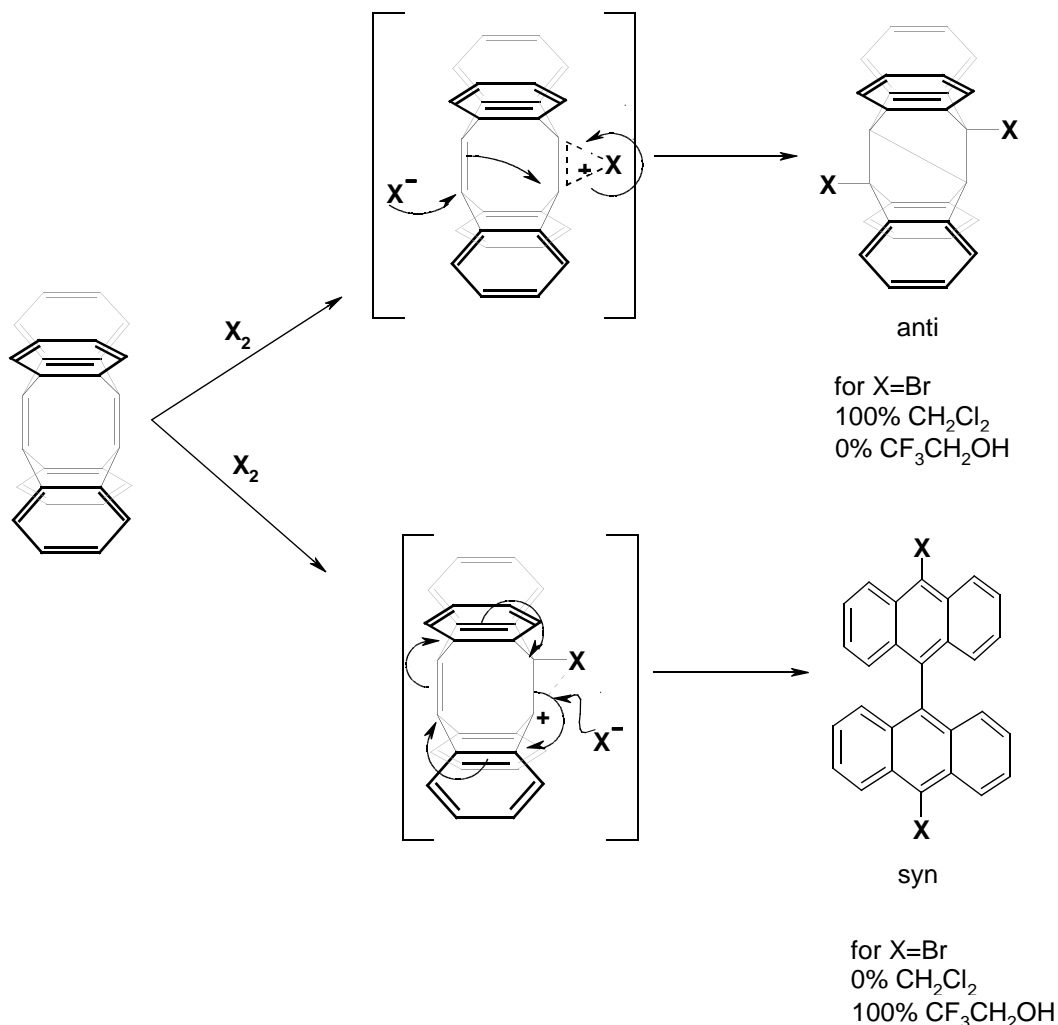
Scheme 2.4: Qualitative MO diagram of the individual effects on the olefinic π -orbitals of TDDA.^[45]

2.4 Reactivity

2.4.1 Electrophilic addition to TDDA **9**

TDDA **9** reacts with halogens to give transannular (*anti*) and ring opened (*syn*) products. The addition of iodine exclusively gives the transannular *anti* product in all

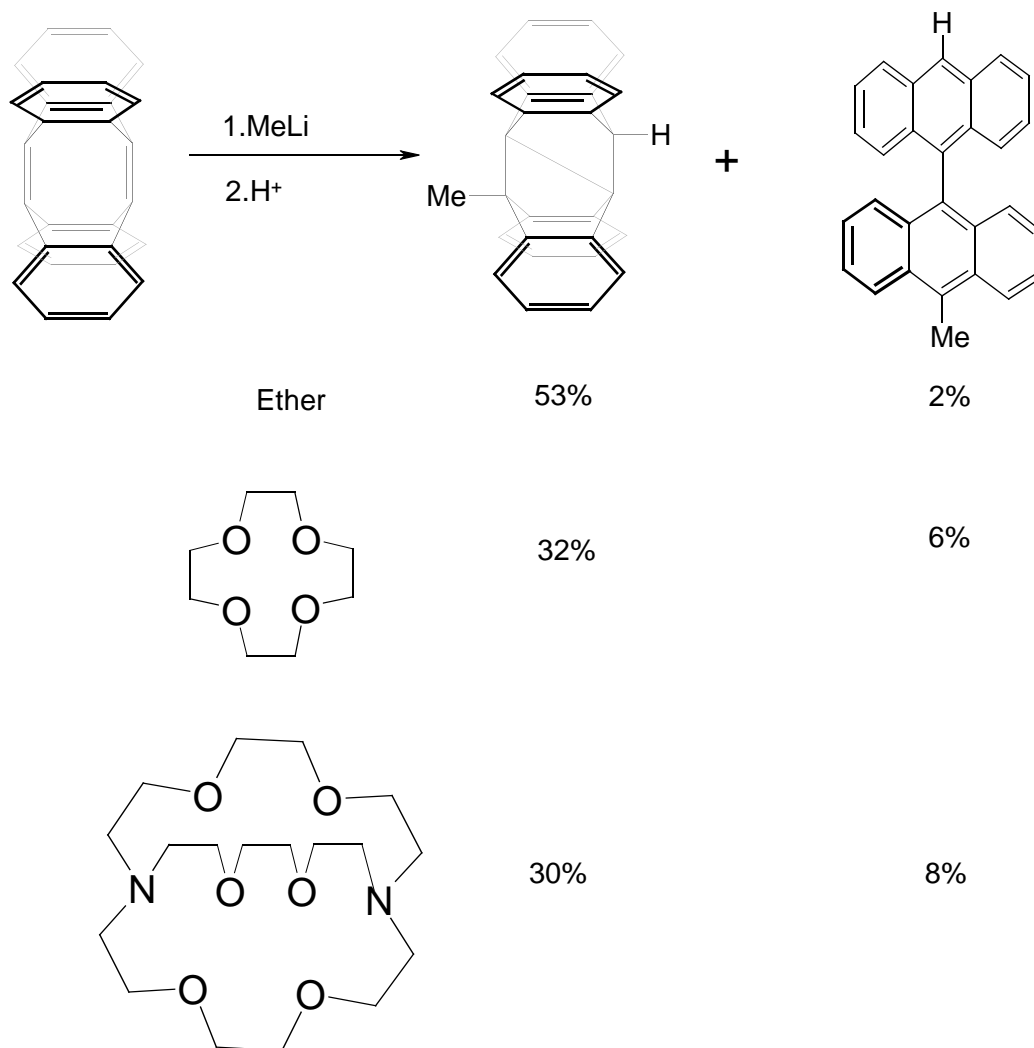
solvents. However, for bromine and chlorine the product ratio has a remarkable dependence upon the solvent polarity. Solvents of medium polarity favour the *anti* addition, whereas *syn* addition is observed with increasing and decreasing polarity (scheme 2.5).^[33]



Scheme 2.5: Electrophilic additions to TDDA.^[45]

2.4.2 Nucleophilic Additions to TDDA 9

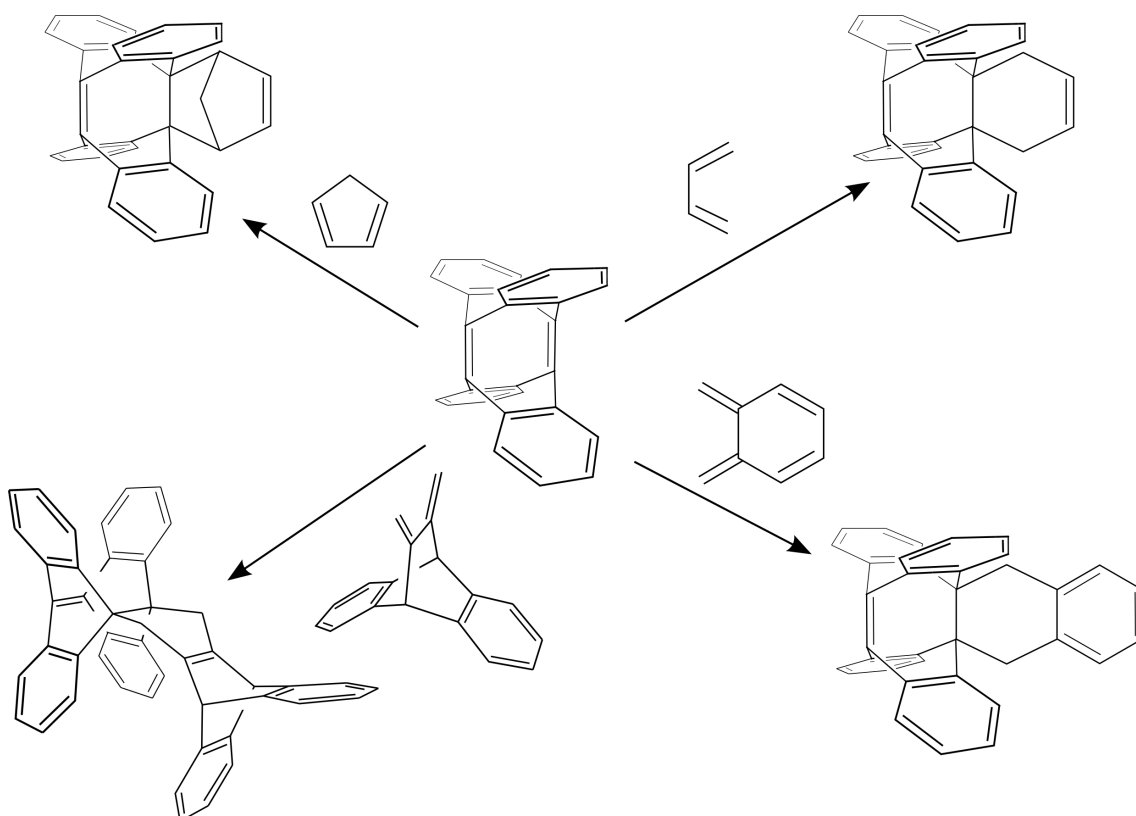
TDDA **9**, due to its peculiar electronic structure reacts with nucleophiles such as MeLi. Similar to electrophilic addition both transannular (*anti*) and ring opened (*syn*) products are observed.^[34] The addition of lithium-complexing ligands such as crown ethers and cryptands favours the formation of the ring-opened product (scheme 2.6).



Scheme 2.6: Nucleophilic additions to TDDA.^[45]

2.4.3 Diels-Alder Reactions with Electron-Rich Dienes

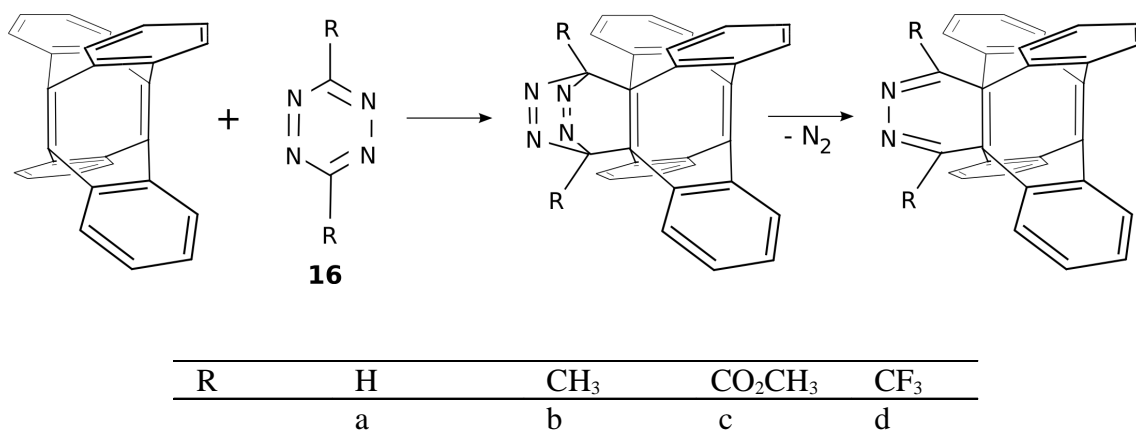
TDDA **9** reacts with electron rich dienes^[32] under ambient conditions. Only mono Diels-Alder adducts were observed even when a large excess of dienes and drastic conditions were applied (even though two strained and highly pyramidalized double bonds are available). The reactivity change of TDDA **9** compared to its mono Diels-Alder adduct is due to the through-bond and through-space interaction of the two olefinic double bonds (scheme 2.7).



Scheme 2.7: Diels-Alder reaction of TDDA with electron rich dienes.

2.4.4 Diels-Alder Reaction with Electron-Poor Dienes

TDDA **9** also reacts with electron poor dienes in Diels-Alder reactions with inverse electron demand. In [4+2] cycloaddition reactions of TDDA **9** with 1,2,4,5-tetrazines **16**^[35] the electronic effect of 3,6-substituents in tetrazines is far outweighed by steric factors resulting in an unexpected reactivity sequence: **16a** > **16b** = **16c** > **16d** (scheme 2.8).

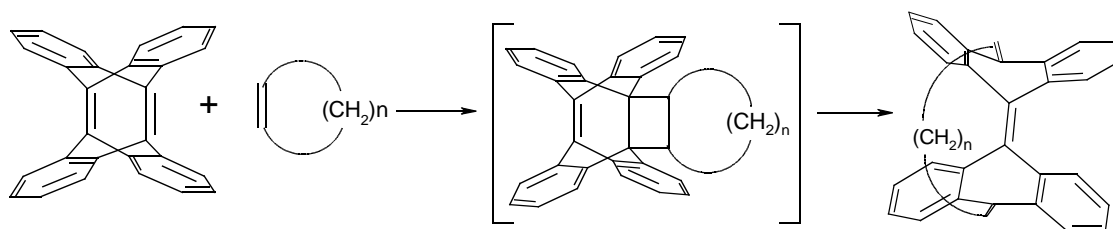


Scheme 2.8: Diels-Alder reactions of TDDA **9** with electron-poor dienes.

2.4.5 Photochemically Induced Metathesis Reactions of TDDA

2.4.5.1 Photochemical Reaction with Cycloalkenes

TDDA **9** undergoes photochemical reactions. With cyclic olefins it forms cyclophane-like bridged bianthraquinodimethanes. In the first step photochemical [2+2] cycloadditions yielded short-lived cyclobutane intermediates, which undergo [2+2] cycloreversions to give the final metathesis product (scheme 2.9). This concept of two-step (photochemical and thermal) metathesis can be used to synthesize spherically deformed, polycyclic aromatic hydrocarbons.^[35]

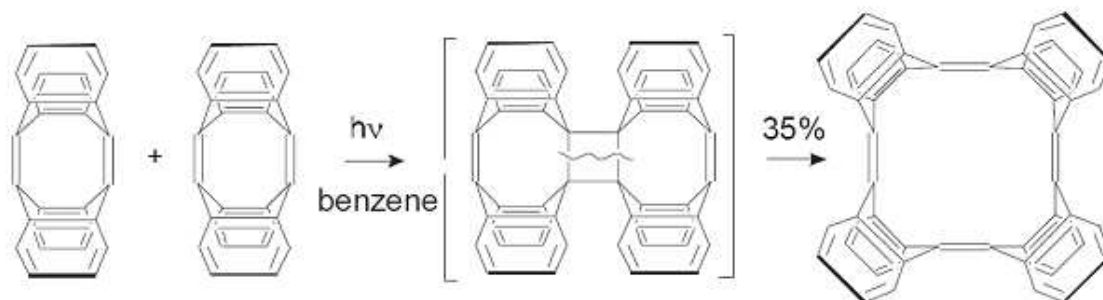


n		Yield %
3	cyclopentene	11
4	cyclohexene	0
5	cycloheptene	29
6	cyclooctene	60
8	cyclodecene	26

Scheme 2.9: Photochemical reactions of TDDA with cycloalkenes.

2.4.5.2 Photodimerization of TDDA

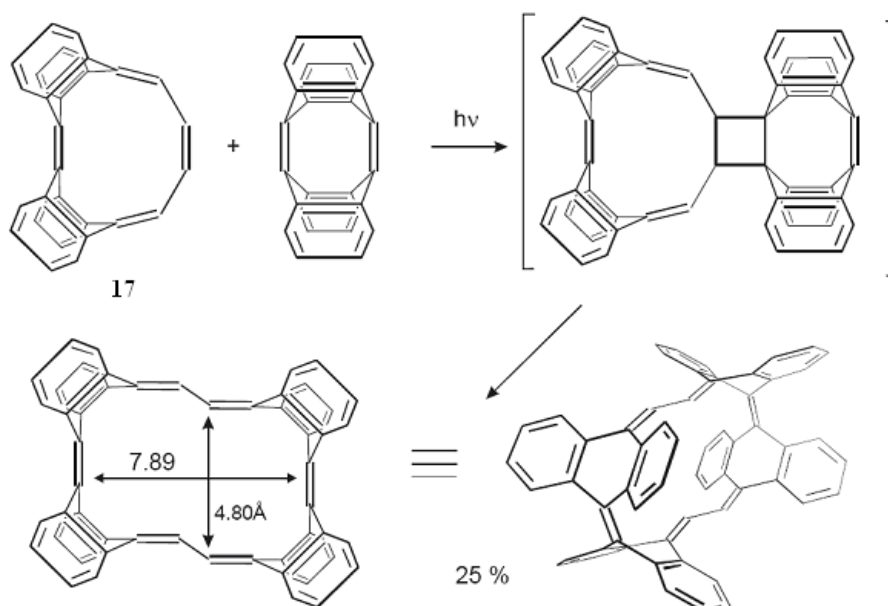
TDDA **9** dimerizes when the suspension in benzene is irradiated with a high pressure mercury lamp in a quartz apparatus^[37] (scheme 2.10).



Scheme 2.10: Photodimerization of TDDA **9**.^[45]

2.4.5.3 Synthesis of Kammerphane **8**

Under photochemical conditions TDDA reacts with double bonds like in the cyclophane bridge of **17** to form kammerphane **8**^[36] (scheme 2.11).



Scheme 2.11: Formation of kammerphane **8**.^[45]

2.5 Conclusion

TDDA **9** due to its peculiar electronic structure is reactive towards electrophiles, nucleophiles, in Diels-Alder reactions with different dienes, and also in photochemically induced metathesis reactions. Thus, TDDA is well suitable for the synthesis of tubular compounds.

3 9,9',9'',10,10',10''-Hexadehydrotrianthracene (Trimer 19)

3.1 General

Several research groups were trying to make the smallest single-walled nanotubes. The metallic properties of these small nanotubes depend upon the helicity. Even super conductivity was observed in 4\AA nanotubes.^[44] So far the smallest nanotubes with diameters of 0.7 ,^[40] 0.5 ^[41] and 0.4 nm ^[42,43] were synthesized (figure 3.1).

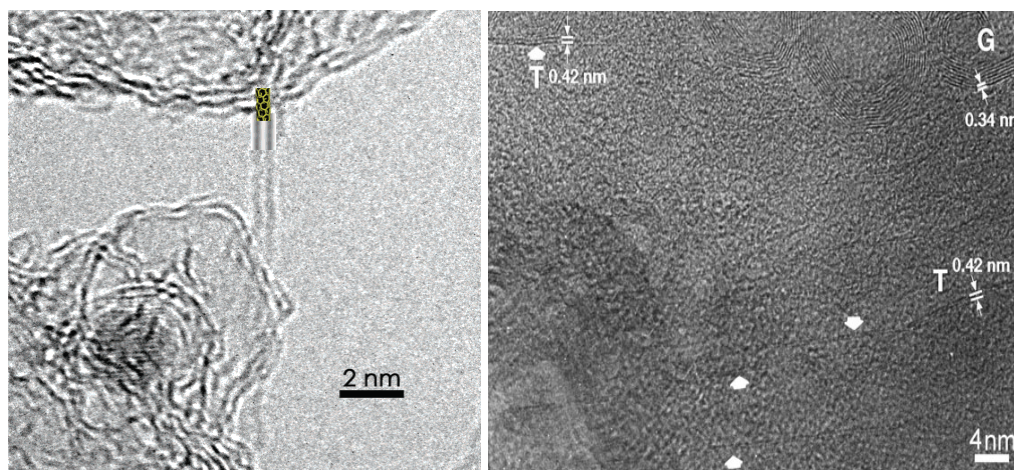


Figure 3.1: High-resolution transmission electron microscope images of small single walled nanotubes.^[42,43]

Our approach to synthesize the smallest single walled nanotube follows the rational synthesis of the dehydrocyclization of 9,9',9'',10,10',10''-hexadehydrotrianthracene (trimer **19**) (figure 3.2). Moreover, the trimer **19** is an interesting building block for the synthesis of larger tubular aromatic compounds (e.g. pentamer, hexamer, octamer etc.), which possibly can be achieved by using the photochemically induced ring enlargement metathesis reaction.

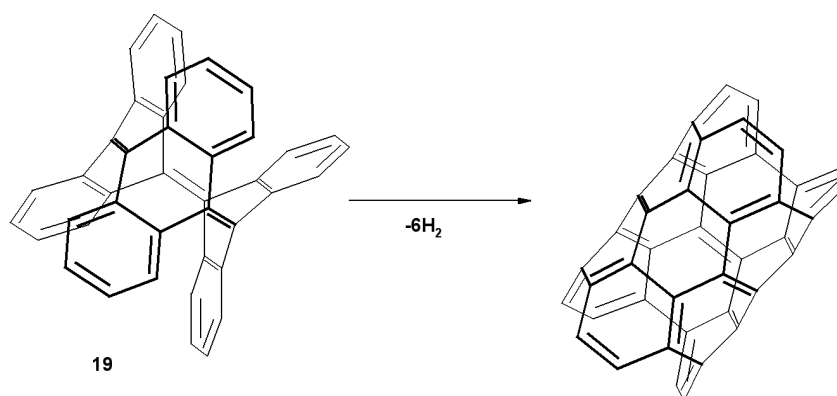
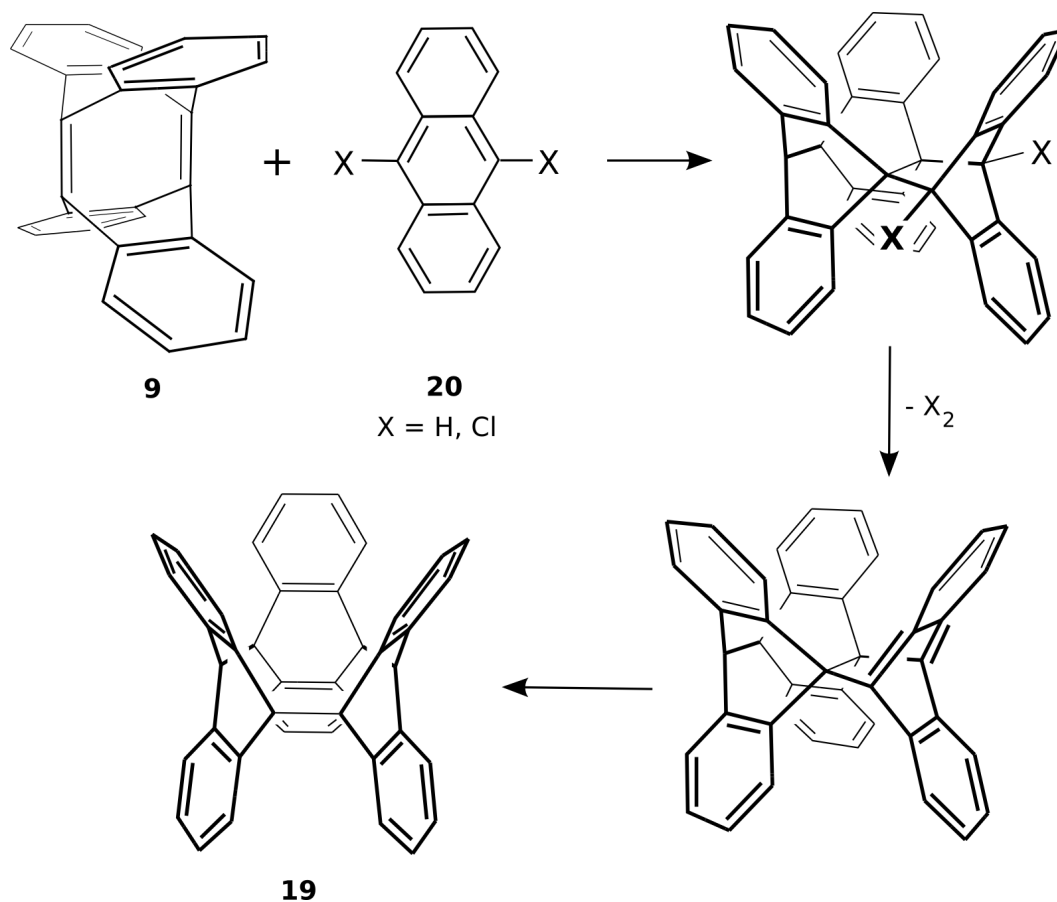


Figure 3.2: Hypothetical rational synthesis of 4\AA nanotube by dehydrocyclization of the trimer **19**.^[45]

Ajami *et al.* [45] tried to synthesize the trimer **19** by the Diels-Alder reaction of TDDA **9** with 9,10-dihaloanthracene and anthracene **20** followed by oxidation (scheme 3.1).



Scheme 3.1: Attempted trimer synthesis strategy based on Diels-Alder reaction.^[45]

But all of their attempts failed most probably because of the steric hindrance between the four hydrogens of the anthracene **10** and four hydrogens of TDDA **9** (figure 3.3).

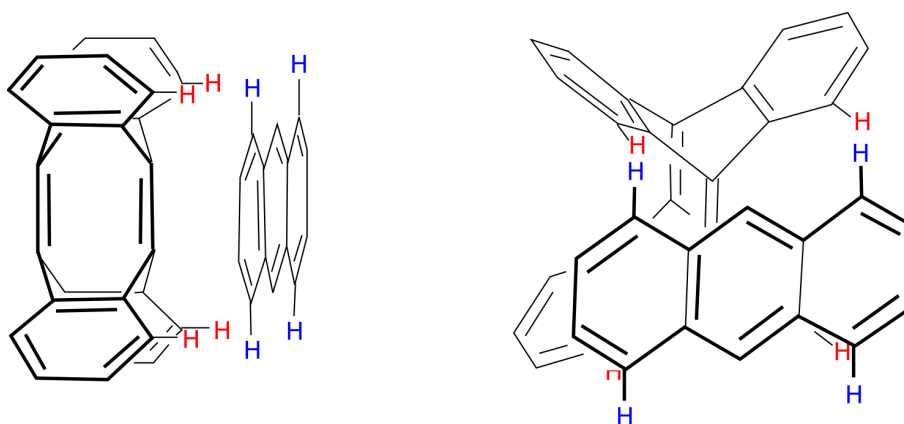
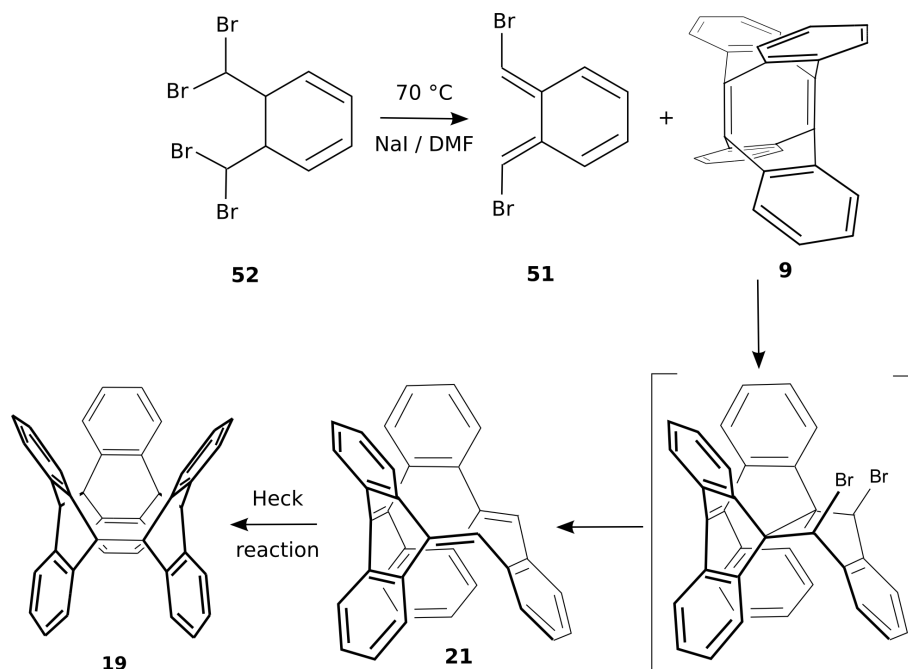


Figure 3.3: Sterical hindrance of four hydrogen atoms of TDDA **9** with four hydrogen atoms of anthracene during Diels-Alder reaction.^[45]

In order to overcome the effect of steric hindrance they tried to synthesize the trimer stepwise, initially adding half anthracene and in the second step converting the formed semitrimer **21** to trimer **19** through a double Heck reaction.

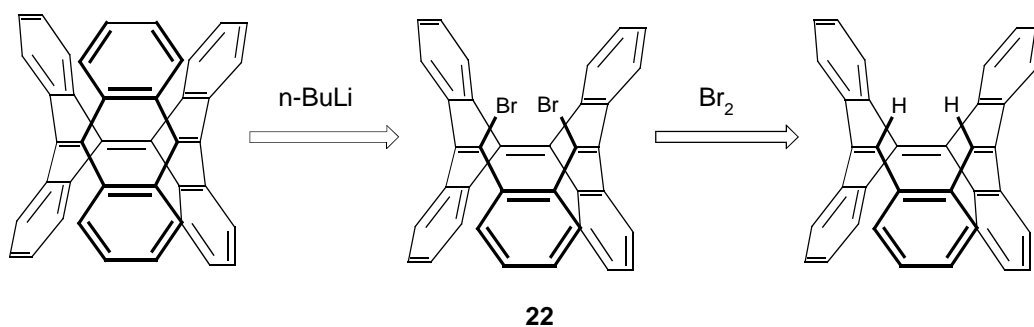


Scheme 3.2: Synthesis of semitrimer **21** and attempted Heck reaction

Unfortunately, the conversion of the semitrimer **21** to the trimer **19** with 1,2- diiodobenzene under Heck reaction conditions was not successful (scheme 3.2).

3.2 Bromination of the Semitrimer **21**

Another way to form the trimer **19** from the semitrimer **21** is to replace the olefinic hydrogen atoms by bromine and to bridge the two double bonds with a benzene ring. This could be achieved by treatment with butyl lithium followed by quenching with 1,2-diiodobenzene (scheme 3.3).



Scheme 3.3: Retrosynthetic strategy to prepare the trimer **19** from semitrimer **21** by bromination, dehydrobromination, lithiation, coupling with 1,2 diiodobenzene.

The semitrimer was treated with bromine in carbon tetrachloride at 0 °C. This reaction yielded many products. The separation of all compounds was difficult, but a product with the mass of the dibromo semitrimer **22** was separated by HPLC using a normal phase column by eluting with hexane and dichloromethane (4:1) as the mobile phase. The remaining compounds were separated with reversed phase HPLC using acetonitrile and water (90:10) as the mobile phase. The NMR of the compound with the mass of the dibromo semitrimer **22** is shown below (figure 3.5).

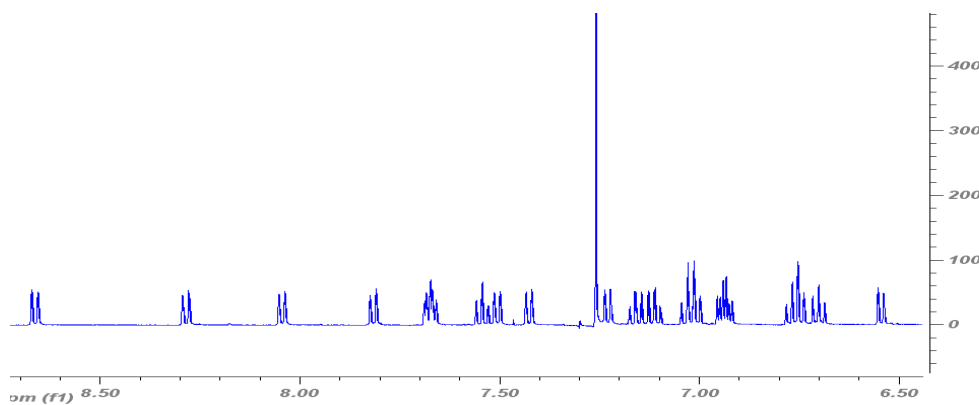


Figure 3.5: NMR of the compound with the mass of dibromo semitrimer.

In the ^1H -NMR spectra, the singlet corresponding to the olefinic protons of the semitrimer **21** disappeared, but a doubled signal set is observed instead. Hence this could be a mixture of *syn* **22** and *anti* **23** dibromo semitrimer. The *anti* dibromo semitrimer has C_2 symmetry and Möbius topology. To assign the NMR peaks for *syn* and *anti* isomers, calculations were performed at the B3LYP/6-31G* level theory. The calculated values of the NMR shifts are as follows for the C_3 isomer and the C_2 isomer (figure 3.6).

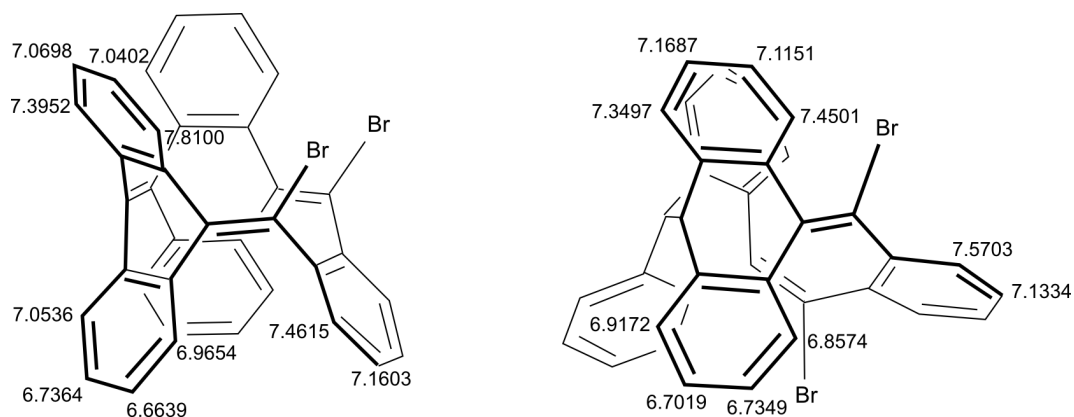


Figure 3.6: The calculated $^1\text{H-NMR}$ shift values of *syn* (left) and *anti* (right) isomers of the expected dibromo semitrimer.

The difference in the calculated and observed NMR values could be caused by the large spin orbit coupling of bromine which has a stronger effect on the neighbouring atoms, including those which are not directly connected to bromine (through-space). Unfortunately, the methods for treating these effects on an adequate level of theory are extremely expensive and not yet implemented in standard quantum chemical programs.

But the gas chromatography, reversed phase HPLC and normal phase HPLC analysis were giving evidence that it is one pure compound. To understand the structure, crystals were grown from a mixture of acetonitrile and carbon disulfide (figure 3.7).

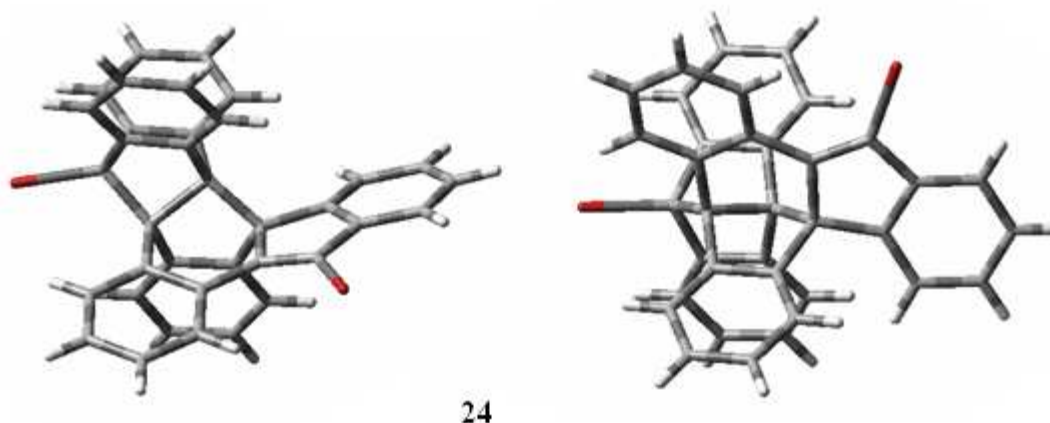
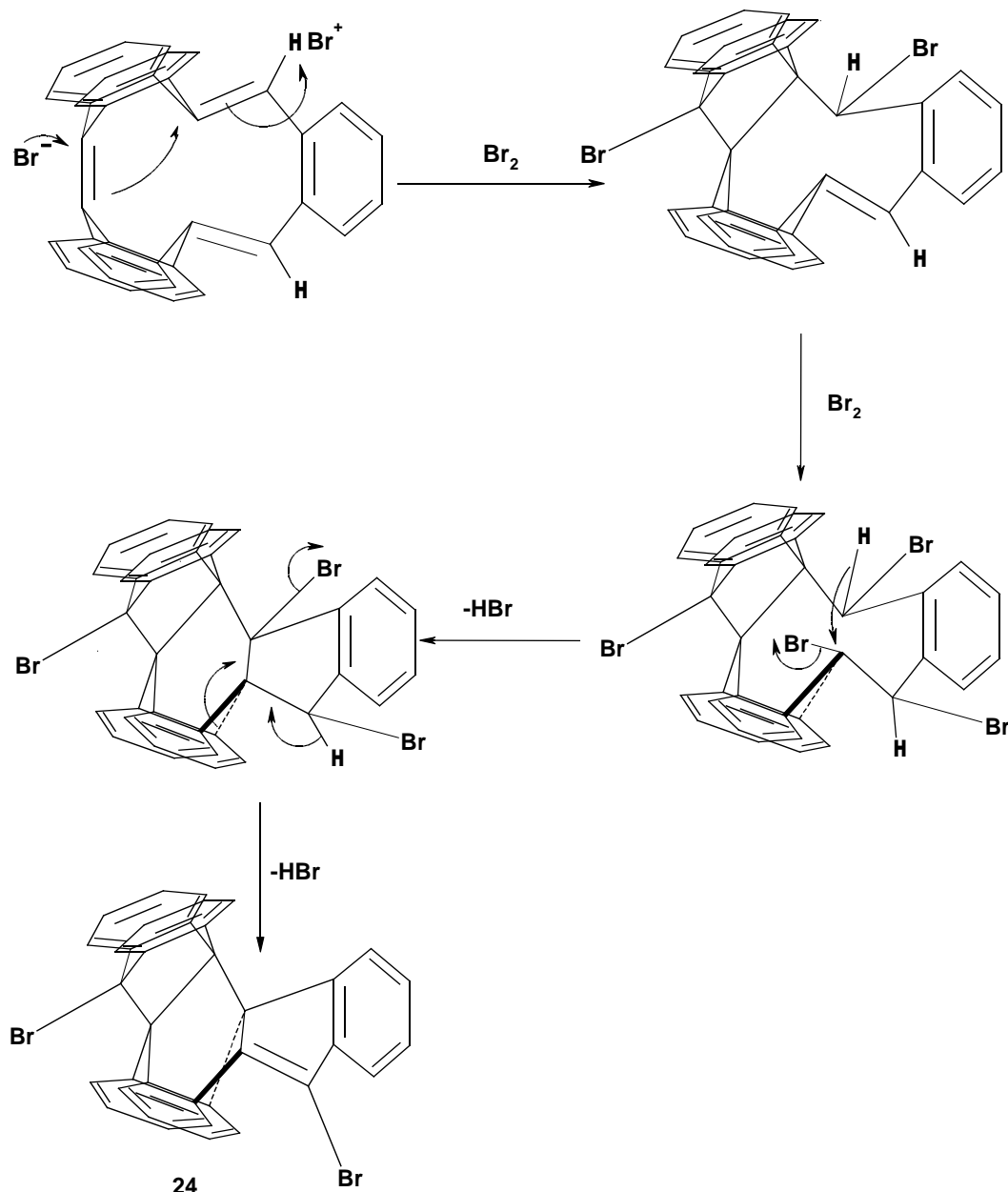


Figure 3.7: Two views of the X-ray structure of the dibromo semitrimer **24** formed upon the treatment of the semitrimer **21** with bromine.

The structure of the observed compound was completely different from the expected one. Instead of a *syn*-like addition on the bridged double bonds of semitrimer **21**, bromine attacked the sterically hindered strained double bond of the semitrimer **21** in an *anti*-like fashion. Mechanistic details for the formation of this compound **24** are unclear, but the following mechanism seems plausible (scheme 3.4):



Scheme 3.4: A possible mechanism of the addition of bromine to the semitrimer.

Obviously, bromine attacked the semitrimer **21** in an *anti* like addition. Close survey of literature^[33] shows the fact that *anti* addition is favourable in non-polar solvents while polar solvents favour the *syn* addition. Consequently, the bromination was carried out in the highly polar solvent trifluoroethanol. However, no addition product was observed.

3.3 Iodination of the Semitrimer 21

Since iodine has a larger atomic radius than bromine, this might prevent the attack to the sterically hindered strained double bond of the semitrimer **21** that was observed with bromine. Iodination of the semitrimer **21** was carried out in carbon tetrachloride under reflux conditions. The observed conversion was very low. The resulting products were separated with reversed phase HPLC using acetonitrile and water (90:10) as the mobile phase. The HPLC chromatogram is as follows (figure 3.8):

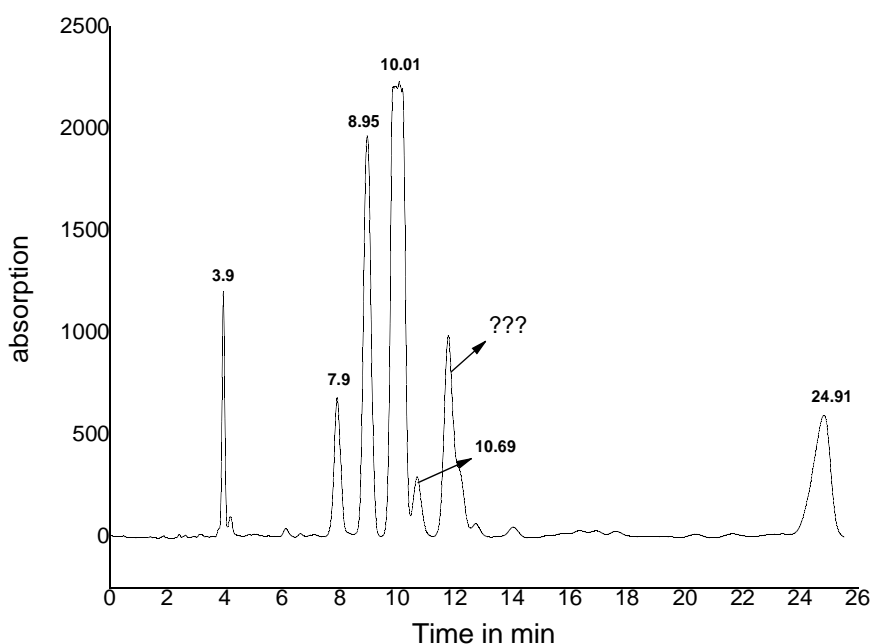


Figure 3.8: The HPLC chromatogram of the reaction of semitrimer with iodine

The substance at 7.9 minutes retention time has exactly the mass of the monoiodo semitrimer and the following $^1\text{H-NMR}$ (figure 3.9). The NMR spectra of the compound lead to the following structure propositions (figure 3.10).

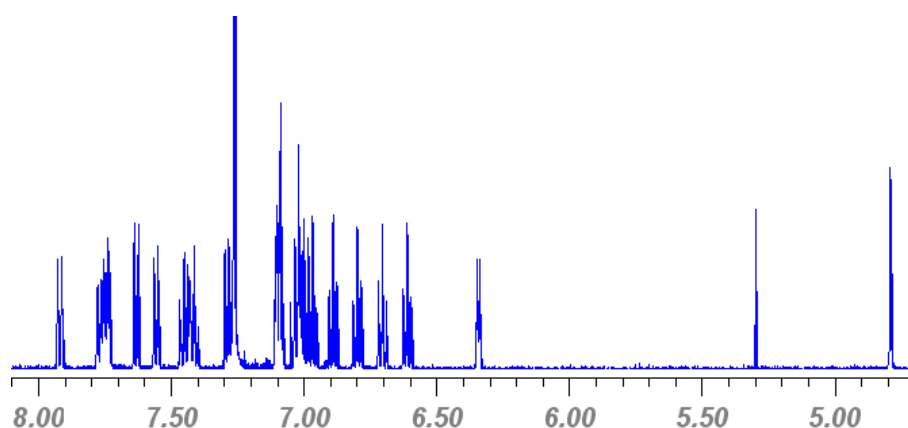


Figure 3.9: The NMR spectrum of the compound with the exact mass of the monoiodo semitrimer.

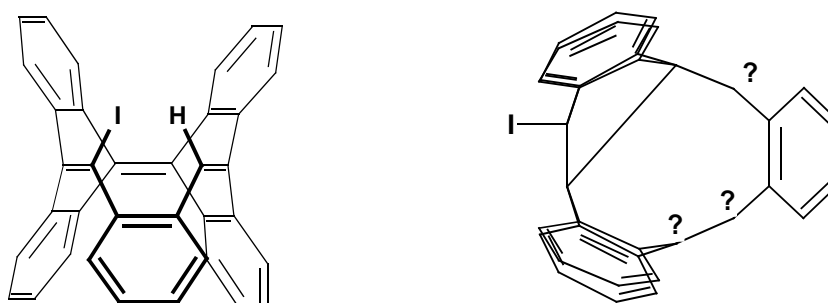


Figure 3.10: The proposed structures for the monoiodo semitrimer.

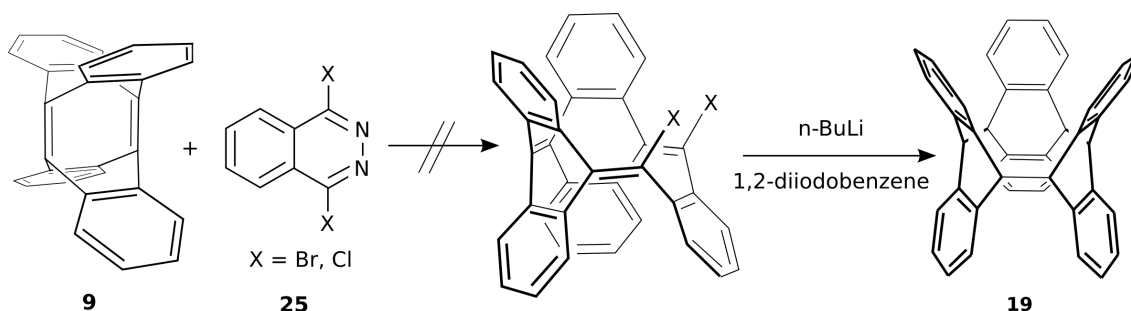
The exact structure determination is only possible by X-ray structure analysis. Attempts to get crystals are still in progress.

The peak at ten minutes retention time can be identified as unreacted semitrimer **21**. The product at 24 minutes retention time has one mass unit more than the monoiodo semitrimer. Attempts to get suitable crystals were not successful. The substances with 8.9 and 10.6 minutes retention time are oxidized forms of semitrimer.^[45] The peak at 3.9 minutes retention could be assigned to anthraquinone.

Since iodine is less reactive compared to bromine, it did not react with semitrimer to give the required diiodo semitrimer.

3.4 Diels-Alder Reaction of TDDA **9** with Phthalazines

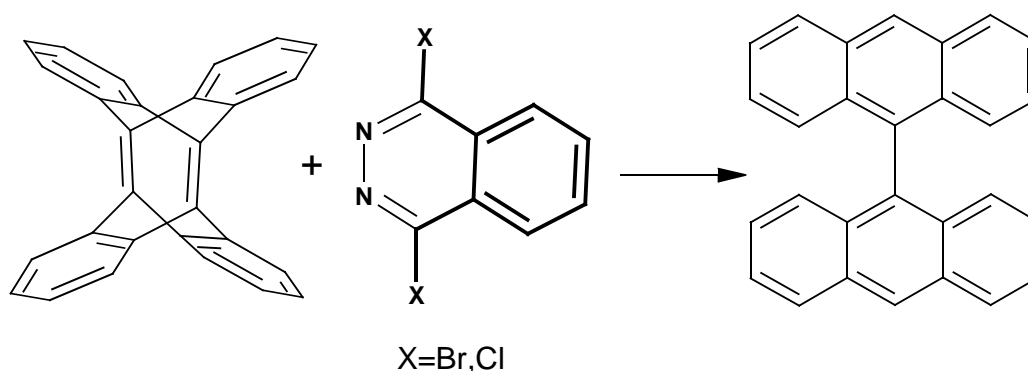
TDDA **9** reacts with the electron poor dienes.^[36] The dibromo semitrimer could be directly prepared by the Diels-Alder reaction of the TDDA with 1,4-dihalophthalazine^[46] **25** (scheme 3.5).



Scheme 3.5: Retrosynthetic route to prepare the trimer **19** by Diels-Alder reaction of TDDA **9** with dihalophthalazine **25**, then coupling the dihalosemitrimer with 1,2-diiodobenzene through lithiation or by Suzuki coupling.

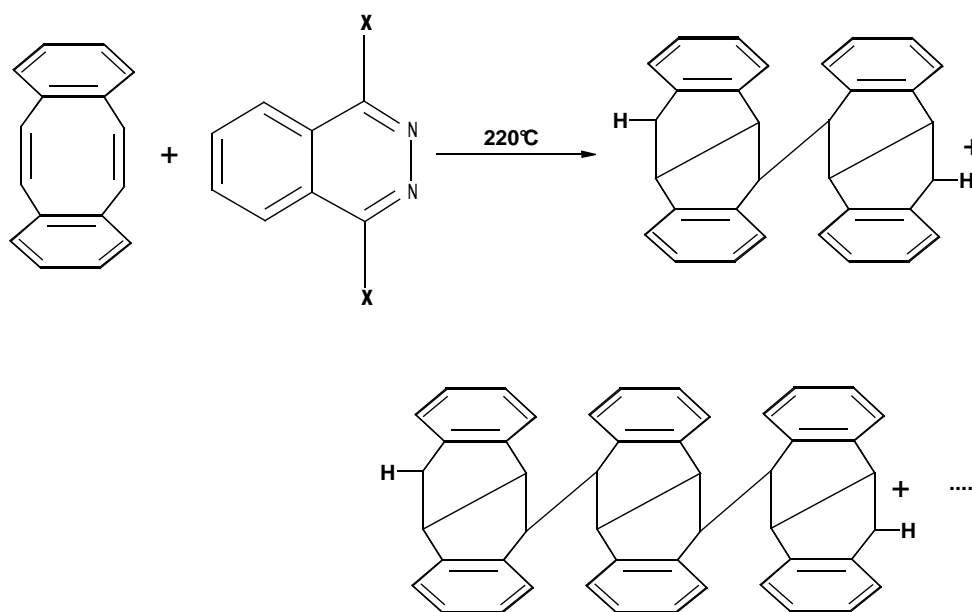
TDDA **9** was treated with 1,4-dibromophthalazine **25** in dichloromethane, tetrahydrofuran, benzene, toluene, xylene and in 1,2-dichlorobenzene at room temperature and under reflux conditions. Unfortunately, only bianthracene was observed which forms by the ring opening of TDDA and no other addition product was observed (scheme 3.6).

Since 1,4-dichlorophthalazine is more reactive than the bromine derivative, the reaction with TDDA **9** was also probed in all solvents similar to dibromo derivative but no addition product was observed.



Scheme 3.6: The Diels-Alder reaction of TDDA **9** with 1,4-dihalophthalazine **25** yields bianthryl in various solvents.

In another attempt a solid mixture of TDDA **9** and 1,4-dihalophthalazine **25** was exposed directly to 220°C for 30 min. Under these conditions many products were formed. Attempts to separate them were not successful because of the insolubility of the products and the difficulties in the chromatographic separation. According to the mass spectra one product can be interpreted as bianthryl and some others are in favour of a radical addition product of TDDA to TDDA (scheme 3.7).



Scheme 3.7: Solid state reaction of TDDA with 1,4-dihalo phthalazines.

To avoid the radical formation, the reaction was carried out in the presence of the radical quencher *tert*-butyl catechol at 220 °C. As anticipated, some addition product was observed between TDDA **9** and dihalophthalazine **25**. The ESI spectra of the reaction mixture before workup show a product which exhibits a similar isotopic pattern to the required dihalo semitrimer but has 10 units less in mass. The MALDI shows that a product which has 33 units less in mass. The observed product in the ESI spectrum can be interpreted as the product mass observed in the MALDI spectrum with additional sodium (figure 3.11, 3.12).

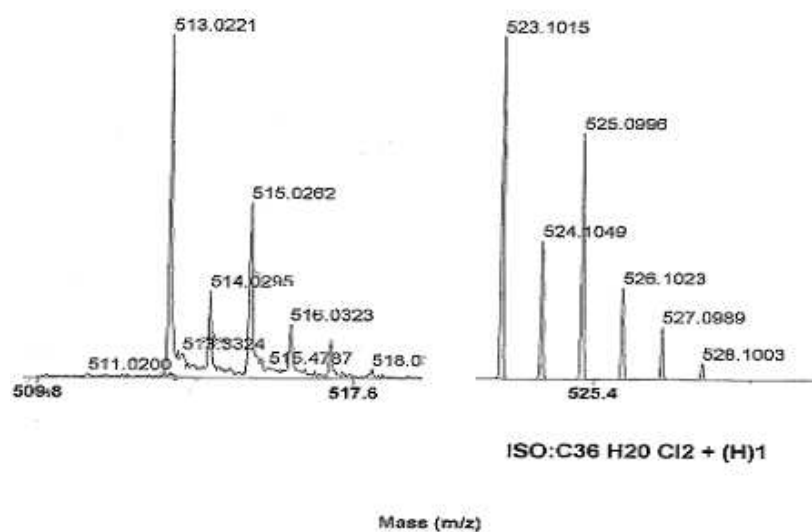


Figure 3.11: Observed (left) and theoretical (right) ESI spectrum of the solid state Diels-Alder reaction of TDDA with 1,4-dichloro phthalazine.

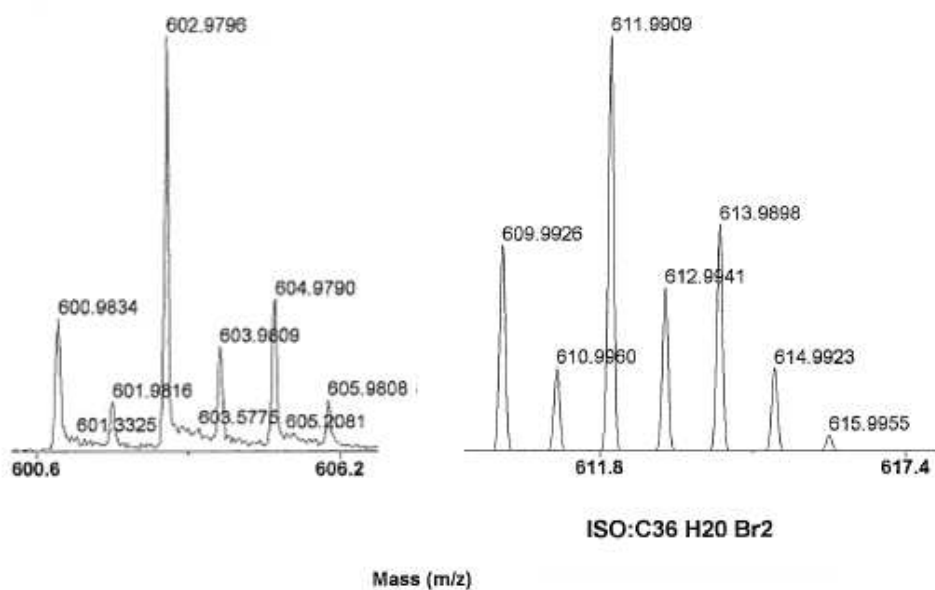
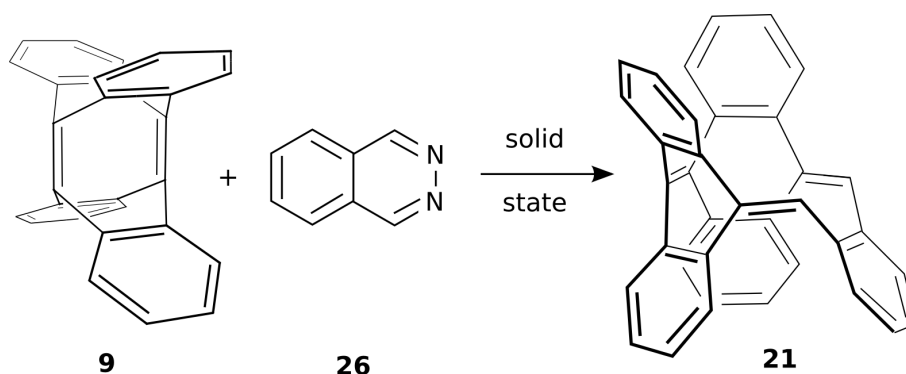


Figure 3.12: Observed (left) and theoretical (right) ESI spectrum of the solid state Diels-Alder reaction of TDDA with 1,4-dibromo phthalazine.

The products with $m/z=513$ and 602 were not observed any more after passing the mixture through a short column of alumina or silica. Probably the product rearranged or decomposed on the column. The reason for the failure of the two step synthesis of the trimer via a Diels-Alder reaction of 1,4-dihalophthalazine **25** with TDDA **9** could be the sterical hindrance of the two halogens and the two hydrogens of 1,4-dihalo phthalazine **25** and the four hydrogens of TDDA **9** (figure 3.13).

Since the semitrimer **21** is an interesting precursor for the trimer formation and for metal complexations, it was important to scale up and simplify the formation of the semitrimer **21**.

TDDA was mixed with phthalazine **26** in toluene at room temperature and reflux conditions. Unfortunately, no evidence of the reaction was obtained. However, solid state exposure of TDDA and phthalazine in the presence of the radical quencher *tert*-butyl catechol yielded the semitrimer **21** in lower yields (17%) than in the reaction of TDDA **9** with tetrabromo-*o*-xylene^[45] (scheme 3.8).



Scheme 3.8: Successful Diels-Alder reaction of TDDA **9** with phthalazine **26**.

The lower yields again can be accounted for on the basis of the steric hindrance of two hydrogens of phthalazine and the four hydrogens of TDDA (figure 3.13).

Since the reaction of TDDA **9** with dihalophthalazines **25** and phthalazine **26** is a Diels-Alder reaction with inverse electron demand, the expected reactivity order would be dichloro phthalazine > dibromo phthalazine > phthalazine. However, the observed order was dichloro phthalazine = dibromo phthalazine < phthalazine. The reason for this behaviour again can be explained on the basis of steric hindrance (figure 3.13).

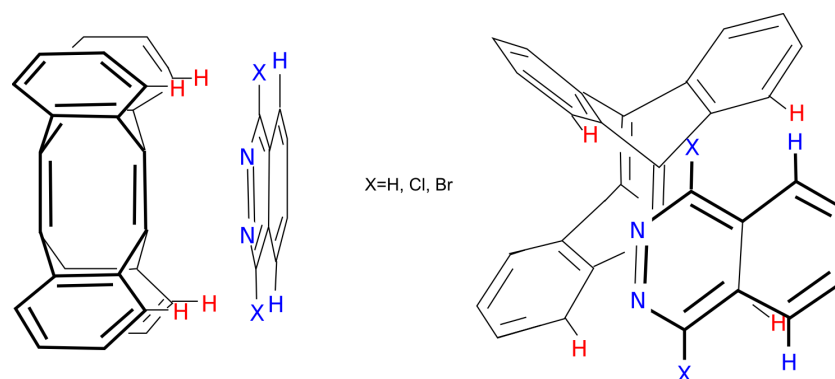


Figure 3.13: Sterical hindrance of four hydrogens of TDDA with two hydrogens of phthalazine during Diels-Alder reaction.

3.5 Treatment with Schlosser's Base

Schlosser's base^[47] is a combination of *n*-butyl lithium and potassium *tert*-butoxide (super base). In solution, *n*-butyl lithium exists as four or six-membered aggregates, which are kinetically slow to react. The tertiary alcoholate serves forms a complex with the lithium ion, which breaks the *n*-butyl lithium clusters. This makes butyl lithium kinetically more reactive (figure 3.14).

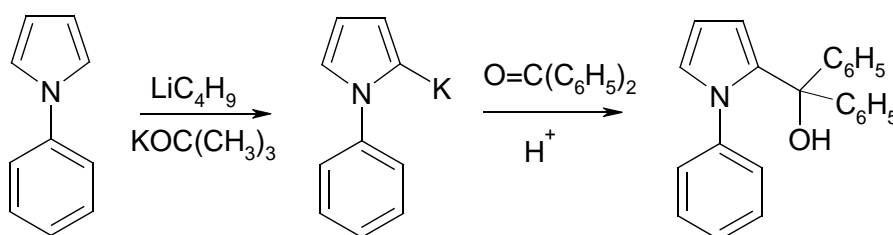
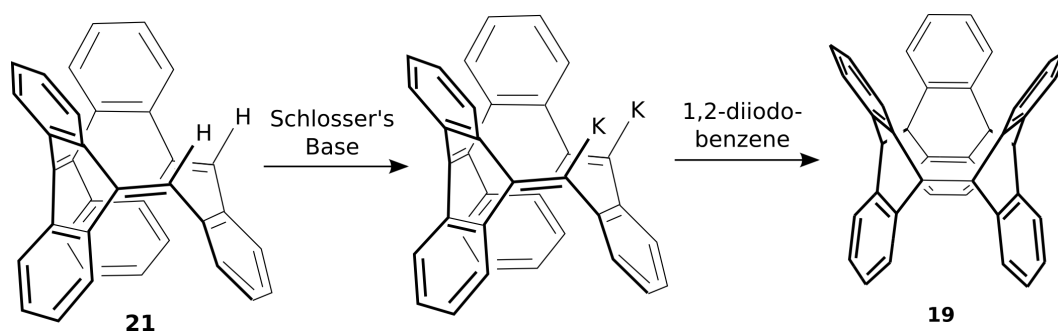


Figure 3.14: An example for the abstraction of a proton by the Schlosser's base^[49].

The trimer **19** also could be formed from semitrimer **21** by replacing the olefinic hydrogens with potassium by treatment with Schlosser's base and coupling the salt with the *ortho*-diiodobenzene (scheme 3.9).



Scheme 3.9: Proposed synthetic route for the conversion of the semitrimer **21** to the trimer **19** by deprotonation with Schlosser's base followed by coupling with 1,2-diiodobenzene.

At first, the semitrimer **21** was treated with *n*-butyl lithium at 0 °C in THF. The colour of the solution immediately changed to green. Upon slow warming up to room temperature the colour changed to yellow. After quenching with D₂O the only isolated substance was the semitrimer **21**. The same results were obtained when the reaction was carried out at room temperature.

In one more attempt a mixture of potassium *tert*-butoxide and semitrimer **21** was treated with *n*-butyl lithium in hexane at -76 °C and then slowly warmed up to 0 °C. The colour of the solution changed from light pink to dark pink during the temperature rise but after quenching with methyl iodide, only the reactant could be recovered. A number of different conditions were applied. In all cases the colour changed but after quenching the analysis shows only the semitrimer **21**.

The semitrimer **21** has a cavity of 4.2 Å in diameter, probably it might incorporate water and dichloromethane, which might hinder the reaction. So in order to remove the water and dichloromethane sublimation of the semitrimer **21** was carried out using a high vacuum pump. The semitrimer sublimated at 250 °C and 5.3×10^{-5} mbar. The sublimation yielded the semitrimer **21** free of dichloromethane and water. However, 40% of the semitrimer **21** was decomposed. Upon treatment of the sublimated semitrimer with Schlosser's base, again the colour changed but after quenching no new product could be observed.

To understand the reasons for the colour change, a sample of the semitrimer **21** in THF-d₈ (figure 3.15) was treated with *n*-butyl lithium at room temperature in an NMR tube under nitrogen. The colour changed immediately to dark green and a number of new signals were observed in the NMR spectra (figure 3.16). Upon exposure of the NMR tube to air the colour disappeared and the compound reverted back to the semitrimer **21**. Probably, *n*-butyl lithium is reducing the semitrimer **21** to its di-anion **27** (scheme 3.10).

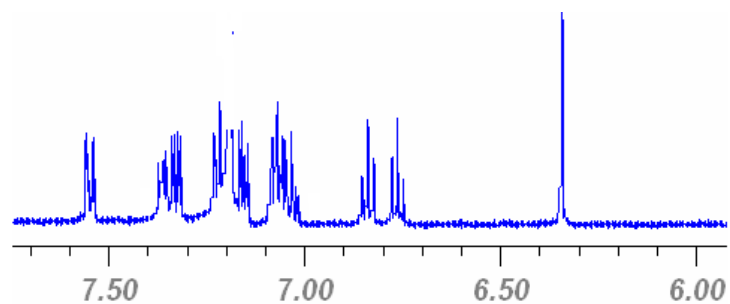


Figure 3.15: The NMR spectrum of semitrimer **21** in THF-d₈.

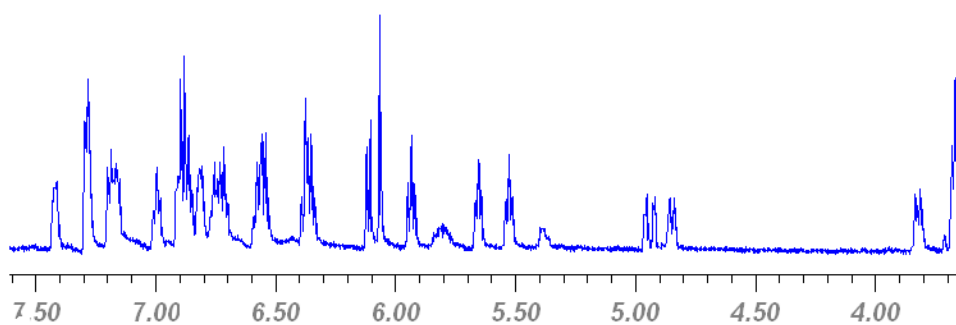
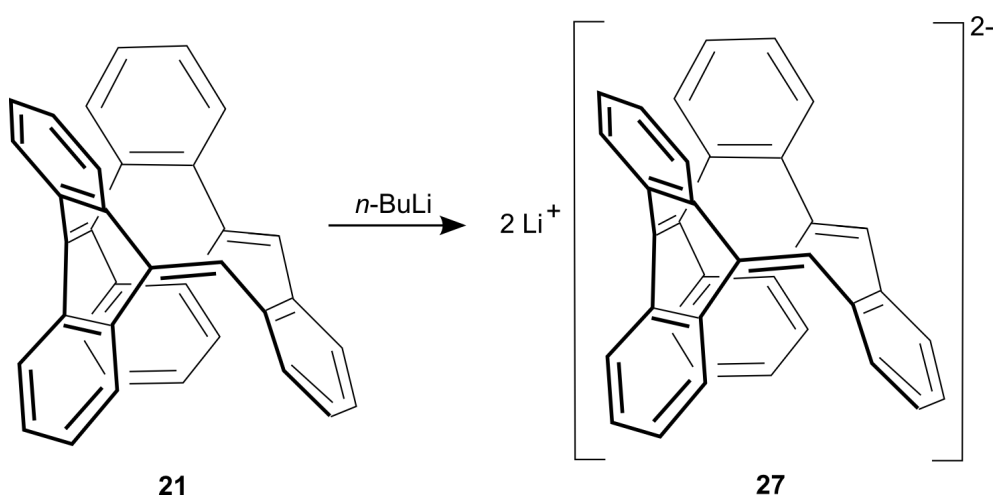


Figure 3.16: Treatment of the semitrimer **21** in THF-d₈ in an NMR tube with *n*-butyl lithium.

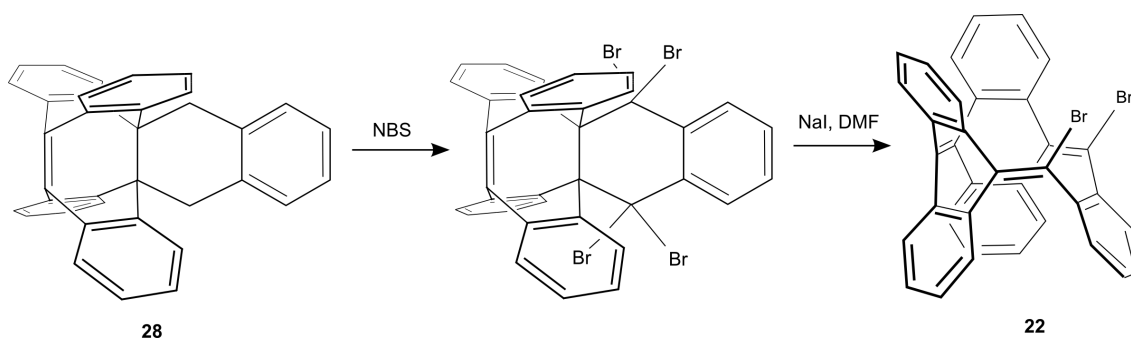


Scheme 3.10: Expected reduction of the semitrimer **21** to its dianion **27**.

The dianion derivative of the semitrimer **27** is an interesting precursor for the metal complexations with transition metals. Systematic reduction of the semitrimer **21** to its dianion **27** with lithium wire in an NMR tube under vacuum in THF is under progress. Since it is very difficult to abstract a proton from a pure hydrocarbon, the reaction with Schlosser's base probably failed.

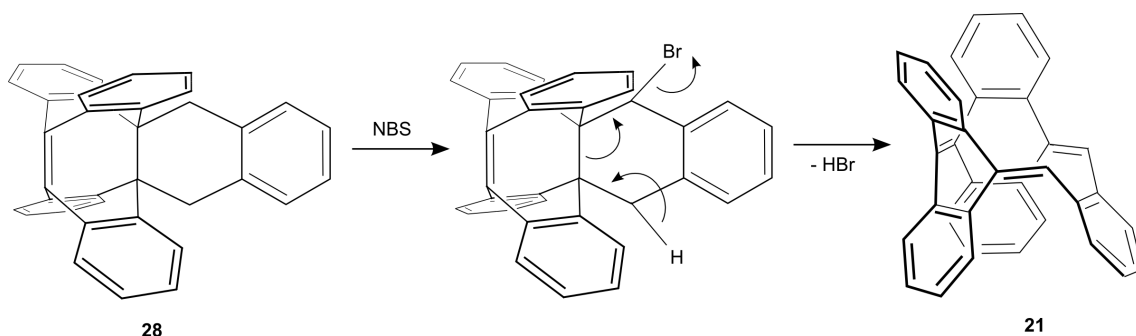
3.6 *N*-Bromo Succinimide Treatment of the *o*-Chinodimethane adduct

The dibromo semitrimer **22** can also be prepared by the reaction of *o*-chinodimethane adduct^[48] **28** with *N*-bromo succinimide (NBS) followed by treatment with sodium iodide in dimethyl formamide (scheme 3.11).



Scheme 3.11: Synthetic route to the dibromo semitrimer **22** by reacting the *o*-chinodimethane adduct **28** with NBS, followed by treatment with sodium iodide.

The NBS treatment of the *o*-chinodimethane adduct **28** yielded a large amount of compounds. These compounds were separated using reversed phase HPLC. Two compounds can be characterized. One of them could be identified as the semitrimer **21**. A possible mechanism for its formation is shown in scheme 3.12.

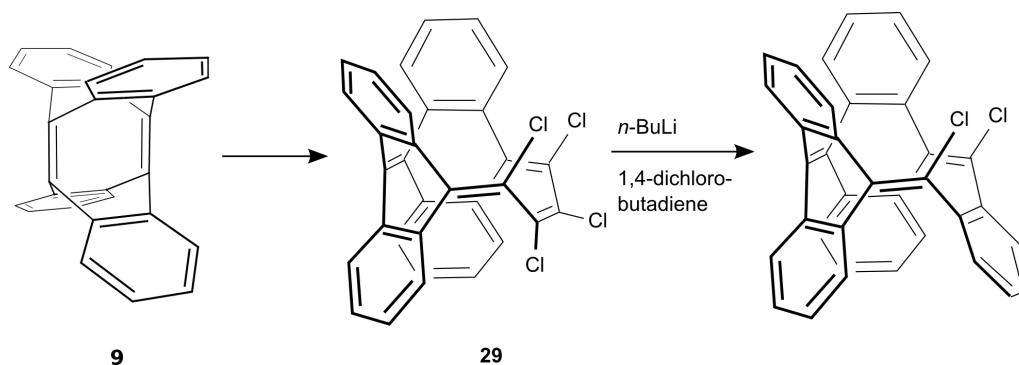


Scheme 3.12: Mechanism for the formation of the semitrimer **21** from the NBS treatment of the *o*-chinodimethane product **28**.

The second product could be identified as the same product obtained by the treatment of the semitrimer **21** with bromine (figure 3.8). Mechanistic details for the formation of this compound are unclear. To understand the mechanism, the semitrimer **21** was treated with NBS. A number of products were observed, one of them can be recognized as the same product obtained by the reaction of bromine with the semitrimer **21** (figure 3.8). Probably, the first step could be the reaction of the *o*-chinodimethane adduct **28** with NBS to form the semitrimer **21** (scheme 3.12).

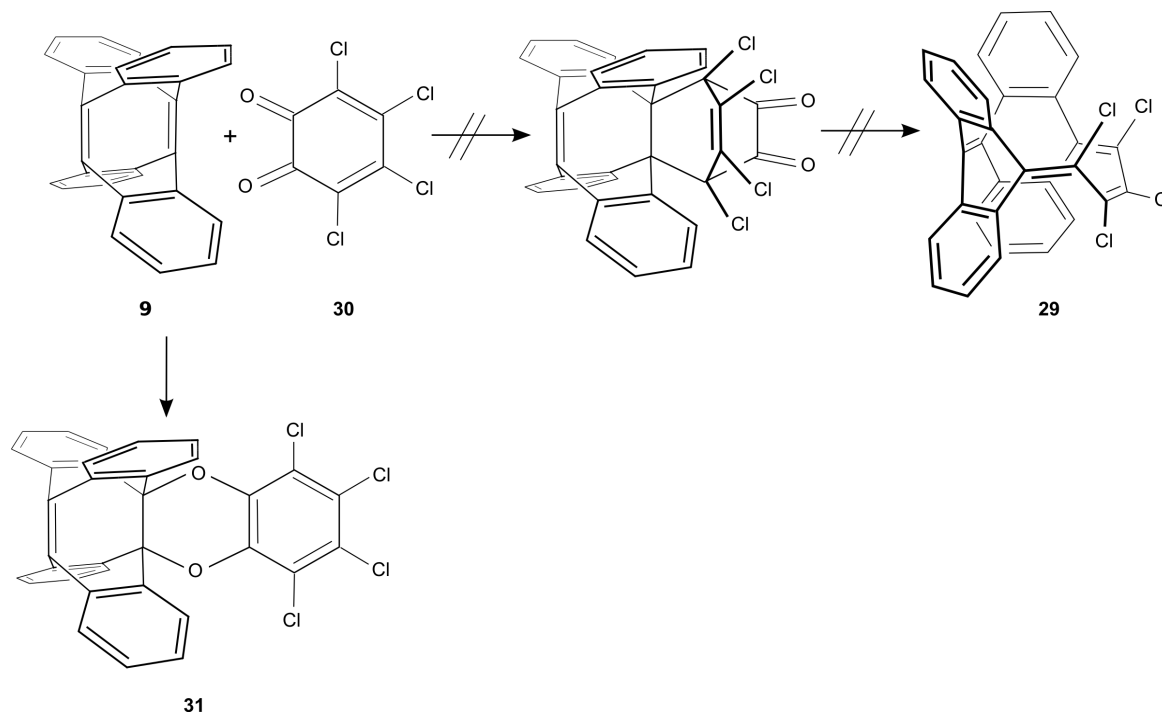
3.7 Diels-Alder Reaction of TDDA **9** with *o*-Chloranil and Tetrachlorothiophene dioxide **32**.

The dichloro semitrimer could be also be prepared from TDDA **9** by first converting the TDDA **9** to its tetrachloro C₄ adduct **29** and coupling the middle two chlorines with 1,4-dichlorobutadiene (scheme 3.13).



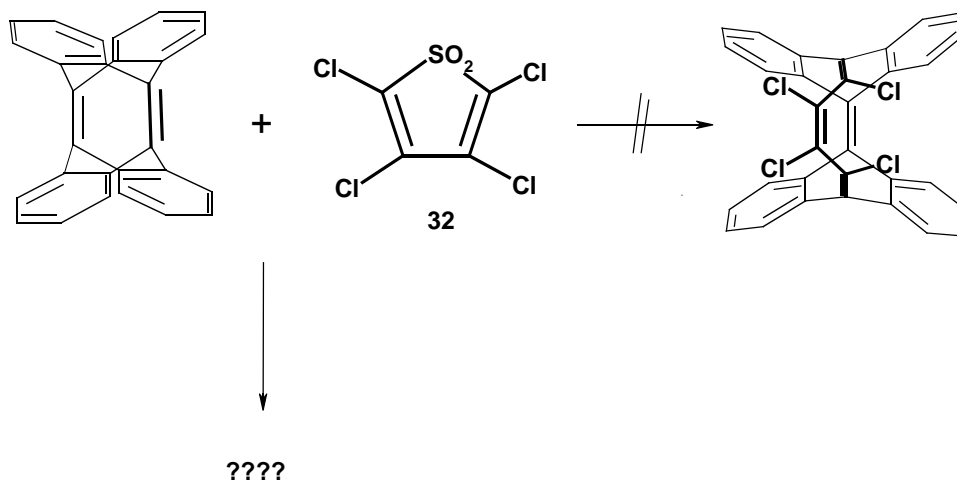
Scheme 3.13: Synthetic route to the dichloro semitrimer from TDDA **9** via the tetrachloro C₄ adduct **29**.

To prepare the tetrachloro C₄-adduct, TDDA **9** was reacted with *o*-chloranil **30** in toluene at room temperature. However, *o*-chloranil **30** underwent the Diels-Alder reaction using its carbonyl oxygens instead of the carbon diene system (scheme 3.14). A possible explanation is steric hindrance and the advantage of aromaticity the formed product.



Scheme 3.14: Diels-Alder reaction of TDDA **9** with *o*-chloranil **30**

In another attempt TDDA **9** was treated with tetrachlorothiophene dioxide **32**^[50,51,52,53] in solid state at 220 °C for 30 min in presence of the radical quencher *tert*-butyl catechol, but there was no evidence for the formation of the required product. The characterization of the formed product is in progress (scheme 3.15).



Scheme 3.15: Diels-Alder reaction of TDDA **9** with tetrachlorothiophene dioxide **32**

3.8 Conclusion

9,9',9'',10,10',10''-Hexadehydrotrianthracene (trimer **19**) is an interesting building block for the synthesis of larger tubular aromatic compounds (e.g. pentamer, hexamer, etc.), using the photochemically induced ring enlargement metathesis. Additionally the rational synthesis of (3,3) armchair nanotubes should be possible by dehydrocyclization of the trimer **19**. The synthesis of trimer **19** based on Diels-Alder reaction of TDDA with anthracene **10** was unsuccessful. In a step by step synthesis the semitrimer **21** was prepared^[45] which is lacking one benzene ring compared to the trimer itself.

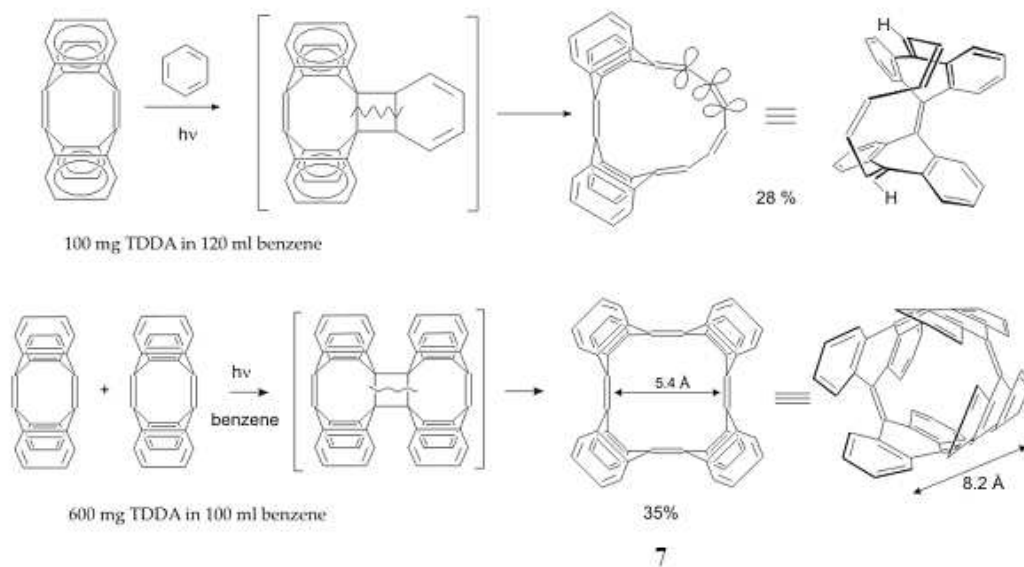
However, the conversion of the semitrimer **21** to the trimer **19** by reaction with Schlosser's base was unsuccessful. Formation of dihalo semitrimer through the bromination of the semitrimer, NBS treatment of the *o*-chinodimethane, Diels-Alder reaction of TDDA **9** with 1,4-dihalophthalazine **25**, *o*-chloranil and with tetrachlorothiophene dioxide **32** was not successful.

4 Photochemical Reactions of the Tetramer 7

4.1 Synthesis of the Tetramer 7

The photochemically induced metathesis reaction of TDDA **9** was extensively investigated. Photochemical dimerization of TDDA **9** to the tetramer **7** was achieved after numerous variations of the reaction conditions.^[48] In most solvents such as toluene or hexane mainly hydrogen transfer takes place to form bianthryl or anthracene **10**. The metathesis product of TDDA **9** with the solvent is the main product in the homogeneous solution in benzene. The tetramer **7** has been prepared in 35% yield by irradiation of a TDDA **9** suspension in benzene with a 700 W high pressure mercury lamp in a quartz apparatus for 40h^[54] (scheme 4.1). The longer irradiation time and the lack of reproducibility are disadvantages of this method. Shortly, after the beginning of the irradiation, a layer of product is formed on the quartz surface which hinders further irradiation of the reaction mixture. Separation of the unreacted TDDA **9** is difficult because both tetramer **7** and TDDA **9** have low solubility and similar retention times on HPLC. Therefore, it is highly desirable to drive the reaction to completion. Under these conditions the reaction conditions are extensively investigated. The following factors can be accounted for the faster completion of the reaction:

1. Good quality of TDDA
2. Concentration of TDDA in benzene
3. Mixing of solution
4. Temperature of the reaction
5. Good design of the apparatus



Scheme 4.1: Metathesis reactions of TDDA.^[45]

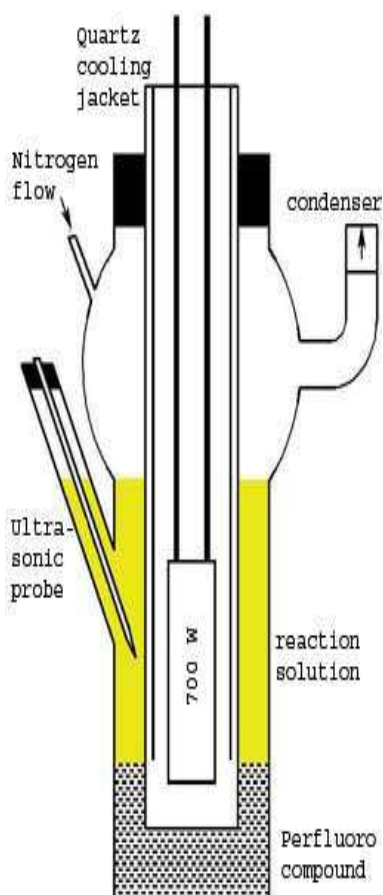


Figure 4.1: Schematic representation of the photo reactor with ultrasonic probe.

For a better mixing of the solution and to destroy the clusters of tetramer **7** and TDDA **9** a cell disruptor (ultra sound generator) was applied and the temperature of the reaction was held above 60°C (reflux of benzene) by controlling the water flow. Surprisingly, the reaction is completed in 3 hours with a fairly reproducible yield of 35% (figure 4.1). Solid phase irradiation of TDDA **9** under inert gas atmosphere did not yield the tetramer **7**.

To understand these reasons, the structure of TDDA **9** was thoroughly examined. In the crystal, the double bonds of TDDA are oriented in a favourable arrangement for a [2+2] cycloaddition with parallel π planes at a distance of 4.3 Å. The four olefinic carbons and the π planes of the double bonds form an angle of 64° (figure 4.2).

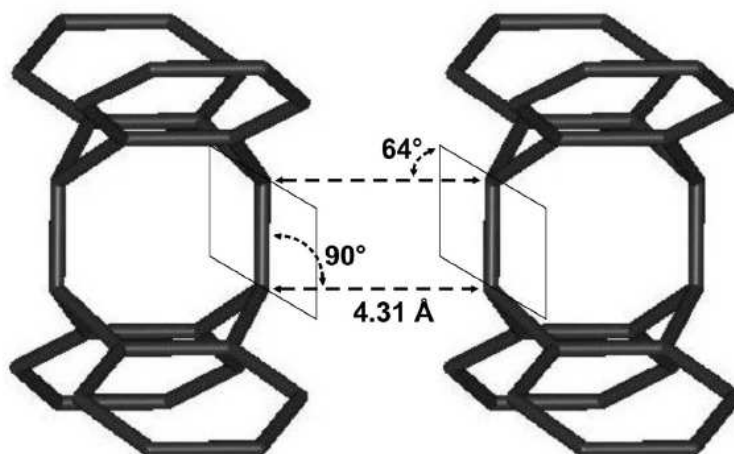


Figure 4.2: Arrangement of TDDA molecules in the crystal structure.^[45]

Solid state irradiation failed because the crystals are “passivated” with layers of tetramer **7** at the crystal surface which has a strong UV absorption in the range of the π - π^* transition of TDDA **9** (282 nm). In the suspension the reaction proceeds to completion because the surface is always renewed (cell disruptor and refluxing of benzene facilitates the renewal of the surface by breaking the crystals or washing off the product).

The structure of the tetramer **7** has interesting aspects. Although four anthracenyliene units are linked with each other one can call this molecule tubular. Because of rigidity and small distance between peri hydrogen atoms an approximately van der Waals closed surface is formed.

Ajami *et al.*^[45] obtained single crystals of tetramer **7** from a mixture of carbon disulfide and acetonitrile. Solvent molecules were included in the crystals. Six molecules of carbon disulfide and six molecules of acetonitrile were found in the unit cell. There are two arrays of tetramer molecules in the crystal unit cell, in which their C_4 axes form an angle of 45° and one benzene ring of the tetramer **7** is located above the cavity of an adjacent tetramer (figure 4.3).

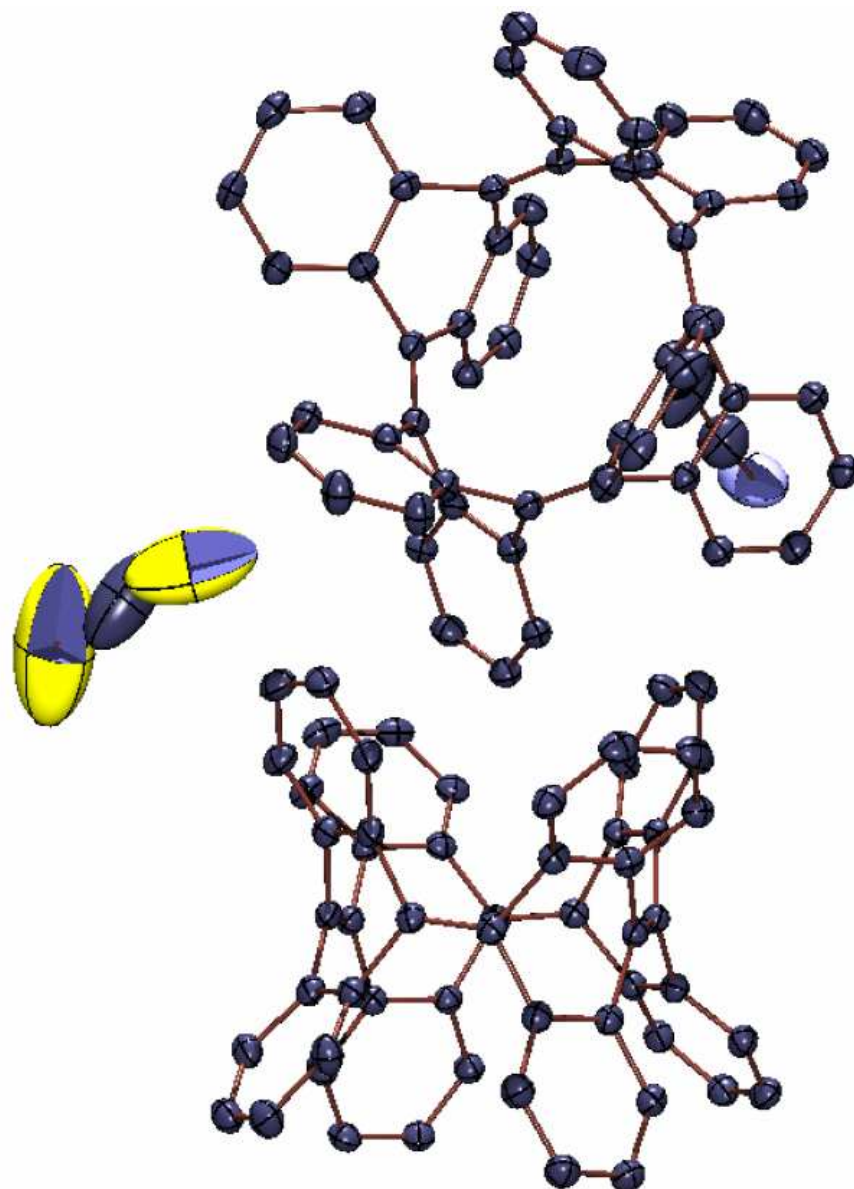


Figure 4.3: Arrangement of tetramer molecules in the crystal.^[45]

The most important aspect is the symmetry of the tetramer. The $^1\text{H-NMR}$ spectrum shows two signals, the $^{13}\text{C-NMR}$ spectrum shows four signals and the X-ray structure is in good agreement with D_{4h} symmetry, but theoretical calculations at the density functional level of theory B3LYP/6-31G* predict that tetramer has D_{2d} symmetry. The D_{2d} structure is 4.4 kcal/mol lower in energy than the D_{4h} symmetric structure. This seeming contradiction can be resolved if one assumes a fast equilibrium of two D_{2d} structures, in which the D_{4h} structure is the transition state of the conformational interconversion. Comparison of the matrix infrared spectrum of the tetramer **7** with theoretically calculated spectra (B3LYP/6-31G*) proved a D_{2d} minimum structure.^[55] Thus, X-ray and NMR correspond to a time averaged D_{4h} structure (figure 4.4).

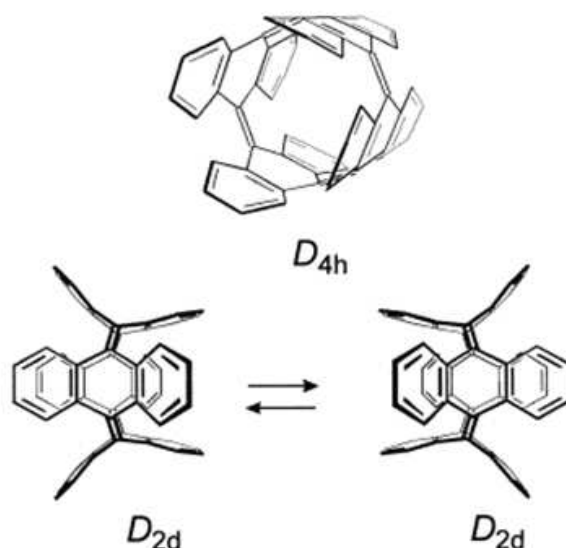
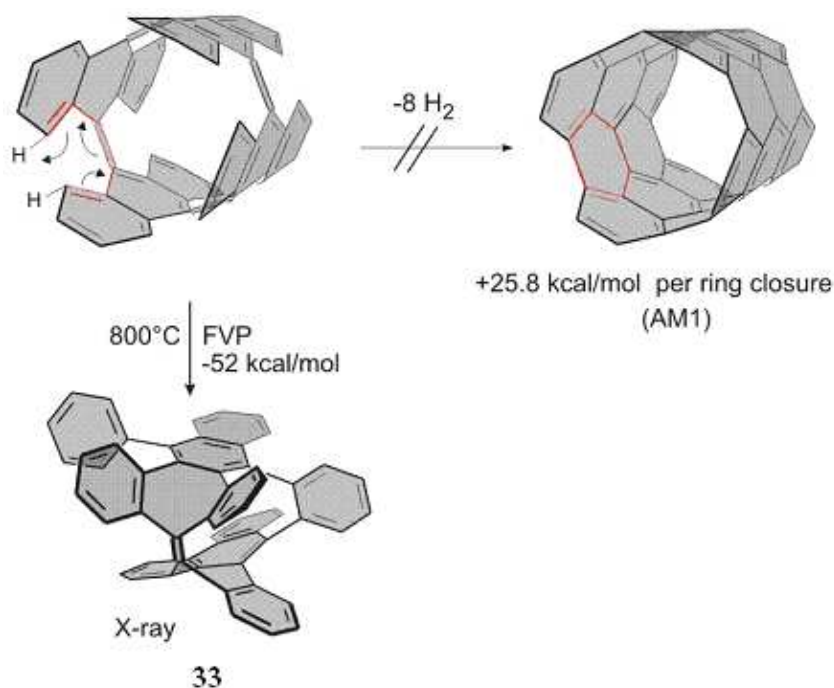


Figure 4.4: Two hypotheses for the structure of the pico tube: Static D_{4h} structure and a fast equilibrium of two D_{2d} structures.

4.2 Pyrolysis of the Tetramer 7

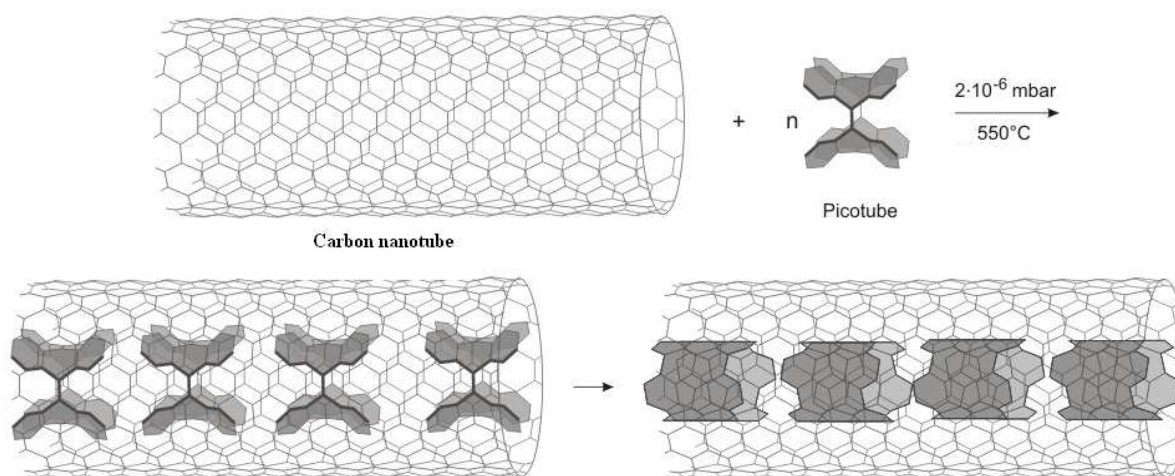
Deichmann *et al.*^[54,56] have attempted to synthesize [4,4] armchair nanotubes based on the dehydrocyclization of the tetramer **9**. Semi-empirical (AM1) calculations predicted the overall elimination of eight hydrogen molecules to be endothermic by 205.9 kcal/mol, on average of 25.7 kcal/mol for each dehydrocyclization step. However, since there is a stepwise increase in the strain energy the first step is endothermic by only 8.5 kcal/mol and the enthalpy of formation of the most stable isomers of the following steps is predicted to be only 3.2, 3.4, and 1.4 kcal/mol. After the fourth step yielding a D_{2h} symmetric compound the strain energy increases dramatically to 60.2 kcal/mol. The subsequent steps are endothermic with 48.2, 43.0 and 38.2 kcal mol⁻¹.

The flash vacuum pyrolysis (FVP) experiments were performed at 800 °C (quartz tube, 20 mm diameter, 30 cm heated length, 15 ml/min Argon, 2.5 mbar). A large number of isomers were formed under these conditions, of which an unsymmetrical compound is the main product **33** (scheme 4.2). Instead of hydrogen elimination one of the C-C single bonds neighbouring the quinoid double bonds is broken in the first step and a cascade of radicaloid rearrangements driven by the release of ring strain leads to the a priori unexpected product **33**.



Scheme 4.2: Flash vacuum pyrolysis of tetramer **9**.^[45]

In collaboration with Prof. Hans Kuzmany, Vienna University, Austria, the dehydrogenated tetramer (closed pico tube = CPT) was achieved.^[57] This was done by placing a mixture of tetramer **7** and carbon nanotubes into a quartz ampoule which was then sealed and evacuated to $p \leq 10^{-7}$ mbar. The ampoule was then heated in a furnace to a temperature of $T = 550^\circ\text{C}$ for 1 hour. Under these conditions the tetramer **7** sublimed into the cavity of the nanotubes and yielded the CPT. From the theoretical predictions and Raman spectra, the formation of CPT is suggested (scheme 4.3).



Scheme 4.3: Successful dehydrogenation of tetramer **7**.

4.3 Solid State Irradiation of the Tetramer 7

Solid tetramer was irradiated with a 700 W high pressure mercury lamp. However, no addition product was observed. The low reactivity of tetramer **7** compared to the TDDA **9** is due to the arrangement of molecules in the crystal structure, in which adjacent molecules form an angle with respect to each other. This arrangement is not suitable for the dimerization reaction in the solid phase or in suspension state. In order to achieve the photodimerization of the tetramer **7** the adjacent molecules should be parallel to each other (figure 4.5). Many attempts were done to crystallize the tetramer **7** in various solvents, but none of them was successful.

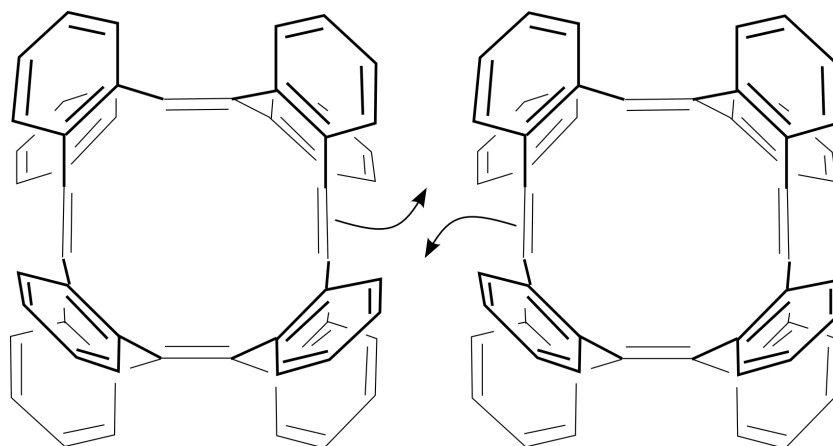


Figure 4.5: Arrangement of tetramer molecules required for cycloaddition.

Finally the use of a laser as the energy source for the dimerization reaction of the tetramer **7** in the solid state was considered. Matrix-assisted laser desorption/ionization mass spectrometers (MALDI-MS) use a nitrogen laser source with 337 nm wavelength, which is the easiest way to investigate the behaviour of the tetramer **7** under laser irradiation. In the MALDI-MS instrument the angle of the laser beam with respect to the sample surface can be tuned by 30° and 75° and the beam is focused with either a single or a multi element optical system and passed through a window into the mass spectrometer. The position of the laser focus with respect to the sample surface can be changed by shifting the optical axis of the sample beneath a fixed axis.^[45]

A saturated solution of tetramer **7** in dichloromethane was used to generate a thick layer of tetramer **7** on the surface of a MALDI plate. The plate was loaded into a Bruker FlexIII™ MALDI-TOF MS instrument to determine the best combination of the intensity of the laser

beam in each shot as well as to vary the number of shots and the position of laser focus during shooting. Indeed, the mass peak of the octamer was detected in the MALDI-MS if the intensity of the laser beam is 20-30% and if one to three shots per run were applied (figure 3.6). The detected isotope distribution is in very good agreement with the theoretical distribution (figure 3.7).

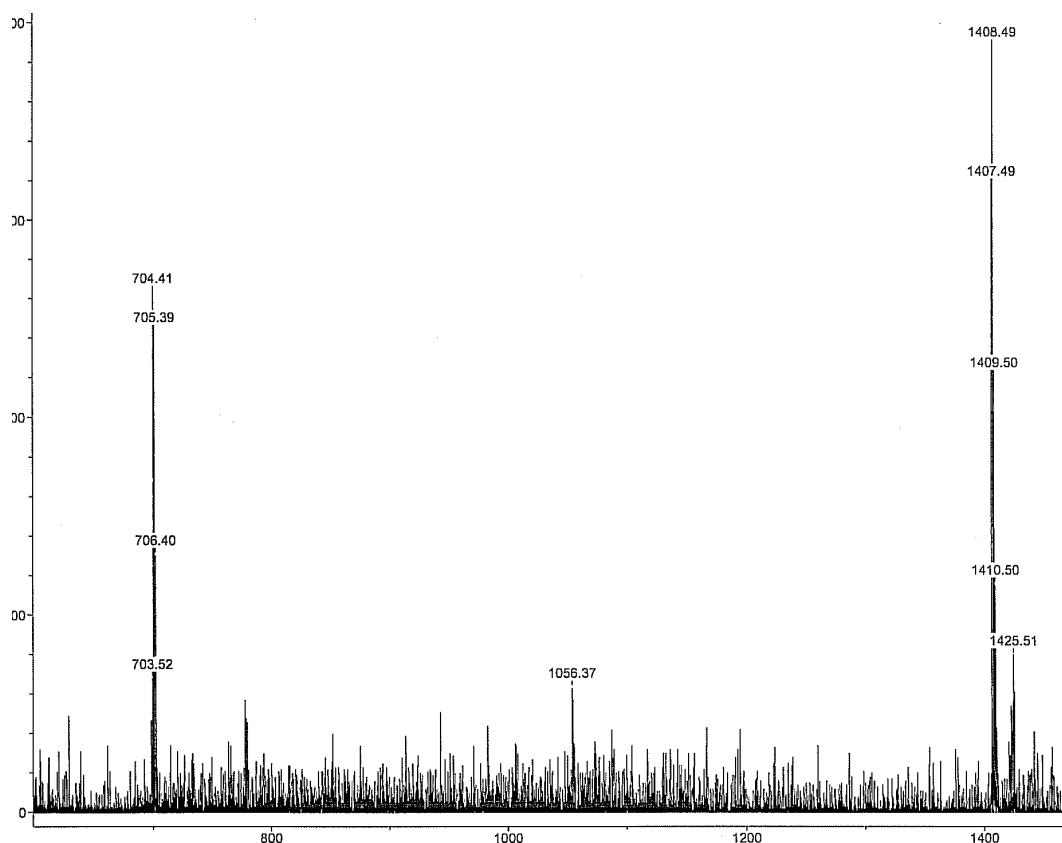


Figure 3.6: MALDI-TOF mass spectra of tetramer **7**, 20-30% laser and one to three shots applied.

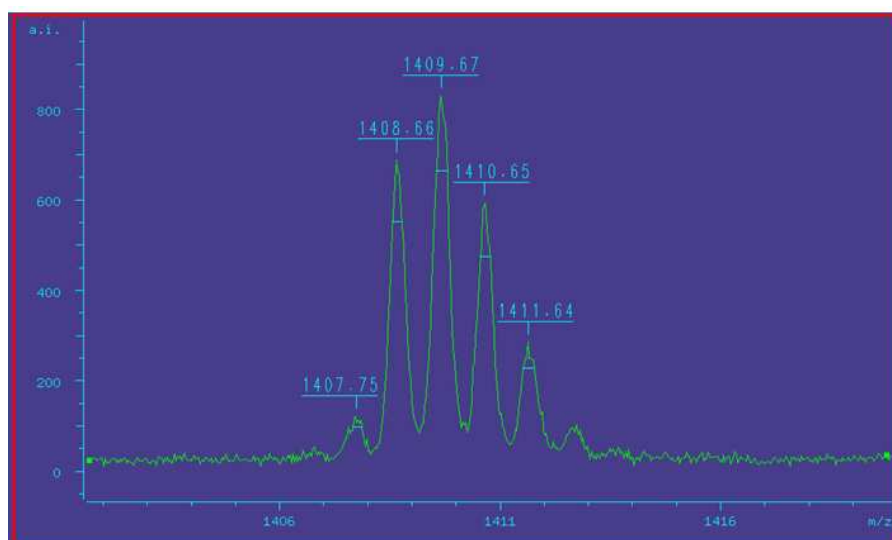


Figure 3.7: Isotopic pattern of the octamer.^[45]

4.4 Heating of the Tetramer **7**

As discussed above, octamer formation was observed in the MALDI spectrometer. To specifically observe the thermal conversion of the tetramer **7** to the octamer in a mass spectrometer, high concentration EI-MS spectra were recorded. At high temperatures indeed the octamer was observed in small amounts. To form the octamer in a larger scale a sample of the tetramer **7** was evacuated in quartz ampoules and flame sealed. The quartz ampoule was exposed directly to 550 °C and 700 °C for 30 min each. The sample was extracted with carbon disulfide and dichloromethane solvents, but most of the content of the ampoule is black lustrous powder which is insoluble in any solvent. The extract contains only anthracene **10**. The analysis of the black lustrous powder by MS spectroscopy failed because the compounds were not volatile. NMR spectroscopy failed because compounds have an extremely low solubility in common organic solvents. Transmission electron microscopy (TEM) or scanning electron microscopy (SEM) of the products probably could provide useful structural information.

4.5 Conclusion

The photochemical reaction of the tetramer **7** was investigated in suspension and in solid state. The anticipated product of this reaction is the octamer with D_{4d} symmetry, which is a very important intermediate for the rational synthesis of carbon nanotubes. According to calculations the dehydrocyclization is exothermic and should form a short piece of an [8,8] armchair nanotube. Sonification and refluxing of the solvent improved the tetramer synthesis, but further reaction to hexamer and octamer could not be achieved.

Preliminary experiments with a nitrogen laser as an energy source in the MALDI-TOF MS instrument were positive. Attempts to overcome technical problems are in progress. Alternatively, the octamer can also be formed by inserting the tetramer **7** into commercially available nanotubes (probably by sublimation or by capillary methods) and followed by heating. Attempts in this direction are in progress.

5 Möbius Aromatic Compounds

5.1 Introduction

The topological shape which is nowadays known as the Möbius strip or Möbius band was originally described independently by the German mathematicians August Ferdinand Möbius and Johann Benedict Listing in 1858. It only contains one side and one boundary component.

To create a model, a paper strip is twisted by 180° before joining the ends together (see figure 5.1). The Möbius strip has developed a life of its own independent of mathematics, in the realms of magic, science, engineering, literature, music, film, art, and elsewhere. There have been technical applications, e.g. giant Möbius strips have been used as durable conveyor belts as the entire surface area of the belt gets the same amount of wear, and as continuous-loop recording tapes (to double the playing time). Möbius strips are common in the manufacture of fabric computer printer and typewriter ribbons, as they allow the ribbon to be twice as wide as the print head whilst using both half-edges evenly. In Physics and electrical engineering, Möbius strips are utilized as inductionless resistor, superconductors with high transition temperature, as knot molecules, molecular engines etc.

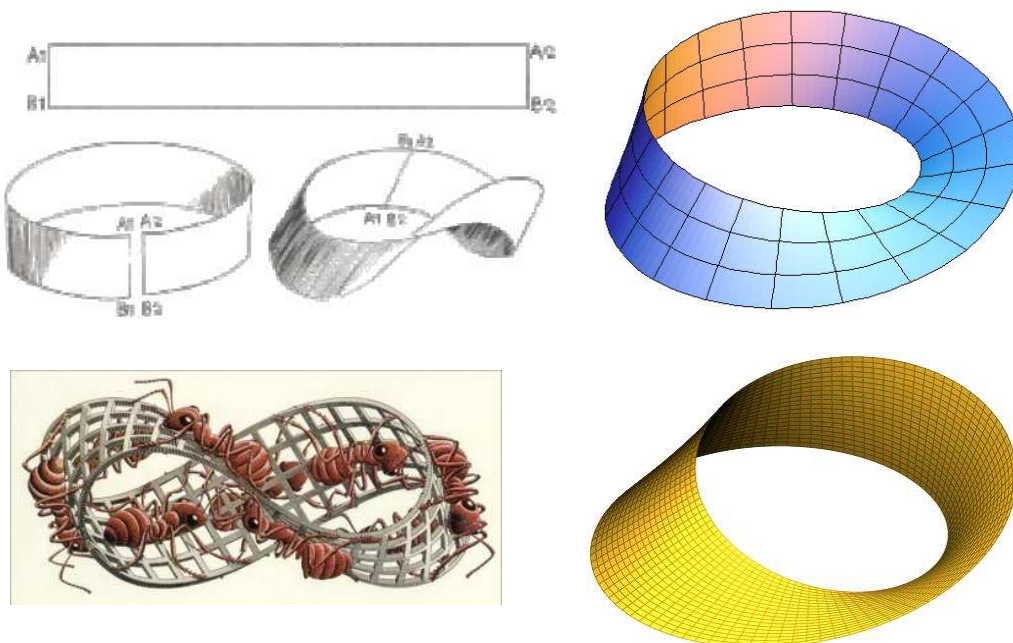


Figure 5.1: Building a Möbius solid with 180° twisting and joining two ends of the band, Escher artistic picture of a Möbius band with ants.^[45]

5.2 Möbius Band of NbSe₃ Crystals

S. Tanda *et al.* were successful to synthesize Möbius structures, rings and figures of eight by crystals of NbSe₃.^[58] The mechanism of ring formation by the ribbon-shaped NbSe₃ crystals depends on their being bent by the surface tension of the viscous selenium droplet on which they have grown. The ribbon grows along the equator of the droplet to minimize bending energy, finally meeting its own tail to form a perfectly seamless ring. Apparently, Möbius crystals are produced when twisting is accompanied by bending or when the selenium droplet is rotating. Such Möbius crystals are about 50 micrometers in diameter and less than 1 micrometer in width (figure 5.2).

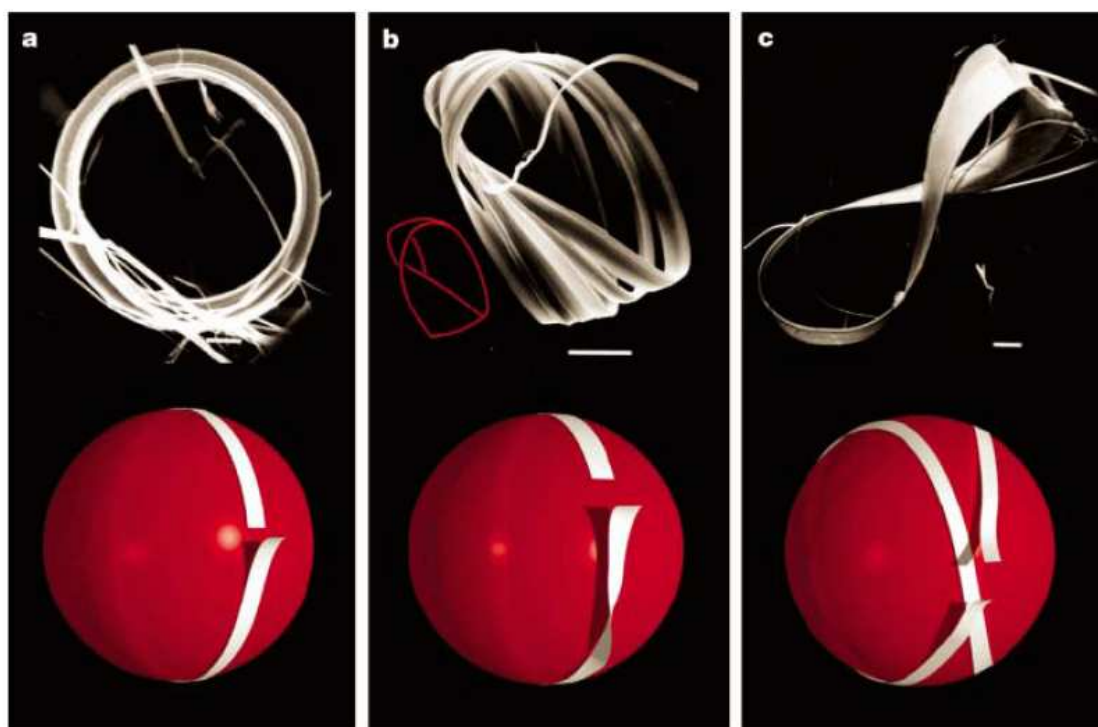


Figure 5.2: SEM image of NbSe₃ crystal topology: **a-** Ring structure **b-**Möbius strip **c-**Figure of eight strip.^[45]

5.3 Non Conjugated Molecular Möbius Strips

In 1982, Walba *et al.* synthesized the first band-type Möbius molecule.^[61,62] They started with a rope-ladder type molecule with ethylene rungs and two polyether ropes. Under high dilution conditions, three different bands are formed: a cylinder **37** and two **35**, **36** enantiomeric Möbius strips (figure 5.3). Cutting down the middle of an untwisted belt gives two separate rings. The same operation performed on a Möbius band gives one large ring with four half twists. Walba *et al.* used the ozonolysis reaction to cut the rungs of their molecular ladder and confirmed the above paper strip experiment on the molecular level. The Möbius ladder yielded a hexaketone with double ring size **39** (figure 5.4).

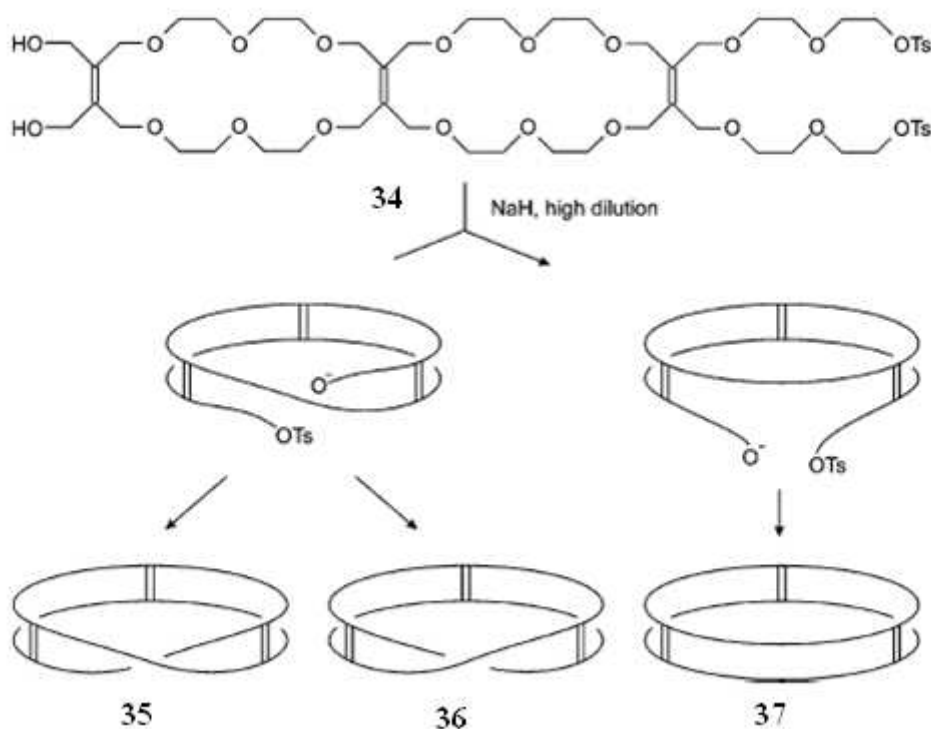


Figure 5.3: The cyclization of a rope ladder type precursor yields an untwisted (**4**) and two enantiomeric Möbius-twisted bands.^[45]

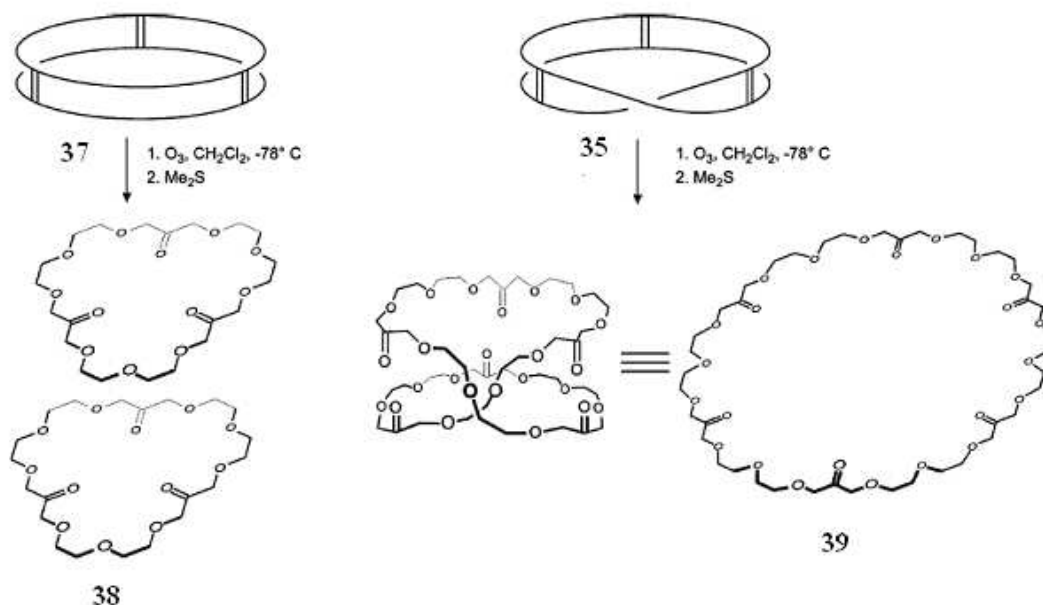


Figure 5.4: Breaking the rungs (ozonolysis) of the Möbius ladder gives one large ring (hexaketone).

5.4 Design and Synthesis of the First Möbius Annulene

Numerous attempts notwithstanding, since Heilbronner's theoretical prediction in 1964, it took almost 40 years to synthesize the first stable Möbius twisted system.^[59,60] The main problem in preparing a Möbius annulene is the fact that all parent annulenes with a ring size of 4-20 (and most probably also the larger ones) are more stable in a non-twisted topology. The stabilization of the π -system in $[4n]$ annulenes by Möbius aromaticity cannot overcome the strain induced by the 180° twist. There are Möbius isomers among the [8]-, [12]-, [16]- and [20]annulenes; however, they are higher in energy and kinetically unstable.

To obtain a stable Möbius annulene, the twist has to be stabilized by proper substitution or incorporation into a rigid molecular framework. To develop a strategy, it is instructive to examine the π system of Möbius annulenes in more detail. There are two types of cyclic π conjugation: (a) the "normal" (anti) aromatics with the p orbitals perpendicular to the ring plane and (b) "in-plane" (belt-like) conjugated systems in which the inner lobes of the p orbitals all point toward the axis of the belt or tube (figure 5.5). In "normal" aromatics, the sp²-hybridized ring atoms retain their preferred trigonal planar configuration, whereas "in-plane" conjugated systems exhibit pyramidalized sp² centers (with partial sp³ character). In smaller rings, pyramidalization causes a considerable amount of strain. Therefore, these

compounds are much less common than “normal” aromatics and usually have a large diameter (e.g, carbon nanotubes). Möbius annulenes exhibit both types of aromaticity “normal” and “in-plane” (figure 5.5).

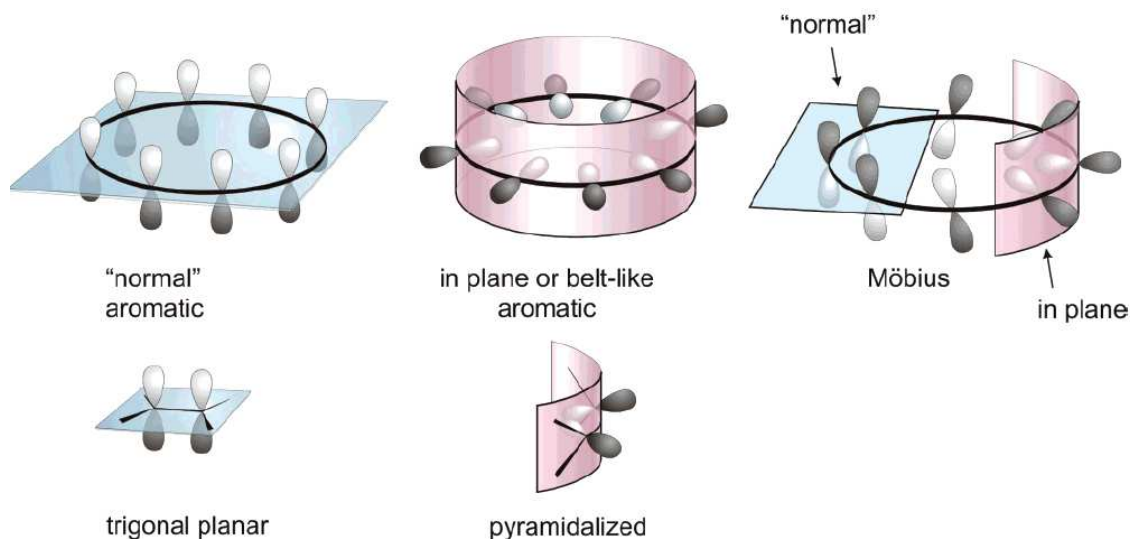
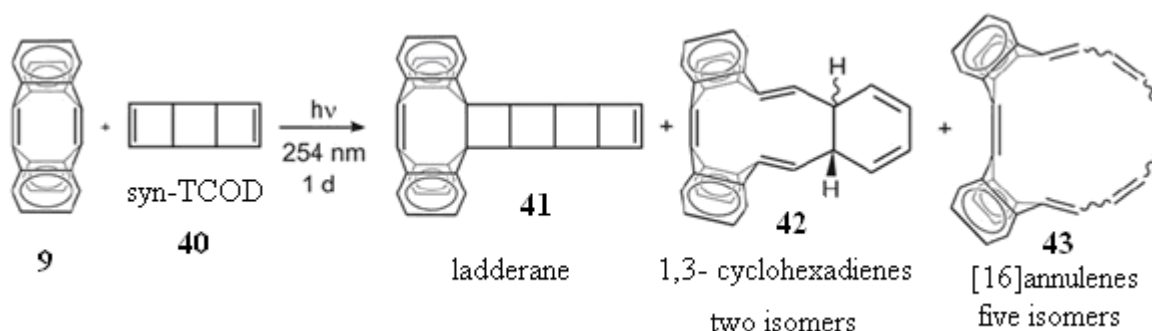


Figure 5.5: Strategy to synthesize Möbius aromatic compounds.



Scheme 5.1: Metathesis reaction between TDDA **7** and *syn*-tricyclooctadiene **40**.^[59]

However, all attempts to react cyclooctatetraene (normal aromatic) with TDDA **7** (in-plane aromatic) upon heating, catalysis (Grubbs' catalysts), and irradiation failed to give addition products. The main product isolated was bianthryl. Further investigations revealed that, upon irradiation, cyclooctatetraene transfers triplet energy to the very low lying triplet state of TDDA **7**, which in turn undergoes electrocyclic ring opening to the 9,10-didehydrodianthracene diradical. To avoid these problems, we used *syn*-tricyclooctadiene (TCOD) **40** as a masked cyclooctatetraene, which does not absorb UV light above 250 nm (scheme 5.1). Upon irradiation of TDDA **7** with TCOD **40** in benzene solution with a low-pressure mercury lamp, a ladderane **41**, two 1,3-cyclohexadienes **42**, and five ring-opened [16]annulene structures **43** (four Möbius and one Hückel) were isolated. A Möbius isomer is not stable at room temperature but undergoes a symmetry allowed electrocyclic ring closure

to form the C_s symmetric 1,3 cyclohexadiene structure. The structure of two Möbius isomers and one Hückel isomer were assigned by X-ray analysis. Experimental values are in good agreement with the computed values.

5.5 Möbius Aromaticity in Expanded Porphyrins

5.5.1 A Hückel-Möbius Aromaticity Switch

Latos-Grażyński and colleagues^[63,64] have synthesized a new kind of ring compound that exhibits Hückel or Möbius behaviour depending on the polarity of the surrounding solvent. Their molecule incorporates a ‘porphyrin’ structure. They have inserted two benzene rings into the porphyrin core, thus increasing the number of mobile electrons from 18 (a $4n+2$ system) to 28 (a $4n$ system). Their nuclear magnetic resonance (NMR) experiments show that the compound is antiaromatic in nonpolar solvents, as expected from the Hückel rule. However, in polar solvents, the antiaromaticity is lost. This change in electronic behaviour can be attributed to a molecular conformation change. The difference in conformation seen in polar and non-polar solvents is brought about by a small twist of one of the molecule’s benzene rings, which acts as a topology switch (figure 5.7). If this benzene ring is perpendicular to the one on the opposite side of the porphyrin 44b, the molecule adopts a twisted, one-sided Möbius topology. However, if the benzene rings are parallel to each other 44a, the structure is untwisted and two-sided. The authors did not observe aromaticity when the molecule was in the Möbius conformation, however, probably because the large amount of twist prevents efficient overlap of the orbitals. This is the first example of a molecule with reversible topology that switches from an antiaromatic to a non-aromatic (or weakly aromatic) state.

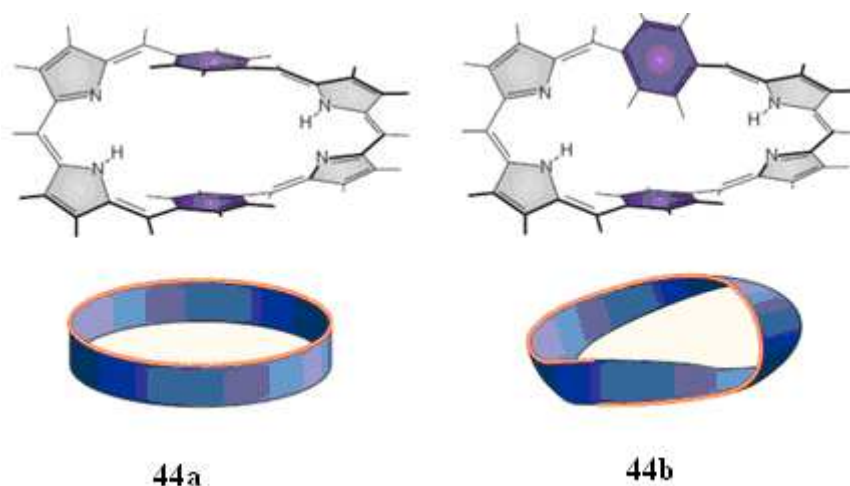


Figure 5.7: A molecular topological switch.^[64]

5.5.2 Möbius Aromaticity by Metallation

Osuka *et al.*^[65,66] reacted the different expanded porphyrins with group 10 metals to form the metal complexes which are Möbius aromatic. They converted [36]Octa-, [32]Hepta- and [26]Hexaphyrines (systems with $4n$ π electrons) with palladium acetate and received Möbius aromatic complexes which are characterized by X-ray crystallography (figure 5.8).

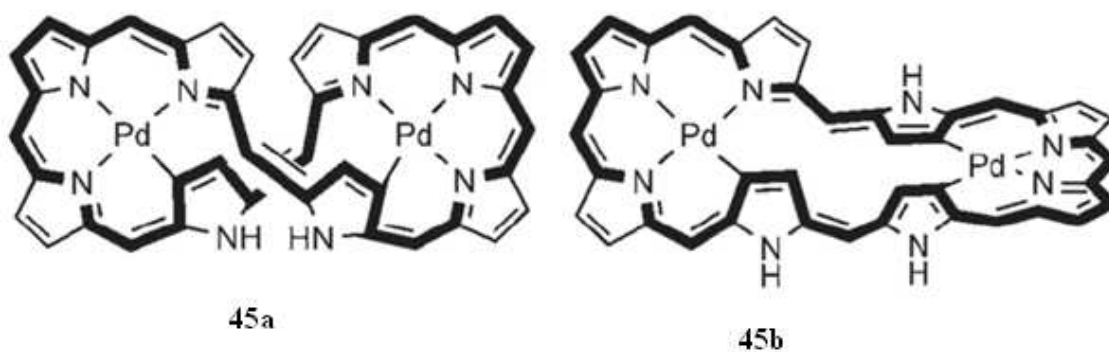
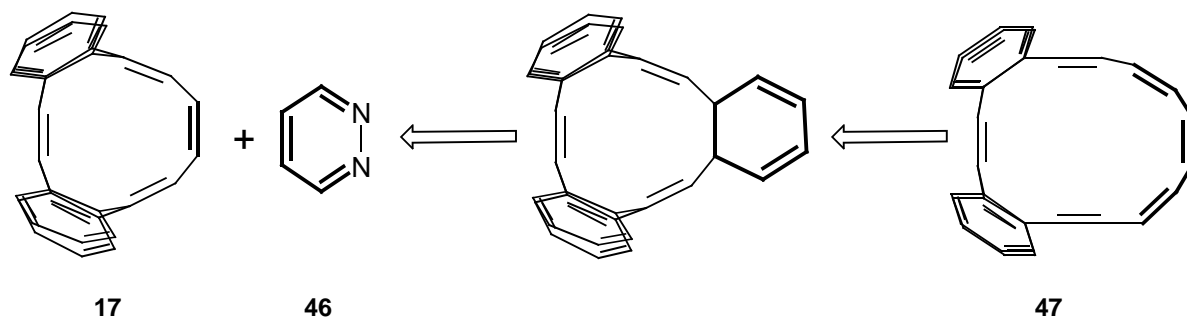


Figure 5.8: The metallation of [36]Octaphyrin yields one Hückel antiaromatic metallo porphyrin (**45a**) and one Möbius aromatic metallo porphyrin (**45b**).

5.6 Diels-Alder Reaction of (CH)₄-Adduct **17** with Pyridazine **46**

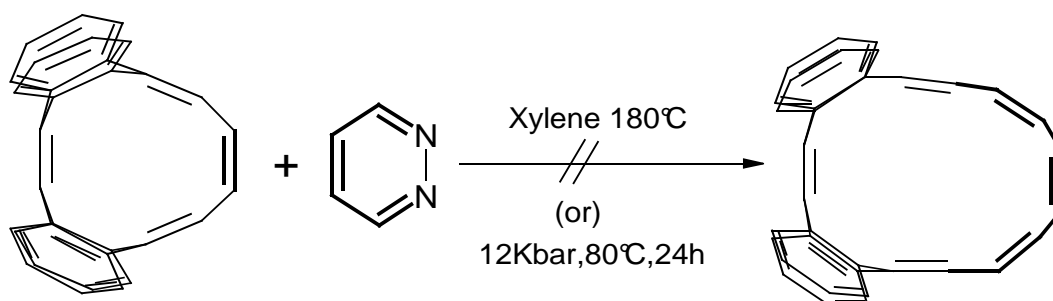
The synthesis of [16]annulene Möbius system **47** can be achieved by Diels-Alder reaction of the (CH)₄-adduct **17** with pyridazine **46** (scheme 5.2).



Scheme 5.2: Possible synthetic route to make [16]annulene.

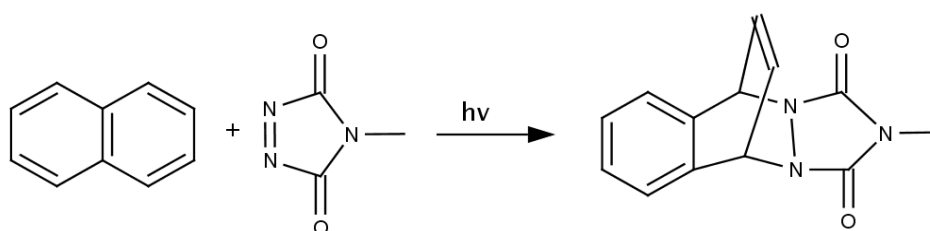
Kammermeier *et al.*^[48] reacted the (CH)₄-adduct **17** with pyridazine **46** in the solvent xylene under reflux conditions, but no addition product was observed.

In one more attempt a mixture of (CH)₄ Adduct **17** and pyridazine **46** in toluene were exposed to 12 Kbar pressure and 80 °C temperature for 24 h. Again, no addition product was observed (scheme 5.3).



Scheme 5.3: Attempted Diels-Alder reaction of (CH)₄ adduct **17** with pyridazine **46**.

Diels-Alder reactions can proceed under photochemical conditions as well as thermally (scheme 5.4).^[68]

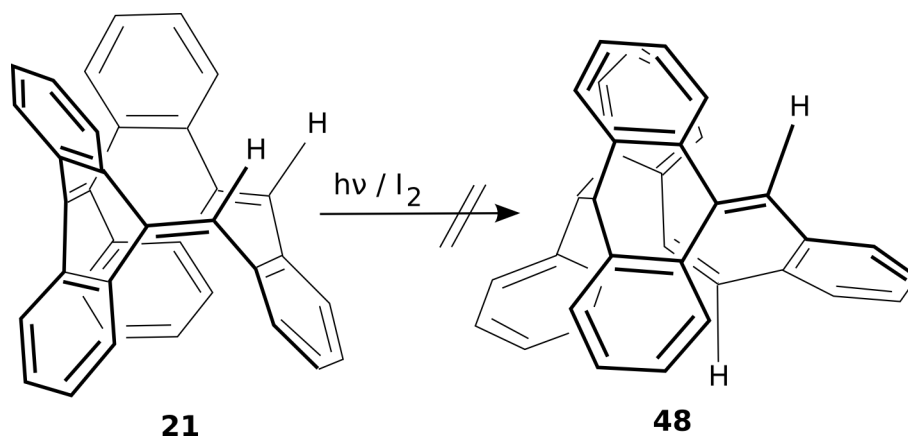


Scheme 5.4: An example of a Diels-Alder reaction under photochemical conditions.^[68]

(CH)₄ adduct **17** was mixed with pyridazine **46** in the solvent benzene and irradiated with 700 and 150 watts high pressure mercury lamps for 20 and 18 hours, respectively. Unfortunately no addition product was observed.

5.7 Irradiation of the Semitrimer **21**

The Hückel *syn* semitrimer **21** has C_s symmetry, whereas the Möbius *anti* semitrimer **48** has C₂ symmetry. Calculations were performed on B3LYP/6-31G* level of theory and it was found that the energy difference between *syn* and *anti* semitrimer is 6 kcal/mol. Since the iodine can act as *cis-trans* catalyst^[69,70] the irradiation of semitrimer **21** was done in presence of iodine. The resulting products were separated with reversed phase HPLC. Only oxidized forms of semitrimer **21**^[45] and unreacted semitrimer **21**, but no new products were observed (scheme 5.5).



Scheme 5.5: Irradiation of semitrimer **21** in presence of iodine.

As the geometry of semitrimer is very rigid, the formation of *anti* semitrimer **48** is very difficult to achieve. The introduction of double bonds into semitrimer **21** between the bridged carbons and the benzene ring makes it more flexible and reduces the activation energy for the formation of *anti* derivative (figure 5.9).

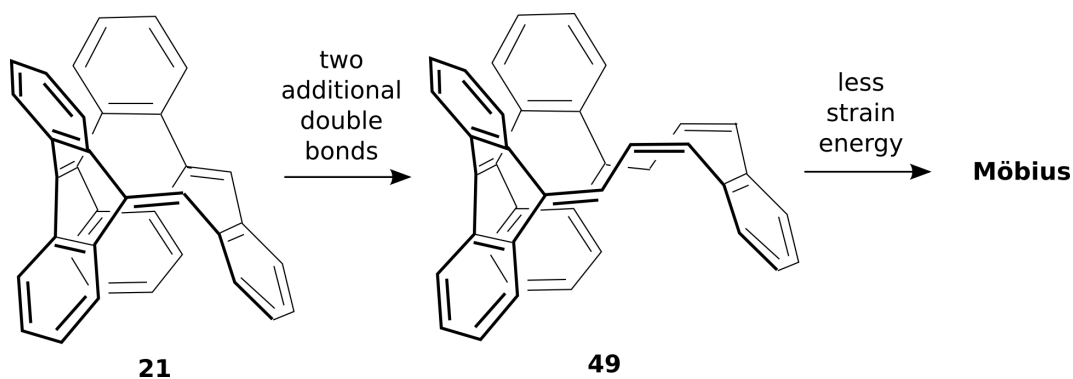
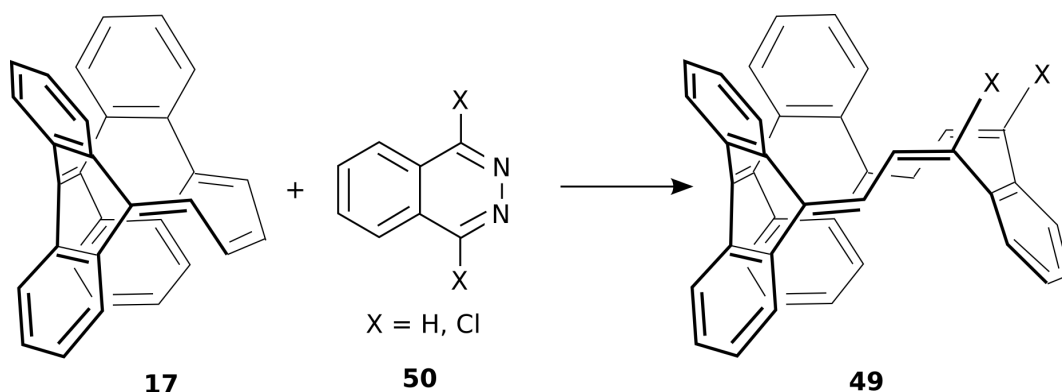


Figure 5.9: Introduction of double bonds between the bridged carbons and benzene of semitrimer **21**.

A possible synthetic route to compound **49** proceeds via a Diels-Alder reaction of phthalazine **50** with $(\text{CH})_4$ -adduct **17** (scheme 5.6).



Scheme 5.6: Proposed synthesis of compound **49**.

The reaction of $(\text{CH})_4$ -adduct **17** with phthalazine **50** was carried out in toluene both at room temperature and under reflux conditions. However, no addition product was observed. Since dichlorophthalazine is more reactive than phthalazine **50**, the reaction was also performed under similar conditions, but again no addition product could be detected. Solid state reaction in presence of *tert*-butyl catechol as a radical quencher was also a failure.

Under these conditions the reactivity of $(\text{CH})_4$ adduct **17** was carefully investigated. The $(\text{CH})_4$ -adduct **17** only reacts with the highly reactive TDDA **7** and tetrachlorothiophene dioxide^[48] but shows no reaction with the comparatively less reactive pyridazine. Compared to phthalazine and 1,4-dichlorophthalazine, dibromo-*o*-quinodimethane **51** is more reactive (figure 5.10).

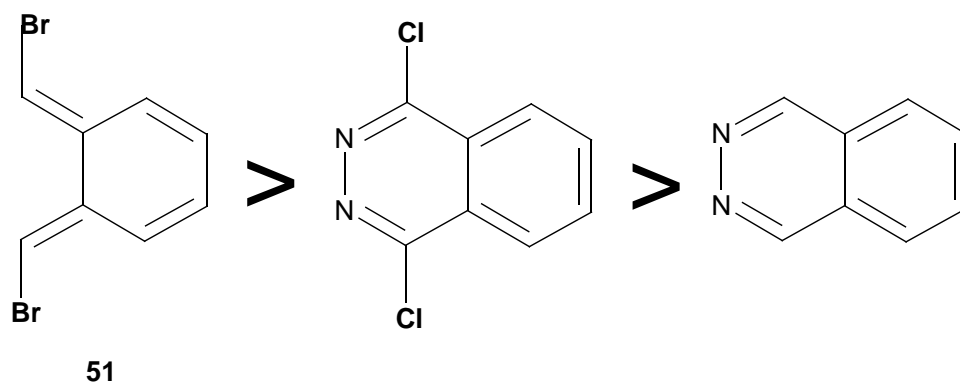


Figure 5.10: The reactivity order of the phthalazines and dibromo-*o*-quinodimethane.

(CH)₄-adduct **17** was reacted with tetrabromo-*o*-xylene **52** in the presence of sodium iodide in dimethyl formamide for 15-20h. As expected, all of the (CH)₄-adduct **17** has vanished during the reaction. The resulting products were separated with reversed phase HPLC using acetonitrile and water (85:15) as a mobile phase (scheme 5.7). The HPLC chromatogram is represented in Figure 5.11.

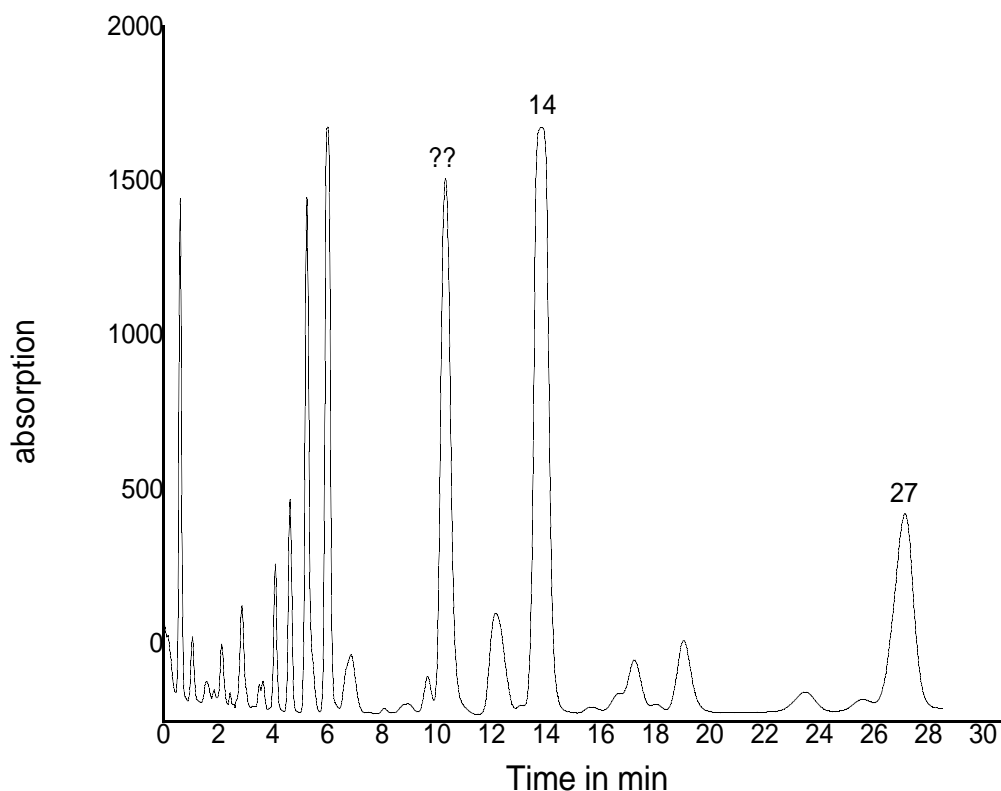


Figure 5.11: The HPLC chromatogram of the reaction of (CH)₄-adduct **17** with tetrabromo-*o*-xylene **52**. The peaks with retention times below seven minutes can be characterized as oxidized forms of (CH)₄ adduct **17**^[48] and excess tetrabromo-*o*-xylene **52**.

The substance with a retention time of 14 minutes exhibits a MS peak which is two units less than the required mass for product . UV and NMR spectral data indicate a fully conjugated tubular aromatic compound with C_s symmetry. Even though the solubility of the compound is low, crystals were grown by dichloromethane and ether diffusion method. The X-ray structure is in agreement with the structure assigned on the basis of spectroscopic data (figure 5.12).

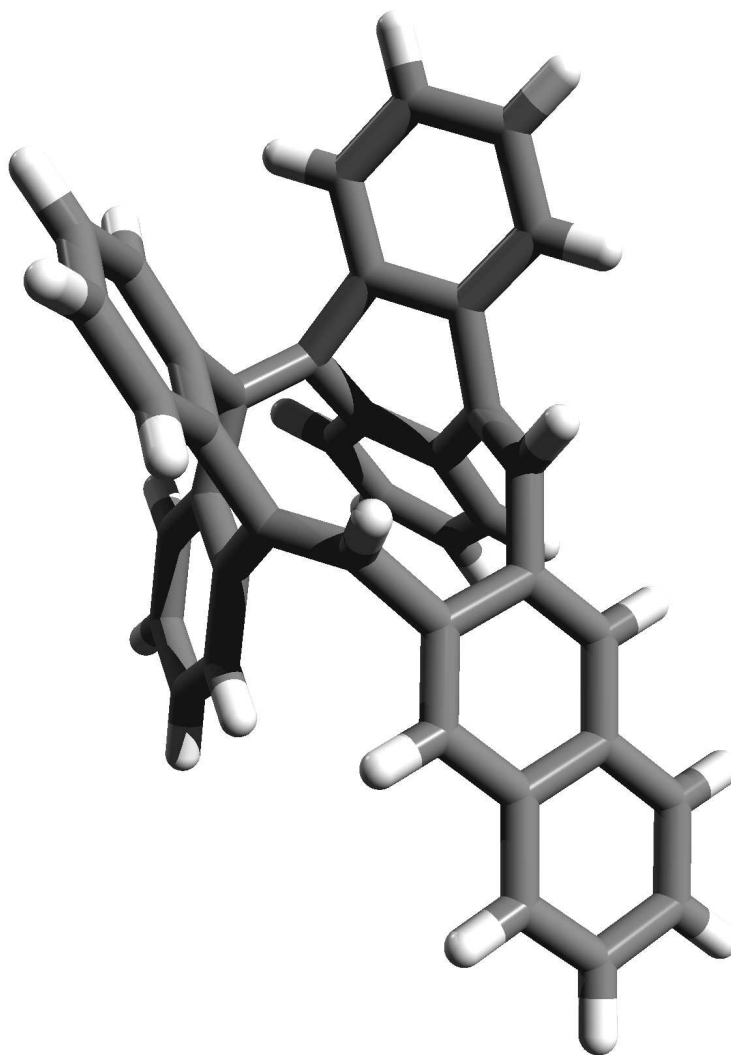
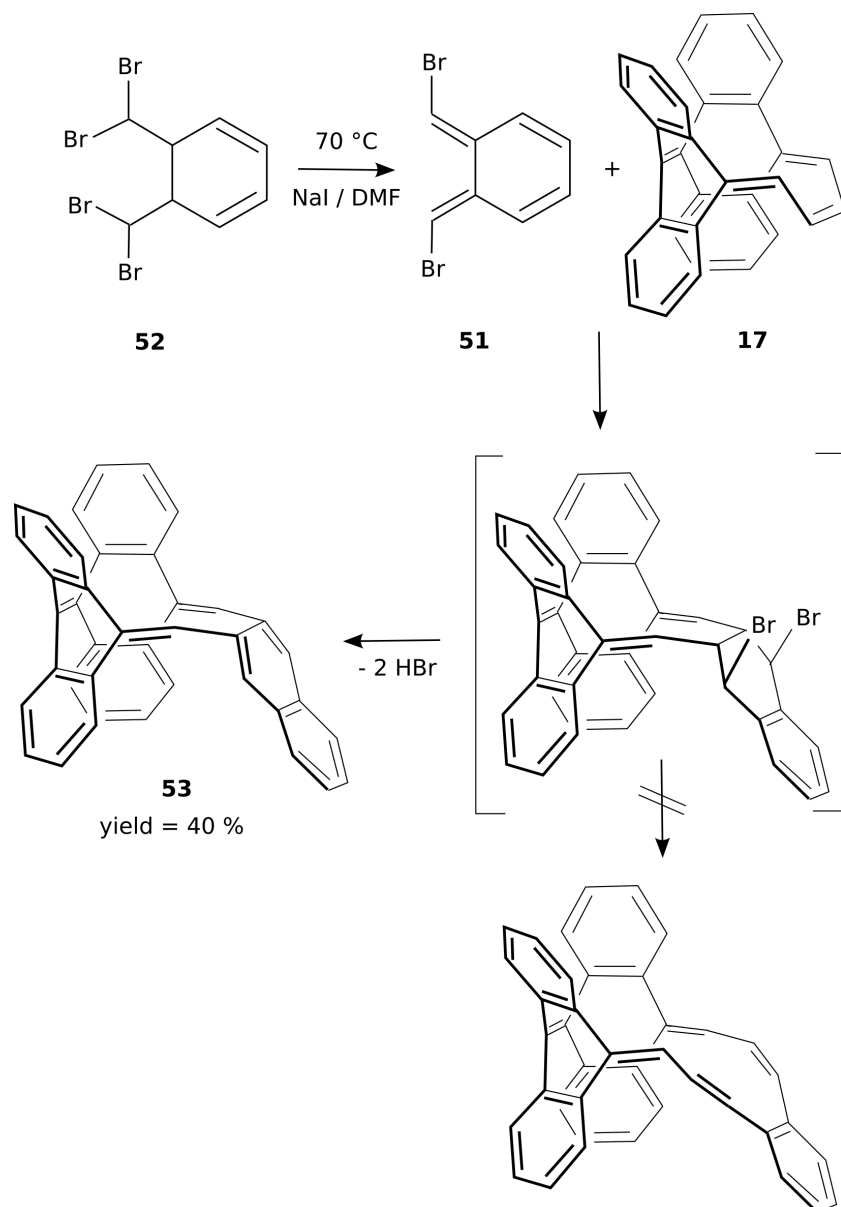


Figure 5.12: X-ray structure of the naphthalene system **53**.

Is the naphthalene system **53** aromatic? The naphthalene system **53** consists of four conjugated benzene rings and one naphthalene ring connected by three double bonds including 40 π electrons. The π perimeter is a [12]annulene with 12 π electrons. According to the $(4n+2)$ π Hückel rule it is antiaromatic. Due to the pyramidalization of the olefinic carbon atoms in the naphthalene system **53**, the olefinic protons are shifted upfield in comparison to the corresponding protons in triphenylethylene (6.49 vs. 6.96 ppm, 500 Mhz, $CDCl_3$)



Scheme 5.7: Mechanism for the formation of the naphthalene system **53**.

The aim of this reaction is the synthesis of a fully conjugated tubular and especially Möbius aromatic compound, but from the mechanism and because of the stability of the aromatic system, the HBr elimination leading to the naphthalene system **53** is preferred over the ring opening. (scheme 5.7).

According to EI and MALDI MS, the substance with a retention time of 27 minutes is 1 unit lighter than the required mass and has the following $^1\text{H-NMR}$ spectrum (figure 5.13).

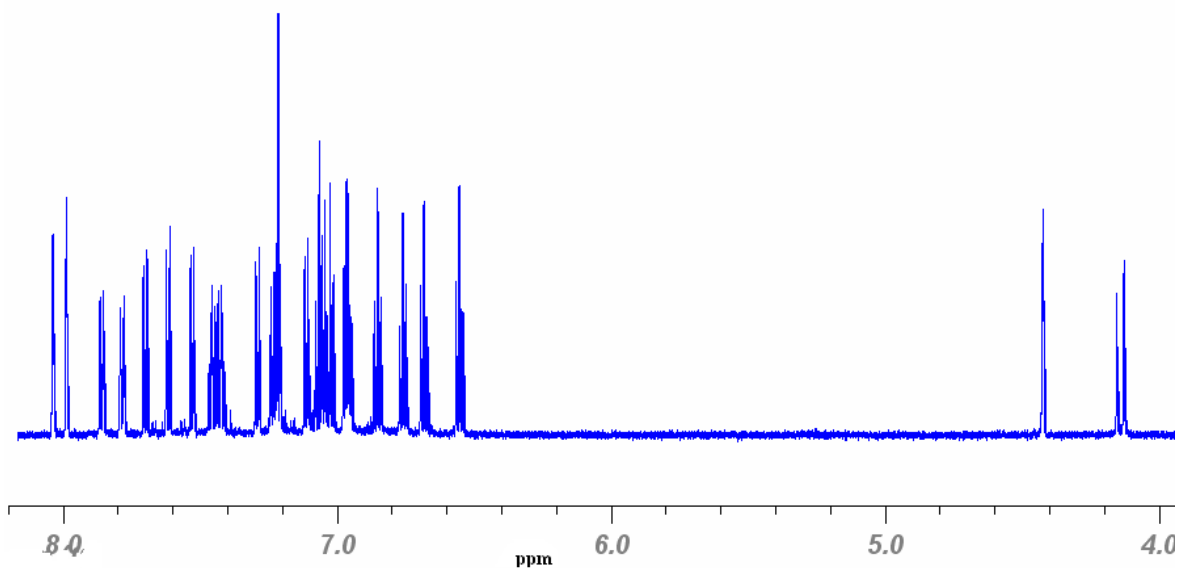


Figure 5.13: $^1\text{H-NMR}$ of the compound with a retention time of 27 minutes.

Based on the NMR spectrum, five benzene rings could be identified. The reduced mass by 1 unit indicates the presence of an allene bond in the structure. However, the IR spectrum gave no evidence for an allene system. To understand the structure, crystals were grown from a mixture of dichloromethane and heptane. The observed structure is completely different from the expected one. An iodide ion has attacked (scheme 5.8) the sterically hindered strained double bond of the naphthalene system leading to an unsymmetrical compound **54** (figure 5.14). Probably, the carbon–iodine bond is too weak for the molecule ion peak to be observed in the mass spectra (EI, MALDI).

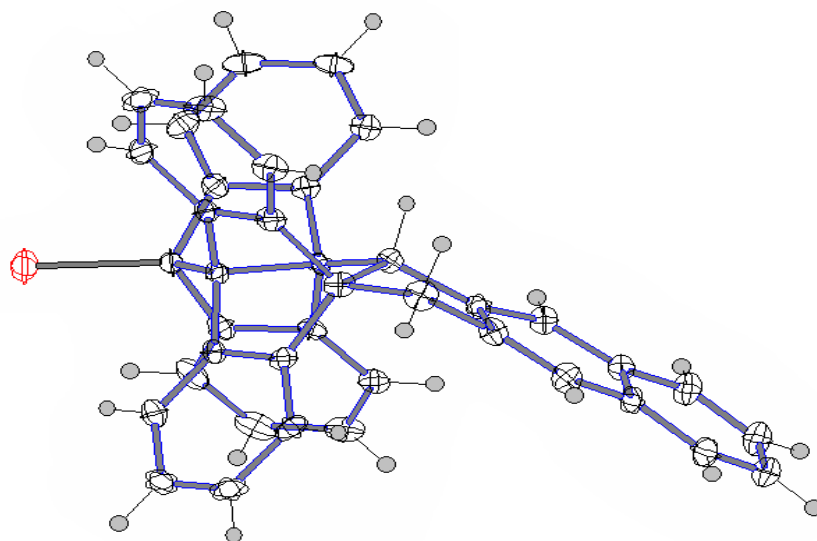
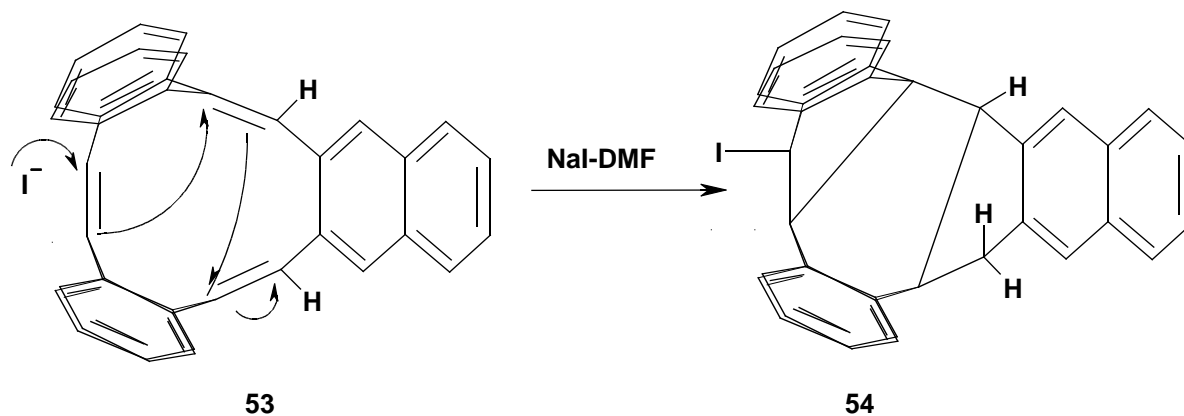


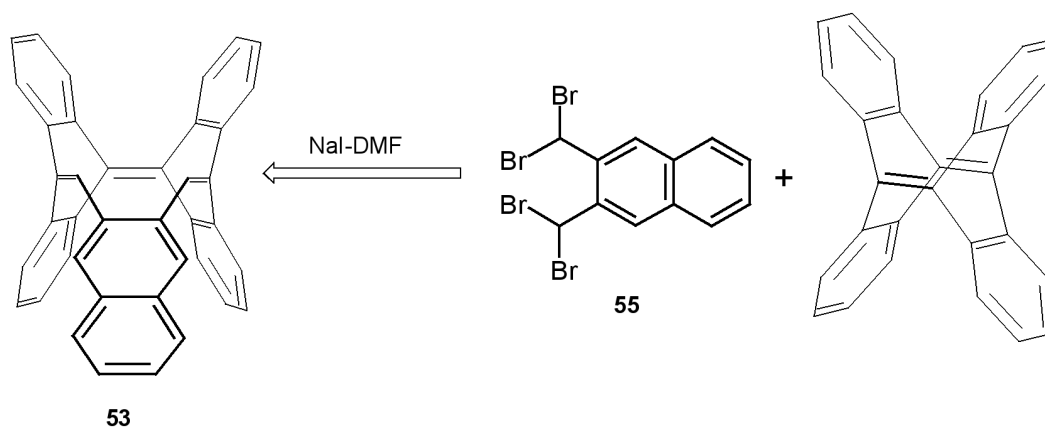
Figure 5.14: X-ray structure of the compound with a retention time of 27 minutes.



Scheme 5.8: Mechanism for the formation of **54**.

5.8 Reaction of TDDA **7** with 2,3-Bis (dibromomethyl) Naphthalene **55**

Alternatively, the naphthalene system **53** can also be prepared directly from TDDA **7** and 2,3-bis(dibromomethyl) naphthalene **55** in the presence of sodium iodide in the solvent DMF (scheme 5.9).



Scheme 5.9: Retrosynthetic route to synthesize the naphthalene system from TDDA **7**.

However, because of steric hindrance between the hydrogens of TDDA **7** and the hydrogens of 2,3-bis(dibromomethyl) naphthalene, the reaction was a failure (figure 5.15).

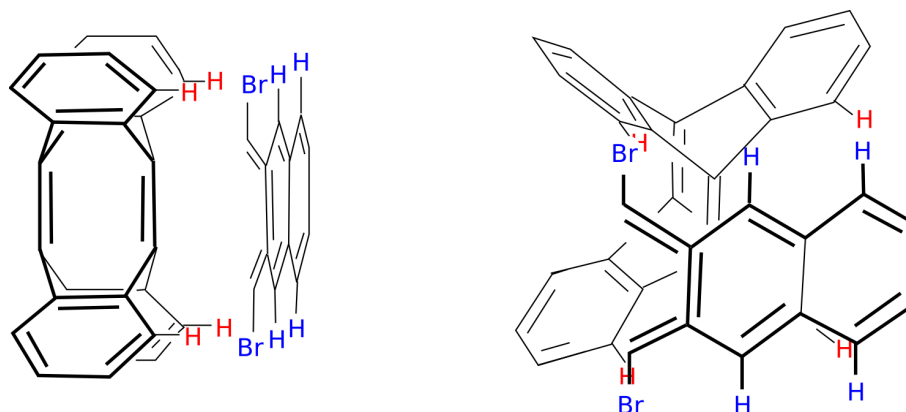
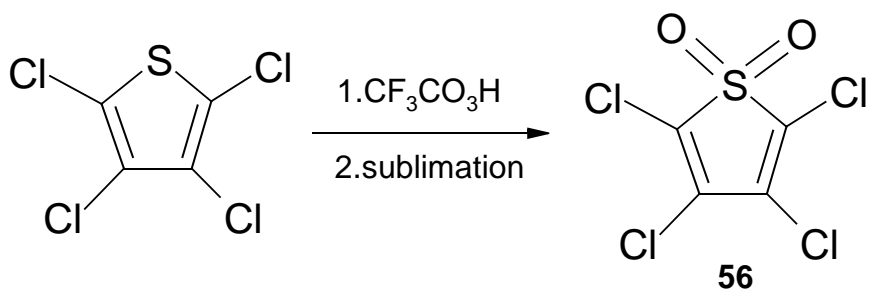


Figure 5.15: Steric hindrance between the hydrogens of TDDA and 2,3-bis(dibromomethyl)-naphthalene.

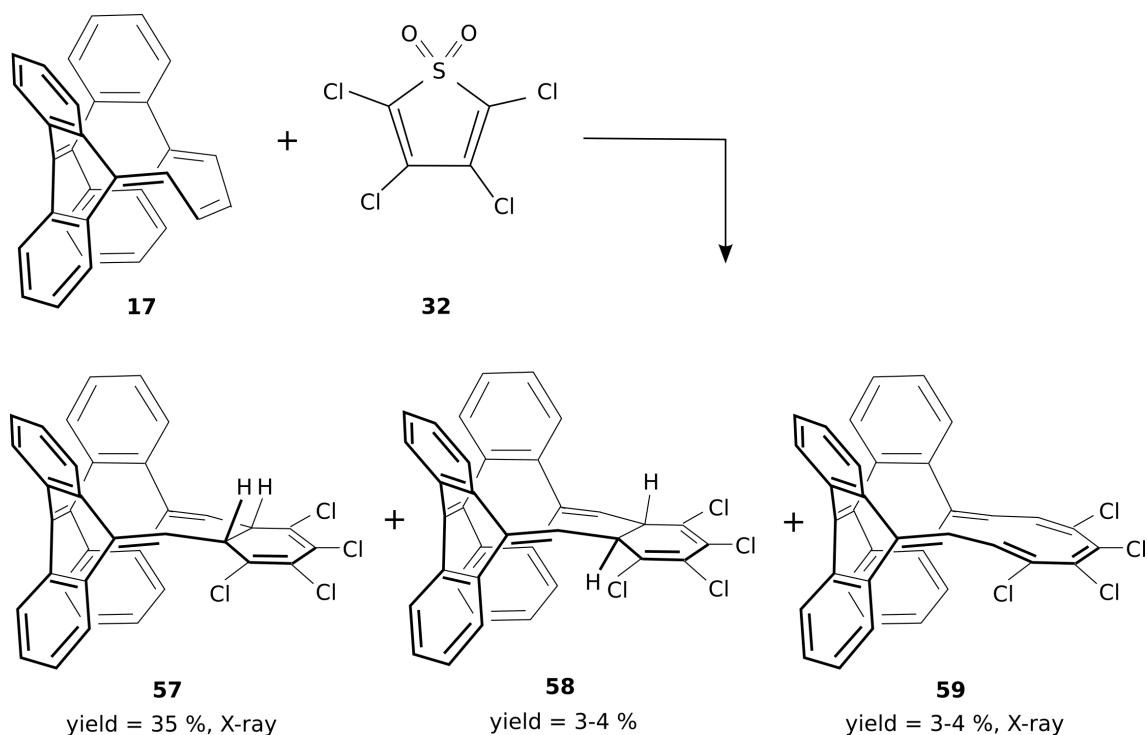
5.9 Reaction of the $(\text{CH})_4$ Adduct **17** with Tetrachlorothiophene Dioxide **32**

Tetrachlorothiophene 1,1-dioxide (TTD) **32** is a reactive electron-poor diene widely used as a Diels-Alder reagent.^[71] The cycloaddition is frequently followed by the cleavage of sulphur dioxide, resulting in the formation of 1,2,3,4-tetrachloro-1,3-cyclohexadiene derivatives. TTD **32** has been prepared by the oxidation of the thiophene using peroxy trifluoro acetic acid as a powerful oxidizing agent.^[72] The purification of TTD **32** was achieved by sublimation (scheme 5.10).



Scheme 5.10: Synthesis of tetrachlorothiophene dioxide **32**.

TTD **32** was reacted with $(\text{CH})_4$ adduct **17** in dry toluene under nitrogen at 90 °C. Under these conditions the reaction yielded three compounds. Two compounds were ring closed isomers **57**, **58** while the third one is a ring opened isomer **59** (scheme 5.11). These compounds were separated by combination of both reversed and normal phase HPLC.



Scheme 5.11: Diels-Alder reaction of TTD **32** with $(\text{CH})_4$ -adduct **17**

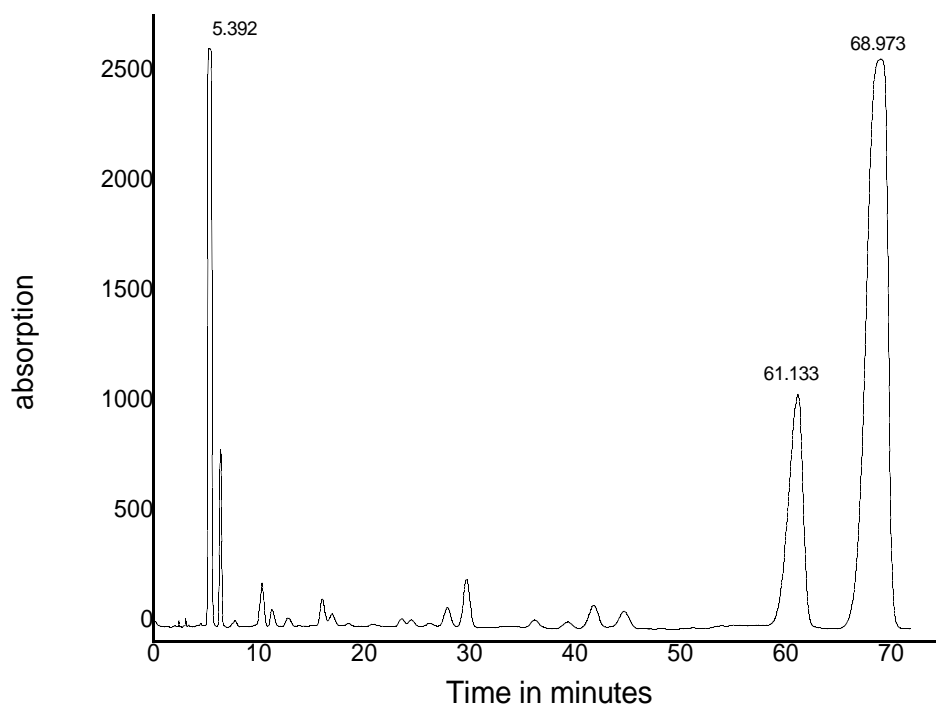


Figure 5.16: Reverse phase HPLC chromatogram of the reaction of $(\text{CH})_4$ adduct **17** with TTD **32**.

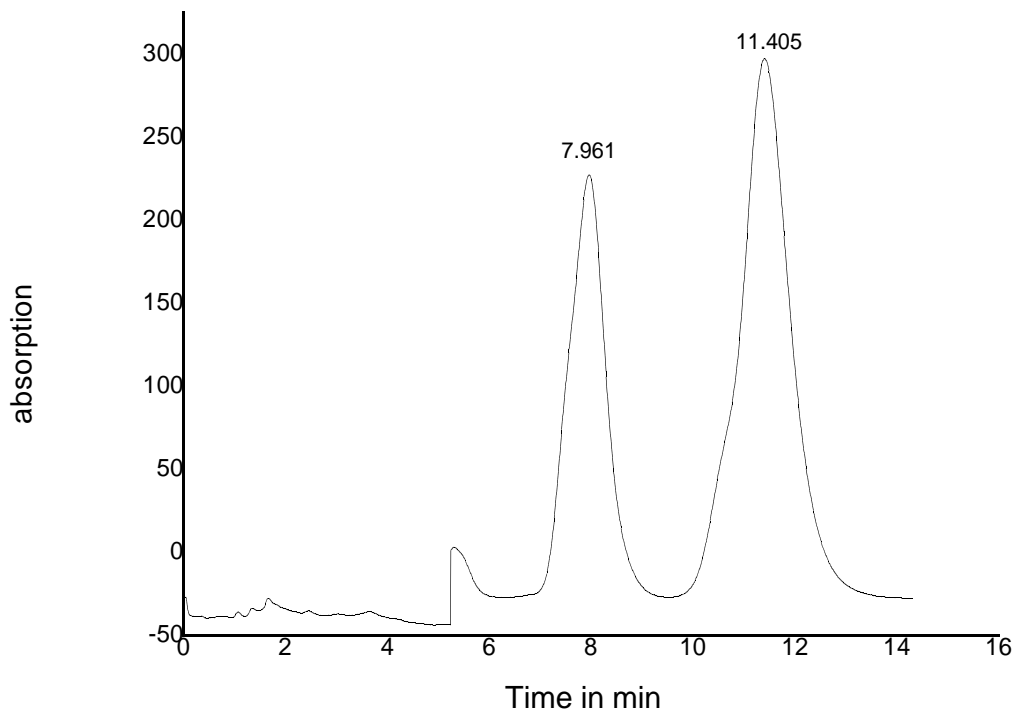


Figure 5.17: Normal phase HPLC chromatogram separating **58** and **59**.

The peak with a retention time of 68.973 minutes represents the ring closed isomer **57** which is formed as the main product (yield=35%). The peak with a retention time of 61.133 minutes contains a mixture of ring opened **59** and ring closed isomer **58**. The peak with a retention time of 5.392 minutes could be identified as excess TTD **32**. The mixture of **58** and **59** was separated using normal phase HPLC (figure 5.17). To understand the structure of **57**, crystals were grown by slow evaporation of its benzene solution.

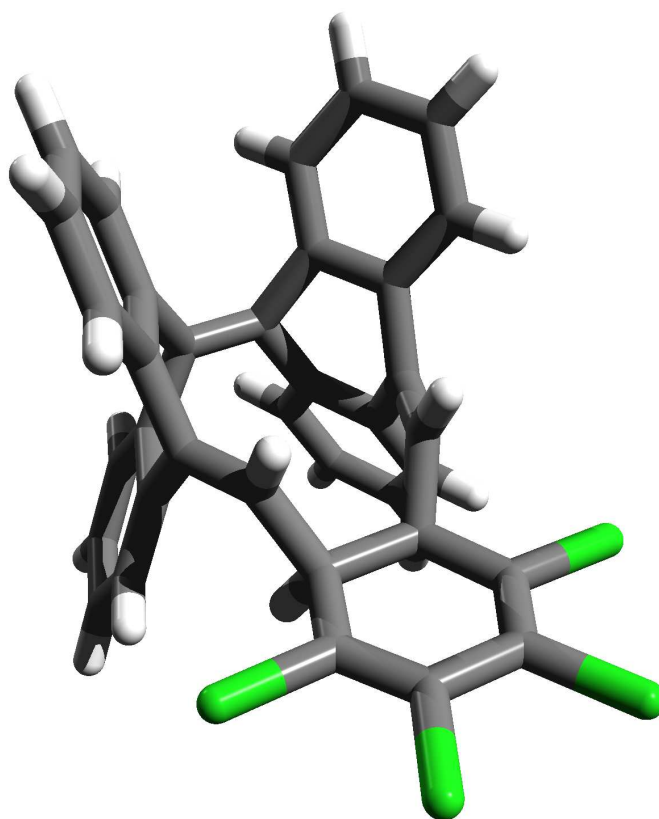


Figure 5.18: X-ray structure of **57**.

The X-ray structure analysis of **57** confirms the proposed structure with C_s symmetry. The molecule contains a tetrachloro 1,3-cyclohexadiene part fused with a bianthraquinodimethane unit (figure 5.18). The hydrogen atoms of both quinoid CH groups in the bianthraquinodimethane part have *syn* configuration with respect to each other and they are in a *trans* relationship with their neighbouring aliphatic hydrogens.

The aim of this reaction was to produce a fully conjugated tubular, especially Möbius aromatic compound. The electrocyclic ring opening leading to isomer **59** can proceed either on a conrotatory or disrotatory stereochemical pathway. In the disrotatory pathway there is a clockwise and anticlockwise rotation of the substituents as the sigma bond breaks. In the

conrotatory process the breaking of a sigma bond is followed by rotation in the same direction. According to the concept of aromatic transition states in pericyclic reactions, the thermal conrotatory electrocyclic ring opening with $(4n+2)$ π electrons proceeds via a Möbius aromatic transition state, as there always is an odd number of sign inversions involved. On the other hand, thermal conrotatory electrocyclic ring opening and ring closing reactions for systems involving $4n$ π electrons involve a Hückel aromatic transition state. This rule is reversed for the corresponding photochemical reactions, as they proceed via the first electronically excited state.^[73] For example, according to the Woodward–Hoffmann rules, the thermal interconversion of 1,3-cyclohexadiene \leftrightarrow hexatriene proceeds via a disrotatory mechanism whereas the corresponding photochemical reaction occurs via a conrotatory mechanism (figure 5.19). The ring opening is much more efficient than the ring closure due to the flexibility of the resulting hexatriene and predominance of all-*trans*-hexatriene in the conformational equilibrium.

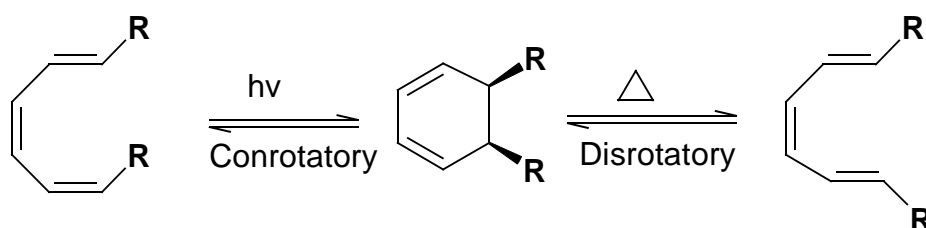


Figure 5.19: Mechanism of the ring opening and ring closure of 1,3-cyclohexadiene and hexatriene based on the Woodward-Hoffmann rules.

The conrotatory opening of a cyclohexadiene ring in a bicyclic system proceeds efficiently, especially if the resulting ring is sufficiently large to provide stability for the E double bonds in the product. Since the triene generally has a higher absorption coefficient and broader absorption bands, longer wavelength irradiation is required for the reverse reaction (figure 5.20).

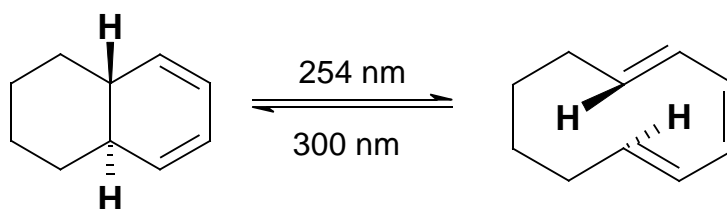


Figure 5.20: The equilibrium of the electrocyclic ring opening and ring closure of a bridged system depends on the wavelength of irradiation.

Since high pressure mercury lamps emit both UV and visible light, they promote both ring closure and ring opening reactions. For the ring opening of **57** a low pressure mercury lamp

was used. Low pressure mercury lamps are miniature U-shape or straight tube fluorescent lamps. A discharge of mercury vapour (10^{-5} atmospheres) converts electrical energy in to UV radiative energy with an efficiency of about 60% in which 95% of this energy is emitted at 253.7 nm. The remaining energy is converted into visible radiation and heat. The arc length of the lamp is a function of the power rating. A typical low pressure lamp has about 35cm arc length with a power consumption of 15 Watt.

5.9.1 Photochemical Irradiation of the Closed Isomer **57**

The *syn* isomer **57** was irradiated with a 15 Watt low pressure mercury lamp in benzene in order to open the cyclohexadiene part of the closed ring. Since the 15 Watt lamp delivers high energy to the compound, it lead to decomposition of most of the compound because of the formation of chlorine radicals. Along with the decomposed product the reaction also yielded **58**, **59** and unreacted **57** (scheme 5.12). All these compounds were separated using normal phase HPLC with heptane as the mobile phase (figure 5.21).

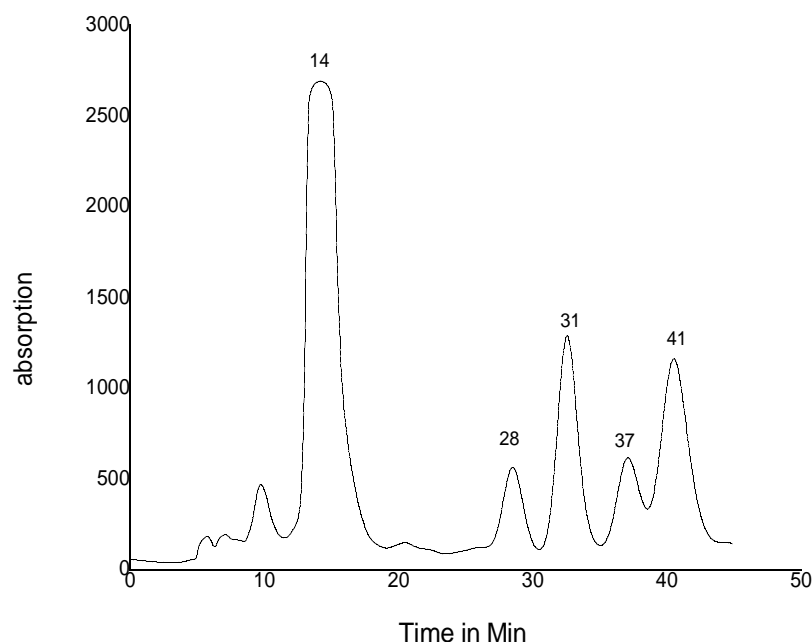
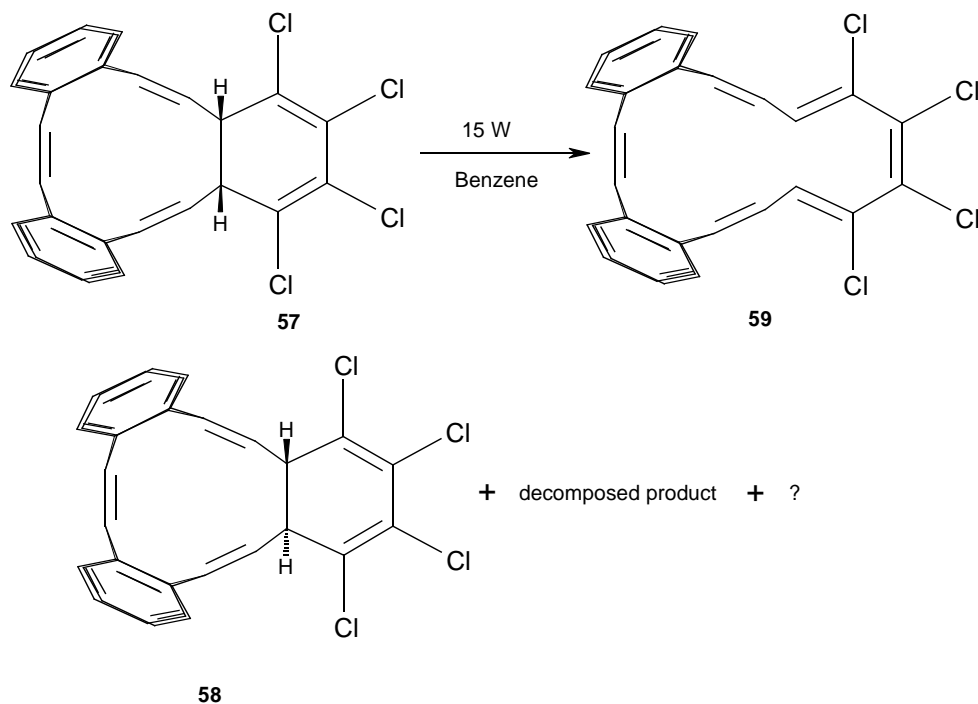


Figure 5.21: Normal phase HPLC chromatogram of photochemical irradiation of **57**.

Thus, photochemical irradiation to form ring-opened isomers from the closed isomer **57** was unsuccessful because of the formation of chlorine radicals.



Scheme 5.12: Photochemical ring opening of closed isomer **57**.

5.9.2 Thermally Induced Ring Opening

The ring closed isomer **57** was heated for 30 min at 170 °C in 1,2-dichlorobenzene in order to thermally open the ring of the cyclohexadiene part. The thermal ring opening was successful. According to the NMR spectra, the ring opened compound **59** was in equilibrium with the ring closed compound **57** (figure 5.22). The open isomer **59** was successfully separated from the closed one **57** with reversed phase HPLC.

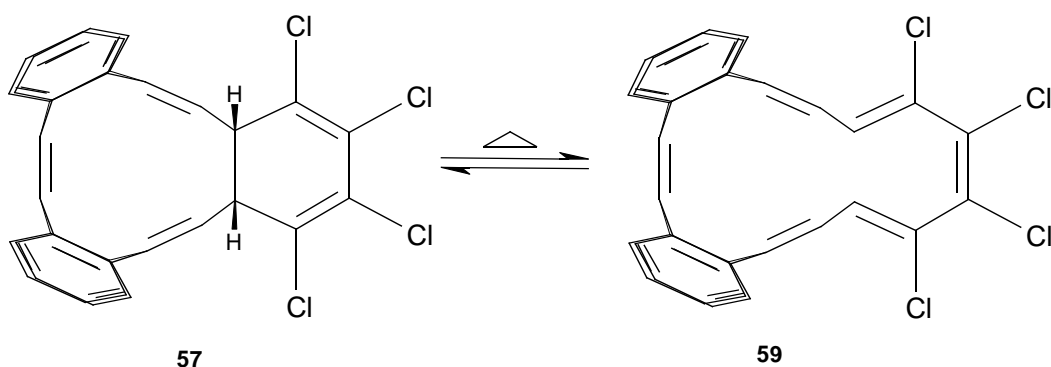


Figure 5.22: Thermal equilibrium of the ring closed isomer **57** with opened one **59**.

According to the NMR spectra, both the thermal and photochemical ring opening yielded the same compound **59**. In order to understand the structure of **59**, crystals were grown by dissolving the compound in chloroform and diffusing pentane into the solution.

The crystal structure is shown in Fig. 5.23:

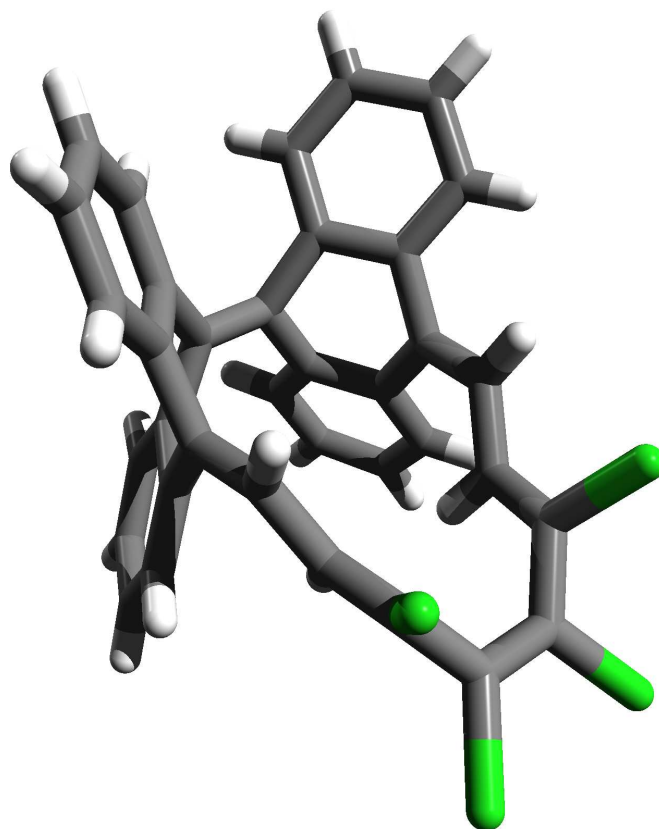
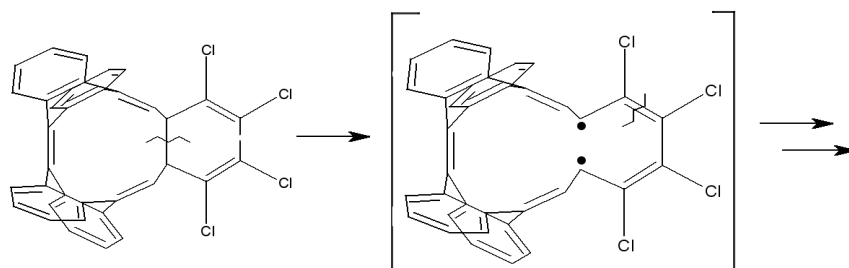


Figure 5.23: Crystal structure of **59**

Compound **59** crystallizes in C_s symmetry and Hückel topology (figure 5.23). Both methods of ring opening (photochemical and thermal) of **57** are leading to the same compound **59**. As the Hückel C_s product **59** can be formed from **57** via a disrotatory mechanism, the results for the thermal ring opening are in agreement with the Woodward-Hoffmann rules for $4n+2$ systems. The photochemical way, however, should proceed via a conrotatory mechanism and lead to a compound with C_2 symmetry and Möbius topology, which could not be observed. In this case probably the reaction is proceeding stepwise, a possible mechanism is shown in Scheme 5.13.



Scheme 5.13: A possible stepwise mechanism for the photochemical ring opening of **57**

5.10 Conclusion

In 1964, Heilbronner propounded his theory about Möbius aromatic [4n]annulenes. He suggested that large cyclic [4n]annulenes might be stabilized if the π orbitals were twisted gradually around a Möbius strip. Numerous attempts have been done in order to synthesize Möbius aromatic compounds, especially Möbius [4n]annulenes, but all of them have failed. Twisted small annulenes are unstable because of the high strain in the molecules and increasing the ring size causes an exponentially increasing number of isomers, whose separation is almost impossible. The combination of in-plane aromaticity and normal aromaticity was considered to stabilize the Möbius structures and to facilitate their synthesis.

Diels-Alder reaction of (CH)₄-adduct **17** with tetrachlorothiopene dioxide **32** formed two closed ring compounds (C_s , C_2) and one open ring compound (C_s). The C_s closed ring **57** and C_s open ring **59** (both Hückel) compounds could be characterized by X-ray crystal analysis. The photochemical irradiation of the C_s -closed isomer **57** to form open isomers was a failure because of the formation of chlorine radicals. The thermal ring opening of the C_s isomer **57** successfully yielded the C_s open isomer **59**. Attempts to form the C_2 open isomer (Möbius) from the C_2 closed isomer **57** by thermally induced ring opening are under progress.

6 Metal Complexations

6.1 Introduction

Cyclophanes are an important class of synthetic receptors, which can complex with various types of substrates varying from organic and inorganic cations and anions to neutral molecules. However the complexation with metal centres is of utmost importance due to the significant alternation of physical and chemical properties of both the cyclophane and metal centre.^[77]

In principle four different types of structurally varied metallocyclophanes are possible (A-D). In the cases A and B either one or both π systems act as ligands. In case B the formation of multidecker systems is also possible as indicated in C. In type D the metal atom is situated inside the cage built up by the cyclophane (figure 6.1).^[78]

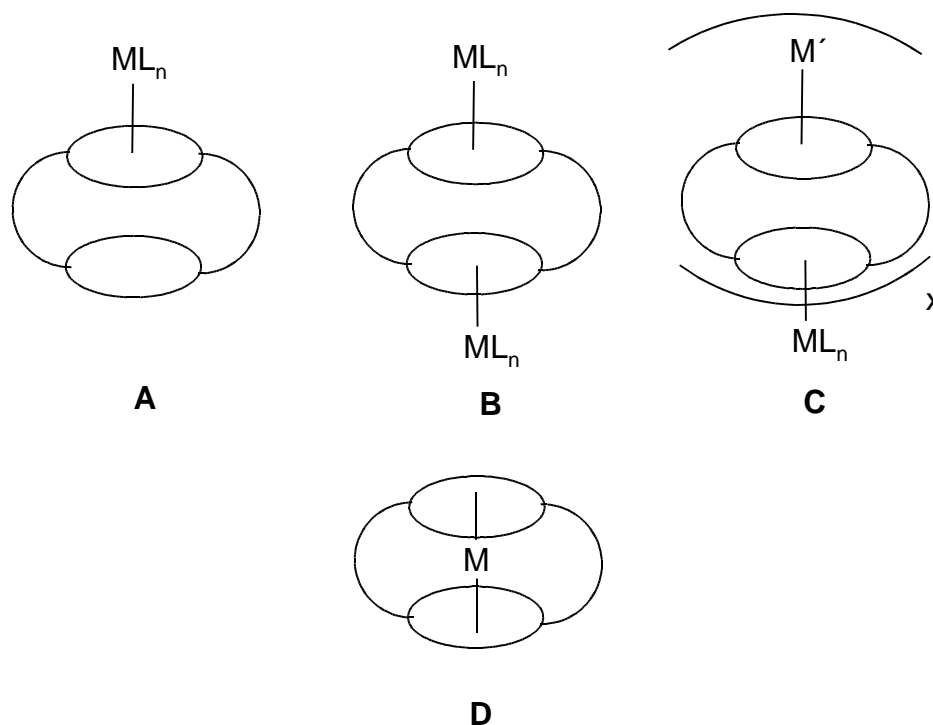


Figure 6.1: Four possible general metallocyclophane structures.

Bonding in these π complexes is due to electron transfer between the aromatic moiety and positively charged metal cations.^[79] Taylor *et al.*^[80] have studied the mechanism of the π bonding between the aromatic ring and the silver ion in the case of bis(*m*-xylene) Ag^+ perchlorate. The conclusion was that in the case of electron donation from the aromatic to the

metal acceptor orbitals the ideal position for the metal ion would be at the point of highest π electron density, above one of the carbon atoms of the aromatic ring. On the other hand, the best overlap between the filled metal d orbitals and the antibonding π MOs of the aromatic moiety for electron back donation from the metal to the aromatic moiety is achieved when the metal ion is located equidistant between two carbon atoms.^[79,80]

Iyoda *et al.*^[81] synthesized the silver(I) and copper(I) complexes of *all-Z*-tribenzo[12]annulene which can be viewed as a simple model of the semitrimer **21** (figure 6.2). In these complexes metal cations are complexed by three olefinic double bonds.

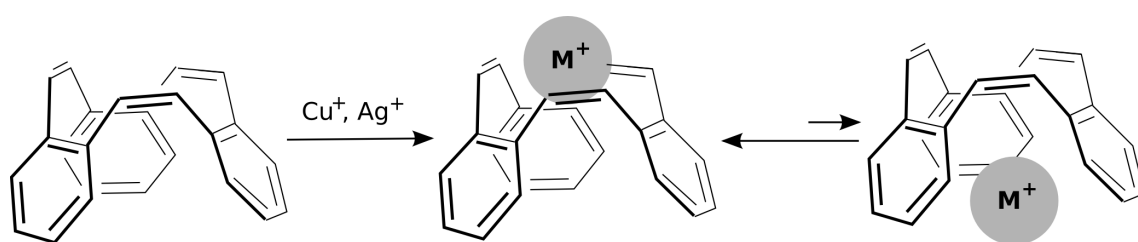


Figure 6.2: Structure of copper (I) and silver (I) complexes of *all-Z*-tribenzo[12]annulene.

The three quinoid double bonds of the semitrimer **21** should provide a planar 6π electron ligand field similar to *all-Z*-tribenzo[12]annulene (figure 6.3). In the following sections the copper and silver complexations of semitrimer were discussed.

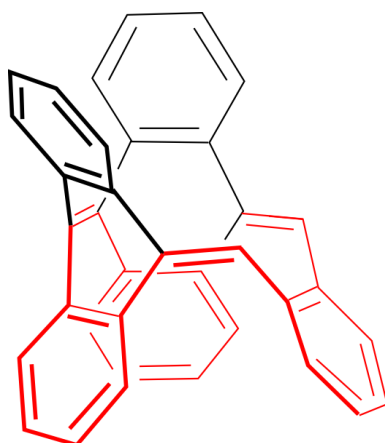


Figure 6.3: View of semitrimer **21** as a simple model of the *all-Z*-tribenzo[12]annulene.

6.2 Copper Complexation of the Semitrimer **21**

The semitrimer **21** was treated with copper(I) trifluoromethane sulfonate salt in benzene and THF. Copper(I) trifluoromethane sulfonate is sparingly soluble in benzene, however it was observed that upon addition of the semitrimer **21** the solution becomes clear. This indicates the formation of metal complexes with the semitrimer **21**. The complexation was further studied by spectroscopy.

Some new peaks appeared and some existing peaks were broadened in the proton NMR spectra upon treatment of the semitrimer with copper (figure 6.5) compared to the NMR spectra of the pure semitrimer **21** (figure 6.4), supporting the formation of the metal complex.

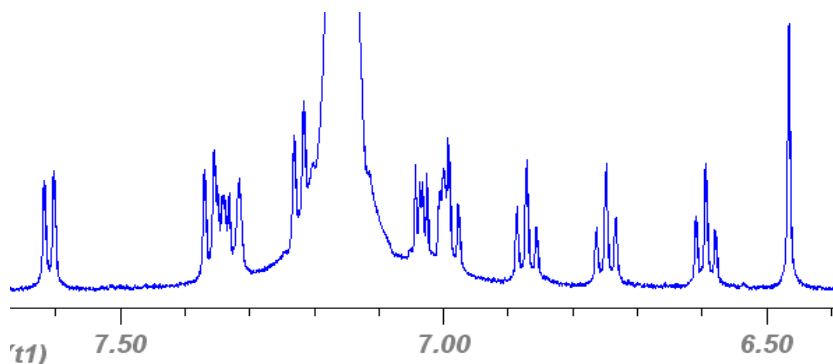


Figure 6.4: NMR spectrum of semitrimer in benzene-D₆.

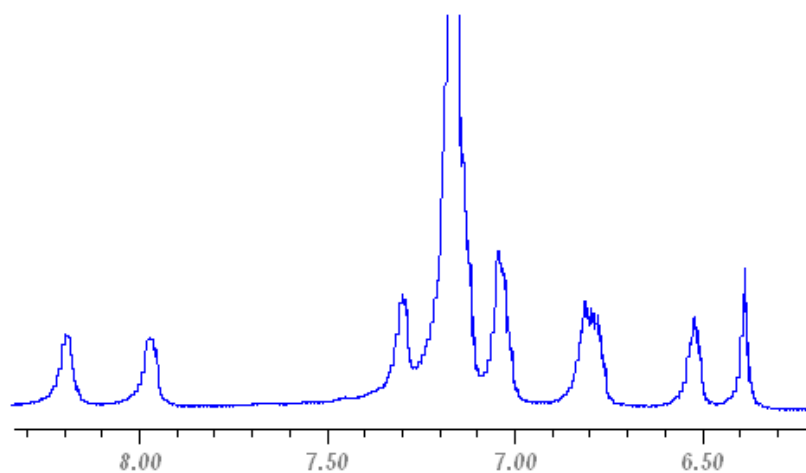


Figure 6.5: NMR spectrum of semitrimer-copper complex in benzene-D₆.

Although the copper complex was stable at room temperature for 3-4 days decomposition occurs in the presence of light and air. From all these observations the possible structure of the metal ion and semitrimer can be designated as follows (figure 6.7).

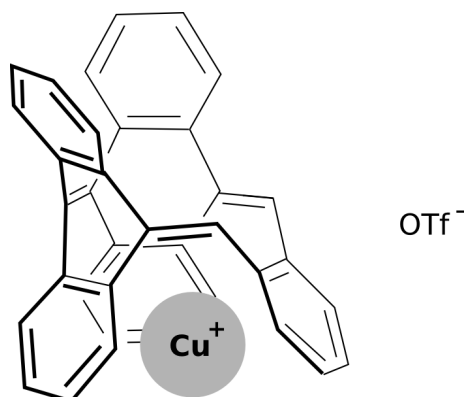


Figure 6.7: Possible copper complex of the semitrimer **21**.

6.3 Silver Complex of the Semitrimer **21**

6.3.1 Reaction with Silver Hexafluorophosphate

Similarly, semitrimer was also reacted with silver hexafluorophosphate. The reaction worked effectively in the various solvents such as THF, chloroform and dichloromethane. In chloroform the silver salt is sparingly soluble but as soon as the semitrimer is added the solution becomes clear, indicating the formation of metal complex. NMR, MALDI and ESI mass spectra supported the formation of metal complex.

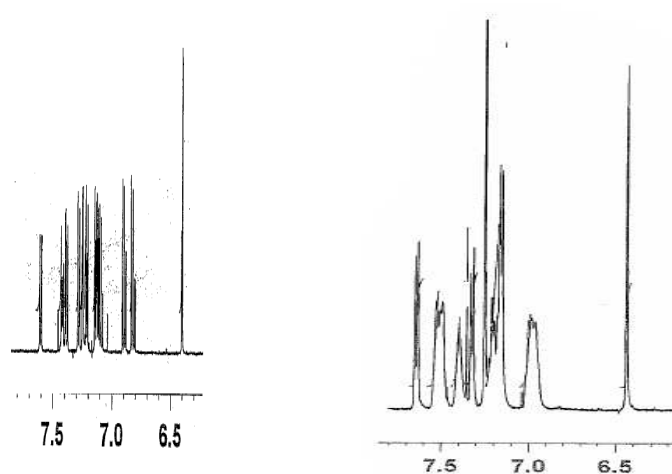


Figure 6.8: NMR spectrum of the pure semitrimer (left) and semitrimer silver complex (right) in CDCl₃

Some new peaks were observed in the NMR spectra of the semitrimer-silver complex compared to the NMR spectra of the pure semitrimer **21**, supporting the formation of a metal complex (figure 6.8). The MALDI and ESI mass spectra are shown in figures 6.9 and 6.10. Unfortunately, all attempts to get crystals suitable for X-ray analysis failed.

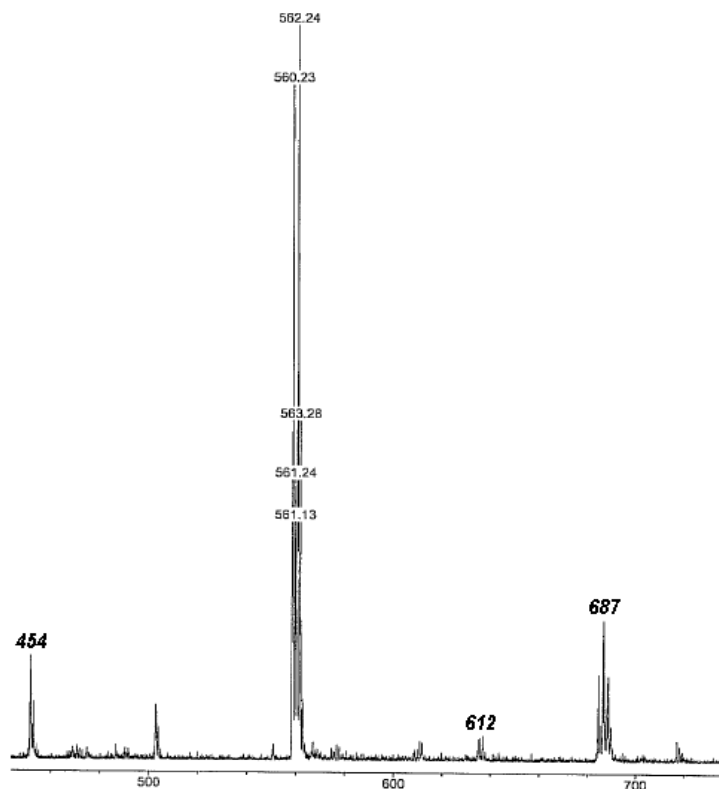


Figure 6.9: MALDI mass spectrum of semitrimer silver complex.

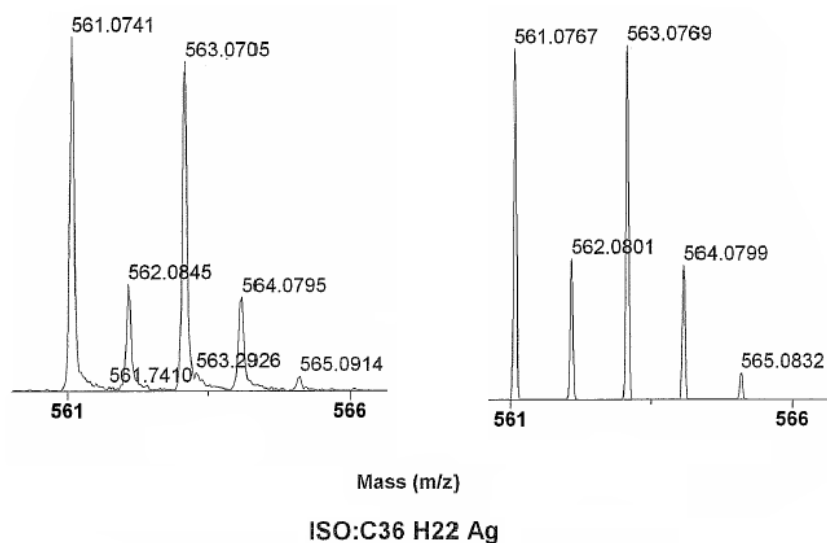


Figure 6.10: Observed (left) and theoretical (right) ESI spectrum of the semitrimer silver complex

6.3.2 Reaction with silver hexafluoroantimonate

The semitrimer **21** reacted with silver hexafluoroantimonate in THF to give the semitrimer silver complex. Single crystals suitable for crystal structure analysis were grown from dichloromethane /ether by diffusion method. The $^1\text{H-NMR}$ analysis of the crystal shows considerable shifts in the signals, indicating the formation of a complex. The crystal structure is determined by X-ray analysis (figure 6.11, 6.12). As anticipated, the silver atom is not coordinated to olefinic bonds (olefinic complex) but is coordinated to benzene rings (benzenoid complex).

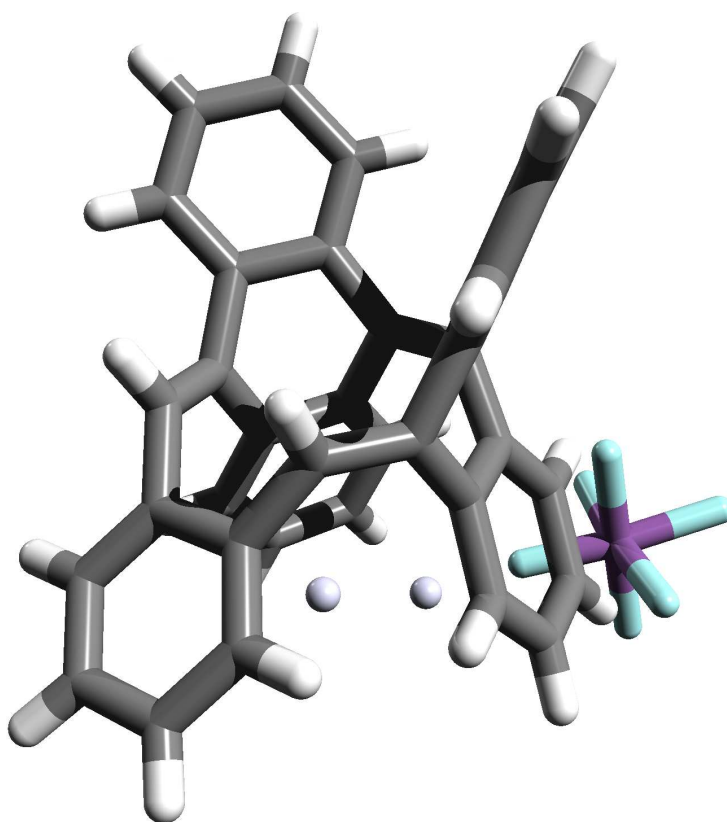


Figure 6.11: Crystal structure of the semitrimer-silver complex (only one complex displayed for clarity, the included molecule of diethyl ether is left out as well).

In the crystal structure, there are two crystallographically independent complexes in the asymmetric unit. Each of the two silver atoms is disordered over two positions and some of the fluorine atoms of both hexafluoroantimonate anions exhibit unusually high anisotropic displacement parameters indicating the disorder. Although the crystals were unstable in the presence of air and light, they were stable for two weeks at -20°C in dark and under argon atmosphere.

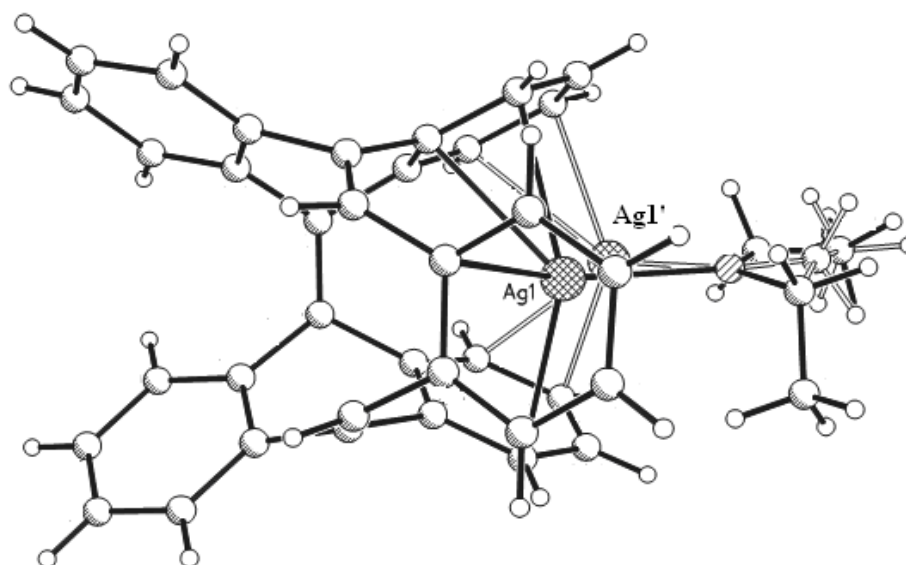


Figure 6.12: Another view of the semitrimer silver complex.

To confirm the presence of the silver-semitrimer complex in solution, a chemical test was performed: when KCN was added to the silver complex, an immediate precipitation of AgCN was observed and the compound reverted back to the semitrimer **21**.

6.4 Silver Complexation of the Naphthalene System **53**

Structurally similar to the semitrimer **21**, the naphthalene system **53** was accidentally (scheme 5.7) synthesized and contains one extra benzene ring compared to the semitrimer **21** (figure 6.13). It could be anticipated that the macrocycle **53** is providing similar structural motif, thus enabling the formation of a silver complex. Similar to the semitrimer **21**, the naphthalene system **53** was treated with silver hexafluoroantimonate in THF. Crystals were grown from dichloromethane/ether by diffusion method.

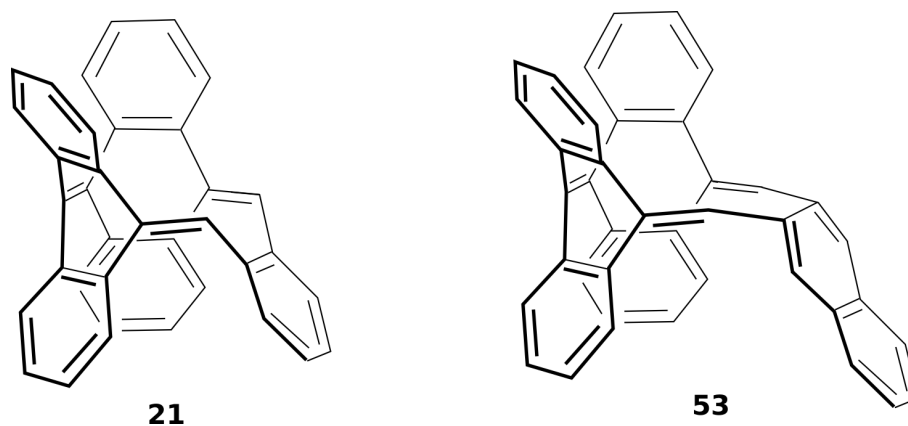


Figure 6.13: Comparing the structures of the semitrimer **21** and the naphthalene system **53**.

The $^1\text{H-NMR}$ spectrum of the crystals of the naphthalene system silver complex (figure 6.15) shows shifts in the peaks compared to the pure naphthalene system (figure 6.14) indicating the formation of a metal complex.

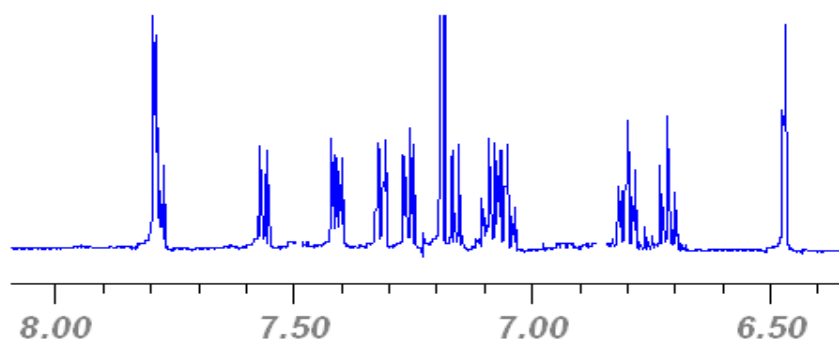


Figure 6.14: $^1\text{H-NMR}$ of naphthalene system

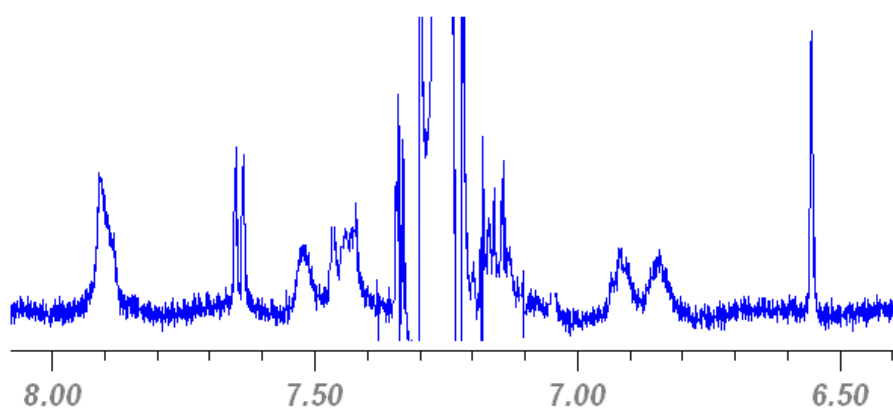


Figure 6.15: $^1\text{H-NMR}$ of silver complex of naphthalene system.

To confirm the presence of the silver naphthalene system complex in solution, a chemical test was performed: When KCN was added to the silver complex, an immediate precipitation of AgCN was observed and the compound reverted back to the naphthalene system **53**.

6.5 Conclusion

The copper and silver complexes of the semitrimer **21** were investigated by NMR and mass spectrometry methods. Moreover, in one case the Ag semitrimer complex was proved by X-ray crystal structure analysis. According to the crystal structure it was observed that silver is coordinated to benzene rings (benzenoid complex) instead of olefinic bonds (olefinic complex). Similarly the silver complex of the naphthalene system **53** was also detected in the proton NMR spectrum.

7. Optimization of Mass Spectrometry

7.1 Electrospray Ionization

Electrospray ionization mass spectrometry (ESI-MS) has established itself as a versatile means for generating intact, gas-phase molecular or pseudomolecular ions (e.g, $(M + nH)^{n+}$) from non-volatile analyte species with little or no fragmentation. Further benefits of ESI-MS include the ability to multiply charge macromolecules at relatively low mass-to-charge ratios (generally $m/z < 2000$) to obtain direct mass information on species present, minimal consumption of solvent and other consumables, and high ionization efficiency.^[74] Analytes are typically detectable by ESI-MS only if they are ionic in solution. Neutral, nonpolar analytes are not amenable to this technique.^[75]

In order to achieve the ESI-MS of non-polar, neutral analytes (in our case polycyclic aromatic hydrocarbons) we employed silver salts as a post column reagent. Silver interacts with aromatic hydrocarbons to form π -complexes. These complexes are charged and hence they can be detected.

A silver salt ($AgPF_6$) was mixed with TDDA **9**, tetramer **7** and semitrimer **21** in various solvents with different stoichiometries. There is an indication that complexes were formed. For semitrimer **21** once ESI-MS showed a positive response (figure 7.1). However, these results could not easily be reproduced. For TDDA **9** and tetramer **7** ESI-MS never showed any positive response. The lack of response and reproducibility can be attributed to technical problems.

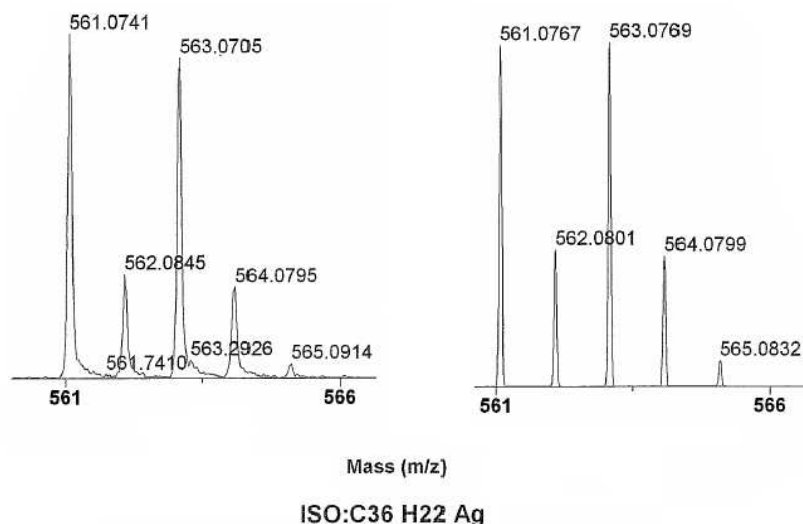


Figure 7.1: Observed (left) and theoretical (right) ESI spectrum of the semitrimer **21** silver complex

7.2 Matrix-Assisted Laser Desorption/Ionization (MALDI)

For MALDI, the analyte is embedded into a second material, the matrix, which is often present in excess and plays an essential part in the overall process of transforming the solid analyte into a gaseous ion. Upon laser irradiation the light absorbing matrix evaporates into the gas phase, assisting the desorption of the analyte. Matrix ions are formed in a primary ionization step as the result of direct laser activation. The ion formation of the analyte then takes place in a secondary ionization step, whereby the matrix-derived ions interact with the analyte. Depending on the nature of both these reactants, different types of analyte ions can be formed, predominantly including protonated, deprotonated, metal cationized analytes and/or true molecular ions.^[76]

Tetramer **7** promotes cycloaddition reaction yielding the octamer when irradiated with the MALDI laser (figure 7.2). Various matrices were investigated for their ability to avoid this reaction or to allow the characterization of octamer. Most of the matrices were promoting the reaction. The matrix DCTB (*trans*-2-[3-(4-*tert*-butylphenyl)-2-methyl-2-propenylidene]-malono nitrile) was able to largely oppress the reaction and produced more pronounced analyte ions when mixed with tetramer in dichloromethane in 10:1 ratio (figure 7.2). Thus, DCTB is a suitable matrix for measuring MALDI mass spectra of our substrates.

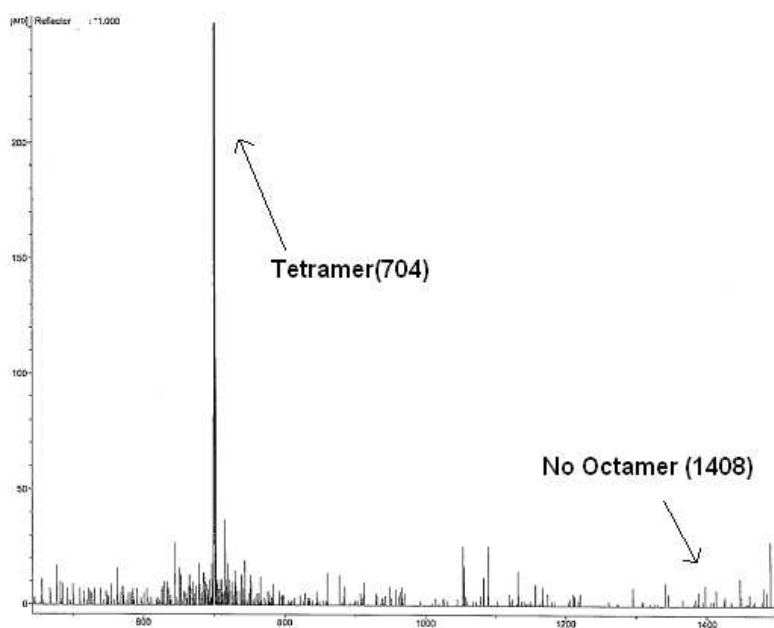


Figure 7.2: MALDI TOF MS spectrum for the tetramer with matrix DCTB

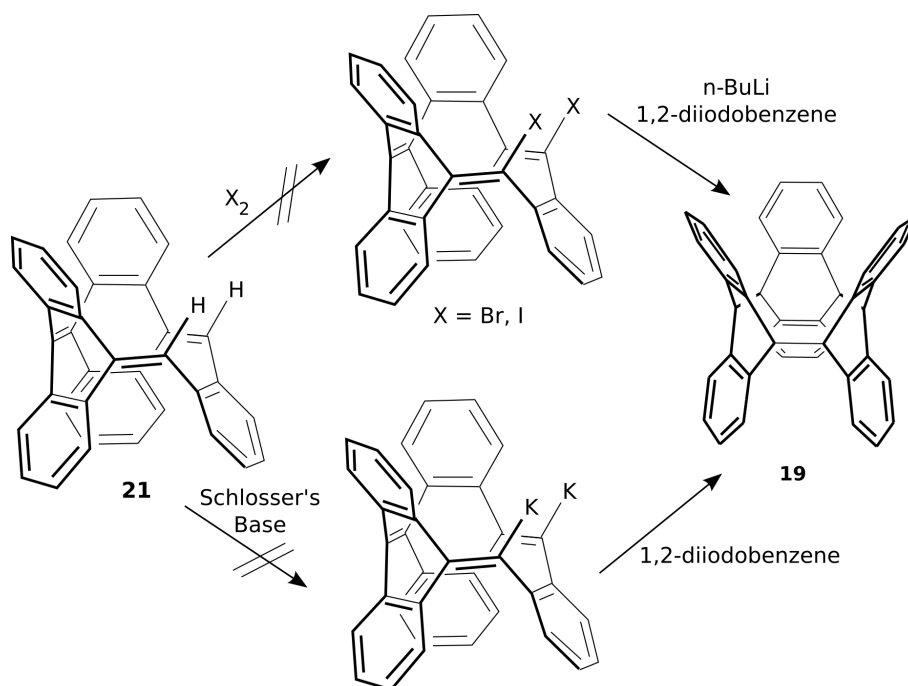
7.3 Conclusion

The mass spectra of polycyclic aromatic hydrocarbons were investigated. In the case of ESI spectra with silver as a post column reagent, there is an indication that complexes were formed but due to technical problems these results could not be finally confirmed. In the MALDI spectra with DCTB as a matrix, the reaction from tetramer **7** to octamer is reduced, thus enabling the characterization of reaction products.

8 Summary

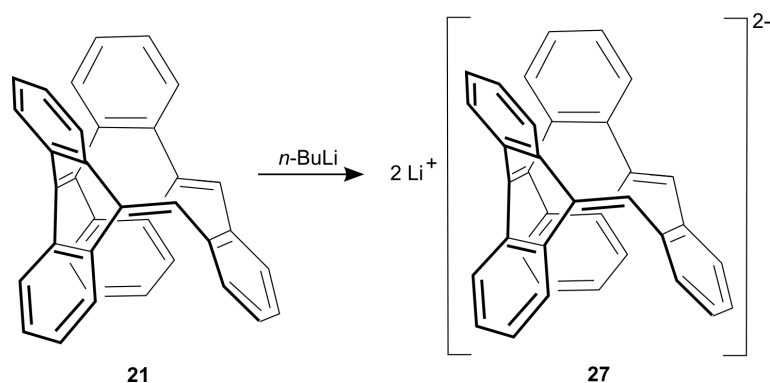
Nanotubes are produced by vaporization of graphite and chemical vapour deposition (CVD) at very high temperatures. Under these rough conditions, the tubes are generated with different lengths, diameters, helicities and endcappings. For technical applications, however, tubes with a uniform geometry and thus with well defined physical properties are required. A rational synthesis of carbon nanotubes was therefore considered.

One of the synthetic targets was 9,9',9'',10,10',10''-hexadehydrotrianthracene (trimer) **19**. The conversion of the semitrimer **21** to the trimer **19** yielded the desired product neither by halogenation, dehydrohalogenation, lithiation, coupling with 1,2-diiodobenzene nor by treatment with Schlosser's base (scheme 8.1).



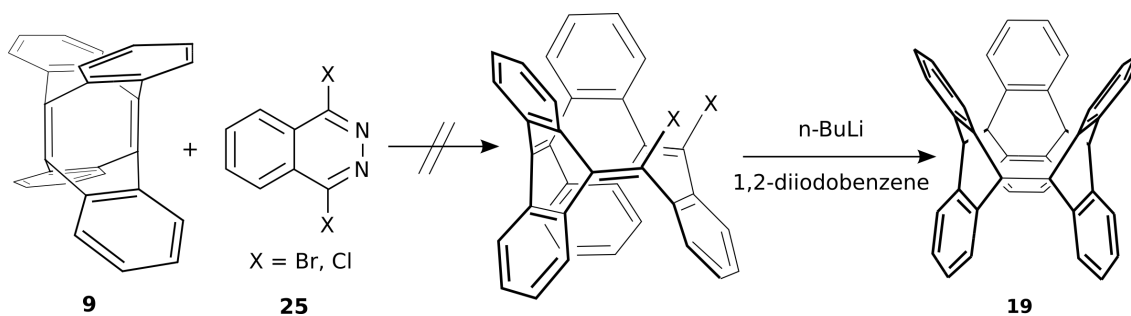
Scheme 8.1: Attempts made to convert semitrimer to trimer.

The treatment of the semitrimer **21** with $n\text{-BuLi}$ in an NMR tube under nitrogen resulted in the reduction of the semitrimer **21** to its dianion (scheme 8.2). Systematic reduction of the semitrimer **21** to its dianion with lithium wire in NMR tube under vacuum in THF has yet to be achieved.



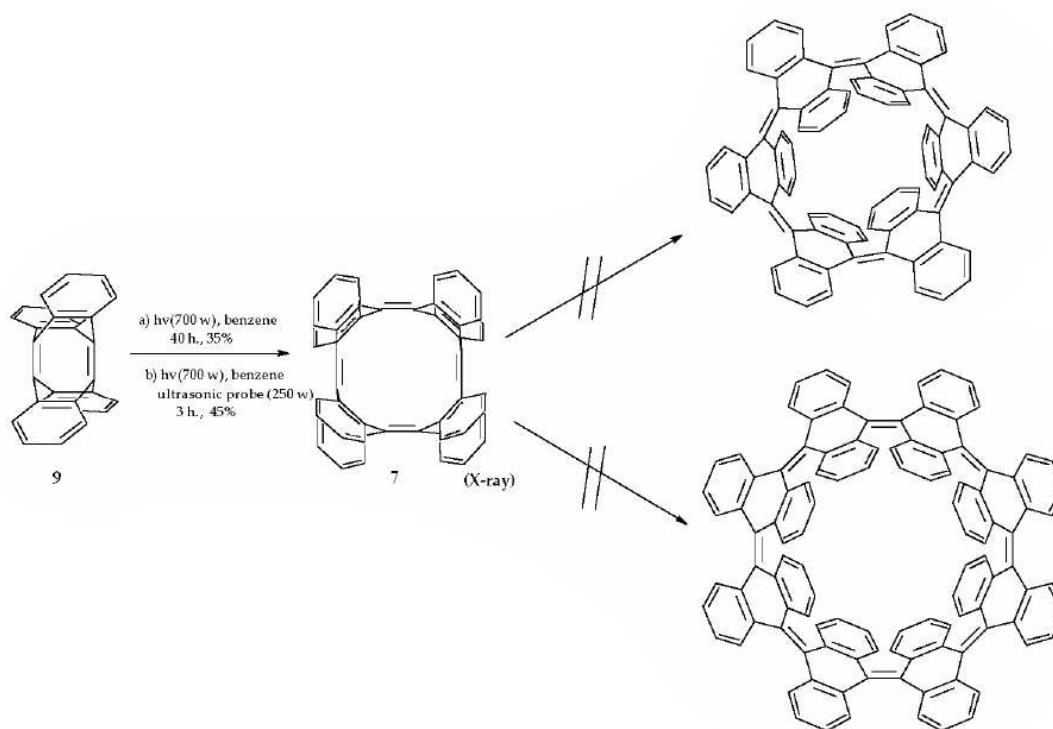
Scheme 8.2: Expected reduction of the semitrimer to its dianion.

In another strategy the Diels-Alder reaction of 1,4-dihalophthalazine **25** with TDDA **9** was supposed to offer a synthetic route towards the trimer **19**, but due to steric hindrance between the reactants, the desired product was not observed (scheme 8.3).



Scheme 8.3: Unsuccessful Diels-Alder reaction between TDDA **9** and dihalophthalazine **25**.

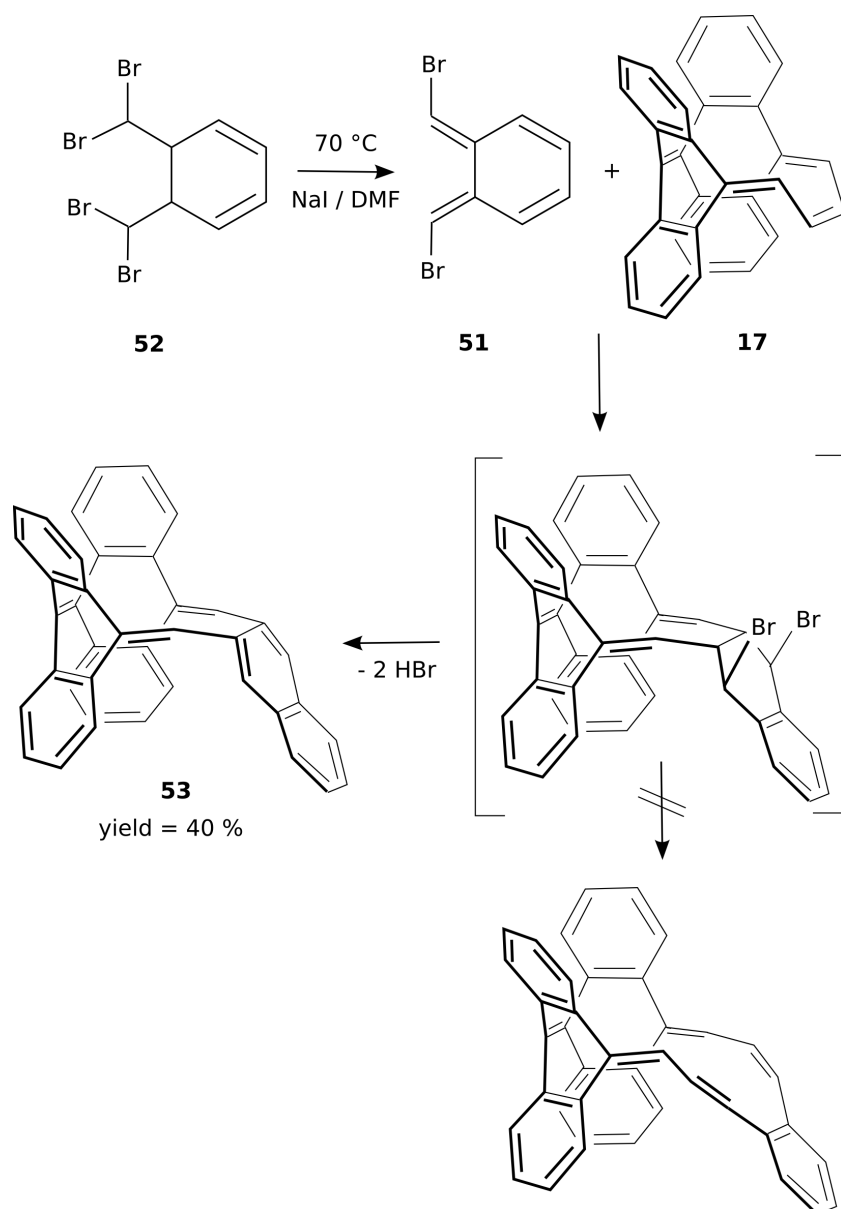
The photochemically induced metathesis reaction of TDDA **9** was extensively investigated. Dimerization of TDDA **9** to tetramer **7** was achieved by irradiation of a suspension of TDDA **9** in benzene in a photochemical reactor for 40 hours. Application of a sonifier (cell disruptor) and refluxing of the reaction mixture during irradiation led to the complete conversion of the starting materials within 3 hours. Further conversion of the tetramer **7** to the octamer and hexamer under similar conditions failed probably because of steric hindrance at the quinoid double bonds in the tetramer **7**. However, the tetramer **7** exhibited the peaks of the hexamer and the octamer upon irradiation by the laser in a MALDI-TOF mass spectrometer. The attempts to circumvent the technical problems are in progress.



Scheme 8.4: The unsuccessful reaction of the tetramer **7** to the hexamer and octamer.

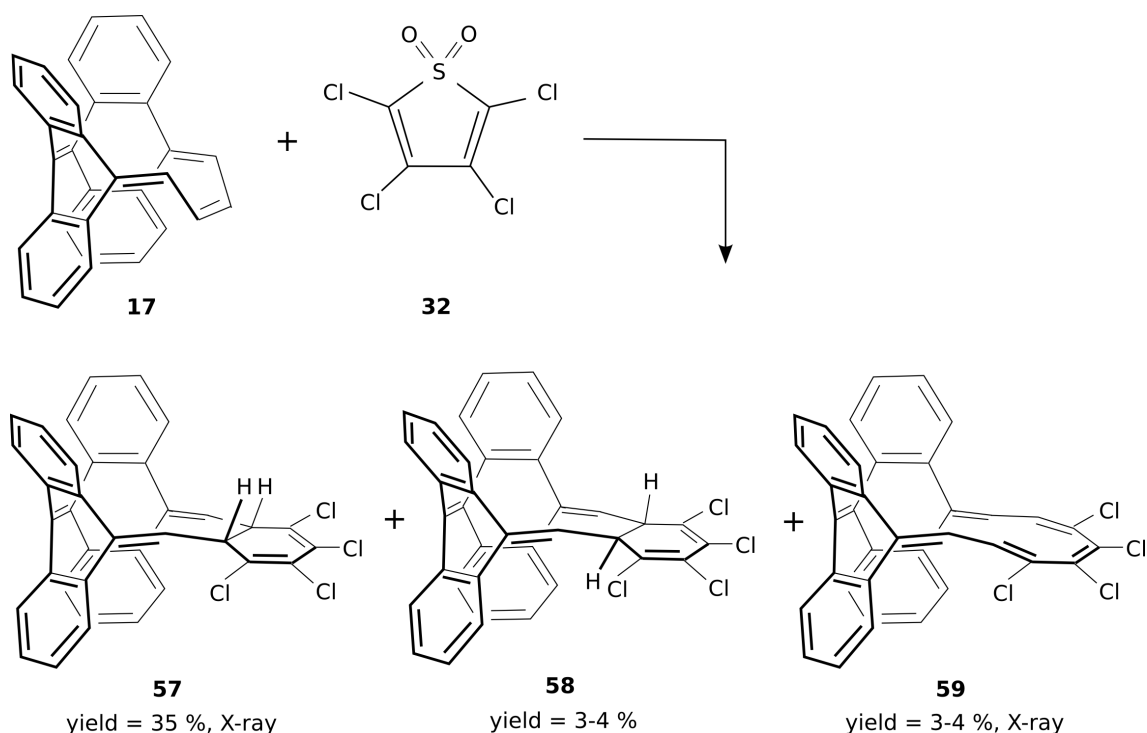
Another task in the course of our investigation was the synthesis of Möbius aromatic systems. The combination of in-plane aromaticity with normal conjugated π systems was supposed to provide a feasible synthetic route towards stable Möbius annulenes.

The Diels-Alder reaction of the $(\text{CH})_4$ -adduct **25** with tetrabromo-*o*-xylene **32** in presence of sodium iodide in dimethyl formamide yielded several products which were separated by reversed phase HPLC. MS analysis of the main product and comparison with the expected product revealed the lack of two mass units. Instead of the ring opening HBr was eliminated leading to the stable aromatic naphthalene system **53** (scheme 8.6).



Scheme 8.6: Mechanism of the formation of the naphthalene system **53**.

Diels-Alder reaction of the $(CH)_4$ -adduct **25** with tetrachlorothiophene dioxide (TTD) **32** yielded three compounds which were separated by combinations of reversed phase HPLC and normal phase HPLC (scheme 8.7).



Scheme 8.7: Diels-Alder reaction of the (CH)₄-adduct **25** with TTD **32**.

Two of the three separated compounds could be characterized by X-ray structure analysis. While compound **57** contains a ring-closed 1,3-hexadiene structure with C_s symmetry **57**, the other one is the ring-opened Hückel isomer **59** with C_s symmetry.

The irradiation of the C_s closed isomer **57** to form open isomers was a failure due to the photochemical formation of chlorine radicals. The thermal ring opening of the C_s isomer **57** successfully formed the C_s ring-opened Hückel isomer **59**. Attempts to thermally convert the C_2 closed isomer **58** to the C_2 ring-opened Möbius isomer have yet to be carried out.

Silver complexation of the semitrimer **21** was achieved by mixing silver hexafluoroantimonate and semitrimer **21** in THF. The resulting 1:1 complex crystals were obtained using the dichloromethane and ether diffusion method (figure 8.1). According to the crystal structure, there are two crystallographically independent complexes in the asymmetric unit. Each of the two silver atoms is disordered over two positions and some of the fluorine atoms of both hexafluoroantimonate anions exhibit unusually high anisotropic displacement parameters indicating disorder.

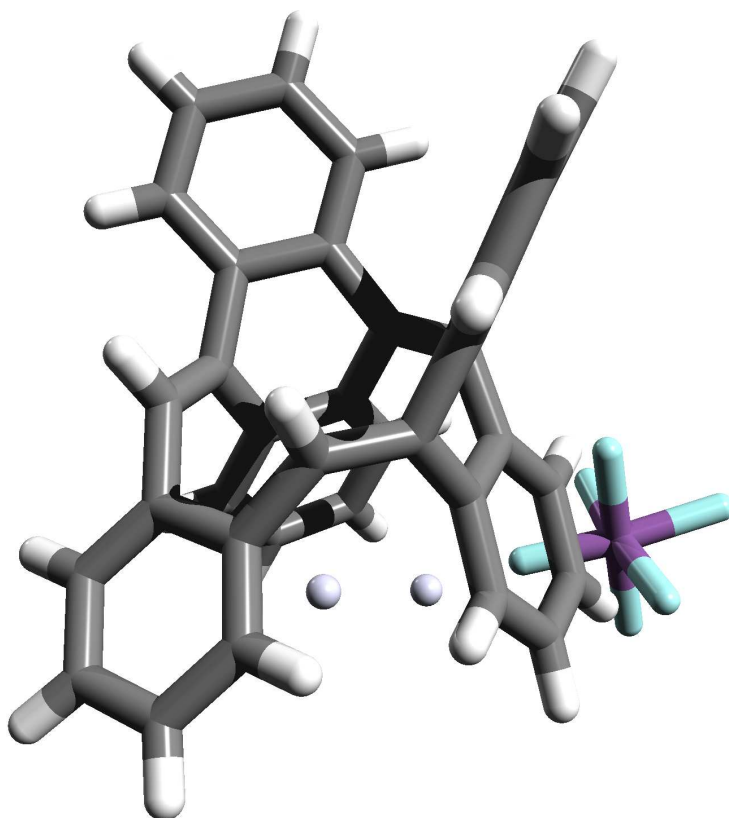


Figure 8.1: Crystal structure of the semitrimer-silver complex (only one complex displayed for clarity, the included molecule of diethyl ether is left out as well).

As anticipated, the silver atom is not coordinated to olefin bonds (olefinic complex) but to benzene rings (benzenoid complex). The crystals of the silver complex decomposed back to the semitrimer **21** upon exposure to air, moisture and light. The crystals were stable for two weeks at -20 °C in the dark and under argon.

9 Experimental Part

9.1 Apparatus

NMR: Samples were dissolved in deuteriochloroform (CDCl_3). Chemical shifts are reported in parts per million (ppm), from either tetramethylsilane (0 ppm) or chloroform (7.26 ppm) used as internal standard. For the multiplicities the following abbreviations were used: s = singlet, d = doublet, t = triplet, m = multiplet, q = quartet, br = broad signal, HP = pseudo. For the allocation of signals two dimensional NMR techniques were used (COSY, HSQC, HMBC and NOESY). The following spectrometers were used:

Bruker AC 200: ^1H -NMR (200.1 MHz), ^{13}C -NMR (50.3 MHz)

Bruker ARX 300: ^1H -NMR (300.1 MHz), ^{13}C -NMR (75.5 MHz)

Bruker DRX 500: ^1H -NMR (500.1 MHz), ^{13}C -NMR (125.8 MHz)

Bruker AV 600: ^1H -NMR (600.1 MHz), ^{13}C -NMR (150.9 MHz)

MS: The mass spectra are measured with the following mass spectrometers:

Finnigan MAT 8200

Applied Biosystems MarinerTM Biospectrometry work station

Bruker MALDI - TOF spectrometer BiflexTM III

IR: The IR spectra were measured with the FT-IR spectrometer Perkin Elmer Paragon 1000.

UV/Vis: The UV/Vis - spectra were recorded with the spectrometer Perkin Elmer Lambda 14.

Melting point: Melting points were recorded in open capillaries with a Büchi melting point B-540 and are not corrected.

Elementary analysis: Elementary analyses were accomplished with a Euro Vector Euro EA 3000 in the institute for inorganic chemistry of the Christian Albrechts - University of Kiel or externally by the micro-analytic laboratory Ilse Beetz.

X-Ray: The crystal structures measured on Image Plate Diffraction System (IPDS) of the company STOE and CIE with molybdenum-K α radiation of the wavelength 71.073 pm at the institute for inorganic chemistry of Christian-Albrechts-University of Kiel. Diffraction information have been solved with SHELXL-97.

HPLC: An analytical system of Agilent series 1100/1200 with configuration of degasser, quaternary pump, auto injector, auto sampler, diode array detector, automatic fraction collector and the following columns was used

Kromasil 100 C18 10 μm , 250 x 10 mm

Kromasil 100 C18 10 μm , 250 x 8 mm

Kromasil 100 C18 10 μm , 250 x 4 mm

Kromasil 100 Sil 10 μm , 250 x 8 mm

Kromasil 100 Sil 10 μm , 250 x 4 mm

LiChrospher 60 Si 10 μm , 250 x 4 mm

LiChrospher 60 Si 5 μm , 250 x 8 mm

LiChrospher 100 RP-18 10 μm , 250 x 4 mm

9.2 Common Procedure

Solvents have been purified and dried with the usual methods. Starting materials were purchased from Acros, Merck, Fluka, Aldrich and TCI companies.

The reaction progress was monitored with thin layer chromatography with silica gel 60 F₂₅₄ and aluminium oxide 60 F₂₅₄ plates from Macherey-Nagel company. New compounds were separated by Flash chromatography and HPLC. Suitable glass columns and silica gel (mesh: 0.04-0.063 μm) were applied in flash chromatography. The configurations of the applied preparative HPLC of Gilson company are M305 major pump, M306 mixing pump, 50 SC head pump, Gilson 117 UV detector and columns:

Kromasil 100 C18 10 μm , 250 x 20 mm (MZ-Analysentechnik)

Silicagel Si 100 (12 μm) 250 x 20 mm (MZ-Analysentechnik)

All photochemical reactions have been done in quartz apparatus with an extra cooling jacket with the following lamps:

High pressure mercury lamps:	150 Watts Heraeus TQ 150
	700 watts Heraeus TQ 718
Low pressure mercury lamp:	15 Watts Heraeus TNN 15/32

9.3 Rational Synthesis of Nanotubes and Möbius Aromatics

9.3.1 Synthesis of TDDA 9

9.3.1.1 Synthesis of 9-Bromoanthracene 11

Anthracene **10** (126.0 g, 0.706 mol) was dissolved in carbon tetrachloride (1000 ml) and under vigorous stirring at -6 °C bromine (35 ml, 0.679 mol) was added in carbon tetrachloride (200 ml). After 1 hour the yellowish precipitate was washed with carbon tetrachloride and dried over night in the air. The precipitate was transferred into a flask containing toluene (900 ml) and phenol (1.8 g). This mixture was stirred at room temperature for 5 days. The mixture was heated to -60 °C in order to drive out the developed HBr. The solution was washed with 1 M sodium hydrogen carbonate (300 ml) and toluene was evaporated. The resulting yellowish solid was washed with water and recrystallization from ethanol yielded light yellow to light green crystals (145.0 g, 80 %).

m.p. 98-100 °C

¹H-NMR (300 MHz, CDCl₃, TMS, 300 K): δ = 8.49 (dd, 3J = 9.1 Hz, 5J = 1.2 Hz, 2 H; H-1,8), 8.39 (s, 2 H; H-10), 7.96 (dd, 3J = 8.5 Hz, 5J = 1.2 Hz, 2 H; H-4,5), 7.58 (ddd, 3J = 9.1 Hz, 3J = 6.8 Hz, 5J = 1.2 Hz, 2 H; H-2,7), 7.47 (ddd, 3J = 8.5 Hz, 3J = 6.8 Hz, 5J = 1.2 Hz, 2 H; H-3,6).

9.3.1.2 Synthesis of 9, 10'-Dibromodianthracene **12**

A solution of 9-bromoanthracene **11** (80.0 g, 0.311 mol) in toluene (1000 ml) was irradiated with usual garden lamp (Osram HQL-R Deluxe, 80 W) for one month in a closed glass container. The resulting greenish crystals (40g) were separated and repeated recrystallization from toluene yielded the colourless crystals of 9, 10'-dibromodianthracene **12** (37.3 g, 47 %).

m.p. 250 °C

¹H-NMR (300 MHz, CDCl₃, TMS, 300 K): δ = 7.79-7.74 (m, 4 H, Ar-H), 7.02-6.88 (m, 12 H, Ar-H), 5.33 (s, 2H, CH).

9.3.1.3 Synthesis of Bistriazolindianthracene **13**

9,10'-dibromodianthracene **12** (14.06 g, 0.027 mol) and sodium azide (48.9 g, 0.752 mol) suspended in dimethylsulphoxide (700 ml). After 1 h stirring potassium *tert*-butoxide (24.4 g, 0.218 mol) in dimethyl sulphoxide (300 ml) was added dropwise. The reaction mixture was stirred for 14 d. at 30-35 °C and then poured on ice water. The light green solid was filtered and washed with water until it is base free and dried *in vacuo* (12 h). The product **13** (12.93 g, little water stays in the crystals) was used in the next step without further purification.

¹H-NMR (500 MHz, CDCl₃, TMS, 300 K): δ = 11.92-11.86 (m, 2 H, NH), 7.07-7.01 (m, 4 H, Ar-H), 6.98-6.82 (m, 12H, Ar-H).

9.3.1.4 Synthesis of *N*-aminobistraizolinedianthracene **14**

To a three neck flask with mechanical stirrer and dropping funnel sodium hydride (7.58 g, 0.158 mol) in dried dimethoxyethane (DME) was added and sonified with an ultrasonic bath. After 1 h the bistriazolinedianthracene **13** (12.93 g, 0.027 mol) was added portionwise. After 1 h of further sonification, a cold solution of *o*-mesitylenesulfonylhydroxylamine (Carpino's Reagent **15**, 16.7 g, 83.8 mmol) in DME was added in 1.5 h. After further 30 min of stirring, the flask was kept in the refrigerator over night. The solid was filtered and washed with

diethyl ether until it becomes colourless and stirred in water (550 ml) for 1.5 h. The solid was filtered and washed with water until it becomes neutral and dried *in vacuo* (9.87 g, 21.1 mmol).

m.p. 388°C

¹H-NMR (500 MHz, DMSO-*d*₆, DMSO, 300 K): δ = 7.05-6.80 (m, 16 H, Ar-H), 6.27, 6.30 (br, 4 H, NH₂).

9.3.1.5 Synthesis of Tetradehydrodianthracene **9**

To a sonicated solution of *N*-aminobistriazolindianthracene **14** (9.87 g, 21.1 mmol) in benzene triflouride (200 ml) lead tetraacetate (18.7 g, 42.2 mmol) was added portionwise until the gas development ceased. The excess of the lead tetraacetate was destroyed with half a pipette of ethylene glycol. The filtered solid was washed with benzene triflouride and dichloromethane and dried in the air. Later the solid was suspended in the sat. aq. sodium hydrogen carbonate and stirred for 1 hr. The solid was filtered, washed with water and dried over night. To remove the impurities, the solid was stirred in dichloromethane (300 ml) for 3 h, filtered and dried. Recrystallization from toluene provided light yellow crystals of TDDA **9** (3 g, 39.6 %).

m.p. 388 °C.

¹H-NMR (500 MHz, CDCl₃, TMS, 300 K): δ = 7.18 (dd, ³*J* = 5.4 Hz, ⁴*J* = 3.2 Hz, 8 H, Ar-H), 6.92 (dd, ³*J* = 5.4 Hz, ⁴*J* = 3.2 Hz, 8 H, Ar-H).

¹³C-NMR (CDCl₃/TMS): δ = 152.2 (s, C=C), 140.0 (s), 125.8 (d), 124.1(d).

9.3.2 Synthesis of *o*-Mesitylsulfonylhydroxylamin (Carpino's Reagent 15)

9.3.2.1 Synthesis of *tert*-Butyl Phenyl Carbonate

To a mechanically stirred solution of *tert*-butyl alcohol (296.5 g, 4.00 mol) and quinoline (519.2 g, 4.02 mol) in dichloromethane (600 ml) phenylchloroformate (500 ml, 3.97 mol) was added during 4 h. while maintaining the temperature below 30 °C. The solution was allowed to stand overnight, sufficient water was added to dissolve the precipitated salt and the layers were separated. The organic layer was washed two times with 250 ml portions of 5 % hydrochloric acid and twice with 200 ml of water. After drying on MgSO₄ the solvent was removed and the product was distilled (499.7 g, 66 %).

b.p. 90-95°C / 1 mbar

¹H-NMR (500 MHz, CDCl₃, TMS, 300 K): δ = 7.40-7.14 (m, 5 H; phenyl), 1.31 (s, 9 H; *tert*-butyl).

9.3.2.2 Synthesis of *tert*-Butyl Carbazate

A mixture of *tert*-butyl phenyl carbonate (499.7 g, 2.58 mol) and 65 % hydrazine (267.5 ml, 7.31 mol) was warmed slowly over a period of 4 h. in an oil bath to 75 °C. At this temperature spontaneously the reaction temperature rises to 103 °C. The clear solution was then stirred at room temperature for additional 12 h. and diluted with ether (1000 ml) and shaken well with 150 g of potassium hydroxide solution. The mixture was extracted with ether for 24 h. in continuous extractor. The solvent was removed under vacuum and the product was distilled (328.9 g, 85 %).

b.p. 85 °C / 1.33 mbar.

¹H-NMR (300 MHz, CDCl₃, TMS, 300 K): δ = 6.48 (s, 1 H; NH), 3.80 (s, 2 H; NH₂), 1.45 (s, 9 H; *tert*-Butyl).

9.3.2.3 Synthesis of *tert*-Butyl Azidoformate

A solution of *tert*-butyl carbazate (264.3 g, 2.00 mol), glacial acetic acid (211 ml) in water (315 ml) was cooled in an ice-bath to 0 °C and with vigorous stirring a solution of sodium nitrite (144.0 g, 2.08 mol) was added dropwise. As soon as the yellowish phase started to get dark, the addition was stopped and phases were separated immediately. The aqueous layer was extracted four times with 100 ml portions of ether. The combined organic layers were washed three times with 150 ml portions of water and three times with 150 ml portions of 1 M sodium bicarbonate solution. The light yellow solution was dried over magnesium sulphate, the solvent was removed and the remaining mixture distilled (154.1 g, 56%).

b.p. 71°C / 93 mbar.

¹H-NMR (300 MHz, CDCl₃, TMS, 300 K): δ = 1.50 (s, 9 H; *tert*-butyl).

9.3.2.4 Synthesis of *tert*-Butyl *N*-hydroxycarbamate

A solution of hydroxylamine hydrochloride (100.2 g, 1.44 mol) in water (200 ml) was cooled in an ice bath and *tert*-butyl azidoformate (154.1 g, 1.08 mol) was added. While stirring vigorously, a cold solution of sodium hydroxide (194.3 g, 4.31 mol) in water (400 ml) was dropped in during 40 min. The mixture was allowed to stir in the ice bath for one hour and water (800 ml) was added to dissolve the formed precipitate. The solution was extracted twice with 500 ml portions of ether and extracts were discarded. The aqueous solution was cooled in an ice bath and acidified to pH 5-6 with 6 N hydrochloric acid (700 ml), the resulting mixture was extracted with five 400 ml portions of ether, then dried on MgSO₄ and the solvent was removed. The thick oil solidified within several hours after placing in a vacuum desiccator giving crystals. (77.9 g, 55%).

m.p. 50°C

¹H-NMR (500 MHz, CDCl₃, 300 K): δ = 7.33 (s, 1 H; NH), 7.14 (s, 1 H; OH), 1.47 (s, 9 H, *tert*-butyl).

9.3.2.5 Synthesis of *tert*-butyl-*N*-*p*-toluenesulfonylcarbamate

To a solution of *tert*-butyl-*N*-hydroxycarbamate (33.2 g, 0.250 mol) and *p*-toluenesulfonyl chloride (54.5 g, 0.249 mol) in ether (800 ml) at 0 °C triethylamine (35 ml, 0.250 mol) was added dropwise. After standing 30 min in the ice bath the solution was filtered and washed with ether. The ether phases were combined and half of the ether was removed. The remaining solution was washed with water, dried on MgSO₄ and evaporated. Upon standing for an hour the collected colourless oil will convert to a colourless solid (65 g, 83%).

m.p. 95-100°C

¹H-NMR (500 MHz, CDCl₃, TMS, 300 K): δ = 8.05 (s, 1 H; NH), 6.95 (s, 2 H; Phenyl), 2.67 (s, 6 H; PhCH₃), 2.32 (s, 3 H; PhCH₃), 1.31 (s, 9 H; *tert*-Butyl).

9.3.2.6 Synthesis of Hydroxyl Amine-*o*-Mesitylene Sulfonate 15 (Carpino's Reagent)

Trifluoroacetic acid (110 g) was added to *tert*-butyl-*N*-*p*-toluenesulfonylcarbamate (30.3 g, 0.102 mol) at 0°C. Vigorous gas development occurred and was allowed to subside between addition and then cooled water (400 ml, 5 °C) was added. The mixture was filtered and the solid was washed with water until its pH is neutral and the compound was dried. The solid was dissolved in the minimum amount of ether (50-70 ml) and the water phase was separated. Pentane (150-200 ml) was added to the ether phase and the resulting white crystals were filtered and dried (16.7 g, 76 %).

¹H-NMR (500 MHz, CDCl₃, 300 K): δ = 7.00 (s, 2 H; phenyl), 4.98 (s, 2 H; NH), 2.65 (s, 6 H; PhCH₃), 2.32 (s, 3 H; PhCH₃).

9.3.3 Synthesis of the Semitrimer **21**

Method A: A mixture of $\alpha,\alpha,\alpha',\alpha'$ -tetrabromo-*o*-xylene **52** (422 mg, 1 mmol), sodium iodide (2 g), TDDA (200 mg, 0.57 mmol) and dry dimethylformamide (10 ml) was stirred at 60-70 °C for 24 h. The reaction mixture was poured into water (150 ml) containing sodium bisulphite (2 g). The brown precipitate was purified by silica gel flash chromatography with 4:1 hexane/dichloromethane as the mobile phase. The semitrimer **21** was obtained as a white powder (155 mg, 60 %).

Method B: A mixture of TDDA **9** (50 mg, 0.14 mmol), phthalazine **26** (200 mg, 1.538 mmol) and the radical quencher 3-*tert*-butyl catechol were heated to 220 °C for 30 min under nitrogen flow. The reaction mixture was separated by silica gel flash chromatography with 4:1 hexane/dichloromethane as the mobile phase. The first fraction was unreacted TDDA **9** and the second fraction yielded the semitrimer **21** in 17 %. Colourless single crystals of the semitrimer **21** were obtained from the mixture of heptane/dichloromethane.

m.p. 335 °C

¹H-NMR (500 MHz, CDCl₃, 300 K, TMS): δ = 7.61 (dd, $^3J = 7.4$ Hz, $^4J = 1.4$ Hz, 2 H, CH arom.), 7.45-7.41 (m, 2 H, CH arom.), 7.39 (dd, $^3J = 7.45$ Hz, $^4J = 1.2$ Hz, 2 H, CH arom.), 7.29 (dd, $^3J = 7.0$ Hz, $^4J = 1.5$ Hz, 2 H, CH arom.), 7.25-7.20 (m, 2 H, CH arom.), 7.16-7.08 (m, 6H), 6.90 (td, $^3J = 7.5$ Hz, $^4J = 1.3$ Hz, 2H, CH arom.), 6.83 (td, $^3J = 7.6$ Hz, $^4J = 1.3$ Hz, 2H, CH arom.), 6.41 (s, 2H, CH olef.).

¹³C-NMR (125 MHz, CDCl₃, 300 K, TMS): δ = 141.80 (C_q, C=C bridgehead), 141.04 (C_q, CR₂=CHR), 140.40 (C_q), 139.90 (C_q), 137.46 (C_q), 137.03 (C_q), 135.25 (C_q), 129.20 (CH, olefinic), 129.02 (CH, arom.), 126.67 (CH, arom.), 126.54 (CH, arom.), 126.40 (CH, arom.), 126.08 (CH, arom.), 125.49 (CH, arom.), 125.32 (CH, arom.), 125.13 (CH, arom.), 124.90 (CH, arom.), 121.90 (CH, arom.).

MS (70 eV): m/z (%): 454 (100) [M⁺].

9.3.4 Attempted Trimer Synthesis

9.3.4.1 Preparation of 1,4-Dibromophthalazine

A mixture of 1,4 dioxophthalazine (0.81 g, 0.005 mol), phosphorus pentabromide (4.75 g, 0.011 mol) and carbon tetrabromide (25 g) were heated at 120-130 °C for 6 h. The reaction mixture was cooled to room temperature and treated with dichloromethane (12.5 ml) until all lumps has been disintegrated. This mixture poured under vigorous stirring into ice water (50 ml) and stirring continued for 2 h. The resulting yellow solid was filtered and washed with ether and petroleum ether. Upon recrystallization from THF white crystals were obtained (0.28 g, 20%).

m.p. 160 °C

9.3.4.2 Attempted Diels-Alder Reaction of 1,4-Dibromophthalazine with TDDA 9

A mixture of 1,4 dibromophthalazine (75 mg, 0.26 mmol) and TDDA 9 (25 mg, 0.071 mmol) were refluxed in 15 ml of toluene. The solvent was removed *in vacuo*. There was no evidence of the addition product after chromatographic analysis.

9.3.4.3 Attempted Diels-Alder reaction of 1,4 dichloro phthalazine with TDDA

A mixture of 1,4 dichlorophthalazine (90 mg, 0.34 mmol) and TDDA 9 (30 mg, 0.085 mmol) were refluxed in 15 ml of toluene. The solvent was removed *in vacuo*. There was no evidence of the addition product after chromatographic analysis.

9.3.4.4 Solid state reaction of 1,4 dihalophthalazine with TDDA 9

A mixture of TDDA 9 (25 mg, 0.071 mmol) and dihalophthalazine (75 mg, 0.26 mmol) and the radical quencher 3-*tert*-butyl catechol were heated to 220 °C for 30 min under nitrogen flow.

The reaction mixture was separated by silica gel flash chromatography with 4:1 hexane/dichloromethane as the mobile phase. The product was decomposed in the process of chromatographic analysis.

9.3.4.5 Reaction of Schlosser's Base with the Semitrimer **21**

Schlosser's base (*n*-butyl lithium (0.08 ml, 2.5 M, 0.2 mmol) + potassium *tert*-butoxide (22.4 mg, 0.2 mmol)) in 5 ml dried THF was added dropwise at 0 °C to the semitrimer **21** (45.4 mg, 0.1 mmol) under nitrogen flow. As soon as the colour changed to green products were quenched with D₂O. The product analysis shows only the semitrimer **21**.

n-Butyl lithium was added drop wise to a mixture of semitrimer **21** (45.4 mg, 0.1 mmol) and potassium *tert*-butoxide (22.4 mg, 0.2 mmol) in 5 ml THF at -78 °C. The reaction temperature was raised to 0 °C over a period of 12 h and the reaction colour changed from light pink to dark pink. At 0 °C a sample of the of reaction mixture was dropped into an excess of methyl iodide in THF. The remaining reaction mixture was cooled to -50 °C and quenched with D₂O and methyl iodide. In all the above cases the product analysis shows only the semitrimer **21**.

9.3.4.6 Halogenation of the Semitrimer **21**

9.3.4.6.1 Bromination of the Semitrimer **21** in Non-polar Solvents

A solution of bromine (70.5 mg, 0.44 mmol) in carbon tetrachloride (5 ml) was added dropwise to a solution of the semitrimer **21** (100 mg, 0.22 mmol) in carbon tetrachloride (20 ml) at 0 °C under nitrogen flow. After stirring for 1.5 h the reaction mixture was treated with sodium carbonate solution. The organic layer was separated, dried and the solvent was removed *in vacuo*. The brown precipitate was filtered through a short silica gel column with dichloromethane as the mobile phase and then the products were separated with reversed phase HPLC (85:15) with acetonitrile and water as mobile phase. The product with the required mass **24** was separated and single crystals were grown from a mixture of CS₂ and acetonitrile.

m.p. 310°C

¹H-NMR (600 MHz, CDCl₃, 300 K, TMS): δ = 8.59 (dd, $^3J = 7.8$ Hz, $^4J = 1.5$ Hz, 1 H; CH arom.), 8.22 (dd, $^3J = 7.8$ Hz, $^4J = 1.4$ Hz, 1 H, CH arom.), 7.98 (d, $^3J = 7.4$ Hz, 1 H, CH arom.), 7.77 (d, $^3J = 7.6$ Hz, 1 H, CH arom.), 7.63 (m, 2 H, CH arom.), 7.50 (dt, $^3J = 7.4$ Hz, $^4J = 1.1$ Hz, 1 H, CH arom.), 7.44 (d, $^3J = 7.3$ Hz, 1 H, CH arom.), 7.36 (d, $^3J = 7.4$ Hz, 1 H, CH arom.) 7.16 (d, $^3J = 7.4$ Hz, 1 H, CH arom.), 7.09 (m, 2H, CH arom.), 6.97 (m, 2H, CH arom.), 6.90 (m, 2H, CH arom.), 6.69 (m, 3H, CH arom.), 6.48 (d, $^3J = 7.3$ Hz, 1 H, CH arom.).

¹³C-NMR (150.9 MHz, CDCl₃, 300 K, TMS): δ = 153.21 (C_q), 148.50 (C_q), 146.70 (C_q), 146.46 (C_q), 146.07 (C_q), 144.22 (C_q), 143.22 (C_q), 142.63 (C_q, C=C-Br), 141.78 (C_q), 139.32 (C_q), 129.25 (C_q), 128.97 (CH, arom.), 128.18 (CH, arom.), 127.15 (CH, arom.), 126.88 (CH, arom.), 126.64 (CH, arom.), 126.51 (CH, arom.), 126.33 (CH, arom.), 126.30 (CH, arom.), 126.07 (CH, arom.), 125.16 (CH, arom.), 124.95 (CH, arom.), 124.15 (CH, arom.), 123.57 (CH, arom.), 122.61 (CH, arom.), 122.40 (CH, arom.), 122.04 (CH, arom.), 121.57 (CH, arom.), 120.79 (CH, arom.), 113.84 (C_q), 90.10 (C_q), 77.71 (C_q, C-Br), 70.12 (C_q), 64.85 (C_q).

9.3.4.6.2 Bromination of the Semitrimer **21** in Polar Solvents

A solution of bromine (35.5 mg, 0.44 mmol) in trifluoro ethanol (5 ml) was added dropwise to a solution of the semitrimer **21** (50 mg, 0.11 mmol) in trifluoro ethanol (10 ml) under nitrogen flow. After 1.5 h the reaction mixture was poured into water and the compound was extracted with dichloromethane. The product analysis shows no evidence of the formation of the addition product.

9.3.4.7 *N*-Bromo Succinimide Treatment of the *o*-Chinodimethane Adduct **28**

9.3.4.7.1 Synthesis of the *o*-Chinodimethane Adduct **28**

75 mg (0.213 mmol) of TDDA was suspended in 10 ml of DMF with 50 mg of zinc powder. Then 84 mg of α,α' -dibromo-*o*-xylene in 10 ml of DMF was added dropwise to the

suspension over a period of 5 h. The solvent was removed under vacuum and the residue was subjected to chromatography on silica gel with 2:1 hexane / dichloromethane as the mobile phase. The required compound was separated with $R_f = 0.37$ (66 mg, 68%).

m.p. 240-243 °C

$^1\text{H-NMR}$ (500 MHz, CDCl_3 , TMS, 300 K): $\delta = 7.58$ (m, 2 H, CH; arom.), 7.30 (m, 4 H, CH; arom.), 7.15 (m, 2 H, CH; arom.), 7.05 (m, 2 H, CH; arom.), 6.93 (m, 4 H, CH; arom.), 6.80 (m, 2 H, CH; arom.), 6.65 (m, 2 H, CH; arom.), 3.92 (d, $^3J = 14.6$ Hz, 2 H, CH_2), 3.36 (d, $^3J = 14.6$ Hz, 2 H, CH_2).

9.3.4.7.2 Treatment of the *o*-Chinodimethane Adduct **28** with NBS

The *o*-chinodimethane adduct **28** (30 mg, 0.0657 mmol) was treated with *N*-bromo succinimide (51.5 mg, 0.29 mmol) in CCl_4 (15 ml) under reflux conditions for 19 h. The reaction mixture was hot filtered to remove the succinimide and the solvent was removed under vacuum. The brown precipitate was filtered through a short column with dichloromethane as the mobile phase and then the products were separated with reversed phase HPLC (85:15) with acetonitrile and water as the mobile phase. The product with the required mass was separated and single crystals were grown from CS_2 and acetonitrile by layering method.

9.3.4.8 Diels-Alder Reaction of TDDA with *o*-Chloranil

A mixture of TDDA **9** (30 mg, 0.085 mmol) and *o*-chloranil **30** (53 mg, 0.21 mmol) was stirred at room temperature in toluene (25 ml) for 2 h. The solvent was removed under vacuum and the mixture was subjected to chromatography on silica gel with 4:1 hexane/dichloromethane as the mobile phase. The first fraction separated was compound **31**.

m.p. 360°C

¹H-NMR (500 MHz, CDCl₃, TMS, 300 K): δ = 7.18 (dd, ³*J* = 7.7 Hz, ⁴*J* = 0.7 Hz, 4H, CH arom.), 7.08 (dd, ³*J* = 7.3 Hz, ⁴*J* = 0.8 Hz, 4 H, CH arom.), 6.92 (dt, ³*J* = 7.4 Hz, ⁴*J* = 1.2 Hz, 4 H, CH arom.), 6.85 (dt, ³*J* = 7.6 Hz, ⁴*J* = 1.3 Hz, 4 H, CH arom.).

9.3.5 Synthesis of the Tetramer **7**

A suspension of TDDA **9** (1.00 g, 2.84 mmol) in benzene (60 ml) in a quartz photo reactor with FC-40 compound (40 ml) with nitrogen gas flow and 250 W ultrasonic probe (50 % output) was irradiated with a 700 W high pressure mercury lamp for 3 h. The benzene phase was separated and evaporated. After chromatography with a silica gel flash column with 2:1 hexane / dichloromethane as the mobile phase, the tetramer **7** was recrystallized several times from pentane/dichloromethane until it is pure (210 mg, 35 %).

¹H-NMR (500 MHz, CS₂, CDCl₃ (1:1), 300 K) δ = 7.93 (dd, ³*J* = 5.7 Hz, ⁴*J* = 3.4 Hz, 16 H; CH arom.), 7.15 (dd, ³*J* = 5.7 Hz, ⁴*J* = 3.4 Hz, 16 H; CH arom.).

MS (70 eV): *m/z* (%): 704 (100) [M⁺], 352 (15) [M²⁺].

9.3.6 Attempted Synthesis of Möbius Hydrocarbons

9.3.6.1 Synthesis of the (CH)₄ Adduct **17**

A mixture of TDDA **9** (100 mg, 0.284 mmol) and pyridazine (350 mg, 4.38 mmol) was refluxed under nitrogen in 70 ml of toluene for 20 h. The solvent was removed under vacuum and the brown solid was subjected to chromatography on silica gel with 4:1 hexane/dichloromethane as the mobile phase. The (CH)₄ adduct **17** was separated as a half white solid (92 mg, 80 %).

m.p. 242 °C.

¹H-NMR (400 MHz, CDCl₃, TMS): δ = 7.58 (dd, ³*J* = 7.3 Hz, ⁴*J* = 1.3 Hz, 2 H; CH arom.), 7.47 (dd, ³*J* = 7.5 Hz, ⁴*J* = 1.4 Hz, 2 H; CH arom.), 7.19 (dd, ³*J* = 7.3 Hz, ⁴*J* = 1.3 Hz, 2 H; CH

arom.), 7.12-7.01 (m, 6 H; CH arom.), 6.96-6.90 (m, 4 H; CH arom.), 6.45 (d, $^3J = 2.0$ Hz, 2 H; HC=C), 5.86 (d, $^3J = 2.0$ Hz, 2 H; HC=C).

MS (70 eV): m/z (%): 404 (100) [M^+].

9.3.6.2 Synthesis of the Naphthalene System 53

A mixture of carbon tetrabromide (188 mg, 0.44 mmol), sodium iodide (0.4 g), (CH)₄ adduct **17** (90 mg, 0.22 mmol) and dry dimethylformamide (1.5 ml) was stirred at 60-70 °C for 15 h. Then the reaction mixture was poured into water (25 ml) containing sodium bisulphite (0.4 g). The brown precipitate was filtered through a short column with dichloromethane as the mobile phase and then the products were separated with reversed phase HPLC. Two products were successfully separated, one is the naphthalene system **53** (40%), the other could be identified as the iodine attacked naphthalene system **54** (5%).

Naphthalene system 53:

Crystals of this compound were grown from dichloromethane and ether in diffusion method.

m.p. 333 °C

¹H-NMR (500 MHz, CDCl₃, TMS, 300K): $\delta = 7.79$ (s, 2H), 7.79-7.77 (m, 2 H, CH arom.), 7.56 (dd, $^3J = 7.1$ Hz, $^4J = 1.6$ Hz, 2 H, CH arom.), 7.42-7.38 (m, 2 H, CH arom.), 7.31 (dd, 2 H, $^3J = 7.4$ Hz, $^4J = 1.2$ Hz, CH arom.), 7.26 (dd, $^3J = 7.3$ Hz, $^4J = 1.4$ Hz, 2 H, CH arom.), 7.16 (dd, $^3J = 7.6$ Hz, $^4J = 0.9$ Hz, 2H, CH arom.), 7.09 (td, $^3J = 7.5$ Hz, $^4J = 1.5$ Hz, 2 H, CH arom.), 7.05 (td, $^3J = 7.4$ Hz, $^4J = 1.5$ Hz, 2 H, CH arom.), 6.80 (td, $^3J = 7.6$ Hz, $^4J = 1.2$ Hz, 2 H, CH arom.), 6.71 (td, $^3J = 7.6$ Hz, $^4J = 1.2$ Hz, 2 H, CH arom.), 6.47 (s, 2 H, CH olef.).

¹³C-NMR (125 MHz, CDCl₃, TMS, 300 K): $\delta = 142.07$ (C_q), 141.21 (C_q), 140.51 (C_q), 139.96 (C_q), 137.2 (C_q), 135.76 (C_q), 135.25 (C_q), 132.73 (C_q), 131.22 (CH, arom.), 128.84 (CH, olef.), 127.92 (CH; naphthalene), 127.74 (CH, arom.), 126.94 (CH, arom.), 126.82 (CH,

arom.), 126.73 (CH, arom.), 126.48 (CH, arom.), 125.95 (CH, arom.), 125.62 (CH, arom.), 122.43 (CH, arom.).

MS (70 eV): m/z (%): 504 (100) [M⁺].

Iodine attacked naphthalene system 54:

Crystals of this compound were obtained from a heptane/dichloromethane mixture.

¹H-NMR (500 MHz, CDCl₃, TMS, 300 K): δ = 8.07 (s, 1 H, CH arom.), 8.03 (s, 1 H, CH arom.), 7.90 (d, 1 H, ³ J = 8.0 Hz, CH arom.), 7.82 (d, 1H, ³ J = 7.8 Hz, CH arom.), 7.74 (dd, 1 H, ³ J = 7.6 Hz, ⁴ J = 1.0 Hz, CH arom.), 7.65 (d, 1 H, ³ J = 7.1 Hz, CH arom.), 7.57 (dd, 1 H, ³ J = 7.4 Hz, ⁴ J = 0.8 Hz, CH arom.), 7.48 (m, 2 H, CH arom.), 7.33 (dd, 1 H, ³ J = 7.6 Hz, ⁴ J = 1.1 Hz, CH arom.), 7.25 (m, 1 H, CH arom.), 7.05 (m, 6 H, CH arom.), 6.89 (dt, 1 H, ³ J = 7.5 Hz, ⁴ J = 0.9 Hz, CH arom.), 6.80 (dt, 1 H, ³ J = 7.5 Hz, ⁴ J = 1.2 Hz, CH arom.), 6.72 (m, 1 H, CH arom.), 6.72 (dt, 1 H, ³ J = 7.5 Hz, ⁴ J = 1.2 Hz, CH arom.), 6.59 (dt, 1 H, ³ J = 7.6 Hz, ⁴ J = 1.1 Hz, CH arom.), 4.46 (s, 1 H, CH aliph.), 4.18 (d, 1 H, ³ J = 15.6 Hz, CH₂), 3.93 (d, 1 H, ³ J = 16.0 Hz, CH₂).

¹³C-NMR (125 MHz, CDCl₃, TMS, 300 K): δ = 152.06 (C_q), 150.90 (C_q), 149.87 (C_q), 147.85 (C_q), 147.61 (C_q), 142.88 (C_q), 142.29 (C_q), 140.39 (C_q), 139.55 (C_q), 138.47 (C_q), 133.29 (C_q), 132.73 (C_q), 127.79 (C_q), 127.60 (C_q), 127.38 (CH, arom.), 126.22 (CH, arom.), 126.15 (CH, arom.), 125.83 (CH, arom.), 125.69 (CH, arom.), 125.59 (CH, arom.), 125.32 (CH, arom.), 125.20 (CH, arom.), 125.03 (CH, arom.), 124.89 (CH, arom.), 124.83 (CH, arom.), 124.77 (CH, arom.), 124.68 (CH, arom.), 124.57 (CH, arom.), 124.18 (CH, arom.), 123.80 (CH, arom.), 123.70 (CH, arom.), 122.45 (CH, arom.), 122.02 (CH, arom.), 121.91 (CH, arom.), 119.47 (CH, arom.), 59.31(CH, aliph), 32.73(CH₂).

9.3.6.3 Attempted Diels-Alder Reaction of the (CH)₄ Adduct 17 with Pyridazine

A mixture of the (CH)₄ adduct **17** (75 mg, 0.185 mmol), pyridazine (18 mg, 0.25 mmol) in toluene (20 ml) were exposed to 80 °C at 12 Kbar for 24 h. The solvent was removed under vacuum. There was no evidence of any addition product after the chromatographic analysis.

9.3.6.4 Reaction of the (CH)₄ Adduct with Tetrachlorothiophene Dioxide 32

9.3.6.4.1 Preparation of Tetrachlorothiophene Dioxide 32 (TTD)

In a 50 ml three-necked flask with a pressure-equalizing dropping funnel, 3.7 ml (38.3 mmol) 30 % H₂O₂ was added and cooled to -10 °C in a NaCl / ice bath. Trifluoroacetic anhydride (8.5 ml, 38.5 mmol) was added dropwise during 1.5 h, and the reaction mixture was stirred for an additional 0.5 h. Concentrated H₂SO₄ (6.9 ml) was added dropwise over 0.5 h, and stirring was continued for another 0.5 h. Volatiles (mainly peroxytrifluoroacetic acid and trifluoroacetic acid) were vacuum transferred into a liquid nitrogen-cooled trap. In another 50 ml round bottom flask, tetrachlorothiophene (500 mg, 2.30 mmol) was dissolved in 10 ml of methylene chloride. The peroxytrifluoroacetic acid solution was added dropwise over 1 h at room temperature, and the mixture was stirred over night. Volatiles were removed using an aspirator. The received crude product was sublimated (7-8 mbar, 65 °C) to get 437.2 mg (76.4 %) of pure product.

m.p. 88-90 °C (lit^[71] 90-91 °C).

MS (EI, 70 eV): m/z (%) = 254 (100) [M⁺]

9.3.6.4.2 Reaction of TTD 32 with the (CH)₄ Adduct 17

The (CH)₄ adduct **17** (176 mg, 0.435 mmol) was treated with TTD **32** (276 mg, 1.09 mmol) in toluene at 90 °C for 15 hrs. After completion of the reaction the solvent was removed under vacuum. The crude product was dissolved in dichloromethane and passed through a short column of silica and then combinations of reversed and normal phase HPLC were used to separate the formed products.

C_s Hückel ring-opened product 59

Crystals of this compound were grown from chloroform and pentane by diffusion method.

m.p. 319°C.

¹H-NMR (600 MHz, CDCl₃, TMS, 300 K): δ = 7.70 (dd, ³*J* = 7.3 Hz, ⁴*J* = 1.3 Hz, 2 H, CH arom.), 7.66 (dd, ³*J* = 7.3 Hz, ⁴*J* = 0.9 Hz, 2 H, CH arom.), 7.38 (dd, ³*J* = 7.6 Hz, ⁴*J* = 1.1 Hz, 2 H, CH arom.) 7.22-7.09 (m, 10 H), 6.50 (d, ³*J* = 10.5 Hz, 2 H), 6.24 (d, ³*J* = 10.5 Hz, 2 H).

¹³C-NMR (150.9 MHz, CDCl₃, TMS, 300 K): δ = 144.75 (C_q), 138.94 (C_q), 138.41 (C_q), 138.33 (C_q), 135.48 (C_q), 134.47 (C_q), 133.89 (C_q), 133.31 (CH, olef.), 128.55 (CH, arom.), 127.88 (CH, arom.), 127.26 (CH, arom.), 127.10 (CH, arom.), 126.53 (CH, arom.), 126.35 (CH, arom.), 125.94 (CH, arom.), 125.94 (C_q), 122.61 (CH, arom.), 120.36 (CH, olef.).

UV/Vis (CHCl₃): λ_{\max} (ϵ) = 268 (20590), 320 (29143) nm.

MS (EI, 70 eV): *m/z* (%) = 594 (55) [M⁺], 557 (100).

C_s ring-closed product 57

Crystals of this compound were grown by slow evaporation its benzene solution.

m.p. 319°C

¹H-NMR (600 MHz, CDCl₃, TMS, 300 K): δ = 7.49 (dd, ³*J* = 7.5 Hz, ⁴*J* = 0.7 Hz, 2 H), 7.47 (dd, ³*J* = 7.4 Hz, ⁴*J* = 0.8 Hz, 2 H), 7.30 (dd, ³*J* = 7.5 Hz, ⁴*J* = 0.7 Hz, 2 H), 7.10 (dd, ³*J* = 7.44 Hz, ⁴*J* = 1.20 Hz, 2 H), 7.03 (ddd, ³*J* = 7.6 Hz, ³*J* = 7.6 Hz, ⁴*J* = 1.3 Hz, 2 H), 7.02 (ddd, ³*J* = 7.6 Hz, ³*J* = 7.6 Hz, ⁴*J* = 1.3 Hz, 2 H), 6.97 (ddd, ³*J* = 7.6 Hz, ³*J* = 7.6 Hz, ⁴*J* = 1.3 Hz, 2 H), 6.96 (ddd, ³*J* = 7.6 Hz, ³*J* = 7.6 Hz, ⁴*J* = 1.3 Hz, 2 H), 5.48-5.42 (m, 2 H), 4.28-4.22 (m, 2 H).

¹³C-NMR (150.9 MHz, CDCl₃, TMS, 300 K): δ = 141.63 (C_q), 140.73 (C_q), 140.70 (C_q), , 139.50 (C_q), 137.52 (C_q), 134.52 (C_q), 131.09 (C_q), 127.40 (CH, arom.), 126.72 (CH, arom.),

126.41 (CH, olef.), 126.41 (CH, arom.), 126.13 (CH, arom.), 126.06 (CH, arom.), 125.64 (CH, arom.), 125.10 (CH, arom.), 123.67 (C_q), 122.24 (CH, arom.), 45.15 (CH, aliph.).

MS (EI, 70 eV): m/z (%) = 594 (55) [M⁺], 557 (100)

C₂ ring-closed product 58

m.p. 319°C

¹H-NMR (500 MHz, CDCl₃, TMS, 300 K): δ = 7.57 (d, ³J = 7.4 Hz, 2H), 7.22 (dd, ³J = 7.1 Hz, ⁴J = 1.6 Hz, 2 H), 7.18-7.06 (m, 8 H) 6.90-6.81 (m, 4 H), 5.08-5.02 (m, 2 H), 3.75-3.69 (m, 2 H).

¹³C NMR (150.9 MHz, CDCl₃, TMS, 300 K): δ = 141.19 (C_q), 140.84 (C_q), 140.48 (C_q), 140.45 (C_q), 137.36 (C_q), 133.50 (C_q), 130.59 (C_q), 129.07 (C_q), 128.26 (CH, arom.), 127.59 (CH, arom.), 127.54 (CH, arom.), 126.66 (CH, olef.), 125.98 (CH, arom.), 125.55 (CH, arom.), 125.37 (CH, arom.), 124.74 (CH, arom.), 121.68 (CH, arom.), 48.75 (CH, aliph.).

MS (EI, 70 eV): m/z (%) = 594 (55) [M⁺], 557 (100)

9.4 Silver complexation of Semitrimer with Silver(I) hexafluoroantimonate

To the (15 mg, 0.033 mmol) of semitrimer in dry THF under nitrogen was added silver hexafluoroantimonate (34 mg., 0.099 mmol). The mixture was stirred for 1 hour at room temperature. The solvent was removed under vacuum. Single crystals were grown by dissolving the residue in little dichloromethane and ether was diffused and colourless crystals were obtained.

9.5 X-ray Structure Data

9.5.1 Semitrimer 21

Table 1. Crystal data and structure refinement for herges32.

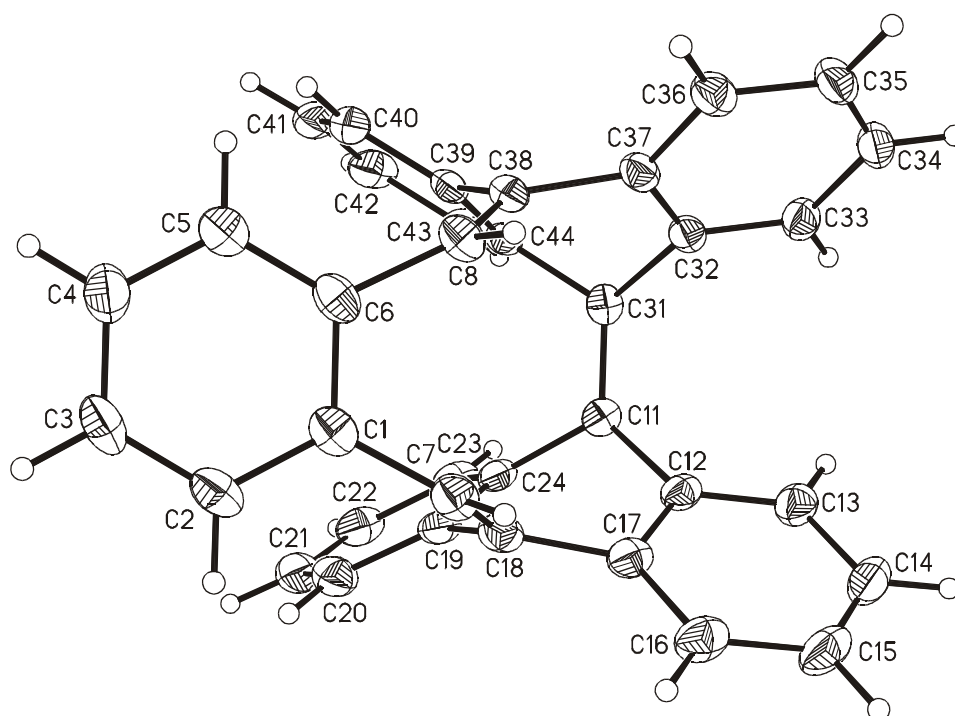
Identification code	herges32	
Empirical formula	C ₃₆ H ₂₂	
Formula weight	454.54	
Temperature	170(2) K	
Wavelength	0.71073 Å	
Crystal system	monoclinic	
Space group	P2 ₁ /n	
Unit cell dimensions	a = 9.0130(6) Å	α = 90°.
	b = 16.8487(13) Å	β = 102.871(8)°.
	c = 16.1977(12) Å	γ = 90°.
Volume	2397.9(3) Å ³	
Z	4	
Density (calculated)	1.259 Mg/m ³	
Absorption coefficient	0.071 mm ⁻¹	
F(000)	952	
Crystal size	0.3 x 0.2 x 0.2 mm ³	
Theta range for data collection	2.61 to 26.02°.	
Index ranges	-10 ≤ h ≤ 11, -20 ≤ k ≤ 20, -13 ≤ l ≤ 19	
Reflections collected	11980	
Independent reflections	4487 [R(int) = 0.0433]	
Completeness to theta = 26.02°	94.9 %	
Refinement method	Full-matrix least-squares on F ²	
Data / restraints / parameters	4487 / 0 / 326	
Goodness-of-fit on F ²	1.009	
Final R indices [I > 2σ(I)]	R1 = 0.0429, wR2 = 0.1073	
R indices (all data)	R1 = 0.0615, wR2 = 0.1168	
Extinction coefficient	0.017(4)	
Largest diff. peak and hole	0.788 and -0.197 e.Å ⁻³	

Comments:

All non-hydrogen atoms were refined anisotropic. The C-H hydrogen atoms were positioned with idealized geometry and refined using a riding model.

Table 2. Atomic coordinates ($\times 10^4$) and equivalent isotropic displacement parameters($\text{\AA}^2 \times 10^3$). U(eq) is defined as one third of the trace of the orthogonalized U_{ij} tensor.

	x	y	z	U(eq)
C(1)	1811(2)	6615(1)	3981(1)	26(1)
C(2)	516(2)	7023(1)	4077(1)	32(1)
C(3)	537(2)	7500(1)	4774(1)	35(1)
C(4)	1865(2)	7577(1)	5390(1)	36(1)
C(5)	3166(2)	7166(1)	5314(1)	33(1)
C(6)	3165(2)	6683(1)	4619(1)	26(1)
C(7)	1869(2)	6103(1)	3239(1)	26(1)
C(8)	4507(2)	6208(1)	4510(1)	26(1)
C(11)	4783(2)	6703(1)	2077(1)	21(1)
C(12)	4085(2)	5939(1)	1715(1)	22(1)
C(13)	4698(2)	5411(1)	1220(1)	28(1)
C(14)	3932(2)	4706(1)	938(1)	33(1)
C(15)	2556(2)	4533(1)	1140(1)	36(1)
C(16)	1928(2)	5055(1)	1636(1)	32(1)
C(17)	2683(2)	5760(1)	1926(1)	25(1)
C(18)	2160(2)	6339(1)	2501(1)	25(1)
C(19)	2318(2)	7178(1)	2243(1)	24(1)
C(20)	1222(2)	7766(1)	2231(1)	31(1)
C(21)	1417(2)	8516(1)	1913(1)	35(1)
C(22)	2689(2)	8676(1)	1595(1)	33(1)
C(23)	3807(2)	8105(1)	1616(1)	27(1)
C(24)	3639(2)	7361(1)	1953(1)	22(1)
C(31)	6074(2)	6753(1)	2701(1)	21(1)
C(32)	6939(2)	6046(1)	3114(1)	21(1)
C(33)	7883(2)	5560(1)	2762(1)	25(1)
C(34)	8635(2)	4924(1)	3228(1)	28(1)
C(35)	8444(2)	4770(1)	4036(1)	30(1)
C(36)	7511(2)	5260(1)	4398(1)	27(1)
C(37)	6765(2)	5900(1)	3942(1)	22(1)
C(38)	5741(2)	6466(1)	4263(1)	22(1)
C(39)	6099(2)	7307(1)	4092(1)	22(1)
C(40)	6267(2)	7917(1)	4689(1)	28(1)
C(41)	6719(2)	8667(1)	4485(1)	33(1)
C(42)	7026(2)	8806(1)	3699(1)	33(1)
C(43)	6852(2)	8203(1)	3092(1)	27(1)
C(44)	6364(2)	7456(1)	3283(1)	21(1)

**Table 3.** Bond lengths [Å] and angles [°].

C(1)-C(2)	1.393(2)	C(19)-C(24)	1.408(2)
C(1)-C(6)	1.417(2)	C(20)-C(21)	1.390(2)
C(1)-C(7)	1.489(2)	C(21)-C(22)	1.384(3)
C(2)-C(3)	1.383(3)	C(22)-C(23)	1.388(2)
C(3)-C(4)	1.383(3)	C(23)-C(24)	1.390(2)
C(4)-C(5)	1.391(2)	C(31)-C(32)	1.497(2)
C(5)-C(6)	1.389(2)	C(31)-C(44)	1.501(2)
C(6)-C(8)	1.493(2)	C(32)-C(33)	1.391(2)
C(7)-C(18)	1.339(2)	C(32)-C(37)	1.408(2)
C(8)-C(38)	1.336(2)	C(33)-C(34)	1.395(2)
C(11)-C(31)	1.363(2)	C(34)-C(35)	1.383(3)
C(11)-C(12)	1.4948(19)	C(35)-C(36)	1.396(2)
C(11)-C(24)	1.496(2)	C(36)-C(37)	1.392(2)
C(12)-C(13)	1.392(2)	C(37)-C(38)	1.498(2)
C(12)-C(17)	1.413(2)	C(38)-C(39)	1.492(2)
C(13)-C(14)	1.399(2)	C(39)-C(40)	1.398(2)
C(14)-C(15)	1.382(3)	C(39)-C(44)	1.405(2)
C(15)-C(16)	1.394(3)	C(40)-C(41)	1.390(2)
C(16)-C(17)	1.397(2)	C(41)-C(42)	1.382(3)
C(17)-C(18)	1.495(2)	C(42)-C(43)	1.397(2)
C(18)-C(19)	1.491(2)	C(43)-C(44)	1.390(2)
C(19)-C(20)	1.396(2)		

Table 3. Bond lengths [Å] and angles [°].

C(2)-C(1)-C(6)	119.00(16)	C(22)-C(21)-C(20)	119.93(15)
C(2)-C(1)-C(7)	123.85(16)	C(21)-C(22)-C(23)	120.90(15)
C(6)-C(1)-C(7)	117.15(14)	C(22)-C(23)-C(24)	119.49(16)
C(3)-C(2)-C(1)	121.27(16)	C(23)-C(24)-C(19)	120.17(14)
C(2)-C(3)-C(4)	119.76(16)	C(23)-C(24)-C(11)	126.05(15)
C(3)-C(4)-C(5)	119.97(17)	C(19)-C(24)-C(11)	113.75(12)
C(6)-C(5)-C(4)	121.07(17)	C(11)-C(31)-C(32)	123.77(12)
C(5)-C(6)-C(1)	118.92(15)	C(11)-C(31)-C(44)	120.97(13)
C(5)-C(6)-C(8)	123.73(15)	C(32)-C(31)-C(44)	110.30(13)
C(1)-C(6)-C(8)	117.33(15)	C(33)-C(32)-C(37)	119.69(14)
C(18)-C(7)-C(1)	126.71(14)	C(33)-C(32)-C(31)	126.23(15)
C(38)-C(8)-C(6)	127.69(14)	C(37)-C(32)-C(31)	114.06(13)
C(31)-C(11)-C(12)	123.96(13)	C(32)-C(33)-C(34)	119.95(16)
C(31)-C(11)-C(24)	120.22(13)	C(35)-C(34)-C(33)	120.49(15)
C(12)-C(11)-C(24)	111.56(13)	C(34)-C(35)-C(36)	119.99(15)
C(13)-C(12)-C(17)	119.68(14)	C(37)-C(36)-C(35)	120.04(16)
C(13)-C(12)-C(11)	126.11(15)	C(36)-C(37)-C(32)	119.82(14)
C(17)-C(12)-C(11)	114.21(13)	C(36)-C(37)-C(38)	124.89(15)
C(12)-C(13)-C(14)	119.99(17)	C(32)-C(37)-C(38)	115.29(13)
C(15)-C(14)-C(13)	120.41(16)	C(8)-C(38)-C(39)	126.38(13)
C(14)-C(15)-C(16)	120.23(15)	C(8)-C(38)-C(37)	120.99(13)
C(15)-C(16)-C(17)	120.11(17)	C(39)-C(38)-C(37)	111.40(13)
C(16)-C(17)-C(12)	119.59(15)	C(40)-C(39)-C(44)	119.91(14)
C(16)-C(17)-C(18)	124.54(15)	C(40)-C(39)-C(38)	124.37(15)
C(12)-C(17)-C(18)	115.78(13)	C(44)-C(39)-C(38)	115.60(13)
C(7)-C(18)-C(19)	125.56(15)	C(41)-C(40)-C(39)	119.77(17)
C(7)-C(18)-C(17)	120.95(13)	C(42)-C(41)-C(40)	120.16(15)
C(19)-C(18)-C(17)	112.37(14)	C(41)-C(42)-C(43)	120.71(15)
C(20)-C(19)-C(24)	119.29(14)	C(44)-C(43)-C(42)	119.56(17)
C(20)-C(19)-C(18)	124.42(15)	C(43)-C(44)-C(39)	119.83(14)
C(24)-C(19)-C(18)	116.21(13)	C(43)-C(44)-C(31)	126.47(15)
C(21)-C(20)-C(19)	120.12(17)	C(39)-C(44)-C(31)	113.70(12)

Table 4. Anisotropic displacement parameters ($\text{\AA}^2 \times 10^3$). The anisotropicdisplacement factor exponent takes the form: $-2\pi^2 [h^2 a^{*2} U_{11} + \dots + 2 h k a^* b^* U_{12}]$

	U_{11}	U_{22}	U_{33}	U_{23}	U_{13}	U_{12}
C(1)	22(1)	23(1)	32(1)	5(1)	9(1)	-2(1)
C(2)	20(1)	34(1)	41(1)	3(1)	6(1)	2(1)
C(3)	24(1)	34(1)	49(1)	0(1)	15(1)	7(1)
C(4)	35(1)	36(1)	38(1)	-4(1)	14(1)	6(1)
C(5)	28(1)	37(1)	33(1)	0(1)	5(1)	5(1)
C(6)	21(1)	26(1)	32(1)	6(1)	10(1)	2(1)
C(7)	22(1)	22(1)	35(1)	1(1)	6(1)	-3(1)
C(8)	24(1)	24(1)	30(1)	5(1)	6(1)	4(1)
C(11)	24(1)	19(1)	20(1)	2(1)	5(1)	-2(1)
C(12)	27(1)	18(1)	19(1)	1(1)	-1(1)	-1(1)
C(13)	34(1)	27(1)	23(1)	0(1)	2(1)	3(1)
C(14)	45(1)	25(1)	26(1)	-5(1)	0(1)	3(1)
C(15)	49(1)	21(1)	32(1)	-4(1)	-3(1)	-6(1)
C(16)	34(1)	25(1)	34(1)	0(1)	1(1)	-8(1)
C(17)	28(1)	20(1)	24(1)	3(1)	-1(1)	-1(1)
C(18)	19(1)	23(1)	31(1)	0(1)	2(1)	-2(1)
C(19)	23(1)	22(1)	23(1)	-2(1)	-4(1)	-1(1)
C(20)	27(1)	29(1)	34(1)	-1(1)	-2(1)	4(1)
C(21)	36(1)	25(1)	38(1)	-3(1)	-7(1)	9(1)
C(22)	43(1)	18(1)	31(1)	2(1)	-8(1)	-1(1)
C(23)	34(1)	21(1)	23(1)	1(1)	-4(1)	-5(1)
C(24)	25(1)	19(1)	19(1)	-2(1)	-3(1)	-1(1)
C(31)	22(1)	18(1)	24(1)	1(1)	8(1)	-2(1)
C(32)	16(1)	18(1)	28(1)	-2(1)	3(1)	-2(1)
C(33)	24(1)	23(1)	29(1)	-5(1)	6(1)	-1(1)
C(34)	23(1)	22(1)	39(1)	-6(1)	5(1)	3(1)
C(35)	27(1)	22(1)	38(1)	2(1)	1(1)	6(1)
C(36)	26(1)	24(1)	29(1)	3(1)	4(1)	3(1)
C(37)	17(1)	20(1)	28(1)	-1(1)	3(1)	0(1)
C(38)	19(1)	22(1)	23(1)	0(1)	1(1)	4(1)
C(39)	15(1)	22(1)	27(1)	-1(1)	0(1)	4(1)
C(40)	25(1)	28(1)	27(1)	-4(1)	-1(1)	5(1)
C(41)	31(1)	24(1)	37(1)	-9(1)	-7(1)	2(1)
C(42)	31(1)	18(1)	44(1)	1(1)	-7(1)	-4(1)
C(43)	23(1)	22(1)	33(1)	2(1)	-2(1)	-2(1)
C(44)	15(1)	19(1)	27(1)	-1(1)	-1(1)	1(1)

Table 5. Hydrogen coordinates ($\times 10^4$) and isotropic displacement parameters ($\text{\AA}^2 \times 10^3$).

	x	y	z	U(eq)
H(2)	-399	6972	3656	38
H(3)	-357	7773	4830	42
H(4)	1889	7911	5866	43
H(5)	4069	7216	5744	39
H(7)	1681	5553	3294	32
H(8)	4481	5657	4631	31
H(13)	5636	5530	1072	34
H(14)	4360	4344	606	40
H(15)	2036	4056	940	43
H(16)	985	4932	1776	38
H(20)	340	7653	2441	38
H(21)	678	8918	1914	42
H(22)	2798	9183	1360	40
H(23)	4680	8223	1400	32
H(33)	8016	5660	2206	30
H(34)	9282	4594	2987	34
H(35)	8949	4332	4346	35
H(36)	7385	5156	4954	32
H(40)	6074	7820	5233	34
H(41)	6816	9085	4887	39
H(42)	7359	9316	3569	40
H(43)	7064	8303	2553	32

9.5.2 Naphthalene System 53

Table 1. Crystal data and structure refinement for herges37.

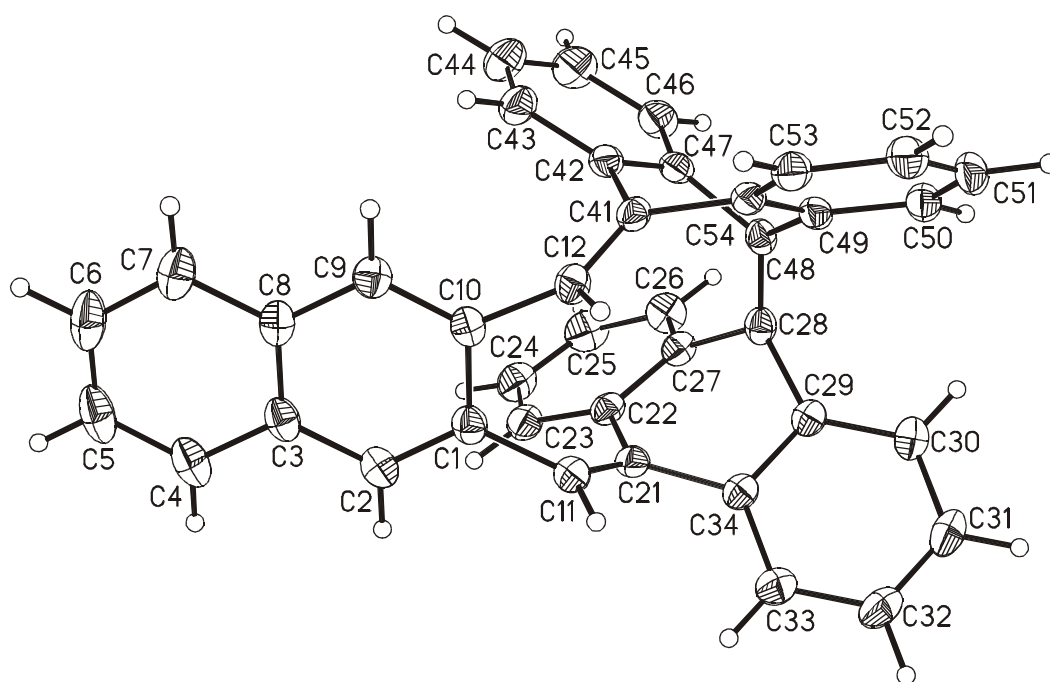
Identification code	herges37	
Empirical formula	C ₄₀ H ₂₄	
Formula weight	504.59	
Temperature	170(2) K	
Wavelength	0.71073 Å	
Crystal system	monoclinic	
Space group	P2 ₁ /c	
Unit cell dimensions	a = 9.3217(7) Å	α = 90°.
	b = 14.4237(6) Å	β = 98.185(9)°.
	c = 19.5029(14) Å	γ = 90°.
Volume	2595.5(3) Å ³	
Z	4	
Density (calculated)	1.291 Mg/m ³	
Absorption coefficient	0.073 mm ⁻¹	
F(000)	1056	
Crystal size	0.4 x 0.3 x 0.3 mm ³	
Theta range for data collection	2.54 to 28.11°.	
Index ranges	-12 ≤ h ≤ 12, -17 ≤ k ≤ 18, -22 ≤ l ≤ 25	
Reflections collected	22114	
Independent reflections	6230 [R(int) = 0.0359]	
Completeness to theta = 28.11°	98.3 %	
Refinement method	Full-matrix least-squares on F ²	
Data / restraints / parameters	6230 / 0 / 362	
Goodness-of-fit on F ²	1.022	
Final R indices [I > 2σ(I)]	R1 = 0.0415, wR2 = 0.1071	
R indices (all data)	R1 = 0.0557, wR2 = 0.1141	
Extinction coefficient	0.022(3)	
Largest diff. peak and hole	0.250 and -0.226 e.Å ⁻³	

Comments:

All non-hydrogen atoms were refined anisotropic. The C-H H atoms were positioned with idealized geometry and refined using a riding model.

Table 2. Atomic coordinates ($\times 10^4$) and equivalent isotropic displacement parameters ($\text{\AA}^2 \times 10^3$).U(eq) is defined as one third of the trace of the orthogonalized U_{ij} tensor.

	x	y	z	U(eq)
C(1)	6318(1)	3150(1)	2549(1)	24(1)
C(2)	6972(1)	2697(1)	3129(1)	27(1)
C(3)	7485(1)	3185(1)	3748(1)	26(1)
C(4)	8158(1)	2726(1)	4355(1)	34(1)
C(5)	8659(1)	3227(1)	4939(1)	39(1)
C(6)	8532(1)	4195(1)	4944(1)	38(1)
C(7)	7872(1)	4660(1)	4370(1)	33(1)
C(8)	7323(1)	4163(1)	3759(1)	25(1)
C(9)	6644(1)	4621(1)	3154(1)	26(1)
C(10)	6143(1)	4141(1)	2561(1)	23(1)
C(11)	5816(1)	2676(1)	1879(1)	25(1)
C(12)	5494(1)	4596(1)	1901(1)	23(1)
C(21)	4504(1)	2313(1)	1668(1)	22(1)
C(22)	3306(1)	2191(1)	2090(1)	23(1)
C(23)	3467(1)	1797(1)	2747(1)	28(1)
C(24)	2256(2)	1610(1)	3068(1)	33(1)
C(25)	881(2)	1804(1)	2732(1)	36(1)
C(26)	701(1)	2226(1)	2083(1)	32(1)
C(27)	1906(1)	2437(1)	1767(1)	24(1)
C(28)	1921(1)	2989(1)	1121(1)	23(1)
C(29)	2708(1)	2490(1)	616(1)	23(1)
C(30)	2253(1)	2373(1)	-91(1)	29(1)
C(31)	3097(2)	1864(1)	-492(1)	34(1)
C(32)	4404(2)	1485(1)	-193(1)	34(1)
C(33)	4886(1)	1613(1)	507(1)	29(1)
C(34)	4048(1)	2108(1)	917(1)	23(1)
C(41)	4118(1)	4857(1)	1709(1)	21(1)
C(42)	2929(1)	4807(1)	2139(1)	23(1)
C(43)	3010(1)	5189(1)	2800(1)	30(1)
C(44)	1819(2)	5143(1)	3153(1)	39(1)
C(45)	546(2)	4733(1)	2848(1)	38(1)
C(46)	449(1)	4349(1)	2190(1)	31(1)
C(47)	1639(1)	4373(1)	1833(1)	23(1)
C(48)	1776(1)	3922(1)	1153(1)	22(1)
C(49)	2343(1)	4585(1)	670(1)	22(1)
C(50)	1770(1)	4744(1)	-19(1)	27(1)
C(51)	2386(1)	5413(1)	-399(1)	31(1)
C(52)	3594(1)	5909(1)	-104(1)	31(1)
C(53)	4197(1)	5744(1)	581(1)	26(1)
C(54)	3573(1)	5092(1)	971(1)	22(1)

**Table 3.** Bond lengths [Å] and angles [°].

C(1)-C(2)	1.3713(16)	C(28)-C(48)	1.3547(17)
C(1)-C(10)	1.4402(17)	C(28)-C(29)	1.4940(15)
C(1)-C(11)	1.4900(16)	C(29)-C(30)	1.3936(16)
C(2)-C(3)	1.4217(17)	C(29)-C(34)	1.4139(16)
C(3)-C(8)	1.4185(18)	C(30)-C(31)	1.3942(18)
C(3)-C(4)	1.4216(16)	C(31)-C(32)	1.387(2)
C(4)-C(5)	1.373(2)	C(32)-C(33)	1.3888(18)
C(5)-C(6)	1.402(2)	C(33)-C(34)	1.3908(16)
C(6)-C(7)	1.3732(19)	C(41)-C(42)	1.4836(15)
C(7)-C(8)	1.4217(17)	C(41)-C(54)	1.4941(15)
C(8)-C(9)	1.4198(16)	C(42)-C(43)	1.3940(16)
C(9)-C(10)	1.3712(16)	C(42)-C(47)	1.4107(16)
C(10)-C(12)	1.4932(15)	C(43)-C(44)	1.3891(18)
C(11)-C(21)	1.3403(16)	C(44)-C(45)	1.383(2)
C(12)-C(41)	1.3384(16)	C(45)-C(46)	1.3897(18)
C(21)-C(22)	1.4895(15)	C(46)-C(47)	1.3914(15)
C(21)-C(34)	1.4951(15)	C(47)-C(48)	1.4982(15)
C(22)-C(23)	1.3904(16)	C(48)-C(49)	1.4911(15)
C(22)-C(27)	1.4115(16)	C(49)-C(50)	1.3914(15)
C(23)-C(24)	1.3927(17)	C(49)-C(54)	1.4152(16)
C(24)-C(25)	1.383(2)	C(50)-C(51)	1.3897(18)
C(25)-C(26)	1.3930(18)	C(51)-C(52)	1.388(2)
C(26)-C(27)	1.3890(16)	C(52)-C(53)	1.3935(16)
C(27)-C(28)	1.4927(16)	C(53)-C(54)	1.3893(16)

Table 3. Bond lengths [Å] and angles [°].

C(2)-C(1)-C(10)	119.82(11)	C(30)-C(29)-C(34)	119.34(11)
C(2)-C(1)-C(11)	123.54(11)	C(30)-C(29)-C(28)	126.96(11)
C(10)-C(1)-C(11)	116.59(10)	C(34)-C(29)-C(28)	113.69(10)
C(1)-C(2)-C(3)	121.46(12)	C(29)-C(30)-C(31)	120.14(12)
C(8)-C(3)-C(4)	119.08(11)	C(32)-C(31)-C(30)	120.25(12)
C(8)-C(3)-C(2)	118.73(10)	C(31)-C(32)-C(33)	120.21(12)
C(4)-C(3)-C(2)	122.19(12)	C(32)-C(33)-C(34)	120.23(12)
C(5)-C(4)-C(3)	120.24(14)	C(33)-C(34)-C(29)	119.79(11)
C(4)-C(5)-C(6)	120.66(12)	C(33)-C(34)-C(21)	123.99(10)
C(7)-C(6)-C(5)	120.65(13)	C(29)-C(34)-C(21)	116.15(10)
C(6)-C(7)-C(8)	120.17(14)	C(12)-C(41)-C(42)	126.21(10)
C(3)-C(8)-C(9)	119.10(10)	C(12)-C(41)-C(54)	120.99(10)
C(3)-C(8)-C(7)	119.16(11)	C(42)-C(41)-C(54)	112.09(9)
C(9)-C(8)-C(7)	121.72(12)	C(43)-C(42)-C(47)	119.79(11)
C(10)-C(9)-C(8)	121.62(11)	C(43)-C(42)-C(41)	123.83(11)
C(9)-C(10)-C(1)	119.27(10)	C(47)-C(42)-C(41)	116.33(10)
C(9)-C(10)-C(12)	123.55(11)	C(44)-C(43)-C(42)	119.92(12)
C(1)-C(10)-C(12)	117.07(10)	C(45)-C(44)-C(43)	120.27(12)
C(21)-C(11)-C(1)	127.39(10)	C(44)-C(45)-C(46)	120.47(12)
C(41)-C(12)-C(10)	128.29(10)	C(45)-C(46)-C(47)	120.05(12)
C(11)-C(12)-C(22)	126.85(10)	C(46)-C(47)-C(42)	119.47(11)
C(11)-C(12)-C(34)	119.85(10)	C(46)-C(47)-C(48)	127.34(11)
C(22)-C(12)-C(34)	112.79(9)	C(42)-C(47)-C(48)	113.05(9)
C(23)-C(22)-C(27)	119.07(11)	C(28)-C(48)-C(49)	124.07(10)
C(23)-C(22)-C(21)	124.54(11)	C(28)-C(48)-C(47)	119.64(10)
C(27)-C(22)-C(21)	116.23(10)	C(49)-C(48)-C(47)	111.32(10)
C(22)-C(23)-C(24)	120.32(12)	C(50)-C(49)-C(54)	119.50(11)
C(25)-C(24)-C(23)	120.29(12)	C(50)-C(49)-C(48)	126.43(11)
C(24)-C(25)-C(26)	120.15(12)	C(54)-C(49)-C(48)	114.06(9)
C(27)-C(26)-C(25)	119.90(12)	C(51)-C(50)-C(49)	119.88(12)
C(26)-C(27)-C(22)	120.10(11)	C(52)-C(51)-C(50)	120.66(11)
C(26)-C(27)-C(28)	126.64(11)	C(51)-C(52)-C(53)	120.07(11)
C(22)-C(27)-C(28)	113.06(10)	C(54)-C(53)-C(52)	119.89(12)
C(48)-C(28)-C(27)	118.46(10)	C(53)-C(54)-C(49)	119.97(10)
C(48)-C(28)-C(29)	124.85(10)	C(53)-C(54)-C(41)	124.72(11)
C(27)-C(28)-C(29)	111.37(10)	C(49)-C(54)-C(41)	115.31(10)

Table 4. Anisotropic displacement parameters ($\text{\AA}^2 \times 10^3$). The anisotropicdisplacement factor exponent takes the form: $-2\pi^2 [h^2 a^{*2} U_{11} + \dots + 2 h k a^* b^* U_{12}]$

	U_{11}	U_{22}	U_{33}	U_{23}	U_{13}	U_{12}
C(1)	19(1)	28(1)	24(1)	0(1)	2(1)	-1(1)
C(2)	25(1)	28(1)	29(1)	4(1)	1(1)	0(1)
C(3)	18(1)	36(1)	24(1)	6(1)	3(1)	-2(1)
C(4)	25(1)	47(1)	30(1)	12(1)	1(1)	1(1)
C(5)	26(1)	67(1)	23(1)	13(1)	0(1)	-2(1)
C(6)	30(1)	65(1)	20(1)	-2(1)	3(1)	-11(1)
C(7)	30(1)	45(1)	24(1)	-3(1)	5(1)	-9(1)
C(8)	20(1)	36(1)	20(1)	1(1)	4(1)	-5(1)
C(9)	27(1)	26(1)	25(1)	2(1)	4(1)	-2(1)
C(10)	19(1)	28(1)	21(1)	3(1)	4(1)	-1(1)
C(11)	25(1)	26(1)	24(1)	0(1)	3(1)	2(1)
C(12)	26(1)	25(1)	19(1)	1(1)	5(1)	-2(1)
C(21)	26(1)	19(1)	22(1)	0(1)	4(1)	2(1)
C(22)	28(1)	18(1)	22(1)	-2(1)	5(1)	-2(1)
C(23)	36(1)	22(1)	24(1)	1(1)	4(1)	0(1)
C(24)	46(1)	28(1)	27(1)	4(1)	12(1)	-2(1)
C(25)	39(1)	34(1)	37(1)	4(1)	18(1)	-6(1)
C(26)	28(1)	33(1)	35(1)	2(1)	8(1)	-4(1)
C(27)	27(1)	23(1)	23(1)	-2(1)	6(1)	-2(1)
C(28)	19(1)	29(1)	21(1)	0(1)	2(1)	-2(1)
C(29)	24(1)	23(1)	22(1)	-1(1)	4(1)	-3(1)
C(30)	30(1)	33(1)	23(1)	-1(1)	1(1)	-4(1)
C(31)	44(1)	37(1)	21(1)	-4(1)	6(1)	-5(1)
C(32)	41(1)	35(1)	28(1)	-6(1)	14(1)	0(1)
C(33)	30(1)	29(1)	29(1)	-2(1)	8(1)	1(1)
C(34)	25(1)	21(1)	23(1)	-1(1)	5(1)	-3(1)
C(41)	28(1)	19(1)	18(1)	0(1)	5(1)	0(1)
C(42)	28(1)	21(1)	19(1)	3(1)	6(1)	5(1)
C(43)	38(1)	30(1)	22(1)	-2(1)	7(1)	3(1)
C(44)	49(1)	47(1)	25(1)	-5(1)	15(1)	8(1)
C(45)	38(1)	48(1)	31(1)	2(1)	19(1)	9(1)
C(46)	27(1)	37(1)	29(1)	4(1)	9(1)	6(1)
C(47)	25(1)	24(1)	21(1)	4(1)	6(1)	7(1)
C(48)	18(1)	29(1)	19(1)	2(1)	2(1)	3(1)
C(49)	22(1)	26(1)	19(1)	2(1)	5(1)	7(1)
C(50)	25(1)	36(1)	21(1)	0(1)	3(1)	8(1)
C(51)	35(1)	40(1)	17(1)	6(1)	5(1)	13(1)
C(52)	43(1)	29(1)	23(1)	7(1)	11(1)	7(1)
C(53)	34(1)	24(1)	23(1)	2(1)	8(1)	3(1)
C(54)	26(1)	22(1)	18(1)	1(1)	6(1)	6(1)

Table 5. Hydrogen coordinates ($\times 10^4$) and isotropic displacement parameters ($\text{\AA}^2 \times 10^3$).

	x	y	z	U(eq)
H(2)	7084	2043	3116	33
H(4)	8261	2071	4357	41
H(5)	9096	2913	5344	47
H(6)	8907	4533	5348	46
H(7)	7782	5316	4380	39
H(9)	6535	5275	3160	31
H(11)	6505	2626	1565	30
H(12)	6141	4716	1577	28
H(23)	4408	1655	2979	33
H(24)	2375	1348	3519	40
H(25)	56	1649	2944	43
H(26)	-243	2369	1856	38
H(30)	1366	2641	-300	35
H(31)	2774	1777	-972	41
H(32)	4972	1136	-469	40
H(33)	5791	1361	708	34
H(43)	3878	5480	3008	36
H(44)	1880	5395	3606	47
H(45)	-269	4714	3090	46
H(46)	-431	4070	1983	37
H(50)	960	4395	-228	33
H(51)	1976	5532	-864	37
H(52)	4011	6361	-370	37
H(53)	5033	6077	780	32

9.5.3 Iodine attacked naphthalene system 54

Table 1. Crystal data and structure refinement for herges35.

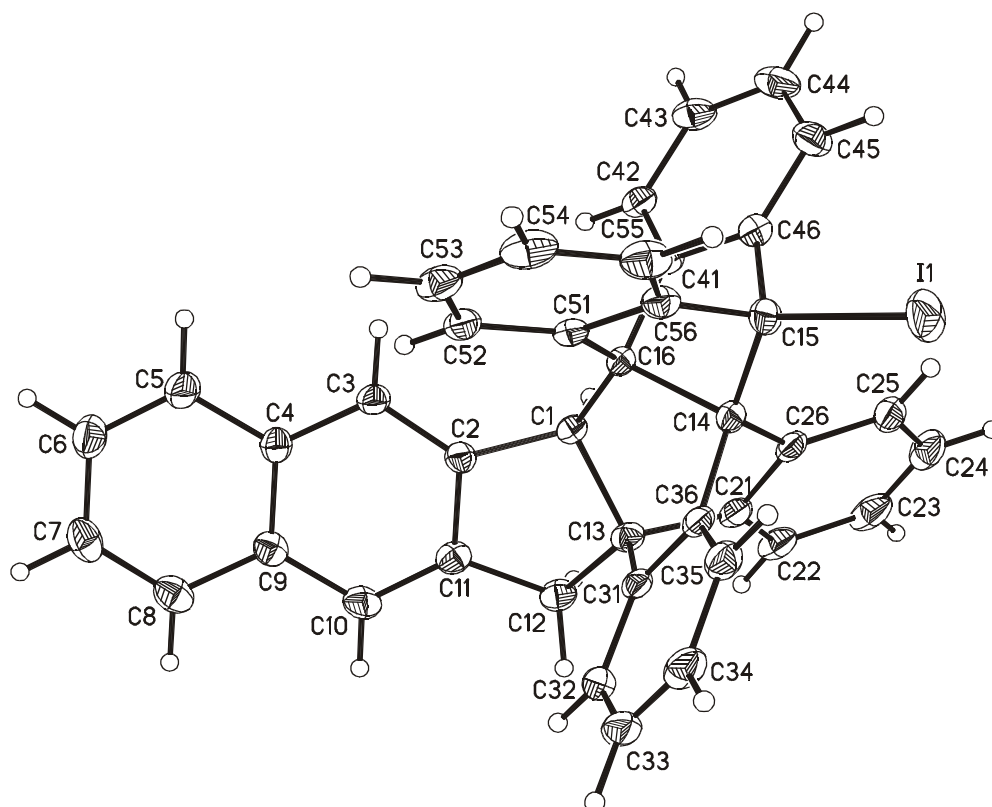
Identification code	herges35	
Empirical formula	C ₄₀ H ₂₅ I	
Formula weight	632.50	
Temperature	170(2) K	
Wavelength	0.71073 Å	
Crystal system	monoclinic	
Space group	P2 ₁ /c	
Unit cell dimensions	a = 9.0700(5) Å	α = 90°.
	b = 17.2327(11) Å	β = 92.850(7)°.
	c = 17.4789(11) Å	γ = 90°.
Volume	2728.6(3) Å ³	
Z	4	
Density (calculated)	1.540 Mg/m ³	
Absorption coefficient	1.203 mm ⁻¹	
F(000)	1272	
Crystal size	0.14 x 0.11 x 0.08 mm ³	
Theta range for data collection	2.25 to 28.08°.	
Index ranges	-11 ≤ h ≤ 11, -22 ≤ k ≤ 22, -23 ≤ l ≤ 23	
Reflections collected	31237	
Independent reflections	6511 [R(int) = 0.0360]	
Completeness to theta = 28.08°	98.2 %	
Refinement method	Full-matrix least-squares on F ²	
Data / restraints / parameters	6511 / 0 / 371	
Goodness-of-fit on F ²	1.042	
Final R indices [I > 2σ(I)]	R1 = 0.0303, wR2 = 0.0833	
R indices (all data)	R1 = 0.0409, wR2 = 0.0873	
Extinction coefficient	0.0091(5)	
Largest diff. peak and hole	0.704 and -0.696 e.Å ⁻³	

Comments:

All non-hydrogen atoms were refined anisotropic. The C-H H atoms were positioned with idealized geometry (CH₃ allowed to rotate but not to tip) and refined using a riding model. A numerical absorption correction was performed (Tmin./Tmax.: 0.7038, 0.7840).

Table 2. Atomic coordinates ($\times 10^4$) and equivalent isotropic displacement parameters ($\text{\AA}^2 \times 10^3$).U(eq) is defined as one third of the trace of the orthogonalized U_{ij} tensor.

	x	y	z	U(eq)
I(1)	7195(1)	14(1)	1914(1)	35(1)
C(1)	6323(2)	3271(1)	1472(1)	16(1)
C(2)	6896(2)	3971(1)	1063(1)	18(1)
C(3)	6768(2)	4173(1)	304(1)	20(1)
C(4)	7447(2)	4865(1)	53(1)	20(1)
C(5)	7445(3)	5068(1)	-736(1)	27(1)
C(6)	8190(3)	5701(1)	-970(1)	30(1)
C(7)	8991(2)	6171(1)	-442(1)	29(1)
C(8)	9000(2)	6006(1)	327(1)	26(1)
C(9)	8228(2)	5352(1)	595(1)	21(1)
C(10)	8209(2)	5163(1)	1388(1)	23(1)
C(11)	7538(2)	4498(1)	1613(1)	20(1)
C(12)	7263(2)	4207(1)	2414(1)	23(1)
C(13)	7151(2)	3328(1)	2295(1)	18(1)
C(14)	6987(2)	1876(1)	1889(1)	17(1)
C(15)	6705(2)	1125(1)	1411(1)	20(1)
C(16)	6399(2)	2430(1)	1186(1)	15(1)
C(21)	6220(2)	2841(1)	2810(1)	20(1)
C(22)	5475(2)	3109(1)	3433(1)	25(1)
C(23)	4605(2)	2597(2)	3828(1)	31(1)
C(24)	4473(2)	1828(2)	3606(1)	31(1)
C(25)	5211(2)	1555(1)	2977(1)	26(1)
C(26)	6088(2)	2060(1)	2578(1)	19(1)
C(31)	8639(2)	2923(1)	2282(1)	17(1)
C(32)	10002(2)	3255(1)	2480(1)	22(1)
C(33)	11271(2)	2796(1)	2510(1)	27(1)
C(34)	11185(2)	2014(1)	2333(1)	27(1)
C(35)	9829(2)	1678(1)	2117(1)	23(1)
C(36)	8556(2)	2129(1)	2097(1)	17(1)
C(41)	4919(2)	2033(1)	1003(1)	17(1)
C(42)	3581(2)	2332(1)	736(1)	20(1)
C(43)	2402(2)	1815(1)	600(1)	26(1)
C(44)	2578(2)	1028(1)	731(1)	29(1)
C(45)	3932(2)	721(1)	1004(1)	26(1)
C(46)	5089(2)	1236(1)	1144(1)	20(1)
C(51)	7421(2)	2117(1)	574(1)	16(1)
C(52)	8077(2)	2445(1)	-49(1)	19(1)
C(53)	8860(2)	1964(1)	-531(1)	25(1)
C(54)	8987(2)	1179(1)	-398(1)	28(1)
C(55)	8345(2)	841(1)	236(1)	27(1)
C(56)	7584(2)	1315(1)	710(1)	20(1)

**Table 3.** Bond lengths [Å] and angles [°].

I(1)-C(15)	2.1447(18)	C(16)-C(51)	1.546(2)
C(1)-C(2)	1.508(2)	C(21)-C(22)	1.388(3)
C(1)-C(16)	1.536(2)	C(21)-C(26)	1.410(3)
C(1)-C(13)	1.593(2)	C(22)-C(23)	1.390(3)
C(2)-C(3)	1.371(2)	C(23)-C(24)	1.385(3)
C(2)-C(11)	1.426(2)	C(24)-C(25)	1.397(3)
C(3)-C(4)	1.422(3)	C(25)-C(26)	1.390(3)
C(4)-C(5)	1.423(3)	C(31)-C(32)	1.390(3)
C(4)-C(9)	1.427(3)	C(31)-C(36)	1.407(3)
C(5)-C(6)	1.358(3)	C(32)-C(33)	1.395(3)
C(6)-C(7)	1.404(3)	C(33)-C(34)	1.384(3)
C(7)-C(8)	1.374(3)	C(34)-C(35)	1.395(3)
C(8)-C(9)	1.418(3)	C(35)-C(36)	1.392(3)
C(9)-C(10)	1.424(3)	C(41)-C(42)	1.378(3)
C(10)-C(11)	1.365(3)	C(41)-C(46)	1.402(3)
C(11)-C(12)	1.519(3)	C(42)-C(43)	1.402(3)
C(12)-C(13)	1.532(3)	C(43)-C(44)	1.384(3)
C(13)-C(21)	1.517(3)	C(44)-C(45)	1.400(3)
C(13)-C(31)	1.520(3)	C(45)-C(46)	1.387(3)
C(14)-C(36)	1.515(2)	C(51)-C(52)	1.387(3)
C(14)-C(26)	1.521(3)	C(51)-C(56)	1.410(3)
C(14)-C(15)	1.555(2)	C(52)-C(53)	1.400(3)
C(14)-C(16)	1.625(2)	C(53)-C(54)	1.376(3)
C(15)-C(46)	1.528(3)	C(54)-C(55)	1.403(3)
C(15)-C(56)	1.529(3)	C(55)-C(56)	1.374(3)
C(16)-C(41)	1.526(2)		

Table 3. Bond lengths [Å] and angles [°].

C(2)-C(1)-C(16)	125.36(15)	C(41)-C(16)-C(14)	98.51(13)
C(2)-C(1)-C(13)	102.73(14)	C(1)-C(16)-C(14)	109.07(13)
C(16)-C(1)-C(13)	109.00(14)	C(51)-C(16)-C(14)	97.62(13)
C(3)-C(2)-C(11)	120.23(17)	C(22)-C(21)-C(26)	120.26(18)
C(3)-C(2)-C(1)	130.32(16)	C(22)-C(21)-C(13)	126.07(18)
C(11)-C(2)-C(1)	109.18(15)	C(26)-C(21)-C(13)	113.59(15)
C(2)-C(3)-C(4)	119.60(16)	C(21)-C(22)-C(23)	119.4(2)
C(3)-C(4)-C(5)	121.68(17)	C(24)-C(23)-C(22)	120.7(2)
C(3)-C(4)-C(9)	119.79(17)	C(23)-C(24)-C(25)	120.3(2)
C(5)-C(4)-C(9)	118.43(18)	C(26)-C(25)-C(24)	119.5(2)
C(6)-C(5)-C(4)	120.85(19)	C(25)-C(26)-C(21)	119.77(18)
C(5)-C(6)-C(7)	120.96(19)	C(25)-C(26)-C(14)	127.60(18)
C(8)-C(7)-C(6)	120.1(2)	C(21)-C(26)-C(14)	112.63(16)
C(7)-C(8)-C(9)	120.59(19)	C(32)-C(31)-C(36)	119.58(18)
C(8)-C(9)-C(10)	122.17(18)	C(32)-C(31)-C(13)	125.93(18)
C(8)-C(9)-C(4)	119.00(17)	C(36)-C(31)-C(13)	114.36(16)
C(10)-C(9)-C(4)	118.83(18)	C(31)-C(32)-C(33)	119.88(19)
C(11)-C(10)-C(9)	119.94(17)	C(34)-C(33)-C(32)	120.4(2)
C(10)-C(11)-C(2)	120.90(17)	C(33)-C(34)-C(35)	120.3(2)
C(10)-C(11)-C(12)	129.66(17)	C(36)-C(35)-C(34)	119.58(19)
C(2)-C(11)-C(12)	109.37(16)	C(35)-C(36)-C(31)	120.23(18)
C(11)-C(12)-C(13)	102.30(14)	C(35)-C(36)-C(14)	127.78(17)
C(21)-C(13)-C(31)	105.99(15)	C(31)-C(36)-C(14)	111.98(16)
C(21)-C(13)-C(12)	120.07(16)	C(42)-C(41)-C(46)	120.86(17)
C(31)-C(13)-C(12)	113.77(16)	C(42)-C(41)-C(16)	130.84(17)
C(21)-C(13)-C(1)	104.46(14)	C(46)-C(41)-C(16)	108.30(16)
C(31)-C(13)-C(1)	109.74(14)	C(41)-C(42)-C(43)	118.11(18)
C(12)-C(13)-C(1)	102.09(14)	C(44)-C(43)-C(42)	120.93(19)
C(36)-C(14)-C(26)	106.47(14)	C(43)-C(44)-C(45)	121.27(19)
C(36)-C(14)-C(15)	119.78(16)	C(46)-C(45)-C(44)	117.45(19)
C(26)-C(14)-C(15)	121.25(16)	C(45)-C(46)-C(41)	121.37(18)
C(36)-C(14)-C(16)	106.36(14)	C(45)-C(46)-C(15)	132.77(18)
C(26)-C(14)-C(16)	107.91(14)	C(41)-C(46)-C(15)	105.78(16)
C(15)-C(14)-C(16)	92.46(12)	C(52)-C(51)-C(56)	119.05(17)
C(46)-C(15)-C(56)	105.01(14)	C(52)-C(51)-C(16)	134.20(16)
C(46)-C(15)-C(14)	100.93(15)	C(56)-C(51)-C(16)	106.65(15)
C(56)-C(15)-C(14)	100.06(14)	C(51)-C(52)-C(53)	118.83(18)
C(46)-C(15)-I(1)	114.38(13)	C(54)-C(53)-C(52)	121.38(19)
C(56)-C(15)-I(1)	114.45(13)	C(53)-C(54)-C(55)	120.49(19)
C(14)-C(15)-I(1)	119.82(11)	C(56)-C(55)-C(54)	118.03(19)
C(41)-C(16)-C(1)	115.98(16)	C(55)-C(56)-C(51)	122.21(19)
C(41)-C(16)-C(51)	104.50(13)	C(55)-C(56)-C(15)	130.84(18)
C(1)-C(16)-C(51)	126.25(15)	C(51)-C(56)-C(15)	106.85(16)

Table 4. Anisotropic displacement parameters ($\text{\AA}^2 \times 10^3$). The anisotropicdisplacement factor exponent takes the form: $-2\pi^2 [h^2 a^{*2} U_{11} + \dots + 2 h k a^* b^* U_{12}]$

	U_{11}	U_{22}	U_{33}	U_{23}	U_{13}	U_{12}
I(1)	38(1)	20(1)	45(1)	11(1)	-3(1)	2(1)
C(1)	18(1)	18(1)	13(1)	-1(1)	0(1)	0(1)
C(2)	19(1)	15(1)	19(1)	0(1)	0(1)	0(1)
C(3)	24(1)	17(1)	18(1)	-1(1)	-3(1)	-1(1)
C(4)	22(1)	18(1)	21(1)	3(1)	1(1)	2(1)
C(5)	34(1)	22(1)	24(1)	4(1)	-4(1)	-2(1)
C(6)	36(1)	28(1)	26(1)	8(1)	3(1)	-1(1)
C(7)	28(1)	20(1)	39(1)	7(1)	4(1)	-1(1)
C(8)	26(1)	18(1)	34(1)	-2(1)	1(1)	0(1)
C(9)	22(1)	15(1)	25(1)	0(1)	1(1)	2(1)
C(10)	27(1)	17(1)	25(1)	-6(1)	0(1)	-1(1)
C(11)	23(1)	19(1)	19(1)	-3(1)	0(1)	2(1)
C(12)	28(1)	23(1)	17(1)	-6(1)	1(1)	-1(1)
C(13)	20(1)	22(1)	13(1)	-3(1)	1(1)	-1(1)
C(14)	17(1)	17(1)	17(1)	4(1)	-1(1)	0(1)
C(15)	22(1)	14(1)	23(1)	4(1)	-3(1)	1(1)
C(16)	16(1)	16(1)	14(1)	2(1)	-1(1)	0(1)
C(21)	17(1)	28(1)	13(1)	1(1)	-1(1)	0(1)
C(22)	22(1)	38(1)	15(1)	-1(1)	0(1)	2(1)
C(23)	21(1)	57(2)	16(1)	3(1)	1(1)	1(1)
C(24)	21(1)	51(1)	22(1)	12(1)	2(1)	-5(1)
C(25)	21(1)	32(1)	23(1)	10(1)	-4(1)	-5(1)
C(26)	16(1)	27(1)	13(1)	5(1)	-3(1)	0(1)
C(31)	16(1)	24(1)	11(1)	2(1)	0(1)	-2(1)
C(32)	24(1)	26(1)	17(1)	2(1)	0(1)	-7(1)
C(33)	18(1)	41(1)	22(1)	6(1)	-3(1)	-7(1)
C(34)	17(1)	39(1)	24(1)	8(1)	-2(1)	4(1)
C(35)	22(1)	25(1)	22(1)	4(1)	-2(1)	3(1)
C(36)	17(1)	23(1)	12(1)	2(1)	-2(1)	0(1)
C(41)	17(1)	20(1)	13(1)	-1(1)	0(1)	-2(1)
C(42)	20(1)	26(1)	15(1)	-1(1)	0(1)	0(1)
C(43)	17(1)	36(1)	25(1)	-5(1)	-3(1)	-1(1)
C(44)	22(1)	34(1)	31(1)	-8(1)	0(1)	-9(1)
C(45)	29(1)	21(1)	27(1)	-4(1)	1(1)	-6(1)
C(46)	20(1)	21(1)	18(1)	1(1)	-1(1)	-1(1)
C(51)	14(1)	20(1)	15(1)	-2(1)	-3(1)	0(1)
C(52)	18(1)	24(1)	16(1)	-1(1)	-1(1)	-1(1)
C(53)	19(1)	37(1)	17(1)	-5(1)	1(1)	0(1)
C(54)	24(1)	36(1)	24(1)	-13(1)	0(1)	6(1)
C(55)	27(1)	23(1)	29(1)	-8(1)	-4(1)	6(1)
C(56)	19(1)	19(1)	21(1)	-2(1)	-3(1)	1(1)

Table 5. Hydrogen coordinates ($\times 10^4$) and isotropic displacement parameters ($\text{\AA}^2 \times 10^3$).

	x	y	z	U(eq)
H(1)	5258	3377	1552	20
H(3)	6228	3852	-52	24
H(5)	6915	4756	-1104	32
H(6)	8170	5828	-1500	36
H(7)	9528	6604	-616	34
H(8)	9527	6332	683	31
H(10)	8663	5500	1760	27
H(12A)	6335	4422	2602	27
H(12B)	8092	4342	2780	27
H(22)	5559	3636	3587	30
H(23)	4095	2777	4256	38
H(24)	3878	1484	3883	38
H(25)	5113	1028	2823	31
H(32)	10069	3793	2594	27
H(33)	12199	3022	2654	33
H(34)	12054	1705	2359	32
H(35)	9775	1144	1983	28
H(42)	3461	2872	646	24
H(43)	1470	2009	416	31
H(44)	1763	690	634	35
H(45)	4055	180	1091	31
H(52)	7997	2986	-147	23
H(53)	9314	2184	-958	29
H(54)	9513	864	-737	33
H(55)	8435	300	334	32

9.5.4 C_s Ring-Closed 57

Table 1. Crystal data and structure refinement for herges48 (Benzene solvate)

Identification code	herges48	
Empirical formula	C ₄₂ H ₂₅ Cl ₄	
Formula weight	671.42	
Temperature	170(2) K	
Wavelength	0.71073 Å	
Crystal system	hexagonal	
Space group	P6 ₃ /m	
Unit cell dimensions	a = 19.5210(10) Å	α = 90°.
	b = 19.5210(10) Å	β = 90°.
	c = 15.7070(7) Å	γ = 120°.
Volume	5183.6(4) Å ³	
Z	6	
Density (calculated)	1.291 Mg/m ³	
Absorption coefficient	0.372 mm ⁻¹	
F(000)	2070	
Crystal size	0.4 x 0.1 x 0.1 mm ³	
Theta range for data collection	2.41 to 25.02°.	
Index ranges	-23 ≤ h ≤ 23, -23 ≤ k ≤ 19, -18 ≤ l ≤ 18	
Reflections collected	28215	
Independent reflections	3169 [R(int) = 0.0550]	
Completeness to theta = 25.02°	99.7 %	
Refinement method	Full-matrix least-squares on F ²	
Data / restraints / parameters	3169 / 0 / 212	
Goodness-of-fit on F ²	1.062	
Final R indices [I > 2σ(I)]	R1 = 0.0572, wR2 = 0.1410	
R indices (all data)	R1 = 0.0722, wR2 = 0.1503	
Extinction coefficient	0.0049(10)	
Largest diff. peak and hole	0.498 and -0.344 e.Å ⁻³	

Comments:

All non-hydrogen atoms were refined anisotropic. All H atoms were positioned with idealized geometry and refined isotropic using a riding model. The molecule is located on a crystallographic mirror plane. The structure contain one benzene molecule which is also located on a crystallographic mirror plane. There is one additional benzene molecule located on a -6 axis. This molecule is completely disordered and therefore, the data were corrected for disordered solvent using the SQUEEZE option in Platon.

Table 2. Atomic coordinates ($\times 10^4$) and equivalent isotropic displacement parameters ($\text{\AA}^2 \times 10^3$).U(eq) is defined as one third of the trace of the orthogonalized U_{ij} tensor.

	x	y	z	U(eq)
C(1)	3202(2)	485(2)	6327(2)	31(1)
C(2)	2848(2)	-388(2)	6232(2)	31(1)
C(3)	3196(2)	-758(2)	5796(2)	36(1)
C(4)	2811(2)	-1565(2)	5724(2)	42(1)
C(5)	2051(2)	-2036(2)	6070(2)	43(1)
C(6)	1689(2)	-1676(2)	6495(2)	36(1)
C(7)	2083(2)	-860(2)	6584(2)	30(1)
C(8)	1802(1)	-391(2)	7069(2)	27(1)
C(9)	1878(2)	295(2)	6563(2)	29(1)
C(10)	1315(2)	522(2)	6467(2)	34(1)
C(11)	1482(2)	1206(2)	6014(2)	41(1)
C(12)	2227(2)	1669(2)	5666(2)	41(1)
C(13)	2792(2)	1453(2)	5749(2)	36(1)
C(14)	2630(2)	761(2)	6188(2)	30(1)
C(15)	3926(2)	979(2)	6637(2)	33(1)
C(16)	4507(2)	758(2)	6994(2)	34(1)
C(17)	5314(2)	1276(2)	6603(2)	38(1)
Cl(1)	6865(1)	2281(1)	6514(1)	58(1)
C(18)	5978(2)	1711(2)	7035(2)	36(1)
Cl(2)	5314(1)	1248(1)	5500(1)	67(1)
C(21)	-370(5)	-3598(4)	7500	103(3)
C(22)	339(4)	-4036(3)	6730(4)	116(3)
C(23)	-144(4)	-3746(3)	6788(4)	100(2)
C(24)	645(6)	-4205(4)	7500	150(6)

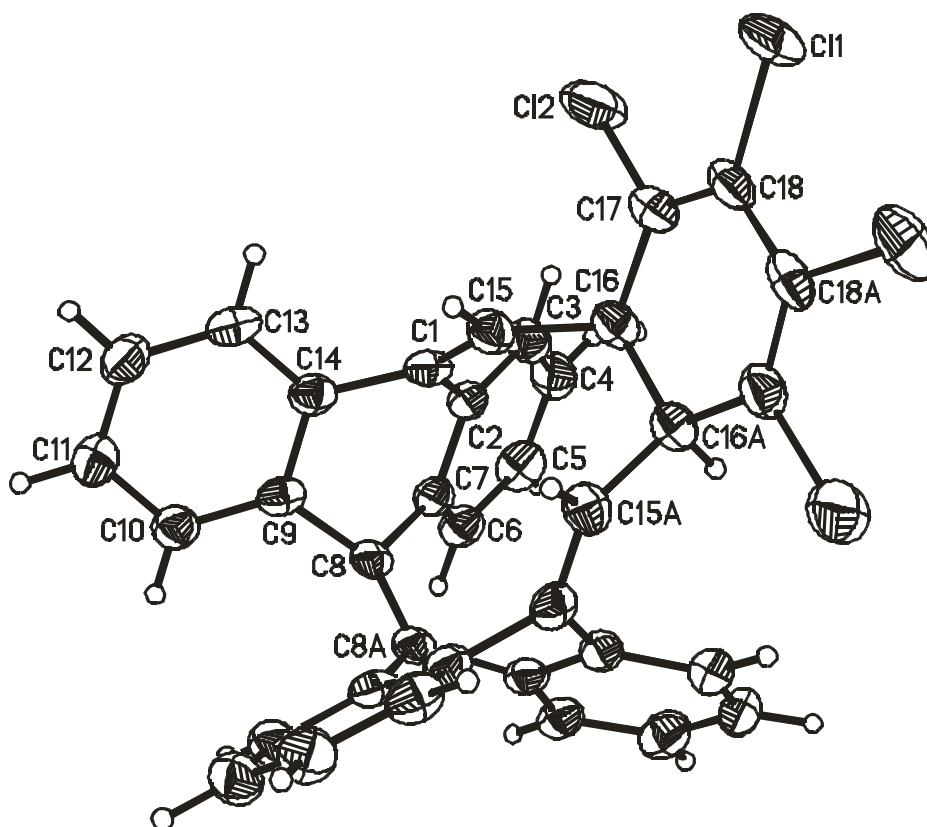


Table 3. Bond lengths [Å] and angles [°].

C(1)-C(15)	1.342(4)	C(11)-C(12)	1.384(5)
C(1)-C(14)	1.479(4)	C(12)-C(13)	1.371(4)
C(1)-C(2)	1.492(4)	C(13)-C(14)	1.405(4)
C(2)-C(3)	1.394(4)	C(15)-C(16)	1.509(4)
C(2)-C(7)	1.417(4)	C(16)-C(17)	1.513(4)
C(3)-C(4)	1.369(4)	C(16)-C(16A)	1.590(6)
C(4)-C(5)	1.406(5)	C(17)-C(18)	1.328(4)
C(5)-C(6)	1.393(4)	C(17)-Cl(2)	1.733(3)
C(6)-C(7)	1.386(4)	Cl(1)-C(18)	1.725(3)
C(7)-C(8)	1.492(4)	C(18)-C(18A)	1.462(6)
C(8)-C(8A)	1.355(5)	C(21)-C(23A)	1.288(8)
C(8)-C(9)	1.499(4)	C(21)-C(23)	1.288(8)
C(9)-C(10)	1.382(4)	C(22)-C(23)	1.322(10)
C(9)-C(14)	1.412(4)	C(22)-C(24)	1.458(10)
C(10)-C(11)	1.401(4)	C(24)-C(22A)	1.458(10)
C(15)-C(1)-C(14)	120.5(2)	C(12)-C(11)-C(10)	119.3(3)
C(15)-C(1)-C(2)	125.2(3)	C(13)-C(12)-C(11)	120.5(3)
C(14)-C(1)-C(2)	113.5(2)	C(12)-C(13)-C(14)	120.9(3)
C(3)-C(2)-C(7)	118.8(3)	C(13)-C(14)-C(9)	119.1(3)
C(3)-C(2)-C(1)	125.0(2)	C(13)-C(14)-C(1)	125.0(2)
C(7)-C(2)-C(1)	116.1(2)	C(9)-C(14)-C(1)	115.8(2)
C(4)-C(3)-C(2)	120.5(3)	C(1)-C(15)-C(16)	126.9(3)
C(3)-C(4)-C(5)	120.9(3)	C(15)-C(16)-C(17)	109.7(2)
C(6)-C(5)-C(4)	119.4(3)	C(15)-C(16)-C(16A)	111.81(15)
C(7)-C(6)-C(5)	119.9(3)	C(17)-C(16)-C(16A)	113.96(16)
C(6)-C(7)-C(2)	120.5(3)	C(18)-C(17)-C(16)	125.3(3)
C(6)-C(7)-C(8)	126.4(2)	C(18)-C(17)-Cl(2)	121.0(2)
C(2)-C(7)-C(8)	113.0(2)	C(16)-C(17)-Cl(2)	113.7(2)
C(8A)-C(8)-C(7)	120.71(15)	C(17)-C(18)-C(18A)	120.73(18)
C(8A)-C(8)-C(9)	121.97(14)	C(17)-C(18)-Cl(1)	121.0(3)
C(7)-C(8)-C(9)	112.1(2)	C(18A)-C(18)-Cl(1)	118.30(11)
C(10)-C(9)-C(14)	119.0(3)	C(23A)-C(21)-C(23)	120.6(10)
C(10)-C(9)-C(8)	127.2(2)	C(23)-C(22)-C(24)	120.0(6)
C(14)-C(9)-C(8)	113.8(2)	C(21)-C(23)-C(22)	123.6(8)
C(9)-C(10)-C(11)	121.2(3)	C(22A)-C(24)-C(22)	112.1(9)

Symmetry transformations used to generate equivalent atoms: A = x,y,-z+3/2

Table 4. Anisotropic displacement parameters ($\text{\AA}^2 \times 10^3$). The anisotropicdisplacement factor exponent takes the form: $-2\pi^2 [h^2 a^{*2} U_{11} + \dots + 2 h k a^* b^* U_{12}]$

	U_{11}	U_{22}	U_{33}	U_{23}	U_{13}	U_{12}
C(1)	29(1)	34(1)	24(1)	3(1)	6(1)	12(1)
C(2)	31(1)	43(2)	21(1)	2(1)	1(1)	21(1)
C(3)	35(2)	45(2)	32(2)	-4(1)	0(1)	22(1)
C(4)	50(2)	57(2)	32(2)	-6(1)	1(1)	37(2)
C(5)	55(2)	38(2)	37(2)	-5(1)	-3(1)	24(1)
C(6)	39(2)	42(2)	26(1)	-1(1)	-1(1)	20(1)
C(7)	28(1)	39(2)	20(1)	-1(1)	-4(1)	16(1)
C(8)	16(1)	31(1)	27(1)	-1(1)	-2(1)	7(1)
C(9)	27(1)	29(1)	20(1)	-3(1)	-2(1)	6(1)
C(10)	31(1)	41(2)	30(2)	1(1)	0(1)	16(1)
C(11)	45(2)	48(2)	36(2)	5(1)	-2(1)	29(2)
C(12)	52(2)	44(2)	33(2)	8(1)	2(1)	28(2)
C(13)	38(2)	35(2)	25(1)	5(1)	6(1)	12(1)
C(14)	32(1)	35(1)	22(1)	-2(1)	0(1)	14(1)
C(15)	27(1)	31(1)	38(2)	3(1)	3(1)	12(1)
C(16)	25(1)	38(2)	39(2)	-1(1)	1(1)	14(1)
C(17)	26(1)	46(2)	41(2)	3(1)	6(1)	18(1)
Cl(1)	23(1)	60(1)	77(1)	15(1)	14(1)	11(1)
C(18)	19(1)	32(1)	55(2)	6(1)	5(1)	12(1)
Cl(2)	37(1)	112(1)	41(1)	5(1)	10(1)	29(1)
C(21)	90(6)	57(4)	130(9)	0	0	14(4)
C(22)	129(5)	54(3)	111(5)	-14(3)	62(4)	5(3)
C(23)	122(5)	54(3)	82(4)	4(3)	-7(4)	13(3)
C(24)	86(6)	35(4)	310(20)	0	0	14(4)

Table 5. Hydrogen coordinates ($\times 10^4$) and isotropic displacement parameters ($\text{\AA}^2 \times 10^3$).

	x	y	z	U(eq)
H(3)	3704	-448	5547	44
H(4)	3061	-1809	5436	50
H(5)	1788	-2596	6014	51
H(6)	1172	-1988	6723	43
H(10)	806	208	6713	41
H(11)	1087	1351	5946	49
H(12)	2347	2139	5369	49
H(13)	3301	1776	5506	43
H(15)	4090	1526	6631	40
H(16)	4326	203	6808	41
H(21)	-707	-3377	7500	124
H(22)	486	-4134	6187	140
H(23)	-334	-3642	6276	120

9.5.5 C_s Ring-Opened 59

Table 1. Crystal data and structure refinement for C₃₆H₂₀Cl₄-chloroform solvate.

Identification code	herges49	
Empirical formula	C ₃₇ H ₂₁ Cl ₇	
Formula weight	713.69	
Temperature	293(2) K	
Wavelength	0.71073 Å	
Crystal system	monoclinic	
Space group	P2 ₁ /n	
Unit cell dimensions	a = 13.2695(9) Å	α = 90°.
	b = 8.7070(3) Å	β = 90.036(8)°.
	c = 27.6283(18) Å	γ = 90°.
Volume	3192.1(3) Å ³	
Z	4	
Density (calculated)	1.485 Mg/m ³	
Absorption coefficient	0.650 mm ⁻¹	
F(000)	1448	
Crystal size	0.13 x 0.10 x 0.07 mm ³	
Theta range for data collection	2.45 to 25.95°.	
Index ranges	-16 ≤ h ≤ 16, -9 ≤ k ≤ 10, -33 ≤ l ≤ 33	
Reflections collected	21311	
Independent reflections	6221 [R(int) = 0.0326]	
Completeness to theta = 25.95°	99.5 %	
Refinement method	Full-matrix least-squares on F ²	
Data / restraints / parameters	6221 / 0 / 414	
Goodness-of-fit on F ²	1.037	
Final R indices [I > 2σ(I)]	R1 = 0.0387, wR2 = 0.1003	
R indices (all data)	R1 = 0.0491, wR2 = 0.1057	
Extinction coefficient	0.0063(7)	
Largest diff. peak and hole	0.441 and -0.590 e.Å ⁻³	

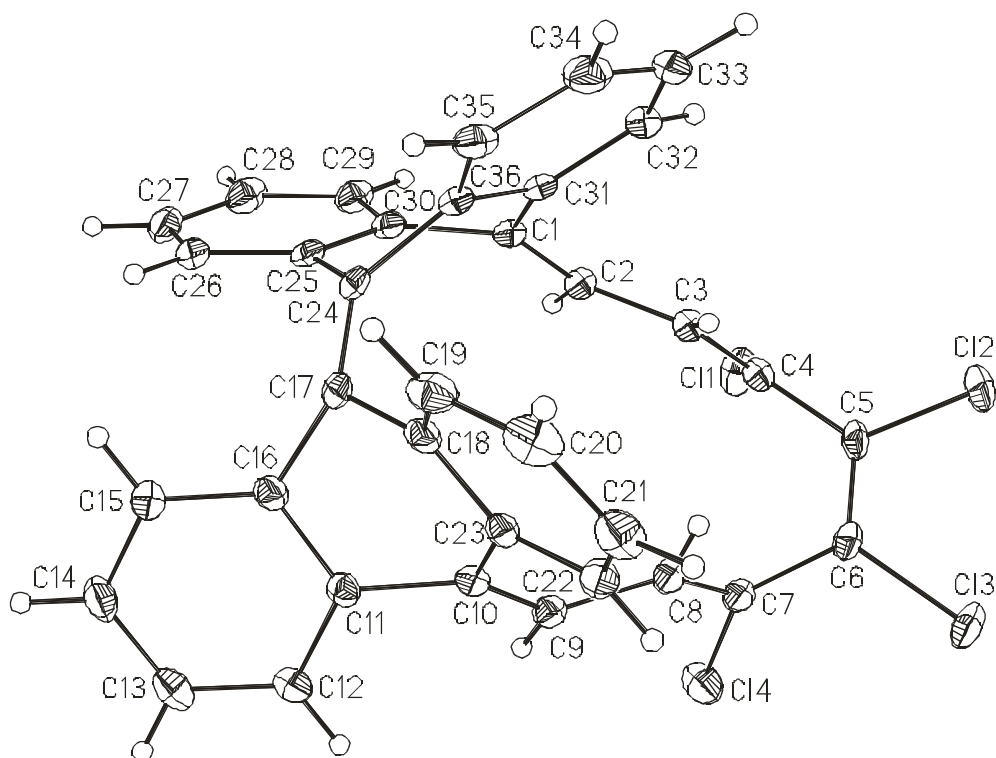
Comments:

All non-hydrogen atoms were refined anisotropic. All H atoms were located in difference map. The aromatic H atoms were positioned with idealized geometry and refined isotropic using a riding model. The H atoms at C2, C3, C8 and C9 were refined with varying coordinates and varying isotropic displacement parameters.

A numerical absorption correction was performed (T_{min}/t_{max}: 0.8192 / 0.9479).

Table 2. Atomic coordinates ($\times 10^4$) and equivalent isotropic displacement parameters ($\text{\AA}^2 \times 10^3$).U(eq) is defined as one third of the trace of the orthogonalized U_{ij} tensor.

	x	y	z	U(eq)
C(1)	4027(1)	8883(2)	6606(1)	17(1)
C(2)	3374(2)	8112(2)	6320(1)	18(1)
C(3)	3686(2)	7244(2)	5897(1)	18(1)
C(4)	3095(1)	6437(2)	5597(1)	18(1)
Cl(1)	1783(1)	6595(1)	5604(1)	28(1)
C(5)	3459(1)	5278(2)	5251(1)	19(1)
Cl(2)	3264(1)	5692(1)	4644(1)	30(1)
C(6)	3842(1)	3927(2)	5391(1)	18(1)
Cl(3)	4161(1)	2523(1)	4971(1)	30(1)
C(7)	3914(1)	3461(2)	5904(1)	17(1)
Cl(4)	2925(1)	2268(1)	6082(1)	28(1)
C(8)	4623(2)	3923(2)	6215(1)	18(1)
C(9)	4596(1)	3738(2)	6736(1)	17(1)
C(10)	5296(1)	4342(2)	7039(1)	16(1)
C(11)	5091(1)	4522(2)	7565(1)	15(1)
C(12)	4637(1)	3384(2)	7844(1)	19(1)
C(13)	4508(2)	3605(3)	8339(1)	23(1)
C(14)	4827(2)	4953(3)	8556(1)	26(1)
C(15)	5263(2)	6101(2)	8280(1)	23(1)
C(16)	5396(1)	5914(2)	7782(1)	17(1)
C(17)	5877(1)	7035(2)	7443(1)	16(1)
C(18)	6659(1)	6241(2)	7145(1)	17(1)
C(19)	7662(2)	6677(2)	7091(1)	23(1)
C(20)	8282(2)	5890(3)	6770(1)	27(1)
C(21)	7914(2)	4651(3)	6508(1)	25(1)
C(22)	6935(2)	4149(2)	6579(1)	20(1)
C(23)	6299(1)	4928(2)	6900(1)	15(1)
C(24)	5471(1)	8390(2)	7301(1)	16(1)
C(25)	4485(2)	9019(2)	7472(1)	17(1)
C(26)	4235(2)	9320(2)	7955(1)	20(1)
C(27)	3300(2)	9933(2)	8074(1)	23(1)
C(28)	2605(2)	10278(2)	7714(1)	24(1)
C(29)	2827(2)	9959(2)	7233(1)	21(1)
C(30)	3756(1)	9321(2)	7109(1)	17(1)
C(31)	5075(1)	9265(2)	6477(1)	17(1)
C(32)	5337(2)	9832(2)	6020(1)	20(1)
C(33)	6320(2)	10271(2)	5923(1)	25(1)
C(34)	7042(2)	10204(2)	6288(1)	25(1)
C(35)	6789(2)	9675(2)	6749(1)	21(1)
C(36)	5815(1)	9154(2)	6844(1)	17(1)
C(37)	8787(2)	7659(3)	4959(1)	46(1)
Cl(5)	8574(1)	9636(1)	4879(1)	58(1)
Cl(6)	9822(1)	7046(1)	4612(1)	61(1)
Cl(7)	8965(1)	7214(1)	5569(1)	81(1)

**Table 3.** Bond lengths [Å] and angles [°].

C(1)-C(2)	1.350(3)	C(17)-C(24)	1.355(3)
C(1)-C(31)	1.475(3)	C(17)-C(18)	1.496(3)
C(1)-C(30)	1.486(3)	C(18)-C(19)	1.391(3)
C(2)-C(3)	1.452(3)	C(18)-C(23)	1.411(3)
C(3)-C(4)	1.339(3)	C(19)-C(20)	1.392(3)
C(4)-C(5)	1.472(3)	C(20)-C(21)	1.386(3)
C(4)-Cl(1)	1.747(2)	C(21)-C(22)	1.385(3)
C(5)-C(6)	1.339(3)	C(22)-C(23)	1.400(3)
C(5)-Cl(2)	1.7332(19)	C(24)-C(25)	1.495(3)
C(6)-C(7)	1.478(3)	C(24)-C(36)	1.499(3)
C(6)-Cl(3)	1.7374(19)	C(25)-C(26)	1.400(3)
C(7)-C(8)	1.335(3)	C(25)-C(30)	1.419(3)
C(7)-Cl(4)	1.744(2)	C(26)-C(27)	1.390(3)
C(8)-C(9)	1.448(3)	C(27)-C(28)	1.388(3)
C(9)-C(10)	1.357(3)	C(28)-C(29)	1.390(3)
C(10)-C(23)	1.477(3)	C(29)-C(30)	1.395(3)
C(10)-C(11)	1.486(3)	C(31)-C(32)	1.399(3)
C(11)-C(12)	1.393(3)	C(31)-C(36)	1.414(3)
C(11)-C(16)	1.412(3)	C(32)-C(33)	1.385(3)
C(12)-C(13)	1.392(3)	C(33)-C(34)	1.391(3)
C(13)-C(14)	1.385(3)	C(34)-C(35)	1.396(3)
C(14)-C(15)	1.385(3)	C(35)-C(36)	1.395(3)
C(15)-C(16)	1.397(3)		
C(16)-C(17)	1.494(3)		
C(37)-Cl(7)	1.745(3)	C(37)-Cl(5)	1.759(3)
C(37)-Cl(6)	1.757(3)		

Table 3. Bond lengths [Å] and angles [°].

C(2)-C(1)-C(31)	125.14(17)	C(16)-C(17)-C(18)	109.88(16)
C(2)-C(1)-C(30)	121.32(17)	C(19)-C(18)-C(23)	119.55(18)
C(31)-C(1)-C(30)	113.37(16)	C(19)-C(18)-C(17)	126.67(18)
C(1)-C(2)-C(3)	123.14(18)	C(23)-C(18)-C(17)	113.78(16)
C(4)-C(3)-C(2)	127.14(18)	C(18)-C(19)-C(20)	120.0(2)
C(3)-C(4)-C(5)	124.75(18)	C(21)-C(20)-C(19)	120.49(19)
C(3)-C(4)-Cl(1)	122.34(15)	C(22)-C(21)-C(20)	120.10(19)
C(5)-C(4)-Cl(1)	112.84(14)	C(21)-C(22)-C(23)	120.17(19)
C(6)-C(5)-C(4)	122.56(17)	C(22)-C(23)-C(18)	119.47(17)
C(6)-C(5)-Cl(2)	121.28(15)	C(22)-C(23)-C(10)	122.73(18)
C(4)-C(5)-Cl(2)	115.94(15)	C(18)-C(23)-C(10)	117.45(16)
C(5)-C(6)-C(7)	122.92(17)	C(17)-C(24)-C(25)	125.08(17)
C(5)-C(6)-Cl(3)	121.17(15)	C(17)-C(24)-C(36)	120.65(17)
C(7)-C(6)-Cl(3)	115.55(14)	C(25)-C(24)-C(36)	111.78(16)
C(8)-C(7)-C(6)	125.41(18)	C(26)-C(25)-C(30)	118.50(18)
C(8)-C(7)-Cl(4)	121.86(16)	C(26)-C(25)-C(24)	125.35(18)
C(6)-C(7)-Cl(4)	112.68(14)	C(30)-C(25)-C(24)	116.15(16)
C(7)-C(8)-C(9)	126.02(19)	C(27)-C(26)-C(25)	120.60(19)
C(10)-C(9)-C(8)	123.61(18)	C(28)-C(27)-C(26)	120.46(18)
C(9)-C(10)-C(23)	126.19(17)	C(27)-C(28)-C(29)	120.04(19)
C(9)-C(10)-C(11)	121.27(17)	C(28)-C(29)-C(30)	120.1(2)
C(23)-C(10)-C(11)	112.51(16)	C(29)-C(30)-C(25)	120.21(18)
C(12)-C(11)-C(16)	119.99(17)	C(29)-C(30)-C(1)	123.08(18)
C(12)-C(11)-C(10)	123.05(18)	C(25)-C(30)-C(1)	116.69(17)
C(16)-C(11)-C(10)	116.95(16)	C(32)-C(31)-C(36)	119.90(18)
C(13)-C(12)-C(11)	119.95(19)	C(32)-C(31)-C(1)	122.18(18)
C(14)-C(13)-C(12)	120.35(19)	C(36)-C(31)-C(1)	117.75(17)
C(15)-C(14)-C(13)	120.03(19)	C(33)-C(32)-C(31)	120.35(19)
C(14)-C(15)-C(16)	120.84(19)	C(32)-C(33)-C(34)	119.85(19)
C(15)-C(16)-C(11)	118.81(18)	C(33)-C(34)-C(35)	120.53(19)
C(15)-C(16)-C(17)	126.46(18)	C(36)-C(35)-C(34)	120.2(2)
C(11)-C(16)-C(17)	114.68(16)	C(35)-C(36)-C(31)	119.06(18)
C(24)-C(17)-C(16)	125.46(17)	C(35)-C(36)-C(24)	125.82(18)
C(24)-C(17)-C(18)	121.20(17)	C(31)-C(36)-C(24)	115.03(16)
Cl(7)-C(37)-Cl(6)	110.72(17)	Cl(6)-C(37)-Cl(5)	110.79(15)
Cl(7)-C(37)-Cl(5)	111.13(17)		

Table 4. Anisotropic displacement parameters ($\text{\AA}^2 \times 10^3$). The anisotropicdisplacement factor exponent takes the form: $-2\pi^2 [h^2 a^{*2} U_{11} + \dots + 2 h k a^* b^* U_{12}]$

	U_{11}	U_{22}	U_{33}	U_{23}	U_{13}	U_{12}
C(1)	24(1)	11(1)	17(1)	0(1)	-1(1)	1(1)
C(2)	22(1)	15(1)	16(1)	-1(1)	-1(1)	1(1)
C(3)	23(1)	16(1)	15(1)	0(1)	0(1)	1(1)
C(4)	21(1)	18(1)	15(1)	2(1)	-1(1)	1(1)
Cl(1)	22(1)	38(1)	25(1)	-7(1)	-5(1)	4(1)
C(5)	21(1)	25(1)	10(1)	-2(1)	-2(1)	-5(1)
Cl(2)	43(1)	37(1)	11(1)	2(1)	-3(1)	2(1)
C(6)	19(1)	21(1)	14(1)	-6(1)	-1(1)	-2(1)
Cl(3)	40(1)	28(1)	21(1)	-12(1)	2(1)	4(1)
C(7)	21(1)	16(1)	16(1)	-1(1)	-2(1)	2(1)
Cl(4)	31(1)	29(1)	23(1)	4(1)	-7(1)	-12(1)
C(8)	21(1)	16(1)	16(1)	-3(1)	-1(1)	1(1)
C(9)	19(1)	15(1)	17(1)	-1(1)	-2(1)	-1(1)
C(10)	19(1)	13(1)	15(1)	2(1)	-1(1)	2(1)
C(11)	14(1)	17(1)	15(1)	2(1)	-3(1)	1(1)
C(12)	19(1)	18(1)	20(1)	4(1)	-2(1)	-1(1)
C(13)	22(1)	27(1)	20(1)	8(1)	2(1)	0(1)
C(14)	33(1)	31(1)	14(1)	3(1)	1(1)	4(1)
C(15)	31(1)	21(1)	16(1)	-2(1)	-3(1)	0(1)
C(16)	18(1)	17(1)	15(1)	2(1)	-3(1)	1(1)
C(17)	20(1)	17(1)	12(1)	-3(1)	-5(1)	-5(1)
C(18)	19(1)	16(1)	15(1)	4(1)	-4(1)	1(1)
C(19)	20(1)	20(1)	27(1)	5(1)	-5(1)	-3(1)
C(20)	17(1)	29(1)	35(1)	8(1)	-1(1)	2(1)
C(21)	21(1)	29(1)	26(1)	6(1)	2(1)	9(1)
C(22)	23(1)	19(1)	18(1)	0(1)	-2(1)	5(1)
C(23)	17(1)	16(1)	14(1)	2(1)	-4(1)	2(1)
C(24)	21(1)	14(1)	14(1)	-4(1)	-2(1)	-4(1)
C(25)	24(1)	10(1)	18(1)	-3(1)	1(1)	-5(1)
C(26)	29(1)	14(1)	17(1)	-1(1)	0(1)	-5(1)
C(27)	32(1)	20(1)	18(1)	-6(1)	8(1)	-8(1)
C(28)	23(1)	21(1)	28(1)	-6(1)	8(1)	-4(1)
C(29)	22(1)	17(1)	24(1)	-3(1)	1(1)	-3(1)
C(30)	22(1)	11(1)	18(1)	-1(1)	2(1)	-3(1)
C(31)	24(1)	8(1)	18(1)	-2(1)	1(1)	0(1)
C(32)	29(1)	14(1)	18(1)	0(1)	1(1)	0(1)
C(33)	38(1)	15(1)	20(1)	1(1)	9(1)	-5(1)
C(34)	26(1)	19(1)	31(1)	-1(1)	7(1)	-6(1)
C(35)	24(1)	14(1)	26(1)	0(1)	1(1)	-3(1)
C(36)	23(1)	10(1)	18(1)	-2(1)	1(1)	0(1)
C(37)	48(2)	48(2)	43(2)	7(1)	-15(1)	-20(1)
Cl(5)	60(1)	46(1)	67(1)	2(1)	-4(1)	-6(1)
Cl(6)	72(1)	52(1)	61(1)	2(1)	-4(1)	-1(1)
Cl(7)	103(1)	97(1)	43(1)	22(1)	-13(1)	-18(1)

Table 5. Hydrogen coordinates ($\times 10^4$) and isotropic displacement parameters ($\text{\AA}^2 \times 10^3$).

	x	y	z	U(eq)
H(2)	2656(17)	7980(30)	6434(8)	20(5)
H(3)	4420(17)	7180(20)	5852(8)	14(5)
H(8)	5153(19)	4530(30)	6084(9)	27(6)
H(9)	3983(18)	3290(30)	6866(9)	24(6)
H(12)	4421	2477	7699	23
H(13)	4205	2843	8524	28
H(14)	4748	5088	8888	31
H(15)	5470	7007	8427	27
H(19)	7917	7494	7270	27
H(20)	8948	6197	6730	33
H(21)	8326	4158	6285	30
H(22)	6700	3291	6414	24
H(26)	4698	9108	8199	24
H(27)	3138	10114	8396	28
H(28)	1990	10722	7795	29
H(29)	2355	10172	6993	25
H(32)	4849	9914	5780	24
H(33)	6496	10610	5616	29
H(34)	7700	10513	6224	30
H(35)	7271	9669	6994	26
H(37)	8189	7107	4845	55

9.5.6 Silver Complex

Table 1. Crystal data and structure refinement for herge39a.

Identification code	herge39a	
Empirical formula	C ₄₀ H ₃₂ AgF ₆ OSb	
Formula weight	872.28	
Temperature	170(2) K	
Wavelength	0.71073 Å	
Crystal system	monoclinic	
Space group	Cc	
Unit cell dimensions	a = 17.7185(14) Å	α = 90°.
	b = 23.6763(16) Å	β = 108.196(9)°.
	c = 16.7757(13) Å	γ = 90°.
Volume	6685.6(9) Å ³	
Z	8	
Density (calculated)	1.733 Mg/m ³	
Absorption coefficient	1.460 mm ⁻¹	
F(000)	3456	
Crystal size	0.2 x 0.15 x 0.08 mm ³	
Theta range for data collection	2.56 to 26.02°.	
Index ranges	-21 ≤ h ≤ 21, -29 ≤ k ≤ 29, -20 ≤ l ≤ 20	
Reflections collected	24672	
Independent reflections	12620 [R(int) = 0.0547]	
Completeness to theta = 26.02°	99.2 %	
Refinement method	Full-matrix least-squares on F ²	
Data / restraints / parameters	12620 / 46 / 871	
Goodness-of-fit on F ²	1.080	
Final R indices [I > 2σ(I)]	R1 = 0.0691, wR2 = 0.1684	
R indices (all data)	R1 = 0.0968, wR2 = 0.1904	
Absolute structure parameter	0.00(3)	
Extinction coefficient	0.00145(19)	
Largest diff. peak and hole	1.223 and -1.252 e.Å ⁻³	

Comments:

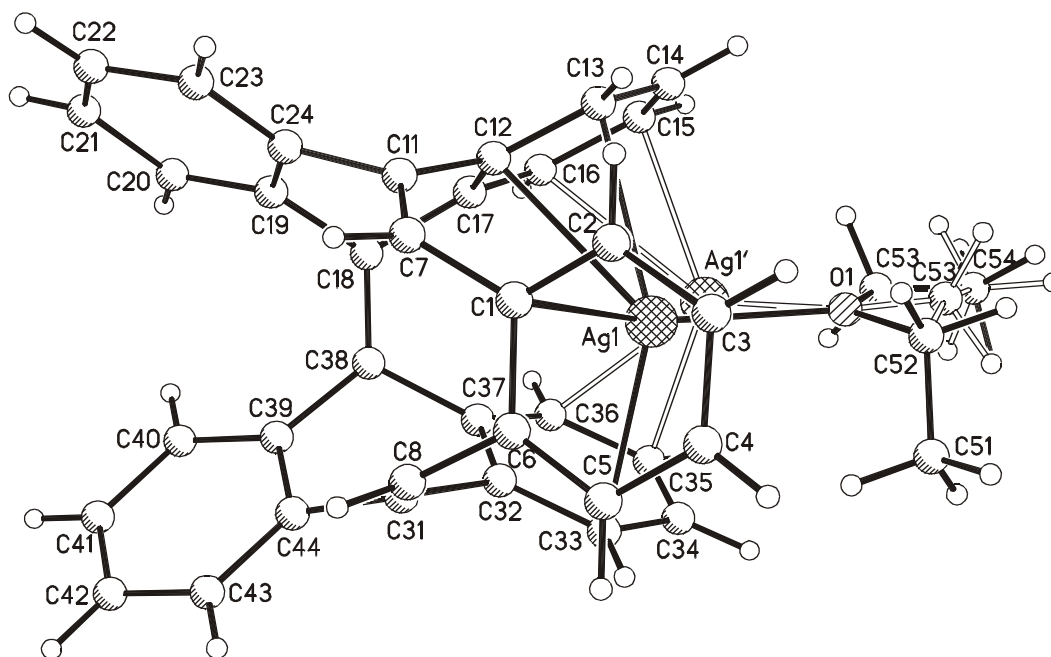
All non-hydrogen atoms except one fluoro atom were refined anisotropic. The H atoms were positioned with idealized geometry and refined using a riding model. A numerical absorption correction was performed Tmin./max= 0.5840 / 0.8766. There are two crystallographically independent complexes in the asymmetric unit. Each of the two silver atoms is disordered over two positions and was refined using a riding model. Some of the fluoro atoms of both hexafluoroantimonate anions exhibit unusual high anisotropic displacement parameters indicating for disorder. One of these fluoro atoms was refined only isotropic. Analysis of the structure shows that both crystallographically independent complexes can be transferred into each other by half a translation into the direction of the a-axis. However, if the structure is refined in the smaller cell, disorder and unusual short bond distances between carbon and fluoro atoms occurs.

Table 2. Atomic coordinates ($\times 10^4$) and equivalent isotropic displacement parameters ($\text{\AA}^2 \times 10^3$).U(eq) is defined as one third of the trace of the orthogonalized U_{ij} tensor.

	x	y	z	U(eq)
Sb(1)	6699(1)	9378(1)	5395(1)	55(1)
F(1)	6696(6)	8586(3)	5372(6)	85(2)
F(2)	6712(7)	10178(3)	5408(6)	91(3)
F(3)	6707(9)	9394(4)	4310(5)	113(4)
F(4)	7841(5)	9368(3)	5729(7)	95(3)
F(5)	6839(8)	9357(4)	6537(6)	113(4)
F(6)	5705(7)	9377(6)	5227(13)	156(6)
Sb(2)	11589(1)	9382(1)	5321(1)	76(1)
F(11)	11681(7)	8612(3)	5274(7)	134(5)
F(12)	11613(7)	10169(4)	5335(6)	134(5)
F(13)	12753(6)	9394(4)	5658(8)	133(5)
F(14)	11811(7)	9333(5)	6452(6)	166(7)
F(15)	11736(9)	9394(4)	4261(7)	159(7)
F(16)	10544(7)	9330(6)	5128(10)	183(7)
Ag(1)	3437(1)	8084(1)	2620(1)	41(1)
Ag(1')	4429(2)	8696(1)	3628(3)	52(1)
C(1)	2861(5)	7189(4)	1681(6)	43(2)
C(2)	2628(7)	7532(5)	983(6)	53(3)
C(3)	1908(6)	7842(5)	778(6)	52(3)
C(4)	1408(6)	7771(5)	1261(7)	60(3)
C(5)	1640(6)	7436(5)	1978(7)	57(3)
C(6)	2355(5)	7147(4)	2200(6)	42(2)
C(7)	3537(5)	6796(4)	1848(5)	38(2)
C(8)	2631(5)	6756(5)	2936(7)	47(2)
C(11)	4319(5)	6906(4)	2201(5)	36(2)
C(12)	4666(4)	7461(4)	2464(5)	33(2)
C(13)	4595(6)	7937(5)	1948(7)	49(2)
C(14)	5024(7)	8422(5)	2252(8)	61(3)
C(15)	5520(7)	8462(6)	3063(8)	64(3)
C(16)	5598(7)	7986(4)	3598(7)	47(2)
C(17)	5170(5)	7500(4)	3308(5)	34(2)
C(18)	5141(4)	6988(4)	3799(5)	33(2)
C(19)	5337(4)	6483(4)	3398(5)	34(2)
C(20)	5855(5)	6054(4)	3760(6)	41(2)
C(21)	5975(7)	5593(5)	3280(7)	53(3)
C(22)	5534(7)	5555(5)	2449(8)	62(3)
C(23)	4996(7)	5986(5)	2060(6)	52(3)
C(24)	4899(5)	6442(4)	2533(5)	37(2)
C(31)	3125(5)	6865(4)	3691(6)	40(2)
C(32)	3418(5)	7447(4)	3997(5)	39(2)
C(33)	2940(7)	7913(5)	3969(7)	53(3)
C(34)	3264(9)	8419(6)	4331(7)	78(4)
C(35)	4076(8)	8466(5)	4766(6)	59(3)
C(36)	4550(7)	7998(5)	4805(6)	50(2)
C(37)	4242(5)	7504(4)	4417(5)	32(2)
C(38)	4700(4)	6978(3)	4336(5)	29(2)
C(39)	4378(5)	6466(4)	4608(5)	36(2)
C(40)	4821(6)	6039(4)	5120(5)	41(2)
C(41)	4436(8)	5579(5)	5338(7)	59(3)
C(42)	3610(8)	5543(6)	5041(8)	64(3)
C(43)	3176(6)	5956(5)	4534(8)	58(3)
C(44)	3539(5)	6418(4)	4309(6)	44(2)

Table 2. Atomic coordinates ($\times 10^4$) and equivalent isotropic displacement parameters ($\text{\AA}^2 \times 10^3$).U(eq) is defined as one third of the trace of the orthogonalized U_{ij} tensor.

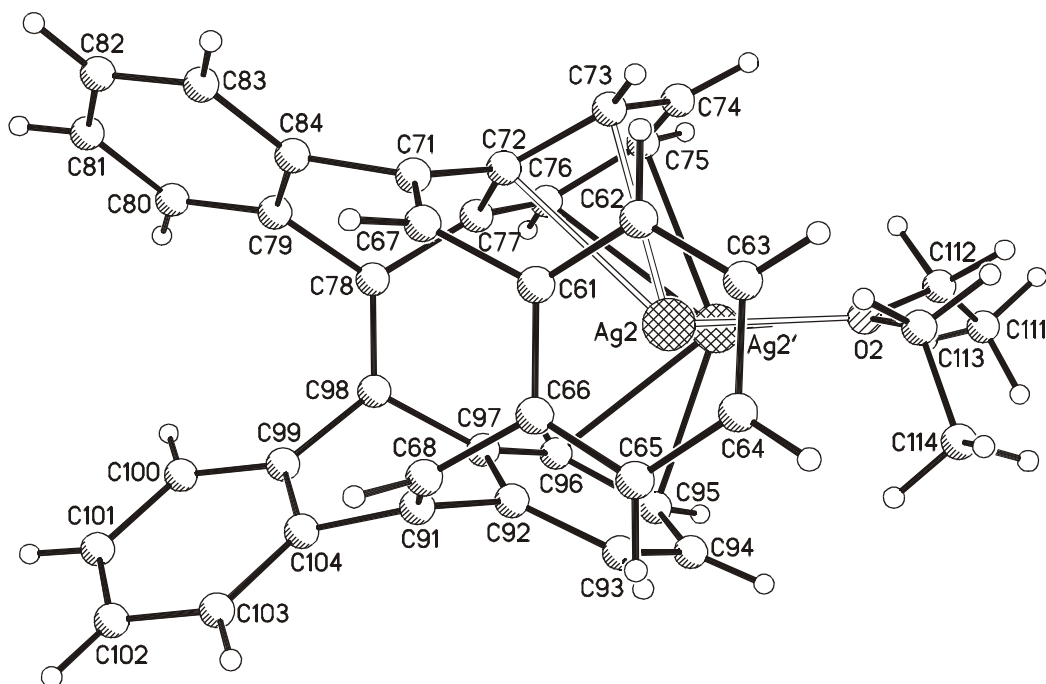
	x	y	z	U(eq)
C(51)	1935(11)	9164(8)	2204(12)	97(5)
C(52)	2569(9)	9226(7)	1883(11)	84(4)
O(1)	3322(5)	9069(4)	2491(6)	67(2)
C(53)	3860(20)	9434(15)	2950(20)	146(13)
C(53')	3400(50)	9642(16)	2540(60)	170(40)
C(54)	3930(20)	10026(16)	3090(20)	187(13)
Ag(2)	9383(1)	8675(1)	3620(1)	46(1)
Ag(2')	8469(1)	8064(1)	2643(1)	44(1)
C(61)	7853(5)	7138(4)	1665(5)	43(2)
C(62)	7607(7)	7489(5)	964(7)	56(3)
C(63)	6904(7)	7795(5)	767(7)	57(3)
C(64)	6437(6)	7734(5)	1274(6)	53(3)
C(65)	6666(6)	7402(6)	1993(7)	61(3)
C(66)	7378(6)	7099(4)	2199(6)	47(2)
C(67)	8539(6)	6742(5)	1826(6)	47(2)
C(68)	7633(5)	6696(5)	2915(7)	47(2)
C(71)	9314(6)	6873(4)	2178(5)	38(2)
C(72)	9645(6)	7426(4)	2443(6)	42(2)
C(73)	9570(7)	7899(5)	1920(7)	51(2)
C(74)	10003(8)	8408(5)	2245(9)	63(3)
C(75)	10490(7)	8434(5)	3034(8)	58(3)
C(76)	10569(7)	7976(5)	3593(7)	49(2)
C(77)	10144(5)	7473(4)	3298(6)	36(2)
C(78)	10113(5)	6962(4)	3781(5)	33(2)
C(79)	10326(5)	6449(4)	3388(5)	32(2)
C(80)	10871(5)	6026(4)	3767(6)	37(2)
C(81)	10982(6)	5578(5)	3300(7)	52(3)
C(82)	10569(7)	5533(5)	2462(7)	56(3)
C(83)	10019(7)	5936(5)	2072(6)	56(3)
C(84)	9890(5)	6399(4)	2526(5)	35(2)
C(91)	8122(5)	6830(4)	3693(6)	42(2)
C(92)	8405(6)	7402(4)	4007(5)	42(2)
C(93)	7873(7)	7851(5)	3945(6)	58(3)
C(94)	8181(9)	8357(6)	4339(7)	69(4)
C(95)	8966(9)	8402(5)	4784(7)	68(4)
C(96)	9517(7)	7963(4)	4817(5)	48(2)
C(97)	9210(6)	7452(4)	4412(6)	42(2)
C(98)	9685(5)	6947(4)	4330(5)	33(2)
C(99)	9378(5)	6439(4)	4609(5)	36(2)
C(100)	9821(5)	6012(4)	5124(5)	41(2)
C(101)	9436(8)	5545(5)	5323(7)	58(3)
C(102)	8608(8)	5493(6)	5032(8)	68(4)
C(103)	8161(7)	5914(6)	4499(8)	61(3)
C(104)	8536(5)	6374(4)	4290(6)	40(2)
C(111)	8940(30)	10050(30)	3280(30)	290(30)
C(112)	8810(40)	9660(30)	2770(40)	340(40)
O(2)	8412(7)	9099(6)	2604(8)	103(4)
C(113)	7705(15)	9097(12)	1997(17)	139(8)
C(114)	7030(10)	9166(8)	2253(11)	93(5)

**Table 3.** Bond lengths [Å] and angles [°].

Ag(1)-O(1)	2.345(8)	Ag(1')-C(35)	2.251(13)
Ag(1)-C(1)	2.647(9)	Ag(1')-O(1)	2.434(10)
Ag(1)-C(13)	2.654(10)	Ag(1')-C(15)	2.468(14)
Ag(1)-C(33)	2.703(10)	Ag(1')-C(36)	2.531(11)
Ag(1)-C(12)	2.708(8)	Ag(1')-C(16)	2.681(12)
C(1)-C(2)	1.377(14)	C(22)-C(23)	1.411(15)
C(1)-C(6)	1.436(14)	C(23)-C(24)	1.382(13)
C(1)-C(7)	1.472(13)	C(31)-C(32)	1.505(14)
C(2)-C(3)	1.418(15)	C(31)-C(44)	1.505(13)
C(3)-C(4)	1.384(17)	C(32)-C(33)	1.384(14)
C(4)-C(5)	1.391(17)	C(32)-C(37)	1.414(11)
C(5)-C(6)	1.384(14)	C(33)-C(34)	1.38(2)
C(6)-C(8)	1.497(14)	C(34)-C(35)	1.401(19)
C(7)-C(11)	1.352(13)	C(35)-C(36)	1.380(15)
C(8)-C(31)	1.320(14)	C(36)-C(37)	1.367(14)
C(11)-C(12)	1.459(13)	C(37)-C(38)	1.514(12)
C(11)-C(24)	1.489(12)	C(38)-C(39)	1.473(12)
C(12)-C(13)	1.403(13)	C(39)-C(40)	1.397(13)
C(12)-C(17)	1.422(11)	C(39)-C(44)	1.416(12)
C(13)-C(14)	1.384(16)	C(40)-C(41)	1.395(14)
C(14)-C(15)	1.372(17)	C(41)-C(42)	1.394(16)
C(15)-C(16)	1.421(16)	C(42)-C(43)	1.366(17)
C(16)-C(17)	1.379(13)	C(43)-C(44)	1.379(14)
C(17)-C(18)	1.476(12)	C(51)-C(52)	1.40(2)
C(18)-C(38)	1.366(12)	C(52)-O(1)	1.452(17)
C(18)-C(19)	1.465(13)	C(52)-C(53')	1.83(5)
C(19)-C(20)	1.377(13)	O(1)-C(53)	1.34(3)
C(19)-C(24)	1.419(11)	O(1)-C(53')	1.36(4)
C(20)-C(21)	1.412(14)	C(53)-C(54)	1.42(4)
C(21)-C(22)	1.372(16)	C(53')-C(54)	1.42(4)

Table 3. Bond lengths [Å] and angles [°].

O(1)-Ag(1)-C(1)	137.3(3)	C(35)-Ag(1')-O(1)	112.5(4)
O(1)-Ag(1)-C(13)	98.5(3)	C(35)-Ag(1')-C(15)	136.8(5)
C(1)-Ag(1)-C(13)	81.3(3)	O(1)-Ag(1')-C(15)	108.4(4)
O(1)-Ag(1)-C(33)	100.6(4)	C(35)-Ag(1')-C(36)	32.9(4)
C(1)-Ag(1)-C(33)	102.3(4)	O(1)-Ag(1')-C(36)	134.4(4)
C(13)-Ag(1)-C(33)	146.5(3)	C(15)-Ag(1')-C(36)	105.5(4)
O(1)-Ag(1)-C(12)	125.6(3)	C(35)-Ag(1')-C(16)	106.6(4)
C(1)-Ag(1)-C(12)	71.3(3)	O(1)-Ag(1')-C(16)	130.6(4)
C(13)-Ag(1)-C(12)	30.3(3)	C(15)-Ag(1')-C(16)	31.7(4)
C(33)-Ag(1)-C(12)	118.8(3)	C(36)-Ag(1')-C(16)	74.2(3)
C(2)-C(1)-C(6)	118.5(9)	C(8)-C(31)-C(32)	124.2(9)
C(2)-C(1)-C(7)	123.1(10)	C(8)-C(31)-C(44)	123.9(10)
C(6)-C(1)-C(7)	117.7(8)	C(32)-C(31)-C(44)	111.5(8)
C(1)-C(2)-C(3)	121.4(11)	C(33)-C(32)-C(37)	117.8(9)
C(4)-C(3)-C(2)	119.1(10)	C(33)-C(32)-C(31)	125.2(9)
C(3)-C(4)-C(5)	120.3(10)	C(37)-C(32)-C(31)	116.7(8)
C(6)-C(5)-C(4)	120.8(11)	C(32)-C(33)-C(34)	120.7(11)
C(5)-C(6)-C(1)	119.7(9)	C(33)-C(34)-C(35)	121.0(11)
C(5)-C(6)-C(8)	124.3(10)	C(36)-C(35)-C(34)	118.2(11)
C(1)-C(6)-C(8)	116.0(8)	C(37)-C(36)-C(35)	121.2(10)
C(11)-C(7)-C(1)	128.6(9)	C(36)-C(37)-C(32)	121.0(9)
C(31)-C(8)-C(6)	128.2(10)	C(36)-C(37)-C(38)	126.8(8)
C(7)-C(11)-C(12)	125.7(8)	C(32)-C(37)-C(38)	112.1(7)
C(7)-C(11)-C(24)	121.0(9)	C(18)-C(38)-C(39)	125.1(8)
C(12)-C(11)-C(24)	112.0(7)	C(18)-C(38)-C(37)	118.6(7)
C(13)-C(12)-C(17)	117.9(9)	C(39)-C(38)-C(37)	112.3(7)
C(13)-C(12)-C(11)	126.1(8)	C(40)-C(39)-C(44)	119.0(8)
C(17)-C(12)-C(11)	115.8(8)	C(40)-C(39)-C(38)	126.0(8)
C(14)-C(13)-C(12)	120.5(10)	C(44)-C(39)-C(38)	114.9(8)
C(15)-C(14)-C(13)	122.0(11)	C(41)-C(40)-C(39)	120.0(9)
C(14)-C(15)-C(16)	118.5(11)	C(42)-C(41)-C(40)	119.9(10)
C(17)-C(16)-C(15)	120.3(10)	C(43)-C(42)-C(41)	120.2(10)
C(16)-C(17)-C(12)	120.7(9)	C(42)-C(43)-C(44)	121.2(10)
C(16)-C(17)-C(18)	126.9(8)	C(43)-C(44)-C(39)	119.7(9)
C(12)-C(17)-C(18)	112.3(7)	C(43)-C(44)-C(31)	125.3(9)
C(38)-C(18)-C(19)	123.8(8)	C(39)-C(44)-C(31)	114.8(8)
C(38)-C(18)-C(17)	120.6(8)	C(51)-C(52)-O(1)	112.1(15)
C(19)-C(18)-C(17)	111.1(7)	C(51)-C(52)-C(53')	115(4)
C(20)-C(19)-C(24)	118.4(8)	O(1)-C(52)-C(53')	47.5(16)
C(20)-C(19)-C(18)	128.3(8)	C(53)-O(1)-C(53')	44(3)
C(24)-C(19)-C(18)	113.2(7)	C(53)-O(1)-C(52)	125.0(17)
C(19)-C(20)-C(21)	121.2(9)	C(53')-O(1)-C(52)	81(3)
C(22)-C(21)-C(20)	119.3(9)	O(1)-C(53)-C(54)	138(3)
C(21)-C(22)-C(23)	120.8(10)	O(1)-C(53')-C(54)	135(4)
C(24)-C(23)-C(22)	119.1(9)	O(1)-C(53')-C(52)	51.7(17)
C(23)-C(24)-C(19)	121.0(8)	C(54)-C(53')-C(52)	169(8)
C(23)-C(24)-C(11)	123.8(8)	C(53)-C(54)-C(53')	42(3)
C(19)-C(24)-C(11)	115.1(8)		

**Table 3.** Bond lengths [Å] and angles [°].

Ag(2)-O(2)	2.245(10)	Ag(2)-C(76)	2.687(11)
Ag(2)-C(95)	2.383(13)	Ag(2')-O(2)	2.452(14)
Ag(2)-C(75)	2.518(11)	Ag(2')-C(73)	2.628(10)
Ag(2)-C(96)	2.577(10)	Ag(2')-C(72)	2.679(9)
C(61)-C(62)	1.394(14)	C(81)-C(82)	1.371(15)
C(61)-C(66)	1.410(15)	C(82)-C(83)	1.374(15)
C(61)-C(67)	1.492(12)	C(83)-C(84)	1.395(13)
C(62)-C(63)	1.390(14)	C(91)-C(92)	1.484(15)
C(63)-C(64)	1.366(17)	C(91)-C(104)	1.497(13)
C(64)-C(65)	1.391(17)	C(92)-C(97)	1.380(14)
C(65)-C(66)	1.398(13)	C(92)-C(93)	1.403(13)
C(66)-C(68)	1.491(14)	C(93)-C(94)	1.39(2)
C(67)-C(71)	1.350(14)	C(94)-C(95)	1.360(19)
C(68)-C(91)	1.359(15)	C(95)-C(96)	1.416(16)
C(71)-C(72)	1.447(14)	C(96)-C(97)	1.409(14)
C(71)-C(84)	1.506(12)	C(97)-C(98)	1.493(12)
C(72)-C(73)	1.404(14)	C(98)-C(99)	1.455(13)
C(72)-C(77)	1.435(13)	C(99)-C(100)	1.399(12)
C(73)-C(74)	1.440(17)	C(99)-C(104)	1.428(12)
C(74)-C(75)	1.336(18)	C(100)-C(101)	1.394(15)
C(75)-C(76)	1.412(16)	C(101)-C(102)	1.400(16)
C(76)-C(77)	1.412(14)	C(102)-C(103)	1.406(17)
C(77)-C(78)	1.468(12)	C(103)-C(104)	1.379(15)
C(78)-C(98)	1.366(12)	C(111)-C(112)	1.23(7)
C(78)-C(79)	1.485(12)	C(112)-O(2)	1.48(7)
C(79)-C(80)	1.399(11)	O(2)-C(113)	1.35(3)
C(79)-C(84)	1.416(11)	C(113)-C(114)	1.40(3)
C(80)-C(81)	1.368(15)		

Table 3. Bond lengths [Å] and angles [°].

O(2)-Ag(2)-C(95)	112.5(5)	C(77)-C(78)-C(79)	111.9(7)
O(2)-Ag(2)-C(75)	108.1(5)	C(80)-C(79)-C(84)	119.0(8)
C(95)-Ag(2)-C(75)	137.5(4)	C(80)-C(79)-C(78)	128.3(8)
O(2)-Ag(2)-C(96)	138.3(4)	C(84)-C(79)-C(78)	112.8(7)
C(95)-Ag(2)-C(96)	32.9(4)	C(81)-C(80)-C(79)	119.8(8)
C(75)-Ag(2)-C(96)	105.2(4)	C(80)-C(81)-C(82)	121.4(9)
O(2)-Ag(2)-C(76)	132.9(4)	C(81)-C(82)-C(83)	120.4(10)
C(95)-Ag(2)-C(76)	106.9(4)	C(82)-C(83)-C(84)	119.9(9)
C(75)-Ag(2)-C(76)	31.3(3)	C(83)-C(84)-C(79)	119.5(8)
C(96)-Ag(2)-C(76)	74.2(3)	C(83)-C(84)-C(71)	125.5(8)
O(2)-Ag(2')-C(73)	99.6(4)	C(79)-C(84)-C(71)	115.0(7)
O(2)-Ag(2')-C(72)	126.0(4)	C(68)-C(91)-C(92)	126.7(9)
C(73)-Ag(2')-C(72)	30.7(3)	C(68)-C(91)-C(104)	120.4(10)
C(62)-C(61)-C(66)	119.0(8)	C(92)-C(91)-C(104)	112.3(8)
C(62)-C(61)-C(67)	123.4(9)	C(97)-C(92)-C(93)	122.6(11)
C(66)-C(61)-C(67)	117.2(9)	C(97)-C(92)-C(91)	115.9(8)
C(63)-C(62)-C(61)	122.1(11)	C(93)-C(92)-C(91)	121.4(10)
C(64)-C(63)-C(62)	118.0(10)	C(94)-C(93)-C(92)	117.5(11)
C(63)-C(64)-C(65)	122.0(9)	C(95)-C(94)-C(93)	120.6(11)
C(64)-C(65)-C(66)	120.0(11)	C(94)-C(95)-C(96)	122.5(11)
C(65)-C(66)-C(61)	118.8(10)	C(97)-C(96)-C(95)	117.0(10)
C(65)-C(66)-C(68)	123.4(10)	C(92)-C(97)-C(96)	119.7(9)
C(61)-C(66)-C(68)	117.6(8)	C(92)-C(97)-C(98)	114.2(9)
C(71)-C(67)-C(61)	126.5(10)	C(96)-C(97)-C(98)	126.0(9)
C(91)-C(68)-C(66)	124.5(10)	C(78)-C(98)-C(99)	125.4(8)
C(67)-C(71)-C(72)	127.0(8)	C(78)-C(98)-C(97)	119.4(8)
C(67)-C(71)-C(84)	118.2(9)	C(99)-C(98)-C(97)	110.8(8)
C(72)-C(71)-C(84)	113.1(8)	C(100)-C(99)-C(104)	118.2(9)
C(73)-C(72)-C(77)	118.1(10)	C(100)-C(99)-C(98)	127.0(8)
C(73)-C(72)-C(71)	125.5(9)	C(104)-C(99)-C(98)	114.8(7)
C(77)-C(72)-C(71)	116.3(8)	C(101)-C(100)-C(99)	119.9(9)
C(72)-C(73)-C(74)	119.7(10)	C(100)-C(101)-C(102)	121.7(9)
C(75)-C(74)-C(73)	121.0(10)	C(101)-C(102)-C(103)	118.7(10)
C(74)-C(75)-C(76)	121.5(11)	C(104)-C(103)-C(102)	120.1(10)
C(77)-C(76)-C(75)	118.8(11)	C(103)-C(104)-C(99)	121.3(9)
C(76)-C(77)-C(72)	120.7(9)	C(103)-C(104)-C(91)	124.4(8)
C(76)-C(77)-C(78)	127.6(9)	C(99)-C(104)-C(91)	114.2(8)
C(72)-C(77)-C(78)	111.7(8)	C(111)-C(112)-O(2)	141(8)
C(98)-C(78)-C(77)	121.1(8)	C(113)-O(2)-C(112)	115(3)
C(98)-C(78)-C(79)	123.4(8)	O(2)-C(113)-C(114)	117(2)

Table 3. Bond lengths [Å] and angles [°].

Sb(1)-F(6)	1.694(11)	Sb(2)-F(16)	1.782(12)
Sb(1)-F(3)	1.824(9)	Sb(2)-F(14)	1.817(10)
Sb(1)-F(5)	1.855(8)	Sb(2)-F(11)	1.833(8)
Sb(1)-F(1)	1.876(7)	Sb(2)-F(12)	1.864(9)
Sb(1)-F(2)	1.895(7)	Sb(2)-F(15)	1.875(10)
Sb(1)-F(4)	1.924(9)	Sb(2)-F(13)	1.960(10)
F(6)-Sb(1)-F(3)	99.6(8)	F(16)-Sb(2)-F(14)	93.3(6)
F(6)-Sb(1)-F(5)	88.1(8)	F(16)-Sb(2)-F(11)	91.4(5)
F(3)-Sb(1)-F(5)	172.3(7)	F(14)-Sb(2)-F(11)	89.3(4)
F(6)-Sb(1)-F(1)	90.0(6)	F(16)-Sb(2)-F(12)	95.1(5)
F(3)-Sb(1)-F(1)	90.1(4)	F(14)-Sb(2)-F(12)	93.0(4)
F(5)-Sb(1)-F(1)	89.6(4)	F(11)-Sb(2)-F(12)	172.9(6)
F(6)-Sb(1)-F(2)	90.6(6)	F(16)-Sb(2)-F(15)	105.9(7)
F(3)-Sb(1)-F(2)	89.2(4)	F(14)-Sb(2)-F(15)	160.4(7)
F(5)-Sb(1)-F(2)	91.0(4)	F(11)-Sb(2)-F(15)	86.3(4)
F(1)-Sb(1)-F(2)	179.2(5)	F(12)-Sb(2)-F(15)	89.3(4)
F(6)-Sb(1)-F(4)	172.9(8)	F(16)-Sb(2)-F(13)	173.3(6)
F(3)-Sb(1)-F(4)	87.5(6)	F(14)-Sb(2)-F(13)	80.5(5)
F(5)-Sb(1)-F(4)	84.8(6)	F(11)-Sb(2)-F(13)	85.8(4)
F(1)-Sb(1)-F(4)	89.4(4)	F(12)-Sb(2)-F(13)	88.0(4)
F(2)-Sb(1)-F(4)	90.0(4)	F(15)-Sb(2)-F(13)	80.1(5)

Table 4. Anisotropic displacement parameters ($\text{\AA}^2 \times 10^3$). The anisotropicdisplacement factor exponent takes the form: $-2\pi^2 [h^2 a^{*2} U_{11} + \dots + 2 h k a^* b^* U_{12}]$

	U_{11}	U_{22}	U_{33}	U_{23}	U_{13}	U_{12}
Sb(1)	73(1)	40(1)	54(1)	-3(1)	25(1)	-2(1)
F(1)	120(6)	33(3)	95(6)	-2(4)	22(5)	-4(4)
F(2)	149(8)	38(4)	84(5)	-11(4)	32(5)	-4(5)
F(3)	213(13)	64(6)	49(4)	6(3)	21(6)	31(6)
F(4)	72(5)	66(5)	126(8)	22(5)	2(5)	-7(4)
F(5)	203(12)	95(7)	62(5)	1(4)	70(7)	-2(7)
F(6)	78(7)	144(12)	267(19)	12(10)	81(9)	14(6)
Sb(2)	134(2)	41(1)	69(1)	-5(1)	56(1)	-7(1)
F(11)	174(11)	48(5)	162(12)	-26(6)	28(9)	-20(6)
F(12)	214(15)	58(5)	108(8)	-16(5)	19(9)	16(7)
F(13)	135(10)	94(8)	175(12)	12(7)	55(9)	-27(7)
F(14)	195(15)	108(10)	136(11)	25(7)	-33(10)	9(9)
F(15)	264(19)	102(10)	157(12)	35(8)	134(13)	60(10)
Ag(1)	44(1)	37(1)	39(1)	-5(1)	9(1)	1(1)
Ag(1')	51(2)	53(2)	52(2)	-3(1)	17(1)	-3(1)
C(1)	39(5)	43(5)	34(4)	-7(4)	-7(4)	6(4)
C(2)	69(7)	53(6)	36(5)	-4(4)	14(5)	5(5)
C(3)	45(5)	65(7)	33(4)	-2(4)	-6(4)	12(5)
C(4)	49(6)	58(7)	55(6)	-6(5)	-8(5)	19(5)
C(5)	40(5)	74(8)	54(6)	0(5)	12(5)	4(5)
C(6)	32(4)	54(6)	32(4)	-6(4)	-2(4)	1(4)
C(7)	35(4)	48(5)	29(4)	-1(4)	6(4)	-1(4)
C(8)	25(4)	64(7)	49(6)	3(5)	5(4)	-8(4)
C(11)	33(4)	46(5)	28(4)	0(3)	10(4)	6(3)
C(12)	24(4)	47(5)	28(4)	4(3)	10(3)	0(3)
C(13)	47(5)	57(6)	49(6)	13(5)	22(5)	0(5)
C(14)	70(7)	52(7)	63(7)	14(5)	23(6)	-10(5)
C(15)	61(7)	59(7)	69(8)	4(6)	14(6)	-20(6)
C(16)	55(6)	45(6)	46(5)	-3(4)	22(5)	-7(5)
C(17)	24(4)	42(5)	36(4)	4(4)	11(3)	-8(3)
C(18)	18(3)	48(5)	29(4)	9(3)	1(3)	-4(3)
C(19)	21(4)	48(5)	33(4)	-2(4)	7(3)	1(3)
C(20)	35(5)	49(5)	35(4)	5(4)	7(4)	-1(4)
C(21)	57(6)	50(6)	54(6)	2(5)	20(5)	19(5)
C(22)	67(7)	55(7)	61(7)	-16(5)	17(6)	26(6)
C(23)	65(6)	59(6)	31(4)	-2(4)	16(4)	24(5)
C(24)	30(4)	49(5)	27(4)	2(4)	2(3)	5(4)
C(31)	26(4)	58(6)	38(5)	6(4)	14(4)	2(4)
C(32)	32(4)	56(6)	28(4)	0(4)	9(3)	7(4)
C(33)	53(6)	64(7)	49(6)	3(5)	26(5)	14(5)
C(34)	106(11)	79(9)	45(6)	-4(6)	19(7)	46(8)
C(35)	88(8)	52(6)	31(4)	-11(4)	10(5)	14(6)
C(36)	63(6)	57(6)	30(4)	-6(4)	13(5)	0(5)
C(37)	28(4)	47(5)	17(3)	3(3)	2(3)	8(3)
C(38)	21(3)	40(4)	20(3)	-1(3)	-1(3)	-4(3)
C(39)	39(4)	44(5)	26(4)	0(3)	14(4)	-6(4)
C(40)	40(5)	50(5)	31(4)	8(4)	7(4)	0(4)
C(41)	82(8)	49(6)	47(6)	21(5)	21(6)	-8(5)
C(42)	57(7)	68(8)	66(8)	16(6)	17(6)	-14(6)
C(43)	44(5)	66(7)	70(7)	9(5)	26(5)	-15(5)
C(44)	36(4)	55(6)	43(5)	12(4)	14(4)	-11(4)

Table 4. Anisotropic displacement parameters ($\text{\AA}^2 \times 10^3$). The anisotropicdisplacement factor exponent takes the form: $-2\pi^2 [h^2 a^{*2} U_{11} + \dots + 2 h k a^* b^* U_{12}]$

	U_{11}	U_{22}	U_{33}	U_{23}	U_{13}	U_{12}
C(51)	96(12)	95(12)	105(13)	9(10)	40(10)	-11(10)
C(52)	67(8)	83(10)	97(11)	-12(8)	16(8)	-8(7)
O(1)	59(5)	54(5)	91(6)	15(4)	30(5)	6(4)
Ag(2)	53(1)	40(1)	45(1)	2(1)	14(1)	2(1)
Ag(2')	44(1)	43(1)	42(1)	-3(1)	9(1)	5(1)
C(61)	31(4)	58(6)	30(4)	-8(4)	-6(4)	13(4)
C(62)	55(6)	68(7)	39(5)	6(5)	8(5)	32(5)
C(63)	58(6)	54(6)	43(5)	0(4)	-7(5)	26(5)
C(64)	34(5)	64(7)	47(5)	-3(5)	-9(4)	22(4)
C(65)	34(5)	91(9)	46(6)	-6(6)	-5(4)	21(5)
C(66)	39(5)	48(6)	45(5)	3(4)	1(4)	14(4)
C(67)	55(6)	47(5)	31(4)	-6(4)	2(4)	23(5)
C(68)	23(4)	58(6)	57(6)	6(5)	10(4)	3(4)
C(71)	39(5)	50(6)	26(4)	5(3)	12(4)	10(4)
C(72)	47(5)	45(5)	42(5)	7(4)	22(4)	17(4)
C(73)	64(6)	51(6)	48(6)	16(5)	31(5)	15(5)
C(74)	84(8)	41(6)	84(9)	22(6)	54(7)	7(5)
C(75)	62(7)	45(6)	79(8)	6(5)	38(6)	-5(5)
C(76)	54(6)	45(6)	53(6)	2(5)	23(5)	-2(5)
C(77)	30(4)	38(5)	44(5)	-1(4)	16(4)	2(3)
C(78)	30(4)	36(4)	35(4)	6(3)	12(3)	7(3)
C(79)	26(4)	32(4)	34(4)	3(3)	6(3)	7(3)
C(80)	23(4)	48(5)	36(4)	7(4)	2(3)	14(4)
C(81)	43(5)	57(6)	54(6)	13(5)	14(5)	22(5)
C(82)	68(7)	55(7)	45(5)	-8(4)	17(5)	26(5)
C(83)	57(6)	71(7)	38(5)	-11(5)	11(5)	24(5)
C(84)	34(4)	40(5)	30(4)	-2(3)	5(3)	12(3)
C(91)	35(5)	50(6)	41(5)	11(4)	15(4)	5(4)
C(92)	46(5)	60(6)	29(4)	14(4)	22(4)	21(4)
C(93)	61(6)	71(8)	42(5)	9(5)	17(5)	40(6)
C(94)	97(10)	70(8)	49(6)	13(6)	36(7)	41(7)
C(95)	110(10)	59(7)	33(5)	-11(5)	19(6)	20(7)
C(96)	64(6)	51(6)	23(4)	-2(4)	5(4)	6(5)
C(97)	53(5)	45(5)	29(4)	7(4)	15(4)	17(4)
C(98)	21(4)	49(5)	26(4)	6(3)	3(3)	9(3)
C(99)	36(4)	43(5)	27(4)	6(3)	8(3)	4(4)
C(100)	38(5)	48(5)	32(4)	11(4)	2(4)	4(4)
C(101)	71(7)	51(6)	53(6)	28(5)	19(6)	19(5)
C(102)	66(7)	65(8)	74(8)	29(6)	22(7)	-11(6)
C(103)	45(5)	74(8)	66(7)	26(6)	17(5)	-5(5)
C(104)	23(4)	58(6)	39(5)	4(4)	7(3)	1(4)
O(2)	68(6)	136(10)	100(8)	52(8)	19(5)	48(7)

Table 5. Hydrogen coordinates ($\times 10^4$) and isotropic displacement parameters ($\text{\AA}^2 \times 10^3$).

	x	y	z	U(eq)
H(2)	2956	7561	633	64
H(3)	1771	8095	315	62
H(4)	904	7951	1102	71
H(5)	1303	7405	2319	68
H(7)	3405	6415	1688	46
H(8)	2424	6383	2849	57
H(13)	4251	7926	1386	59
H(14)	4973	8738	1889	73
H(15)	5805	8801	3262	77
H(16)	5946	8002	4157	57
H(20)	6136	6068	4343	49
H(21)	6358	5311	3531	64
H(22)	5592	5234	2132	74
H(23)	4704	5964	1480	62
H(33)	2384	7886	3698	63
H(34)	2930	8740	4284	94
H(35)	4296	8811	5026	71
H(36)	5101	8019	5107	60
H(40)	5384	6064	5320	50
H(41)	4737	5290	5689	71
H(42)	3348	5229	5192	77
H(43)	2613	5925	4332	70
H(51A)	1439	9271	1774	145
H(51B)	2019	9407	2696	145
H(51C)	1901	8769	2366	145
H(52A)	2597	9624	1714	101
H(52B)	2474	8987	1377	101
H(53A)	4342	9343	2793	175
H(53B)	3974	9284	3529	175
H(53C)	2871	9771	2550	200
H(53D)	3425	9749	1978	200
H(54A)	4493	10127	3337	281
H(54B)	3635	10139	3465	281
H(54C)	3715	10222	2548	281
H(54D)	4474	9953	3078	281
H(54E)	3909	9977	3658	281
H(54F)	3781	10414	2900	281
H(62)	7931	7520	609	67
H(63)	6751	8039	294	68
H(64)	5941	7925	1131	64
H(65)	6338	7381	2345	73
H(67)	8419	6359	1666	56
H(68)	7440	6319	2822	56
H(73)	9235	7884	1355	62
H(74)	9942	8730	1893	76
H(75)	10789	8768	3223	70
H(76)	10902	8005	4158	59
H(80)	11163	6049	4347	45
H(81)	11353	5292	3561	62
H(82)	10664	5222	2149	68
H(83)	9726	5898	1494	68

Table 5. Hydrogen coordinates ($\times 10^4$) and isotropic displacement parameters ($\text{\AA}^2 \times 10^3$).

	x	y	z	U(eq)
H(93)	7324	7812	3646	70
H(94)	7841	8673	4296	83
H(95)	9150	8742	5083	82
H(96)	10068	8010	5100	58
H(100)	10383	6041	5337	49
H(101)	9743	5255	5665	70
H(102)	8353	5179	5191	81
H(103)	7599	5881	4284	74
H(11A)	9132	10377	3041	437
H(11B)	9352	9931	3795	437
H(11C)	8455	10143	3401	437
H(11D)	9354	9563	2757	409
H(11E)	8562	9857	2232	409
H(11F)	7653	8735	1690	166
H(11G)	7709	9402	1595	166
H(11H)	6554	9070	1789	140
H(11I)	6996	9560	2420	140
H(11J)	7068	8918	2731	140

:

10 References

- [1]. H. W. Kroto, J. R. Heath, S. C. O'Brien, R. F. Curl, R. E. Smalley, *Nature* **1985**, *318*, 162.
- [2]. W. Kratschmer, L. D. Lamb, K. Fostiropoulos, D. R. Huffman, *Nature* **1990**, *347*, 354.
- [3]. S. Iijima, *Nature* **1991**, *354*, 57.
- [4]. T. W. Ebbesen, P. M. Ajayan, *Nature* **1992**, *358*, 220.
- [5]. P. J.F. Hariss, *Carbon Nanotubes and related structures new materials for the Twenty first century*, Cambridge University press **1999**.
- [6]. P. M. Ajayan, *Chem. Rev.* **1999**, *99*, 1787.
- [7]. L. Liu, G. Y. Guo, C. S. Jayanthi and S. Y. Wu¹, *Phys. Rev. Lett.* **2002**, *88*, 217206-1.
- [8]. M. Huhtala, A. Kuronen, K. Kaski, *Computer Physics Communications* **2002**, *146*, 30.
- [9]. Y. Tian, D. Chassaing, A. G. Nasibulin, P. Ayala, H. Jiang, A. S. Anisimov, and E. I. Kauppinen, *J. Am. Chem. Soc.* **2008**, *130*, 7188.
- [10]. T. Meng, C. Yu Wang, and S. Wang, *Phys. Rev. B* **2008**, *77*, 033415.
- [11]. R. M Cory, C. L McPhail, A. J Dikmans, J. J. Vittal, *Tetrahedron Lett.*, **1996**, *37*, 1983.
- [12]. R. M. Cory, C. L McPhail, *Tetrahedron Lett.*, **1996**, *37*, 1987.
- [13]. F. H. Kohnke, A. M. Z Slawin, J. F. Stoddart, D. J Williams, *Angew. Chem.* **1987**, *99*, 941.
- [14]. P. R. Ashton, G. R. Brown, N. S. Isaacs, D. Giuffrida, F. H. Kohnke, J. P. Mathias, A. M. Z. Slawin, D. R. Smith, J. F. Stoddart, D. J. Williams, *J. Am. Chem. Soc.* **1992**, *114*, 6330.
- [15]. P. R. Ashton, U. Girreser, D. Giuffrida, F. H Kohnke, J. P Mathias, F. M Raymo, A. M. Z. Slawin, J. F. Stoddart, D. J. Williams, *J. Am. Chem. Soc.*, **1993**, *115*, 5422.
- [16]. B. Esser, F. Rominger, R. Gleiter, *J. Am. Chem. Soc.* **2008**, *130*, 6716.
- [17]. M. Iyoda, Y. Kuwatani, T. Yamauchi, M. Oda, *Chem. Commun*, **1988**, 65.
- [18]. D. L. Mohler, K. P. C. Vollhardt, S. Wolff, *Angew. Chem.* **1990**, *102*, 1200.
- [19]. T. Yoshida, Y. Kuwatani, K. Hara, M. Yoshida, H. Matsuyama, M. Iyoda, S. Nagase, *Tetrahedron Lett.*, **2001**, *42*, 53.
- [20]. (a) E. Nakamura, K. Tahara, Y. Matsuo, M. Sawamura, *J. Am. Chem. Soc.* **2003**, *125*, 2834; (b) E. Nakamura, K. Tahara, Y. Matsuo, M. Sawamura, *J. Am. Chem. Soc.* , **2004**, *126*, 8725.

-
- [21]. K. Tahara, Y. Tobe *Chem.Rev.* **2006**, *106*, 5724.
- [22]. T. Kawase, H. R. Darabi, M. Oda, *Angew. Chem., Int. Ed. Engl.* **1996**, *35*, 2664.
- [23]. T. Kawase, K. Tanaka, N. Fujiwara, H. R. Darabi, M. Oda, *Angew. Chem., Int. Ed.* **2003**, *42*, 1624.
- [24]. S. Kammermeier, P. G. Jones, R. Herges, *Angew. Chem., Int. Ed.* **1996**, *35*, 2669.
- [25]. S. Kammermeier, P. G. Jones, R. Herges, *Angew. Chem., Int. Ed.Engl.* **1997**, *36*, 2200.
- [26]. D. E. Applequist, R. L. Litle, E. C. Friedrich, R. E. Wall, *J. Am. Chem. Soc.* **1959**, *81*, 452-456.
- [27]. R. L. Vivattene, F. D. Greene, L. D. Cheung, R. Majeste, L.M. Tretonas, *J. Am. Chem. Soc.*, **1974**, *96*, 4342.
- [28]. (a) L. A. Carpino, *J. Am. Chem. Soc.* **1957**, *79*, 98 (b) L. A. Carpino, C. A. Giza, B. A. Carpino, *J. Am. Chem. Soc.* **1959**, *81*, 955., (c) L. A. Carpino, *J. Am. Chem. Soc.* **1960**, *82*, 3133.
- [29]. H. Neumann, *Ph.D. Thesis*, Universität Erlangen, **1994**.
- [30]. K. B. Wiberg, M. G. Mattorro, P. J. Okarama, M. E. Jason, *J. Am. Chem. Soc.*, **1984**, *106*, 2194.
- [31]. D. A. Hrovat, W. T. Borden, *J. Am. Chem. Soc.*, **1988**, *110*, 4710.
- [32]. S. Kammermeier, H. Neumann, F. Hampel, R. Herges, *Liebigs Ann. Chem.*, **1996**, 1795.
- [33]. R. Herges, H. Neumann, *Liebigs Ann. Chem.*, **1995**, 1283.
- [34]. R. Herges, H. Neumann, F. Hampel, *Angew. Chem. Int. Ed. Engl.* **1994**, *33*, 993.
- [35]. S. Kammermeier, R. Herges, *Angew. Chem. Int. Ed. Engl.* **1996**, *35*, 417.
- [36]. S. Kammermeier, P. G. Jones, R. Herges, *Angew. Chem. Int. Ed. Engl.* **1997**, *36*, 2200.
- [37]. S. Kammermeier, P. G. Jones, R. Herges, *Angew. Chem. Int. Ed. Engl.*, **1996**, *35*, 2669.
- [38]. M. S. Dresselhaus, G. Dresselhaus, R. Saito, *Carbon* **1995**, *33*, 883.
- [39]. X. Blase, LX. Benedict, EL. Shirley, SG. Louie, *Phys Rev Lett* **1994**, *72*, 1878.
- [40] PM. Ajayan, S. Iijima *Nature* **1992**, *358*, 23.
- [41]. (a) L. F. Sun, S. S. Xie, W. Liu, W. Y. Zhou, Z. Q. Liu, D. S. Tang, *Nature* **2000**, *403*, 384. (b) N. Wang, Z. K. Tang, G. D. Li, J. S. Chen, *Nature* **2000**, *408*, 50.
- [42]. L. C. Qin, X. L. Zhao, K. Hirahara, Y. Miyamoto, Y. Ando, S. Iijima, *Nature* **2000**, *408*, 50.
- [43]. T. Hayashi, Y. A. Kim, T. Matoba, M. Esaka, K. Nishimura, T. Tsukada, M. Endo, M. S. Dresselhaus *Nano letters*, **2003**, *3*, 887.
-

-
- [44]. Z. K. Tang, L. Zhang, N. Wang, X. X. Zhang, G. H. Wen, G. D. Li, J. N. Wang, C. T. Chan, and P. Sheng, *Science*, 2001, 292, 2462.
- [45]. D. Ajami, *Dissertation*, Technische Universität Braunschweig **2003**.
- [46]. A. Hirsch and D. Orphanos, *Canadian Journal of chemistry*, **1965**, 43, 2708.
- [47]. Manfred Schlosser (Ed.), *Organometallics in Synthesis A Manual*, John Wiley & Sons Ltd., New York **2002**.
- [48]. Stefan Kammermeier, *Dissertation*, Universität Erlangen-Nürnberg, **1997**.
- [49]. F. Faigl, M. Schlosser, *Tetrahedron* **1993**, 49, 10271.
- [50]. W. Grimme, K. Pohl, J. Wortmann and D. Frowein, *Liebigs Ann. Chem.* **1996**, 1905.
- [51]. B. A. R. C. Murty, R. Pinkos, P. R. Spurr, W. D. Fessner, G. Lutz, H. Fritz, D. Hunkler, H. Prinzbach, *Chem. Ber.* **1992**, 125, 1719.
- [52]. W. D. Fessner, G. Sedelmeier, P. R. Spurr, G. Rihs, H. Prinzbach, *J. Am. Chem. Soc.* **1987**, 109, 4626.
- [53]. W. D. Fessner, G. Sedelmeier, L. Knothe, H. Prinzbach, G. Rihs, Z. Z. Yang, B. Kovac, E. Heilbronner, *Helv. Chim. Acta* **1987**, 70, 1817.
- [54]. M. Deichmann, *Dissertation*, Technische Universität Braunschweig, **2003**.
- [55]. R. Herges, M. Deichmann, J. Grunenberg, G. Bucher, *Chem. Phys. Lett.*, **2000**, 327, 149.
- [56]. M. Deichman, C. Näther, R. Herges, *Org. Lett.* **2003**, 5, 1269.
- [57]. C. Schaman, R. Pfeiffer, V. Zólyomi, H. Kuzmany, D. Ajami, R. Herges, O. Dubay, J. Sloan, *Phys. Stat. Sol.* **2006**, 243, 3151.
- [58]. S. Tanda, T. Tsuneta, Y. Okajima, K. Inagaki, K. Yamaya, N. Hatakenaka, *Nature* **2003**, 417, 397.
- [59]. D. Ajami, O. Oeckler, A. Simon, R. Herges, *Nature* **2003**, 426, 819.
- [60]. D. Ajami, K. Hess, F. Koehler, C. Näther, O. Oeckler, A. Simon, C. Yamamoto, Y. Okamoto, R. Herges, *Chem. Eur. J.* **2006**, 12, 5434.
- [61]. D. M. Walba, R. M. Richards, R. C. Haltiwanger, *J. Am. Chem. Soc.* **1982**, 104, 3219.
- [62]. D. M. Walba, T. C. Homan, R. M. Richards, R. C. Haltiwanger, *New. J. Chem.* **1993**, 17, 661.
- [63]. M. Stepien, L. Latos-Grazynski, N. Sprutta, P. Chwalisz, L. Szterenberg, *Angew. Chem. Int. Ed.* **2007**, 46, 7869.
- [64]. R. Herges, *Nature* **2007**, 450, 36.
-

-
- [65]. Y. Tanaka, S. Saito, S. Mori, N. Aratani, H. Shinokubo, N. Shibata, Y. Higuchi, Z. S. Yoon, K. S. Kim, S. B. Noh, J. K. Park, D. Kim, A. Osuka, *Angew. Chem. Int. Ed.* **2008**, *47*, 681.
- [66]. J. K. Park, Z. S. Yoon, M. C. Yoon, K. S. Kim, S. Mori, J. Y. Shin, A. Osuka, D. Kim, *J. Am. Chem. Soc.* **2008**, *130*, 1824.
- [67]. R. Herges, *Chem. Rev.* **2006**, *106*, 4820.
- [68]. D. P. Kjell and R. S. Sheridan, *J. Am. Chem. Soc.* **1984**, *106*, 5368.
- [69]. K. Kinko; T. Ikuzo, *J. of Phys. Chem.* **1965**, *69(8)*, 2545.
- [70]. Y. Shigeru, *Bull. Chem. Soc. Jap.* **1961**, *34*, 487.
- [71]. M. S. Raasch, *J. Org. Chem.* **1980** *45*, 856.
- [72]. Y. Lou, J. Chang, J. Jorgensen, and D. M. Lemal, *J. Am. Chem. Soc.* **2002**, *124*, 15302.
- [73]. H. E. Zimmermann, *J. Am. Chem. Soc.*, **1966**, *88*, 1564.
- [74]. M. Takino, S. Daishima, K. Yamaguchi, T. Nakahara, *Journal of Chromatography A*, **2001**, *928*, 53.
- [75]. G. J. Van Berkel and K. G. Asano, *Anal. Chem.*, **1994**, *66*, 2096.
- [76]. Y. V. Vasil'ev, O. G. Khvostenko, A. V. Streletskii, O. V. Boltalina, S. G. Kotsiris, T. Drewello, *J. Phys. Chem. A* **2006**, *110*, 5967.
- [77]. H. Schmidbaur, *Angew. Chem. Int. Ed. Engl.*, **1997**, *24*, 893.
- [78]. R. Gleiter, H. Hopf, *Modern cyclophane chemistry* WILEY-VCH Verlag GmbH & Co. KGaA
- [79]. T. Lahtinen, E. W. Kari Rissanen, *New J. Chem.* **2001**, *25*, 905.
- [80]. I. F. Taylor, E. A. Hall and E. L. Amma, *J. Am. Chem. Soc.*, **1969**, *91*, 5745.
- [81]. T. Yoshi
da, Y. Kuwatani, K. Hara, M. Yoshida, H. Matsuyama, M. Iyoda Nagase,
Tetrahedron Lett., **2001**, *42*, 53.
-

Lebenslauf

Personnel details:

Name: Rajuri Venkataramana
Date of Birth: 22. July 1982
Place of Birth: Sircilla, India
Sex: Male
Marital status: Single
Nationality: Indian
Address: Johann fleck straÙe-8, PHH-839, Kiel

Educational details:

1999-2002 B.Sc. Chemical Technology
Loyola Academy, Secunderabad, India
2002-2004 M.Sc. Chemistry
University of Hyderabad, Hyderabad, India
2004-present Ph.D. Organic Chemistry
Otto- Diels institute of organic chemistry
University of Kiel, in the working group of
Prof. Dr. Rainer Herges